

Plaque stabilizing and destabilizing effects in atherosclerosis

Citation for published version (APA):

Tillie, R. (2024). *Plaque stabilizing and destabilizing effects in atherosclerosis: the role of microvessels, macrophage metabolism and fibroblasts*. [Doctoral Thesis, Maastricht University]. Maastricht University. <https://doi.org/10.26481/dis.20240202rt>

Document status and date:

Published: 01/01/2024

DOI:

[10.26481/dis.20240202rt](https://doi.org/10.26481/dis.20240202rt)

Document Version:

Publisher's PDF, also known as Version of record

Please check the document version of this publication:

- A submitted manuscript is the version of the article upon submission and before peer-review. There can be important differences between the submitted version and the official published version of record. People interested in the research are advised to contact the author for the final version of the publication, or visit the DOI to the publisher's website.
- The final author version and the galley proof are versions of the publication after peer review.
- The final published version features the final layout of the paper including the volume, issue and page numbers.

[Link to publication](#)

General rights

Copyright and moral rights for the publications made accessible in the public portal are retained by the authors and/or other copyright owners and it is a condition of accessing publications that users recognise and abide by the legal requirements associated with these rights.

- Users may download and print one copy of any publication from the public portal for the purpose of private study or research.
- You may not further distribute the material or use it for any profit-making activity or commercial gain
- You may freely distribute the URL identifying the publication in the public portal.

If the publication is distributed under the terms of Article 25fa of the Dutch Copyright Act, indicated by the "Taverne" license above, please follow below link for the End User Agreement:

www.umlib.nl/taverne-license

Take down policy

If you believe that this document breaches copyright please contact us at:

repository@maastrichtuniversity.nl

providing details and we will investigate your claim.

Plaque stabilizing and destabilizing effects in atherosclerosis

The role of microvessels,
macrophage metabolism and fibroblasts

Renée J.H.A. Tillie

Author: Renée Tillie
Cover design: Bennie Tummers, Bram Tummers, Renée Tillie
Layout & figure design: Renée Tillie
Printed by: Gildeprint
ISBN: 978-94-6469-729-2

Copyright © Renée J.H.A. Tillie, Maastricht, The Netherlands, 2023

All rights reserved. No part of this book may be reproduced, stored in a retrieval system of any nature, or transmitted in any form or by any means (electronic, mechanical, photocopying, recording or otherwise) without prior written permission of the author, or when appropriate, by the publisher of the publications.

Plaque stabilizing and destabilizing effects in atherosclerosis

The role of microvessels,
macrophage metabolism and fibroblasts

DISSERTATION

To obtain the degree of Doctor at Maastricht University, on the authority of the
Rector Magnificus, Prof. dr. Pamela Habibović,
in accordance with the decision of the Board of Deans, to be defended in public
on

Friday, February 2nd 2024, at 10:00 hours

by

Renée Jozefien Hubertus Antoinette Tillie

Supervisors

Prof. dr. Judith C. Sluimer

Prof. dr. Erik A.L. Biessen

Assessment committee

Prof. dr. Rory Koenen (chair)

Prof. dr. Elizabeth Jones

Dr. Jeffrey Kroon (Amsterdam University Medical Center, University of Amsterdam)

Dr. Annette Neele (Amsterdam University Medical Center, University of Amsterdam)

Prof. dr. Casper Schalkwijk



Financial support by the Dutch Heart Foundation for the publication of this thesis is gratefully acknowledged. The research described in this thesis was supported by a grant from the Dutch Heart Foundation (DHF 2016T060).

Table of contents

Chapter 1	General introduction and outline of this thesis	7
Chapter 2	A switch from cell-associated to soluble PDGF-B protects against atherosclerosis, despite driving extramedullary hematopoiesis	29
Chapter 3	Partial inhibition of the 6-phosphofructo-2-kinase/fructose-2,6-bisphosphatase-3 (PFKFB3) enzyme in myeloid cells does not affect atherosclerosis	71
Chapter 4	Myeloid PFKFB3 knockdown exacerbates diet-induced MAFLD through stimulation of myeloid cell proliferation and hepatic steatosis	101
Chapter 5	Fibroblasts in atherosclerosis: abundant, heterogeneous and plastic participants	163
Chapter 6	Human and murine fibroblast single-cell transcriptomics reveals fibroblast clusters are differentially affected by ageing and serum cholesterol	177
Chapter 7	Identification of a pan-fibroblast marker and fibroblast subsets in atherosclerosis	241
Chapter 8	General discussion	281
Chapter 9	Summary Samenvatting	313
Chapter 10	Impact	323
Addendum	List of abbreviations	333
	Acknowledgements Dankwoord	343
	Curriculum vitae	353

Chapter 1

General introduction and outline of this thesis

Cardiovascular disease

Cardiovascular disease (CVD) continues to be the leading cause of mortality and morbidity in Europe, posing significant challenges to public health systems and individuals alike¹. CVD encompasses a spectrum of disorders that affect heart and/or blood vessels. Mortality estimates indicate that between 2007 and 2017, the number of deaths attributable to CVD increased with 21.1% to 17.8 million globally². Coronary artery disease and ischaemic stroke accounted for 50% and 15% of CVD deaths, respectively². Both coronary artery disease and ischaemic stroke are major clinical manifestations of atherosclerosis, a progressive condition characterized by the accumulation of fatty deposits, also called plaques, inside large and medium-sized arteries^{3,4}. This emphasizes the importance of understanding the mechanisms underlying atherosclerosis development.

In the sections below, the anatomical structure, cell types and functions of the different layers in the healthy vasculature are addressed, with an emphasis on fibroblasts. Thereafter, the pathogenesis of and risk factors for atherosclerosis, and the different cell types that contribute to disease progression, are discussed.

The healthy arterial wall

To understand and study atherosclerosis development, it is essential to first understand the general structure of the healthy vasculature, including resident cell types and their functions. The healthy arterial wall consists of three main layers: the innermost tunica intima, the middle tunica media, and the outermost tunica adventitia. The intima consists of an endothelial cell (EC) monolayer which lines the vascular lumen, and is supported by a basal lamina⁵. In addition to forming a semipermeable barrier between blood and the arterial wall, the intima plays an important role in controlling vascular tone and maintains homeostasis through regulation of inflammatory responses and coagulation⁶⁻⁸. The intima and media are separated by the internal elastic lamina, a layer of elastic fibers⁹. The media is comprised of circumferentially arranged vascular smooth muscle cells (VSMCs), embedded in a well-organized extracellular matrix (ECM), consisting of elastin and collagen, amongst others¹⁰. The medial layer provides support and elasticity to the blood vessel and is responsible for vasoconstriction and vasodilation, thereby regulating blood flow and blood pressure¹¹. The medial and adventitial layer are separated by the external elastic lamina. Lastly, the adventitia contains small blood vessels that supply the arterial wall (vasa vasorum), and a variety of cell types such as fibroblasts, leukocytes and autonomic nerve cells, next to ECM¹². Traditionally, the tunica adventitia is known to provide support and protection to the artery, and to anchor it to surrounding tissues¹⁰. In addition, it has become increasingly recognized that resident adventitial cells such as fibroblasts and leukocytes are often the first to respond to inflammatory and environmental stresses through stimulation of cell proliferation and the production of ECM, cytokines, chemokines and angiogenic and growth factors. Thereby, the

adventitia is thought to communicate with and influence other resident vascular cell types and the tissue environment, and to modulate inflammatory responses¹²⁻¹⁴.

Fibroblasts in the healthy arterial wall

Fibroblasts are the most abundant cell type in the arterial adventitial layer. Using single-cell RNA-sequencing (scRNA-seq), Kalluri et al. showed that fibroblasts account for 33% of all cells in healthy whole mouse aorta¹⁵. The production of ECM components is the most well-known function of fibroblasts^{16, 17}. However, functions in inflammation, angiogenesis, and wound healing after injury have also been reported^{17, 18}. Indeed, heterogeneity in fibroblast transcriptome and function is observed within and across several organs, in both healthy and disease states¹⁹⁻²³. Fibroblast heterogeneity entails that fibroblast subtypes arise through changes in cellular functions and transcriptome in response to the microenvironment, without altering fibroblast cell identity²⁴. Additionally, fibroblasts are also highly plastic cells, which means that they are capable of adapting their cellular identity upon changes in the microenvironment²⁴. This is demonstrated by their ability to differentiate into osteoblastogenic, chondrogenic, and adipogenic lineages *in vitro*²⁵. Unfortunately, the heterogeneity and plasticity of fibroblasts makes it difficult to define these cells *in vivo*. As a consequence, currently used fibroblast markers lack specificity and sensitivity, complicating further exploration of fibroblast subsets in healthy and diseased vasculature^{21, 23, 26}. The rise of single-cell RNA-sequencing poses a crucial tool to address these issues.

Several groups have also suggested the presence of a heterogeneous population of resident progenitor cells in the adventitial layer, characterized by expression of stem cell antigen-1 (Sca-1, encoded by the *Ly6a* gene, lymphocyte antigen 6 family member A, in mice), but also cluster of differentiation (CD)34, stem cell factor receptor (c-Kit) and/or GLI family zinc finger 1 (Gli1)²⁷. This progenitor population is proposed to maintain mesenchymal and immune populations in the healthy vessel. The potential of adventitial Sca-1+ cells to differentiate into cells that express markers specific to SMCs, macrophages or ECs was reported by several groups²⁸⁻³². However, the identity of these progenitor cells is a subject of discussion as adventitial fibroblasts are also known to express the stemness-associated genes *Ly6a* and *Cd34*^{23, 33, 34}, supporting the plasticity and progenitor-like phenotype of these cells. Indeed, Tang et al. showed expression of fibroblast marker platelet-derived growth factor receptor alpha (PDGFR α) in 40% of lineage-traced Sca-1+ cells in healthy femoral arteries³⁵. Moreover, in healthy human and mouse arteries, cells were annotated as fibroblast or mesenchymal populations, not progenitor or stem cell populations^{15, 36}. These observations indicate striking overlap between (subsets of) the Sca-1+ progenitor, previously studied by many groups, and the fibroblast populations in the arterial adventitia.

The atherosclerotic arterial wall

The behavior of cell types in the arterial wall is significantly altered in atherosclerosis. Atherosclerosis is a chronic, inflammatory, and progressive condition that is typified by the intimal accumulation of lipids, leukocytes, cell debris and fibrous tissue in large and medium-sized arteries. This so-called plaque results in narrowing of the arterial lumen. Clinical complications are mainly caused by erosion or rupture of the plaque, which results in the formation of a thrombus and ensuing blood flow restriction to vital organs, such as the heart or brain³⁷. Broadly, pathogenesis of atherosclerosis is characterized by endothelium dysfunction, lipid retention, accumulation of leukocytes, foam cell formation and intimal fibrosis in the subendothelial space. Mesenchymal cells migrate into the plaque and form a protective fibrous cap by producing ECM components. In later stages, apoptosis of ECM-forming cap cells and thinning of this fibrous cap render the plaque unstable and prone to rupture³⁷. Additionally, advanced stages of atherosclerosis are accompanied by plaque neovascularization and intraplaque hemorrhage, which are also associated with plaque instability³⁸. Importantly, the atherosclerotic environment stimulates changes of cellular characteristics, yielding different cellular subtypes (heterogeneity) or even complete changes in cellular identity (plasticity)²⁴. In the sections below, we will describe the prominent cell types and associated disease processes, plasticity, and heterogeneity in atherogenesis in more detail, with an emphasis on macrophages and fibroblasts.

Endothelial cells in atherosclerosis

Initiation of atherosclerosis development is marked by chronic activation of intimal ECs and increased transendothelial permeability to lipoproteins in response to disturbed blood flow patterns, pro-inflammatory mediators or other aggravating stimuli related to CVD risk factors^{37, 39}. Important risk factors of atherosclerosis include hyperlipidemia, hypertension, smoking, stress and physical inactivity⁴⁰. EC activation also promotes the expression of adhesion molecules, such as vascular cell adhesion molecule 1 (VCAM-1) and intercellular adhesion molecule 1 (ICAM-1), and the expression of secreted and membrane-associated chemokines and other cytokines^{41, 42}. This results in the capture, rolling, adherence and transmigration of circulating leukocytes into the subendothelial space⁴³.

ECs are involved in several other pathogenic events that contribute to atherosclerosis development. In advanced atherosclerosis, as a result of increased oxygen demand in the arterial wall, ECs also contribute to neovascularization of the plaque. This occurs through angiogenesis, which involves the formation of new microvessels, mainly from the vasa vasorum, by EC proliferation, migration and tube formation in response to pro-angiogenic mediators, such as vascular endothelial growth factor (VEGF)^{38, 44, 45}. An intact microvessel consists of an EC layer, interconnected by junctional molecules, embedded in a basement membrane, covered by mural cells^{38, 46}. Platelet derived growth factor B (PDGF-B), which is

secreted by sprouting endothelial cells, is an important mediator of pericyte recruitment towards microvessel walls through its retention in the ECM⁴⁷. However, neomicrovessels in advanced plaque are often fragile and present with reduced structural integrity⁴⁸, making them an important source of intraplaque hemorrhage, the leakage of blood components into the plaque. Thereby, angiogenesis and subsequent intraplaque hemorrhage are thought to further stimulate plaque progression and instability by providing an entry point for leukocytes and erythrocytes, fueling the inflammatory response and lipid accumulation^{38, 49}. However, causality between intraplaque hemorrhage and plaque instability remains to be demonstrated.

Next to plaque neovascularization, ECs contribute to the pool of mesenchymal cells (e.g. fibroblasts, VSMCs) in the atherosclerotic plaque, through a process called endothelial-to-mesenchymal transition (EndMT)⁵⁰. This entails that ECs gradually lose EC identity and expression of EC markers such as vascular endothelial-cadherin (VE-cadherin) and CD31, and gain mesenchymal markers such as alpha smooth muscle actin (α SMA), smoothelin and vimentin⁵⁰. EndMT is reported to occur in both human and mouse atherosclerotic plaques⁵¹. Evrard et al. previously showed that 32.5% and 45.5% of cells that expressed mesenchymal markers, was of EC origin in apolipoprotein E knockout (*ApoE*^{-/-}) mice after 8 and 30 weeks of high fat diet, respectively⁵¹. EndMT is likely driven by disturbed blood flow, transforming growth factor beta (TGF- β) signaling, inflammatory cytokines, hypoxia, and oxidative stress, amongst others⁵¹⁻⁵⁴. Importantly, EndMT is associated with decreased fibrous cap thickness and plaque stability, possibly related to increased inflammatory signatures and increased production of matrix metalloproteinases (MMPs)^{51, 52}.

Leukocytes in atherosclerosis

Circulating monocytes constitute the main leukocyte type that is recruited in response to EC activation during initiation of atherosclerosis. In mice, monocyte subsets are categorized based on the expression of lymphocyte antigen 6C (Ly6C) on the plasma membrane⁵⁵. As such, Ly6C^{low} (non-classical), Ly6C^{intermediate} and Ly6C^{high} (classical) monocytes can be distinguished. It is recognized that the Ly6C^{high} classical monocytes readily extravasate into the subendothelial space and stimulate murine plaque progression, whereas Ly6C^{low} non-classical monocytes are thought to patrol the luminal side of the endothelial wall and secrete cytokines⁵⁶⁻⁵⁸. In humans, monocyte classification is different, as subpopulations are currently categorized based on surface marker expression of CD14 and CD16: CD14⁺⁺CD16⁻ (classical), CD14⁺⁺CD16⁺ (intermediate) and CD14⁺CD16⁺⁺ (non-classical) monocytes⁵⁵. Both classical and intermediate monocytes have been found to correlate with cardiovascular events and plaque characteristics, albeit not consistently. Recent scRNA-seq studies have reported more profound heterogeneity of human monocytes than previously assumed, as reviewed in⁵⁵.

Recruited monocytes that infiltrate the subendothelial space, differentiate into macrophages. Simultaneously, lipoproteins that accumulate in the intima as a result of EC activation, become aggregated or modified by oxidation and other mechanisms^{43, 59}. This triggers the macrophages to engulf these lipoproteins, turning them into lipid-laden foam cells^{43, 59}. The appearance of foam cells marks the first stage of atherosclerosis development, known as intimal xanthoma or fatty streaks⁶⁰. This stage is followed by pathological intimal thickening, in which accumulation of extracellular lipid and foam cells is observed in the intimal layer⁶⁰. Foam cell formation goes hand in hand with increased secretion of pro-inflammatory cytokines, thereby further exacerbating the inflammatory response, attracting more leukocytes and completing the vicious cycle⁴³. Moreover, excessive uptake of lipoproteins by macrophages results in endoplasmic reticulum stress and ultimately, apoptotic cell death. In early stages of atherosclerosis, these dead and dying cells are efficiently cleared by other macrophages through efferocytosis, decreasing inflammation and plaque cellularity^{43, 59}. However, in more advanced stages of atherosclerosis, further dysregulation of lipid metabolism impairs efferocytosis. This induces progression to secondary necrosis, release of intracellular lipid contents and the formation of a lipid-rich necrotic core, which promotes plaque instability^{43, 61}. This stage, characterized by the presence of a necrotic core, is referred to as early fibroatheroma⁶⁰.

Traditionally, macrophages were categorized into pro-inflammatory M1 macrophages or anti-inflammatory, pro-resolving M2 macrophages. However, recent studies have uncovered that this M1/M2 categorization is an oversimplification, as macrophages exist on an extensive functional and phenotypic continuum and adjust their functionality in response to the microenvironment⁶². Using scRNA-seq, the existence of four different macrophage subsets were confirmed in both mouse and human atherosclerotic arteries: triggering receptor expressed on myeloid cells 2 (*TREM2*)+ foamy, tumor necrosis factor (*TNF*)+ interleukin-1 beta (*IL1B*)+ inflammatory, lymphatic vessel endothelial hyaluronan receptor 1 (*LYVE1*)+ resident and interferon-stimulated gene 15 (*ISG15*)+ interferon-inducible macrophages^{63, 64}. The exact functions of these subsets and their contributions to atherosclerosis remain to be explored further, which will be crucial to allow specific macrophage targeting and new therapeutic opportunities to prevent atherosclerosis progression.

Next to macrophages, other leukocyte subsets were also seen to contribute to plaque initiation and progression. Neutrophils are activated and recruited through chemokine secretion by activated ECs and platelets⁶⁵. Activated neutrophils are thought to aggravate the inflammatory response by secreting granule proteins that further stimulate EC activation and permeability, monocyte recruitment and pro-inflammatory macrophage activation^{65, 66}. Neutrophil-derived myeloperoxidase stimulates oxidation of lipoproteins, encouraging the formation of foam cells^{65, 67}. Additionally, neutrophil extracellular traps (NETs) are presumed

to contribute to plaque erosion^{65, 68}. A subpopulation of foam cells in the atherosclerotic plaque seems derived from dendritic cells (DCs). Depletion of CD11c+ DCs previously reduced intimal lipid content in nascent plaques, thereby indicating a role for DCs in atherosclerosis initiation^{69, 70}. However, although controversial, lipid loading has shown to render DC functionality largely unaffected⁷¹. Importantly, DCs regulate T cell recruitment to the inflamed artery site and modulate T cell responses⁷². Indeed, the adaptive immune system also comes into play during atherosclerosis, although for many T cell subsets it remains controversial whether they exert pro- or anti-atherogenic effects⁷³. Both CD4+ T helper 1 cells and natural killer T cells are thought to aggravate atherosclerosis by secreting pro-inflammatory cytokines such as interferon gamma (IFN- γ) and TNF^{73, 74}. In contrast, regulatory T cells are negatively correlated with vulnerable coronary artery plaques⁷⁵. B cells produce both pro- and anti-atherogenic cytokines^{76, 77}. Moreover, the various B cell-secreted immunoglobulin (Ig) isotypes have divergent effects on atherosclerosis progression. IgM natural antibodies have limiting effects of oxidized low-density lipoprotein (LDL) on foam cell formation and EC activation on one hand, and plasma cell-derived IgG and IgE promote macrophage inflammation on the other hand, the latter in part by activating macrophages and mast cells⁷⁸. Activation of mast cells results in their degranulation, resulting in the release of proteases, cytokines, heparin, histamine and other pro-inflammatory mediators from their cytoplasmic granules. These mediators are thought to further stimulate leukocyte recruitment, vascular permeability, foam cell formation, macrophage, EC and SMC apoptosis, MMP activation and angiogenesis, thereby contributing to atherosclerosis progression and destabilization⁷⁹⁻⁸².

It is apparent that atherosclerosis is driven by maladaptive immune and unresolved inflammatory responses. Interestingly, an increased number of studies into immunometabolism has emerged, which focuses on the metabolic adaptations that occur in leukocytes to support their function. Pro-inflammatory macrophages and T cells, both driving forces behind atherosclerosis progression, present with enhanced glycolysis, fatty acid synthesis and pentose phosphate pathway (PPP)⁸³. In contrast, anti-inflammatory, pro-resolving macrophages and T cells exhibit increased rates of oxidative phosphorylation and fatty acid oxidation⁸³. Indeed, high-risk plaques from symptomatic patients were characterized by increased glycolysis, which was associated with plaque inflammation⁸⁴. Additionally, circulating monocytes from patients with coronary artery disease also showed increased inflammatory signaling, accompanied by increased glucose uptake and glycolytic rate⁸⁵. Glucose deprivation, incubation with glycolysis inhibitors or genetic inhibition of glycolytic enzymes such as 6-phosphofructo-2-kinase/fructose-2,6-bisphosphatase 3 (PFKFB3) have all shown to decrease macrophage pro-inflammatory signaling *in vitro*^{85, 86}. Naturally, metabolic pathways are a source of energy and biosynthetic products, prerequisites for inflammatory cells to exert their immune functions. However, several metabolic enzymes and intermediates, such as hexokinase, glyceraldehyde-3-phosphate dehydrogenase and

succinate, also serve as effectors, directly regulating immune cell functions^{83, 87}. These new insights into the relationship between metabolism and immune cell functions open up new avenues for manipulation of immunometabolism in future atherosclerosis research.

Smooth muscle cells in atherosclerosis

VSMCs and VSMC-derived cells in the plaque derive through proliferation and migration of medial VSMCs in response to growth factors, such as PDGF-B, secreted by activated ECs and macrophages⁸⁸. Recent reports using multicolor lineage reporters indicate that this occurs through clonal expansion of a small group of VSMCs in the medial layer^{89, 90}. In humans, plaque VSMCs may also arise from pre-existing intimal VSMCs, which may be present as a result of intimal thickening, a common and natural accumulation of SMCs in the intima^{60, 88}. In early stages of atherosclerosis, similar to macrophages, VSMCs take up (modified) lipoproteins, leading to foam cell formation and apoptosis⁸⁸. Moreover, lineage-tracing studies have shown phenotypic switching of VSMC to macrophage-like cells in both murine and human atherosclerosis^{91, 92}. This phenotypic switching is accompanied by gaining macrophage functions such as phagocytosis^{92, 93}.

In later stages of atherosclerosis, apoptosis and subsequent secondary necrosis of VSMCs and VSMC-derived cells, as a result of build-up of DNA damage, upregulation of pro-apoptotic genes and defective efferocytosis in the plaque, also contribute to formation of the necrotic core^{88, 94-97}. Additionally, in an attempt to heal, phenotypic switching of VSMCs to synthetic VSMCs occurs, which show decreased expression of contractile proteins and increased expression of ECM components and pro-inflammatory cytokines⁸⁸. These synthetic VSMCs stabilize the plaque through the formation of a protective fibrous cap⁸⁸. This stage, characterized by the presence of a necrotic core with a thick overlying fibrous cap, is called late fibroatheroma⁶⁰. Indeed, a recent scRNA-seq study found evidence of VSMC transitioning to an intermediate cell state, called SEM cells (stem cell, endothelial cell, monocyte/macrophage), characterized by expression of *Ly6a*⁹⁸. This SMC-derived intermediate cell type was shown to be a precursor for both macrophage-like cells and fibrochondrocyte-like cells, the latter characterized by increased expression of ECM genes⁹⁸. Apoptosis of synthetic VSMCs and degradation of the fibrous cap by MMPs, mostly produced by VSMCs and macrophages, causes thinning and destabilization of the cap^{88, 99}. This vulnerable plaque is referred to as thin-cap fibroatheroma⁶⁰. Neutrophils also contribute to SMC apoptosis, and thereby to plaque destabilization, through the secretion of NETs¹⁰⁰.

Fibroblasts in atherosclerosis

Next to ECs, leukocytes and VSMCs, the involvement of fibroblasts in atherosclerosis has recently gained attention. Fibroblast presence and heterogeneity in atherosclerosis has become apparent as recent scRNA-seq studies reported two to four fibroblast populations in human and murine atherosclerotic arteries^{98, 101, 102}. In arterial injury, adventitial fibroblasts have been reported to differentiate into myofibroblasts¹⁰³. Myofibroblasts are characterized by acquired expression of α SMA, which is thus not a specific VSMC marker. Additionally, myofibroblasts have been associated with cytokine and matrix metalloproteinase secretion and production of ECM¹⁰⁴. Thus, (myo)fibroblasts could play an important role in (de)stabilization of the atherosclerotic plaque. However, as described previously, fibroblasts are plastic and heterogeneous cells that can change cellular characteristics or identity in response to microenvironmental stimuli. Therefore, exact fibroblast function in atherosclerosis, which is plagued by chronic inflammation, necrosis and altered identity and function of other vascular cells, is currently still unknown. This goes hand in hand with the lack of known specific fibroblast markers in both healthy and atherosclerotic tissue. Next to fibroblast markers and function, origin and fate of plaque fibroblasts remains to be elucidated. Plaque fibroblasts could migrate from the adventitial layer and/or differentiate from ECs, through EndMT⁵¹ as described above, or from SMCs. Indeed, Wirka et al. identified a contractile SMC-derived fibromyocyte population, displaying a fibroblast-like phenotype, although still being transcriptionally different from fibroblast populations¹⁰². Moreover, considering their highly plastic nature, it is likely that fibroblasts contribute to plaque progression by differentiation into other cell types, too. After severe femoral artery injury, Sca-1+PDGFR α + adventitial cells were shown to have the capacity to generate medial SMC-like cells, positive for calponin 1 (CNN1)³⁵. Moreover, Sca-1+ adventitial cells are capable of differentiation to EC-like cells, expressing VE-cadherin and other EC genes¹⁰⁵. Further details on what is known thus far regarding fibroblast presence, heterogeneity, origin and plasticity in health and atherosclerosis can be found in the corresponding review in **chapter 5**. However, it is clear that crucial knowledge on fibroblasts is still lacking. Exploring markers, functions, origin, and fate of fibroblasts in atherosclerosis will be pivotal to fuel the development of therapeutic interventions that can be used to mitigate devastating consequences of atherosclerosis.

In summary, atherosclerosis is a life-long process characterized by the presence of a plethora of plaque stabilizing and -destabilizing cell (sub)types, cellular functions and processes. Moreover, it is clear that atherosclerosis is a significant inducer of cell plasticity and heterogeneity. The complexity of this progressive disease does allow a broad range of leverage points for studying atherosclerosis interventions. A causal role between some atherosclerotic processes, such as intraplaque neovascularization and microvessel leakage, and plaque destabilization remains to be confirmed. Moreover, interventions in key cell types

in atherosclerosis initiation and progression, such as pro-inflammatory macrophages, may prevent or slow down disease progression. Lastly, a new player in atherosclerosis, the fibroblast, and corresponding heterogeneity and functions, remains to be explored. These studies may yield important opportunities for future therapeutic targets in human atherosclerosis.

Aim of this thesis

The general aim of this thesis is to further unravel the role of microvessels, macrophage metabolism and fibroblasts in atherosclerotic plaque (de)stabilization. Specifically, I hypothesized that:

1. Microvascular pericyte loss and subsequent microvascular permeability through deletion of the PDGF-B retention motif results in exacerbated atherosclerosis (**chapter 2**)
2. Decreased pro-inflammatory activation of macrophages through partial inhibition of glycolysis alleviates inflammation in atherosclerosis (**chapter 3**) and diet-induced fatty liver disease (**chapter 4**)
3. The healthy adventitia contains a heterogeneous fibroblast population with divergent functions, differentially regulated by cardiovascular disease risk factors (**chapter 6**)
4. The atherosclerotic plaque contains a heterogeneous fibroblast population with predicted functions in atherosclerosis (**chapter 7**)

Outline of this thesis

Key events in the initiation, progression and escalation of atherosclerosis include lipid accumulation, recruitment of pro-inflammatory macrophages and other leukocytes, foam cell formation and apoptosis, production and thinning of the fibrous cap, and neovascularization of the plaque. As causality between neovascularization, subsequent microvessel hemorrhage, and plaque instability remains to be demonstrated, in **chapter 2**, I explored the effects of microvessel permeability on murine plaque stability. To this end, microvascular pericyte loss was modeled by deletion of the PDGF-B retention motif in low-density lipoprotein receptor knockout (*Ldlr*^{-/-}) mice on a high cholesterol diet¹⁰⁶.

Intervention in one of the aforementioned key processes might pose interesting opportunities to prevent or slow down progression of atherosclerosis. We first focused on pro-inflammatory macrophages, as key drivers of the chronic inflammatory environment in the atherosclerotic plaque, and important contributors to foam cell and necrotic core formation, and fibrous cap thinning. Pro-inflammatory macrophages are dependent on glycolysis for their energy supply and functioning. Silencing of glycolytic enzyme PFKFB3 in macrophages previously reduced both glycolytic rate and pro-inflammatory activation *in vitro*⁸⁶. Therefore, I explored the effects of knockout of myeloid-specific PFKFB3 on murine atherosclerosis, in *Ldlr*^{-/-} mice on a high cholesterol diet, in **chapter 3**. This yielded unforeseen effects on the liver, as it exacerbated fatty liver disease, described in **chapter 4**.

Thereafter, the focus will shift to fibroblasts, as much is still unknown about this cell type in both the healthy and atherosclerotic vasculature. In a review in **chapter 5**, I will provide an in-

depth discussion on what is known thus far about the origin, presence, heterogeneity, and plasticity of fibroblasts in the healthy and atherosclerotic vasculature. In **chapter 6** and **chapter 7**, we performed extensive scRNA-seq transcriptomics to identify pan- and subset-specific fibroblast markers, and explore fibroblast heterogeneity in the healthy aortic adventitia and atherosclerotic aorta, and possible functions of identified subsets.

Lastly, a general discussion of the key findings in this thesis can be found in **chapter 8**.

References

1. Townsend N, Kazakiewicz D, Lucy Wright F, Timmis A, Huculeci R, Torbica A, et al. Epidemiology of cardiovascular disease in Europe. *Nature Reviews Cardiology*. 2022;19(2):133-43.
2. Roth GA, Abate D, Abate KH, Abay SM, Abbafati C, Abbasi N, et al. Global, regional, and national age-sex-specific mortality for 282 causes of death in 195 countries and territories, 1980–2017: a systematic analysis for the Global Burden of Disease Study 2017. *The Lancet*. 2018;392(10159):1736-88.
3. Herrington W, Lacey B, Sherliker P, Armitage J, Lewington S. Epidemiology of Atherosclerosis and the Potential to Reduce the Global Burden of Atherothrombotic Disease. *Circulation Research*. 2016;118(4):535-46.
4. Falk E. Pathogenesis of Atherosclerosis. *Journal of the American College of Cardiology*. 2006;47(8, Supplement):C7-C12.
5. Taylor A, Bordoni B. Histology, Blood Vascular System. *Statpearls*. 2023.
6. Krüger-Genge A, Blocki A, Franke RP, Jung F. Vascular Endothelial Cell Biology: An Update. *Int J Mol Sci*. 2019;20(18).
7. Cahill PA, Redmond EM. Vascular endothelium - Gatekeeper of vessel health. *Atherosclerosis*. 2016;248:97-109.
8. Ricard N, Bailly S, Guignabert C, Simons M. The quiescent endothelium: signalling pathways regulating organ-specific endothelial normalcy. *Nature Reviews Cardiology*. 2021;18(8):565-80.
9. Del Monte-Nieto G, Fischer JW, Gorski DJ, Harvey RP, Kovacic JC. Basic Biology of Extracellular Matrix in the Cardiovascular System, Part 1/4: JACC Focus Seminar. *J Am Coll Cardiol*. 2020;75(17):2169-88.
10. Dave JM, Saito J, Mottola G, Greif DM. Chapter 8 - Out to the tissues: the arterial side (arteries, arterioles—development, structure, functions, and pathologies). In: Galis ZS, editor. *The Vasculome*: Academic Press; 2022. p. 89-98.
11. Brozovich FV, Nicholson CJ, Degen CV, Gao YZ, Aggarwal M, Morgan KG. Mechanisms of Vascular Smooth Muscle Contraction and the Basis for Pharmacologic Treatment of Smooth Muscle Disorders. *Pharmacol Rev*. 2016;68(2):476-532.
12. Majesky MW, Dong XR, Høglund V, Mahoney WM, Jr., Daum G. The adventitia: a dynamic interface containing resident progenitor cells. *Arterioscler Thromb Vasc Biol*. 2011;31(7):1530-9.
13. Stenmark KR, Yeager ME, El Kasmi KC, Nozik-Grayck E, Gerasimovskaya EV, Li M, et al. The adventitia: essential regulator of vascular wall structure and function. *Annu Rev Physiol*. 2013;75:23-47.
14. Mohanta SK, Peng L, Li Y, Lu S, Sun T, Carnevale L, et al. Neuroimmune cardiovascular interfaces control atherosclerosis. *Nature*. 2022;605(7908):152-9.
15. Kalluri AS, Vellarikkal SK, Edelman ER, Nguyen L, Subramanian A, Ellinor PT, et al. Single-Cell Analysis of the Normal Mouse Aorta Reveals Functionally Distinct Endothelial Cell Populations. *Circulation*. 2019;140(2):147-63.
16. Malakpour-Permlid A, Buzzi I, Hegardt C, Johansson F, Oredsson S. Identification of extracellular matrix proteins secreted by human dermal fibroblasts cultured in 3D electrospun scaffolds. *Scientific Reports*. 2021;11(1):6655.

17. Kendall RT, Feghali-Bostwick CA. Fibroblasts in fibrosis: novel roles and mediators. *Frontiers in Pharmacology*. 2014;5.
18. Tieu BC, Ju X, Lee C, Sun H, Lejeune W, Recinos A, 3rd, et al. Aortic adventitial fibroblasts participate in angiotensin-induced vascular wall inflammation and remodeling. *J Vasc Res*. 2011;48(3):261-72.
19. Muhl L, Genové G, Leptidis S, Liu J, He L, Mocci G, et al. Single-cell analysis uncovers fibroblast heterogeneity and criteria for fibroblast and mural cell identification and discrimination. *Nature Communications*. 2020;11(1):3953.
20. Xie T, Wang Y, Deng N, Huang G, Taghavifar F, Geng Y, et al. Single-Cell Deconvolution of Fibroblast Heterogeneity in Mouse Pulmonary Fibrosis. *Cell Rep*. 2018;22(13):3625-40.
21. Stenmark KR, Davie N, Frid M, Gerasimovskaya E, Das M. Role of the adventitia in pulmonary vascular remodeling. *Physiology (Bethesda)*. 2006;21:134-45.
22. Sorrell JM, Caplan AI. Fibroblast heterogeneity: more than skin deep. *Journal of Cell Science*. 2004;117(5):667-75.
23. Kuwabara JT, Tallquist MD. Tracking Adventitial Fibroblast Contribution to Disease: A Review of Current Methods to Identify Resident Fibroblasts. *Arterioscler Thromb Vasc Biol*. 2017;37(9):1598-607.
24. van Kuijk K, Kuppe C, Betsholtz C, Vanlandewijck M, Kramann R, Sluimer JC. Heterogeneity and plasticity in healthy and atherosclerotic vasculature explored by single-cell sequencing. *Cardiovasc Res*. 2019;115(12):1705-15.
25. Soundararajan M, Kannan S. Fibroblasts and mesenchymal stem cells: Two sides of the same coin? *Journal of Cellular Physiology*. 2018;233(12):9099-109.
26. Tillie R, van Kuijk K, Sluimer JC. Fibroblasts in atherosclerosis: heterogeneous and plastic participants. *Curr Opin Lipidol*. 2020;31(5):273-8.
27. Jolly AJ, Lu S, Strand KA, Dubner AM, Mutryn MF, Nemenoff RA, et al. Heterogeneous subpopulations of adventitial progenitor cells regulate vascular homeostasis and pathological vascular remodelling. *Cardiovasc Res*. 2022;118(6):1452-65.
28. Hu Y, Zhang Z, Torsney E, Afzal AR, Davison F, Metzler B, et al. Abundant progenitor cells in the adventitia contribute to atherosclerosis of vein grafts in ApoE-deficient mice. *J Clin Invest*. 2004;113(9):1258-65.
29. Majesky MW, Horita H, Ostriker A, Lu S, Regan JN, Bagchi A, et al. Differentiated Smooth Muscle Cells Generate a Subpopulation of Resident Vascular Progenitor Cells in the Adventitia Regulated by Klf4. *Circ Res*. 2017;120(2):296-311.
30. Passman JN, Dong XR, Wu SP, Maguire CT, Hogan KA, Bautch VL, et al. A sonic hedgehog signaling domain in the arterial adventitia supports resident Sca1+ smooth muscle progenitor cells. *Proc Natl Acad Sci U S A*. 2008;105(27):9349-54.
31. Campagnolo P, Hong X, di Bernardini E, Smyrniak I, Hu Y, Xu Q. Resveratrol-Induced Vascular Progenitor Differentiation towards Endothelial Lineage via MiR-21/Akt/ β -Catenin Is Protective in Vessel Graft Models. *PLoS One*. 2015;10(5):e0125122.
32. Torsney E, Hu Y, Xu Q. Adventitial Progenitor Cells Contribute to Arteriosclerosis. *Trends in Cardiovascular Medicine*. 2005;15(2):64-8.
33. Buechler MB, Pradhan RN, Krishnamurthy AT, Cox C, Calviello AK, Wang AW, et al. Cross-tissue organization of the fibroblast lineage. *Nature*. 2021;593(7860):575-9.

34. Gu W, Ni Z, Tan Y-Q, Deng J, Zhang S-J, Lv Z-C, et al. Adventitial Cell Atlas of wt (Wild Type) and ApoE (Apolipoprotein E)-Deficient Mice Defined by Single-Cell RNA Sequencing. *Arteriosclerosis, Thrombosis, and Vascular Biology*. 2019;39(6):1055-71.
35. Tang J, Wang H, Huang X, Li F, Zhu H, Li Y, et al. Arterial Sca1(+) Vascular Stem Cells Generate De Novo Smooth Muscle for Artery Repair and Regeneration. *Cell Stem Cell*. 2020;26(1):81-96.e4.
36. Hu Z, Liu W, Hua X, Chen X, Chang Y, Hu Y, et al. Single-Cell Transcriptomic Atlas of Different Human Cardiac Arteries Identifies Cell Types Associated With Vascular Physiology. *Arteriosclerosis, Thrombosis, and Vascular Biology*. 2021;41(4):1408-27.
37. Libby P, Buring JE, Badimon L, Hansson GK, Deanfield J, Bittencourt MS, et al. Atherosclerosis. *Nat Rev Dis Primers*. 2019;5(1):56.
38. Parma L, Baganha F, Quax PHA, de Vries MR. Plaque angiogenesis and intraplaque hemorrhage in atherosclerosis. *European Journal of Pharmacology*. 2017;816:107-15.
39. Mundi S, Massaro M, Scoditti E, Carluccio MA, van Hinsbergh VWM, Iruela-Arispe ML, et al. Endothelial permeability, LDL deposition, and cardiovascular risk factors-a review. *Cardiovasc Res*. 2018;114(1):35-52.
40. von Scheidt M, Zhao Y, Kurt Z, Pan C, Zeng L, Yang X, et al. Applications and Limitations of Mouse Models for Understanding Human Atherosclerosis. *Cell Metab*. 2017;25(2):248-61.
41. Bourdillon M-C, Poston RN, Covacho C, Chignier E, Bricca G, McGregor JL. ICAM-1 Deficiency Reduces Atherosclerotic Lesions in Double-Knockout Mice (ApoE^{-/-}/ICAM-1^{-/-}) Fed a Fat or a Chow Diet. *Arteriosclerosis, Thrombosis, and Vascular Biology*. 2000;20(12):2630-5.
42. Gimbrone MA, Jr., García-Cardeña G. Endothelial Cell Dysfunction and the Pathobiology of Atherosclerosis. *Circ Res*. 2016;118(4):620-36.
43. Moore KJ, Sheedy FJ, Fisher EA. Macrophages in atherosclerosis: a dynamic balance. *Nature Reviews Immunology*. 2013;13(10):709-21.
44. Moreno PR, Purushothaman K-R, Sirol M, Levy AP, Fuster V. Neovascularization in Human Atherosclerosis. *Circulation*. 2006;113(18):2245-52.
45. Sluimer JC, Daemen MJ. Novel concepts in atherogenesis: angiogenesis and hypoxia in atherosclerosis. *The Journal of Pathology*. 2009;218(1):7-29.
46. Carmeliet P, Jain RK. Molecular mechanisms and clinical applications of angiogenesis. *Nature*. 2011;473(7347):298-307.
47. Camaré C, Pucelle M, Nègre-Salvayre A, Salvayre R. Angiogenesis in the atherosclerotic plaque. *Redox Biol*. 2017;12:18-34.
48. Sluimer JC, Kolodgie FD, Bijnens APJJ, Maxfield K, Pacheco E, Kutys B, et al. Thin-Walled Microvessels in Human Coronary Atherosclerotic Plaques Show Incomplete Endothelial Junctions: Relevance of Compromised Structural Integrity for Intraplaque Microvascular Leakage. *Journal of the American College of Cardiology*. 2009;53(17):1517-27.
49. Jeney V, Balla G, Balla J. Red blood cell, hemoglobin and heme in the progression of atherosclerosis. *Front Physiol*. 2014;5:379.
50. Dejana E, Hirschi KK, Simons M. The molecular basis of endothelial cell plasticity. *Nature Communications*. 2017;8(1):14361.
51. Evrard SM, Lecce L, Michelis KC, Nomura-Kitabayashi A, Pandey G, Purushothaman KR, et al. Endothelial to mesenchymal transition is common in atherosclerotic lesions and is associated with plaque instability. *Nat Commun*. 2016;7:11853.

52. Chen P-Y, Qin L, Li G, Wang Z, Dahlman JE, Malagon-Lopez J, et al. Endothelial TGF- β signalling drives vascular inflammation and atherosclerosis. *Nature Metabolism*. 2019;1(9):912-26.
53. Alvandi Z, Bischoff J. Endothelial-Mesenchymal Transition in Cardiovascular Disease. *Arteriosclerosis, Thrombosis, and Vascular Biology*. 2021;41(9):2357-69.
54. Kovacic JC, Dimmeler S, Harvey RP, Finkel T, Aikawa E, Krenning G, et al. Endothelial to Mesenchymal Transition in Cardiovascular Disease: JACC State-of-the-Art Review. *J Am Coll Cardiol*. 2019;73(2):190-209.
55. Ruder AV, Wetzels SMW, Temmerman L, Biessen EAL, Goossens P. Monocyte heterogeneity in cardiovascular disease. *Cardiovascular Research*. 2023.
56. Hilgendorf I, Swirski FK, Robbins CS. Monocyte Fate in Atherosclerosis. *Arteriosclerosis, Thrombosis, and Vascular Biology*. 2015;35(2):272-9.
57. Gupta RM, Lee-Kim VS, Libby P. The March of Monocytes in Atherosclerosis. *Circulation Research*. 2020;126(10):1324-6.
58. Swirski FK, Libby P, Aikawa E, Alcaide P, Luscinskas FW, Weissleder R, et al. Ly-6Chi monocytes dominate hypercholesterolemia-associated monocytosis and give rise to macrophages in atheromata. *J Clin Invest*. 2007;117(1):195-205.
59. Moore Kathryn J, Tabas I. Macrophages in the Pathogenesis of Atherosclerosis. *Cell*. 2011;145(3):341-55.
60. Yahagi K, Kolodgie FD, Otsuka F, Finn AV, Davis HR, Joner M, et al. Pathophysiology of native coronary, vein graft, and in-stent atherosclerosis. *Nature Reviews Cardiology*. 2016;13(2):79-98.
61. Tabas I. Consequences and therapeutic implications of macrophage apoptosis in atherosclerosis: the importance of lesion stage and phagocytic efficiency. *Arterioscler Thromb Vasc Biol*. 2005;25(11):2255-64.
62. Barrett TJ. Macrophages in Atherosclerosis Regression. *Arterioscler Thromb Vasc Biol*. 2020;40(1):20-33.
63. Zernecke A, Winkels H, Cochain C, Williams JW, Wolf D, Soehnlein O, et al. Meta-Analysis of Leukocyte Diversity in Atherosclerotic Mouse Aortas. *Circ Res*. 2020;127(3):402-26.
64. Vallejo J, Cochain C, Zernecke A, Ley K. Heterogeneity of immune cells in human atherosclerosis revealed by scRNA-Seq. *Cardiovasc Res*. 2021;117(13):2537-43.
65. Silvestre-Roig C, Braster Q, Ortega-Gomez A, Soehnlein O. Neutrophils as regulators of cardiovascular inflammation. *Nature Reviews Cardiology*. 2020;17(6):327-40.
66. Soehnlein O, Lindbom L, Weber C. Mechanisms underlying neutrophil-mediated monocyte recruitment. *Blood*. 2009;114(21):4613-23.
67. Delporte C, Boudjeltia KZ, Noyon C, Furtmüller PG, Nuyens V, Slomianny MC, et al. Impact of myeloperoxidase-LDL interactions on enzyme activity and subsequent posttranslational oxidative modifications of apoB-100. *J Lipid Res*. 2014;55(4):747-57.
68. Franck G, Mawson TL, Folco EJ, Molinaro R, Ruvkun V, Engelbertsen D, et al. Roles of PAD4 and NETosis in Experimental Atherosclerosis and Arterial Injury: Implications for Superficial Erosion. *Circ Res*. 2018;123(1):33-42.
69. Paulson KE, Zhu SN, Chen M, Nurmohamed S, Jongstra-Bilen J, Cybulsky MI. Resident intimal dendritic cells accumulate lipid and contribute to the initiation of atherosclerosis. *Circ Res*. 2010;106(2):383-90.

70. Subramanian M, Tabas I. Dendritic cells in atherosclerosis. *Semin Immunopathol.* 2014;36(1):93-102.
71. Packard RR, Maganto-García E, Gotsman I, Tabas I, Libby P, Lichtman AH. CD11c(+) dendritic cells maintain antigen processing, presentation capabilities, and CD4(+) T-cell priming efficacy under hypercholesterolemic conditions associated with atherosclerosis. *Circ Res.* 2008;103(9):965-73.
72. Zernecke A. Dendritic Cells in Atherosclerosis. *Arteriosclerosis, Thrombosis, and Vascular Biology.* 2015;35(4):763-70.
73. Saigusa R, Winkels H, Ley K. T cell subsets and functions in atherosclerosis. *Nature Reviews Cardiology.* 2020;17(7):387-401.
74. Nakai Y, Iwabuchi K, Fujii S, Ishimori N, Dashtsoodol N, Watano K, et al. Natural killer T cells accelerate atherogenesis in mice. *Blood.* 2004;104(7):2051-9.
75. George J, Schwartzberg S, Medvedovsky D, Jonas M, Charach G, Afek A, et al. Regulatory T cells and IL-10 levels are reduced in patients with vulnerable coronary plaques. *Atherosclerosis.* 2012;222(2):519-23.
76. Rosser EC, Mauri C. Regulatory B cells: origin, phenotype, and function. *Immunity.* 2015;42(4):607-12.
77. Tay C, Liu YH, Hosseini H, Kanellakis P, Cao A, Peter K, et al. B-cell-specific depletion of tumour necrosis factor alpha inhibits atherosclerosis development and plaque vulnerability to rupture by reducing cell death and inflammation. *Cardiovasc Res.* 2016;111(4):385-97.
78. Sage AP, Tsiantoulas D, Binder CJ, Mallat Z. The role of B cells in atherosclerosis. *Nature Reviews Cardiology.* 2019;16(3):180-96.
79. Sun J, Sukhova GK, Wolters PJ, Yang M, Kitamoto S, Libby P, et al. Mast cells promote atherosclerosis by releasing proinflammatory cytokines. *Nature Medicine.* 2007;13(6):719-24.
80. Lee M, Calabresi L, Chiesa G, Franceschini G, Kovanen PT. Mast cell chymase degrades apoE and apoA-II in apoA-I-knockout mouse plasma and reduces its ability to promote cellular cholesterol efflux. *Arterioscler Thromb Vasc Biol.* 2002;22(9):1475-81.
81. Bot I, de Jager SC, Zernecke A, Lindstedt KA, van Berkel TJ, Weber C, et al. Perivascular mast cells promote atherogenesis and induce plaque destabilization in apolipoprotein E-deficient mice. *Circulation.* 2007;115(19):2516-25.
82. Kovanen PT, Bot I. Mast cells in atherosclerotic cardiovascular disease – Activators and actions. *European Journal of Pharmacology.* 2017;816:37-46.
83. Ketelhuth DFJ, Lutgens E, Bäck M, Binder CJ, Van den Bossche J, Daniel C, et al. Immunometabolism and atherosclerosis: perspectives and clinical significance: a position paper from the Working Group on Atherosclerosis and Vascular Biology of the European Society of Cardiology. *Cardiovasc Res.* 2019;115(9):1385-92.
84. Tomas L, Edsfeldt A, Mollet IG, Perisic Matic L, Prehn C, Adamski J, et al. Altered metabolism distinguishes high-risk from stable carotid atherosclerotic plaques. *Eur Heart J.* 2018;39(24):2301-10.
85. Shirai T, Nazarewicz RR, Wallis BB, Yanes RE, Watanabe R, Hilhorst M, et al. The glycolytic enzyme PKM2 bridges metabolic and inflammatory dysfunction in coronary artery disease. *J Exp Med.* 2016;213(3):337-54.
86. Tawakol A, Singh P, Mojena M, Pimentel-Santillana M, Emami H, MacNabb M, et al. HIF-1 α and PFKFB3 Mediate a Tight Relationship Between Proinflammatory Activation and Anaerobic Metabolism in Atherosclerotic Macrophages. *Arterioscler Thromb Vasc Biol.* 2015;35(6):1463-71.

87. Liu Y, Xu R, Gu H, Zhang E, Qu J, Cao W, et al. Metabolic reprogramming in macrophage responses. *Biomarker Research*. 2021;9(1):1.
88. Basatemur GL, Jørgensen HF, Clarke MCH, Bennett MR, Mallat Z. Vascular smooth muscle cells in atherosclerosis. *Nature Reviews Cardiology*. 2019;16(12):727-44.
89. Chappell J, Harman JL, Narasimhan VM, Yu H, Foote K, Simons BD, et al. Extensive Proliferation of a Subset of Differentiated, yet Plastic, Medial Vascular Smooth Muscle Cells Contributes to Neointimal Formation in Mouse Injury and Atherosclerosis Models. *Circ Res*. 2016;119(12):1313-23.
90. Jacobsen K, Lund MB, Shim J, Gunnarsen S, Füchtbauer EM, Kjolby M, et al. Diverse cellular architecture of atherosclerotic plaque derives from clonal expansion of a few medial SMCs. *JCI Insight*. 2017;2(19).
91. Feil S, Fehrenbacher B, Lukowski R, Essmann F, Schulze-Osthoff K, Schaller M, et al. Transdifferentiation of vascular smooth muscle cells to macrophage-like cells during atherogenesis. *Circ Res*. 2014;115(7):662-7.
92. Shankman LS, Gomez D, Cherepanova OA, Salmon M, Alencar GF, Haskins RM, et al. KLF4-dependent phenotypic modulation of smooth muscle cells has a key role in atherosclerotic plaque pathogenesis. *Nat Med*. 2015;21(6):628-37.
93. Rong JX, Shapiro M, Trogan E, Fisher EA. Transdifferentiation of mouse aortic smooth muscle cells to a macrophage-like state after cholesterol loading. *Proc Natl Acad Sci U S A*. 2003;100(23):13531-6.
94. Gray K, Kumar S, Figg N, Harrison J, Baker L, Mercer J, et al. Effects of DNA damage in smooth muscle cells in atherosclerosis. *Circ Res*. 2015;116(5):816-26.
95. Shah A, Gray K, Figg N, Finigan A, Starks L, Bennett M. Defective Base Excision Repair of Oxidative DNA Damage in Vascular Smooth Muscle Cells Promotes Atherosclerosis. *Circulation*. 2018;138(14):1446-62.
96. Bennett MR, Littlewood TD, Schwartz SM, Weissberg PL. Increased sensitivity of human vascular smooth muscle cells from atherosclerotic plaques to p53-mediated apoptosis. *Circ Res*. 1997;81(4):591-9.
97. Boyle JJ. Vascular smooth muscle cell apoptosis in atherosclerosis. *Int J Exp Pathol*. 1999;80(4):197-203.
98. Pan H, Xue C, Auerbach BJ, Fan J, Bashore AC, Cui J, et al. Single-Cell Genomics Reveals a Novel Cell State During Smooth Muscle Cell Phenotypic Switching and Potential Therapeutic Targets for Atherosclerosis in Mouse and Human. *Circulation*. 2020;142(21):2060-75.
99. Newby AC. Dual role of matrix metalloproteinases (matrixins) in intimal thickening and atherosclerotic plaque rupture. *Physiol Rev*. 2005;85(1):1-31.
100. Silvestre-Roig C, Braster Q, Wichapong K, Lee EY, Teulon JM, Berrebeh N, et al. Externalized histone H4 orchestrates chronic inflammation by inducing lytic cell death. *Nature*. 2019;569(7755):236-40.
101. Conklin AC, Nishi H, Schlamp F, Örd T, Öunap K, Kaikkonen MU, et al. Meta-Analysis of Smooth Muscle Lineage Transcriptomes in Atherosclerosis and Their Relationships to In Vitro Models. *Immunometabolism*. 2021;3(3).
102. Wirka RC, Wagh D, Paik DT, Pjanic M, Nguyen T, Miller CL, et al. Atheroprotective roles of smooth muscle cell phenotypic modulation and the TCF21 disease gene as revealed by single-cell analysis. *Nat Med*. 2019;25(8):1280-9.

103. Shi Y, O'Brien JE, Fard A, Zalewski A. Transforming Growth Factor- β 1 Expression and Myofibroblast Formation During Arterial Repair. *Arteriosclerosis, Thrombosis, and Vascular Biology*. 1996;16(10):1298-305.
104. Singh S, Torzewski M. Fibroblasts and Their Pathological Functions in the Fibrosis of Aortic Valve Sclerosis and Atherosclerosis. *Biomolecules*. 2019;9(9).
105. Le Bras A, Yu B, Issa Bhaloo S, Hong X, Zhang Z, Hu Y, et al. Adventitial Sca1+ Cells Transduced With ETV2 Are Committed to the Endothelial Fate and Improve Vascular Remodeling After Injury. *Arterioscler Thromb Vasc Biol*. 2018;38(1):232-44.
106. Lindblom P, Gerhardt H, Liebner S, Abramsson A, Enge M, Hellstrom M, et al. Endothelial PDGF-B retention is required for proper investment of pericytes in the microvessel wall. *Genes Dev*. 2003;17(15):1835-40.

Chapter 2

A switch from cell-associated to soluble PDGF-B protects against atherosclerosis, despite driving extramedullary hematopoiesis

Renée J.H.A. Tillie, Thomas L. Theelen, Kim van Kuijk, Lieve Temmerman, Jenny de Bruijn, Marion Gijbels, Christer Betsholtz, Erik A.L. Biessen, Judith C. Sluimer

Cells, 2021, Jul 10, 10(7):1746

Abstract

Platelet-derived growth factor B (PDGF-B) is a mitogenic, migratory and survival factor. Cell-associated PDGF-B recruits stabilizing pericytes towards blood vessels through retention in extracellular matrix. We hypothesized that the genetic ablation of cell-associated PDGF-B by retention motif deletion (*Pdgfb^{ret/ret}*) would reduce the local availability of PDGF-B, resulting in microvascular pericyte loss, microvascular permeability and exacerbated atherosclerosis.

To this end, low-density lipoprotein receptor knockout (*Ldlr^{-/-}*) *Pdgfb^{ret/ret}* mice were fed a high cholesterol diet. Although plaque size was increased in the aortic root of these *Pdgfb^{ret/ret}* mice, microvessel density and intraplaque hemorrhage were unexpectedly unaffected. Plaque macrophage content was reduced, which is likely attributable to increased apoptosis, as judged by increased TUNEL+ cells in *Pdgfb^{ret/ret}* plaques (2.1-fold) and increased *Pdgfb^{ret/ret}* macrophage apoptosis upon 7-ketocholesterol or oxidized LDL incubation *in vitro*. Moreover, *Pdgfb^{ret/ret}* plaque collagen content was increased, independent of mesenchymal cell density. Decreased macrophage matrix metalloproteinase activity could partly explain enhanced *Pdgfb^{ret/ret}* collagen content. In addition to the beneficial vascular effects, we observed reduced body weight gain related to smaller fat deposition in *Pdgfb^{ret/ret}* liver and adipose tissue. While dampening plaque inflammation, *Pdgfb^{ret/ret}* paradoxically induced systemic leukocytosis. The increased incorporation of 5-ethynyl-2'-deoxyuridine indicated increased extramedullary hematopoiesis and increased proliferation of circulating leukocytes.

In conclusion, *Pdgfb^{ret/ret}* confers vascular and metabolic effects, which appeared to be protective against diet-induced cardiovascular burden. These effects were unrelated to arterial mesenchymal cell content or adventitial microvessel density and leakage. In contrast, the deletion drives splenic hematopoiesis and subsequent leukocytosis in hypercholesterolemia.

Introduction

The normal artery wall consists of three layers: the intima, the medial layer and the adventitia from luminal inside to outside, respectively¹. The intima consists of a single layer of endothelial cells (ECs), whereas the media consists of smooth muscle cells (SMCs) embedded in extracellular matrix (ECM)¹. The adventitia harbors connective tissue, mesenchymal cells (MCs), immune cells and blood vessels, amongst others¹. Atherosclerosis is characterized by plaque accumulation in the subendothelial space of the intimal layer¹. Despite cholesterol lowering treatment applied in 71% of cardiovascular patients, atherosclerosis remains a major cause of death in western society². Plaque rupture and subsequent luminal thrombus formation can cause life-threatening complications³. The switch from plaques with stabilizing features, such as high mesenchymal cell density and resulting collagen accumulation and a thick fibrous cap, is triggered by the accumulation of immune cells, apoptosis and angiogenesis⁴. These processes degrade the matrix of the plaque and its fibrous cap, which would usually shield thrombogenic content from the arterial lumen, and this biomechanically weakens the fibrous cap and plaque⁴. Indeed, the formation of intra-plaque microvessels originating from adventitia has been identified as a source of intra-plaque hemorrhage, i.e., the leakage of blood components such as erythrocytes and leukocytes into the plaque⁵. Hence, plaque and adventitial microvessels are thought to increase disease progression and severity⁶. Causality between leakage of intraplaque microvessels and plaque instability remains to be addressed.

The important criteria in the association between intraplaque microvessels and disease severity are microvessel quantity and quality. A stable microvessel consists of a single endothelial layer resting on a basement membrane and pericytes that cover the ECs to provide stability⁶. Thus, microvessel quality is defined by healthy EC morphology, intact endothelial junctions and, especially, the presence of surrounding pericytes⁷. Microvessels in ruptured human coronary artery plaques generally present with endothelial abnormalities and the absence of stabilizing pericytes⁸. Platelet-derived growth factor B (PDGF-B) has been identified as an important factor for intercellular communication between ECs and pericytes during early angiogenesis⁹. Sprouting ECs secrete PDGF-B, which binds to heparan sulfate proteoglycans in the ECM and on the cell surface through its retention motif, which is a short amino acid sequence in the protein's C-terminus¹⁰. PDGF-B is thereby thought to form a growth factor gradient, guiding pericytes towards the ECs of the developing vessel¹⁰. Disruption of this gradient by deletion of the retention motif, resulting in a shorter isoform, was previously observed to induce pericyte loss and subsequently to increase microvascular leakage of the blood–brain barrier¹¹. Vice versa, absence of pericyte coverage and vessel dysfunction can be restored by overexpressing PDGF-B¹². Whole-body knockout (KO) of PDGF-B results in embryonic lethality caused by widespread bleedings¹³, which is in line with excessive bleeding as a common side-effect of PDGF receptor tyrosine kinase inhibitors such as imatinib¹⁴.

In addition to its role in microvessel stabilization, PDGF-B may have effects on other cell types involved in atherogenesis. PDGF-B exerts its functions on target cells by homo- or heterodimerization with PDGF-A or PDGF-B and subsequent binding to PDGF receptor alpha (PDGFR α) or -beta (PDGFR β) on the cell surface¹⁵. PDGF-B is naturally produced and secreted with and without its C-terminal retention motif as a cell-associated (or ECM-associated) or soluble isoform, respectively¹⁵. Platelets produce the soluble PDGF-B isoform through intracellular proteolytic processing¹⁶. Furthermore, both isoforms are likely produced by vascular ECs and macrophages, amongst others¹⁵. Both isoforms have been shown to be biologically active¹⁷. PDGF-B is a mitogen that stimulates fibroblast and SMC proliferation and ECM formation^{18, 19}. Indeed, an *in vivo* graft model showed that keratinocyte expression of either soluble or cell-associated PDGF-B results in increased distal or proximal proliferation of dermal mesenchymal cells, respectively¹⁷. Moreover, immune cells have been shown to express PDGF-B, and hematopoietic KO of both PDGF-B forms resulted in a pro-inflammatory phenotype as it increased numbers of activated cluster of differentiation (CD)4+ T cells in blood and caused monocyte accumulation in plaques of apolipoprotein E knockout (*ApoE*^{-/-}) mice²⁰. This is in contrast to immunosuppressive effects of PDGFR tyrosine kinase inhibitors¹⁴. It remains unclear whether functions in atherogenesis are mediated by the soluble or cell-associated isoform of PDGF-B. Thus, we studied the effect of ablation of the cell-associated form of PDGF-B, by removing its retention motif and forcing a switch to soluble PDGF-B, on vascular cell function in atherosclerosis.

Materials and methods

Experimental animals

Animal experiments were conducted according to Dutch governmental and AHA guidelines²¹ and approved by Dutch regulatory authorities. PDGF-B retention motif KO mice were kindly provided by Betsholtz⁹. The murine PDGF-B protein is 241 amino acids long. To delete the retention motif of PDGF-B, a premature translational stop codon was inserted into exon 6 of the *Pdgfb* gene (amino acid position 211). These mice were crossed with low-density lipoprotein receptor KO (*Ldlr*^{-/-}) mice from an in-house breeding colony, with the resulting mice referred to as *Pdgfb*^{ret/ret}. The LDL receptor regulates the amount of circulating cholesterol. Knockout of this receptor results in increased cholesterol levels in the blood, making the mouse susceptible to develop atherosclerosis when fed a high cholesterol diet²². Compared to other murine atherosclerosis models, the lipoprotein profile in *Ldlr*^{-/-} mice most closely resembles the circulating lipoprotein profile in dyslipidemic humans²². PDGF-B wildtype (WT) *Ldlr*^{-/-} mice served as controls in this study (referred to as *Pdgfb*^{WT/WT}). All mice were crossed back on a C57BL/6J *Ldlr*^{-/-} background at least nine times. Animals were housed in the laboratory animal facility of Maastricht University under standard conditions. Food and water were provided *ad libitum* during the experiment. Mice were housed in individually ventilated cages (GM500, Tecniplast, Buguggiate, Italy) with up to five animals per cage. Cages contained bedding (corn cob, Technilab-BMI, Someren, The Netherlands) and cage enrichment and these were changed weekly, which reduced handling of the mice to one handling per week during non-intervention periods.

Atherosclerosis induction, treatments and tissue collection

At 10–25 weeks of age, male mice were fed a 10-week high cholesterol diet (HCD) containing 0.25% cholesterol (824171, Special Diet Services, Essex, UK, 15% cocoa butter, 10% maize starch, 20% casein, 40.5% sucrose and 5.95% cellulose) to induce atherosclerosis²². Only male mice were used to minimize the number of animals per experiment and thus to strictly adhere to the 3R principles (replacement, reduction and refinement). Two separate mouse experiments were performed. The first experiment exclusively entailed mice (*Pdgfb*^{WT/WT} *n* = 19, *Pdgfb*^{ret/ret} *n* = 10) that were fed the HCD. At the start of the second experiment (*Pdgfb*^{WT/WT} *n* = 16, *Pdgfb*^{ret/ret} *n* = 9), blood was collected from vena saphena to assess leukocyte counts on standard laboratory diet (R/M-H 25 kGy, Bio-Services, Uden, The Netherlands) with an automated hematology analyzer (XP-300, Sysmex, Norderstedt, Germany). Thereafter, mice received the 10-week HCD and were housed on metabolic cages once for 24 h to assess food intake. Furthermore, these mice were injected intraperitoneally with 25 mg/kg 5-ethynyl-2'-deoxyuridine (EdU, E10415, Invitrogen, Waltham, MA, US) 24 h before sacrifice. All mice were euthanized by intraperitoneal pentobarbital injection (100 mg/kg).

During the second experiment, glucose concentration of whole blood from splenic artery was measured using a blood glucose meter (Contour TS, Bayer, Leverkusen, Germany). Furthermore, blood was collected from the right ventricle (experiment 1) or vena cava (experiment 2) in the presence of ethylenediamine tetraacetic acid (EDTA) to assess leukocyte counts and other hematological parameters (XP-300, Sysmex), leukocyte EdU incorporation by flow cytometry and plasma cholesterol and triglyceride levels. In all mice, blood collection was followed by phosphate-buffered saline (PBS) perfusion via the left ventricle. Aortic root was excised and immediately embedded in optimal cutting temperature (OCT) compound (361603E, VWR chemicals, Radnor, PA, US). Spleen, pancreas, liver, kidneys, interscapular brown adipose tissue, epididymal white adipose tissue (eWAT) and heart were dissected and weighed during the second experiment. Liver and eWAT were fixed in 4% paraformaldehyde (PFA) overnight and paraffin-embedded. Femur and tibia were dissected followed by the determination of length and weight of the right femur bone. Spleen, femur and tibia were used for leukocyte and/or progenitor cell flow cytometry combined with EdU incorporation detection.

Plasma cholesterol and triglyceride levels

Standard enzymatic techniques were used to assess plasma cholesterol (CHOD-PAP method – Cholesterol FS Ecoline no. 113009990314; DiaSys – Diagnostic Systems GmbH) and plasma triglycerides (FS5' Ecoline no. 157609990314; DiaSys – Diagnostic Systems GmbH) automated on the Cobas Fara centrifugal analyzer (Roche).

Histology and immunohistochemistry

Serial cryosections (5 μ m) from OCT compound embedded aortic roots were cut and stained with hematoxylin and eosin (HE) for blinded quantification of plaque size and necrotic core content in four sections of aortic root (at 25 μ m intervals) using computerized morphometry (Leica QWin V3, Cambridge, UK). Necrotic core was defined as acellular and anuclear plaque areas rich in cholesterol clefts.

Atherosclerotic plaques were assessed for collagen (Sirius red area/plaque area, 09400, Polysciences, Warrington, PA, US), iron (Perls Prussian blue), macrophage content (MOMA-2 area/plaque area), mesenchymal cell content (α smooth muscle actin (α SMA)+ area/plaque area, F3777, Sigma-Aldrich, Saint Louis, MO, US), adventitial microvessel density (number of CD31+ microvessels/adventitial area, 550274, BD Biosciences, Franklin Lakes, NJ, US) and PDGF-B (PDGF-B area/MOMA-2 on adjacent slides, ab23914, Abcam, Cambridge, UK). In short, slides were incubated with primary antibodies (MOMA-2, α SMA, CD31, PDGF-B) followed by peroxidase-based or alkaline-phosphatase-based immunohistochemical staining (see **Supplementary (S) Table S1** for detailed information). For Perls Prussian blue staining, slides were incubated with a freshly prepared mix consisting of 1 part 2% HCl and 1 part 2%

potassium hexacyanoferrate (II) to produce a reaction between ferric ions and potassium hexacyanoferrate (II), resulting in blue staining. Subsequent sensitization was performed using 3,3'-diaminobenzidine (DAB, K346811-2, Agilent, Santa Clara, CA, US). For Sirius red staining, slides were incubated in 0.1% Sirius red in saturated picric acid and subsequently rinsed in 0.01 M HCl.

Quantifications were performed blinded using the Leica QWin software (V3, Cambridge, UK) by one observer with low intra-observer variability (<5%). Mean fibrous cap thickness was determined using ImageJ software Version 1.51S (as described in²³, Bethesda, MD, US). Conversion of pictures to pseudofluorescent images was performed using the deconvoluting option in FIJI software Version 1.53c (Bethesda, MD, US).

Paraffin-embedded liver and eWAT samples were serially sectioned (4 and 7 μ m, respectively) and HE-stained. Fat accumulation was scored blinded through visual analogue scores from 0 to 4.

Isolation and culturing of bone marrow cells

Femur and tibia of *Pdgfb*^{WT/WT} and *Pdgfb*^{ret/ret} mice on standard laboratory diet were dissected. Bone marrow cells were isolated by flushing bones with PBS. Single cell suspensions were obtained by passing cells through a 70 μ m cell strainer.

Bone marrow cells were cultured on non-tissue-culture-treated petri dishes in RPMI 1640 medium (72400047, Gibco, Waltham, MA, US) or DMEM medium (31966021, Gibco) with 15% cell line L929-conditioned medium (LCM), 10% heat-inactivated fetal bovine serum (FBS, FBS-12A, Capricorn Scientific, Ebsdorfergrund, Germany) and 1% Penicillin Streptomycin (P/S, 15070-063, Gibco). LCM was added to ensure differentiation of bone marrow-derived monocytes to macrophages (BMDMs). After 7 days of differentiation, BMDMs were detached with lidocaine and generally plated onto non-tissue culture treated plates for various assays. Prior to the addition of stimuli, BMDMs were always allowed to attach overnight.

RNA and DNA isolation

RNA and DNA were isolated using the TRIzol reagent (15596026, Thermo Fisher Scientific, Waltham, MA, US) and subsequent chloroform phase separation which was performed following manufacturer's protocol. Both DNA and RNA concentrations were determined with a NanoDrop 2000 (Thermo Fisher Scientific).

BMDM genotype confirmation

PDGF-B retention motif KO was assessed in BMDMs through DNA genotyping. A master mix containing REExtract-N-Amp PCR ReadyMix (R4775, Sigma-Aldrich) and specific forward and

reverse primers (10 μ M, **Table S2**) was added per DNA sample (≥ 100 ng) and separately for both the *Pdgfb*^{WT} and *Pdgfb*^{et} gene. Subsequently, PCR was performed in a thermal cycler (MyCycler Thermal Cycler System, Bio-Rad, Hercules, CA, US). An agarose gel was casted using agarose, 0.5 \times TBE buffer (tris-borate-EDTA buffer, 45 mM tris-borate 1 mM EDTA in dH₂O) and SYBR Safe DNA Gel stain (1:35,000 dilution, S33102, Invitrogen). The resulting PCR samples and a DNA ladder (GeneRuler 100 bp Plus DNA ladder, SM0321, Thermo Fisher Scientific) were loaded and electrophoresis was performed for 30 min on 120 V (Powerpac 300, Bio-Rad).

Reverse transcription and quantitative PCR

RNA was reverse transcribed to cDNA with the iScript cDNA synthesis kit following the manufacturer's protocol (1708890, Bio-Rad). Subsequent quantitative polymerase chain reaction (qPCR) was performed using 10 ng cDNA, SYBR Green Supermix (1708885, Bio-Rad) and specific primer sets (**Table S3**). The 18 Svedberg ribosomal RNA (18s rRNA) was used as a housekeeping gene to correct for different mRNA quantities between samples. Analysis was performed with CFX Manager Software Version 3.1 (Bio-Rad).

Pro-inflammatory cytokines in plasma and BMDM-conditioned medium

Cytokine levels in plasma and BMDM-conditioned medium were assessed using a V-PLEX Proinflammatory Panel 1 Mouse Kit following manufacturer's protocol (K15048D-1, Meso Scale Diagnostics).

ELISA PDGF-B

PDGF-B protein levels in BMDM-conditioned medium were determined using ELISA (Quantikine ELISA, MBB00, R&D Systems, Minneapolis, MN, US). The antibodies bind between amino acids 74 and 182 of the PDGF-B protein and, thus, not to the retention motif. ELISA was performed following the manufacturer's protocol and read at 450 nm and 540 nm for wavelength correction with a SpectraMax M2 and SoftMax Pro Software Version 5 (Molecular Devices, San Jose, CA, US).

High Content Analysis of BMDM apoptosis and cholesterol uptake

BMDMs were plated onto Falcon 96-well tissue culture-treated imaging microplates (353219, Corning, Corning, NY, US) for apoptosis and cholesterol uptake assays. BMDMs were stimulated with 7-ketocholesterol (C2394, Sigma-Aldrich, 50 μ M), oxidized LDL (oxLDL, 50 μ g/mL) and/or PDGF-B (SRP3229, Sigma-Aldrich, 140 pg/mL) for the apoptosis assay. After 22–24 h, BMDMs were incubated with Hoechst 33342 (4 μ g/mL, B2261, Sigma-Aldrich) and washed with Annexin binding buffer (10 mM HEPES, 140 mM NaCl, 5 mM CaCl₂, pH 7.4). Subsequently, cells were incubated with Annexin V-OG²⁴ (FP488, 2.6 μ g/mL).

For cholesterol uptake, BMDMs were incubated with oxLDL (8 µg/mL) and Topfluor-labelled Cholesterol (2 µg/mL, 810255, Avanti Polar Lipids, Alabaster, AL, US) for 3 h. Thereafter, BMDMs were incubated with Hoechst 33342 and washed.

Imaging was performed with a BD Pathway 855 High Content Analyzer (HCA, BD Biosciences) and 10-fold objective, taking 9 pictures/well. A digital segmentation mask for each cell based on nuclear Hoechst signal was created with BD Attovision Software Version 1.6. Automated analysis of output parameters for fluorescence probe intensity was performed and BD FACSDiva Software Version 6.1.2 was used for subsequent blinded analyses of apoptosis and lipid uptake by one observer with low intraobserver variability.

TUNEL assay

In order to visualize apoptosis, a TUNEL (terminal deoxynucleotidyl transferase-mediated dUTP nick-end labeling) assay was performed on cryosectioned aortic roots (In Situ Cell Death Detection Kit, TMR Red, 12156792910, Roche, Basel, Switzerland) following the manufacturer's protocol. Cell density, plaque area and number of apoptotic cells were determined blinded using QuPath Version 0.1.2 (Edinburgh, UK) and ImageJ Software Version 1.51S.

BMDM migration

A cross-shaped scratch was applied per well. Subsequently, pictures were taken (Leica DFC300 FX, Leica Microsystems, Wetzlar, Germany) of four fixed positions in each well at several time points (0, 0.5, 1 and 2 h) with a 10× objective (Leica DM IL microscope, Leica Microsystems). Migration over time was assessed with ImageJ Software version 1.51S.

BMDM proliferation

BMDMs were plated onto an E-plate view 96 (Acea, Roche), which was placed into a real-time cell analysis (RTCA) SP station (Acea, Roche) in an incubator on 37 °C with 5% CO₂. Subsequent proliferation of BMDMs measured as change in electrical impedance was assessed with xCELLigence RTCA (Acea, Roche) and analyzed with RTCA Software 1.2.

BMDM matrix metalloproteinase (MMP) activity

BMDMs were lysed with 1% Triton X-100 in PBS and OmniMMP Fluorogenic Substrate (400 µM, BML-P126-0001, Enzo Life Sciences, Farmingdale, NY, US) was added in the 1× Omni-buffer (50 mM HEPES, 10 mM CaCl₂ in dH₂O, pH 7.0). Fluorescence was measured at 2 min intervals from 0–300 min at an excitation of 320 nm and emission of 405 nm with a SpectraMax M2 and SoftMax Pro Software Version 5 (Molecular Devices).

Absolute circulating leukocyte counts by flow cytometry

Flow cytometry was performed to quantify absolute leukocyte subsets in whole blood. Blood was added to BD Trucount Absolute Counting Tubes (340334) containing Fc receptor block (anti-CD16/32 antibody). Thereafter, an antibody cocktail was added (**Table S4**) and erythrocytes were lysed with lysis buffer (8.4 g/L NH₄Cl and 0.84 g/L NaHCO₃ in dH₂O, pH 7.4) prior to measurement. All flow cytometry samples were measured with a BD FACSCanto II and analyzed with BD FACSDiva Software (BD Biosciences).

Leukocyte and progenitor cell Click-iT EdU detection and flow cytometry

Flow cytometry was performed to assess leukocytes in blood and spleen and progenitor cells in bone marrow and spleen. Whole blood was centrifuged (2100 rpm, 10 min, 4 °C) and plasma was stored at -80 °C until further use. The spleen was crushed through a 70 µm cell strainer (542070, Greiner Bio-One, Kremsmünster, Austria) to obtain a single cell suspension. Femur and tibia were flushed with PBS and bone marrow cells were passed through a 70 µm cell strainer. Erythrocytes in all samples were lysed with lysis buffer. For flow cytometry of leukocytes, Fc receptors were blocked and, hereafter, an antibody mix was added. For flow cytometry of progenitor cells, antibody mix was added without prior Fc receptor blocking (**Table S4**). After antibody incubation, the Click-iT reaction with an Alexa Fluor 488-coupled azide was performed following the manufacturer's protocol (Click-iT EdU Alexa Fluor 488 Flow Cytometry Assay Kit, C10420, Invitrogen).

Statistical analyses

Graphs are presented as mean ± standard error of the mean (SEM). Results were statistically analyzed with GraphPad Prism Version 6 (GraphPad Software Inc., San Diego, CA, US). ROUT outlier analysis was performed and any outliers were excluded. Subsequently, normality (Shapiro–Wilk) and equal variances (F-test) analyses and the corresponding parametric or non-parametric testing were performed. * $p < 0.05$, ** $p < 0.01$ and *** $p < 0.001$.

Results

Increased plaque stability in *Pdgfb*^{ret/ret} mice, unaffected adventitial plaque vessel quantity and leakage

Firstly, prior works on PDGF-B protein and mRNA expression in murine plaques and cell types involved therein were confirmed. PDGF-B immunoreactivity was present in macrophages and ECs, which is in line with mRNA expression in these cell types *in vitro* (**Figure 1A** and **B**). Gene expression in SMCs and fibroblasts *in vitro* was neglectably low. Similar to these observations in mice, the single-cell RNA-sequencing dataset by Wirka et al. from human atherosclerotic coronary arteries showed that *PDGFB* was mainly expressed in macrophages and endothelial cells, albeit by a low percentage of cells. *PDGFA* was mainly expressed by mesenchymal cells in the human plaque^{25, 26} (**Supplementary (S) Figure S1**).

To investigate the effect of a switch from the cell-associated to the soluble form of PDGF-B on atherosclerosis, *Pdgfb*^{ret/ret} and *Pdgfb*^{WT/WT} mice were fed a high cholesterol diet (HCD) for 10 weeks (**Figure 1C**). Plaque size was significantly increased (+69%) in aortic roots from *Pdgfb*^{ret/ret} compared to *Pdgfb*^{WT/WT} mice, while the necrotic core content was unchanged (**Figure 1D**). This effect was independent of circulating cholesterol and triglyceride levels, which were comparable between *Pdgfb*^{ret/ret} and *Pdgfb*^{WT/WT} mice (**Figure S2A**).

To clarify the process underlying increased plaque growth, we studied the plaque phenotype in these mice. As PDGF-B^{ret/ret} KO causes microvessel leakage in the blood–brain barrier¹¹, the effect on angiogenesis was studied. However, no CD31 positive microvessels could be detected in either *Pdgfb*^{ret/ret} or *Pdgfb*^{WT/WT} plaques (**Figure 1E**). Due to the lack of intra-plaque vessels, adventitial plaque vessel quantity was assessed as a surrogate parameter, which is in line with the outside-in hypothesis on the role of the adventitia in atherogenesis. However, in contrast to our expectations, adventitial vessel quantity also did not differ between genotypes. In line with these observations, no differences in intra-plaque or adventitial iron residues, potentially originating from lysed erythrocytes after blood vessel leakage, were found in *Pdgfb*^{ret/ret} nor *Pdgfb*^{WT/WT} mice (**Figure 1F**). In contrast, iron-laden macrophages were histologically observed in *Pdgfb*^{ret/ret} versus *Pdgfb*^{WT/WT} livers (**Figure S2B**), indicating that PDGF-B retention motif KO did cause the leakage of blood vessels in other organs. Furthermore, extensive ECM accumulation in *Pdgfb*^{ret/ret} glomeruli was observed, confirming previous observations of microvascular leakage⁹ (**Figure S2C**).

On the other hand, collagen content and mean thickness of the fibrous cap were also increased in *Pdgfb*^{ret/ret} plaques (**Figure 1G**). Plaques were then analyzed for the presence of alpha smooth muscle actin (α SMA)-positive mesenchymal cells (MCs) and MOMA-2 antigen-positive macrophages, as these cell types play an important role in the production and

degradation of collagen in the atherosclerotic plaque, respectively^{27, 28}. Furthermore, PDGF-B is a known inducer of MC proliferation¹⁹. Plaque macrophage content was decreased by half in *Pdgfb^{ret/ret}* mice (**Figure 1H**), whereas α SMA-positive MC content was unaffected (**Figure 1E**). Our data so far suggested that despite an increase in *Pdgfb^{ret/ret}* plaque size, the stability of *Pdgfb^{ret/ret}* plaques is increased due to increased collagen content and fibrous cap thickness and decreased macrophage content. These observations are unrelated to changes in intra-plaque microvessel quantity or leakage.

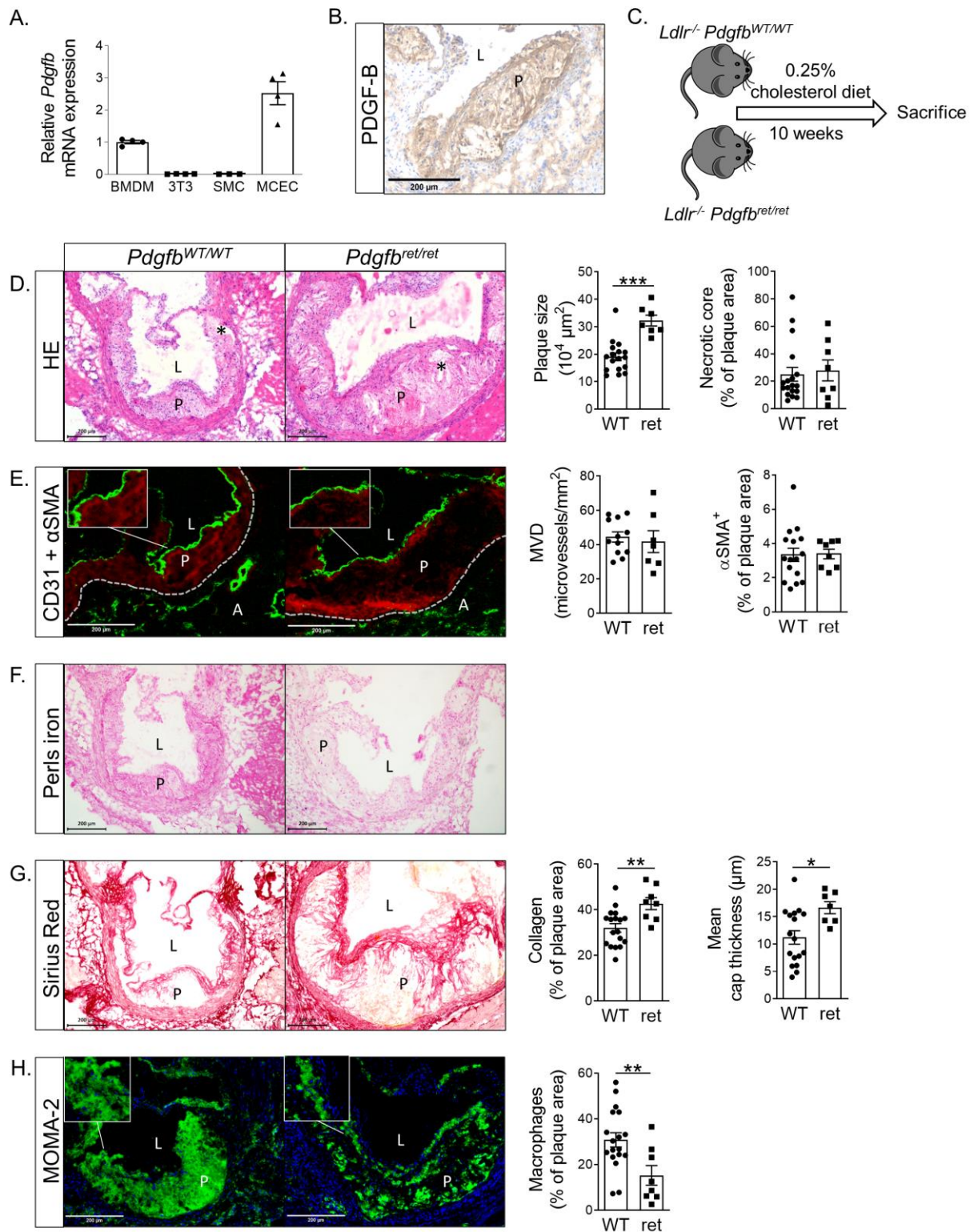


Figure 1: Plaque characteristics show larger but more stable *Pdgfb*^{ret/ret} plaques. (A) *Pdgfb* mRNA expression in mouse cardiac endothelial cells (MCECs²⁹), NIH/3T3 fibroblasts and SMCs relative to BMDMs ($n = 3-4$). **(B)** PDGF-B immunoreactivity in low-density lipoprotein receptor KO (*Ldlr*^{-/-}) aortic root lesions. **(C)** Setup of mouse experiment using *Ldlr*^{-/-} *Pdgfb*^{WT/WT} ($n = 19$) and *Ldlr*^{-/-} *Pdgfb*^{ret/ret} ($n = 10$) mice. Representative photomicrographs of **(D)** HE, **(E)** CD31 + αSMA (green and red, respectively, pseudo-fluorescence), **(F)** Perls iron, **(G)** Sirius Red and **(H)** MOMA-2 (green, pseudo-fluorescence) staining in *Pdgfb*^{WT/WT} ($n = 12-18$) and *Pdgfb*^{ret/ret} ($n = 7-8$) aortic root lesions and the corresponding quantifications. Nuclear staining in MOMA-2 staining of aortic roots was

performed with hematoxylin (blue, pseudo-fluorescence). MVD; adventitial microvessel density. * in photomicrographs indicates necrotic core. P; plaque, L; lumen, A; adventitia. Graphs represent mean \pm standard error of the mean (SEM). * $p < 0.05$, ** $p < 0.01$, *** $p < 0.001$. Scale bars 200 μm . Data were tested for normality (Shapiro-Wilk) and equal variances (F-test). Variables that did or did not pass were analyzed using Student's *t*-test or the Mann-Whitney U test, respectively.

Soluble PDGF-B secretion and *Pdgfb*^{ret/ret} macrophage susceptibility to apoptosis increased

In order to further investigate the decreased *Pdgfb*^{ret/ret} plaque macrophage content and its possible association with increased plaque collagen content, we studied whether the *Pdgfb*^{ret/ret} macrophage function was affected. First, we confirmed the *Pdgfb* genotype in murine bone marrow-derived macrophages (BMDMs) isolated from *Pdgfb*^{ret/ret} and *Pdgfb*^{WT/WT} bone marrow (**Figure 2A**). This confirmation was provided by DNA genotyping as the KO of the retention motif was conferred by the introduction of a translational stop codon into the *Pdgfb* gene. Moreover, the unavailability of specific antibodies directed against the murine PDGF-B retention motif prevented KO confirmation at the protein level. Total *Pdgfb*, *Pdgfrb* and *Pdgfra* mRNA expression levels in *Pdgfb*^{ret/ret} macrophages were unchanged (**Figure 2B**). As expected, based on impaired retention of the protein to heparan sulfate proteoglycans on the cell surface^{9, 30}, ablation of the cell-associated form resulted in the increased secretion of soluble PDGF-B into medium by *Pdgfb*^{ret/ret} macrophages (**Figure 2C**). This PDGF-B secretion was assessed with an antibody that binds between amino acids 100 and 200 of the murine PDGF-B protein and thus not to the retention motif. This observation is in line with higher PDGF-B protein immunoreactivity per macrophage-positive plaque area (**Figure 2D and E**).

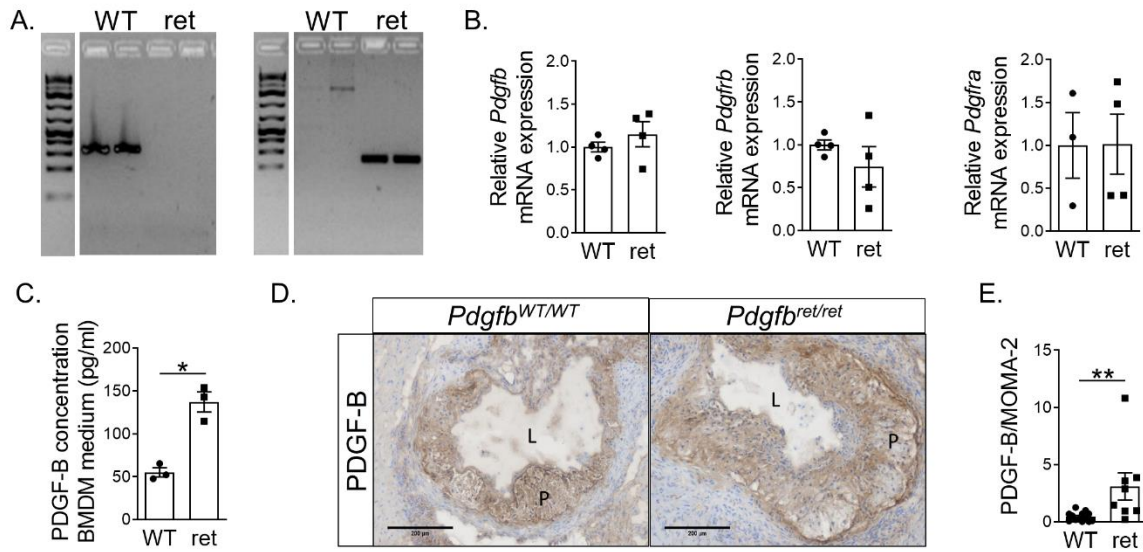


Figure 2: Increased secretion of soluble PDGF-B by *Pdgfb*^{ret/ret} BMDMs. (A) Gel imaging after DNA genotyping. PCR product *Pdgfb*^{WT} 340 bp (left) and *Pdgfb*^{ret} 212 bp (right). (B) *Pdgfb*, *Pdgfrb* and *Pdgfra* mRNA expression in *Pdgfb*^{ret/ret} relative to *Pdgfb*^{WT/WT} BMDMs ($n = 4$). (C) PDGF-B concentration in *Pdgfb*^{WT/WT} and *Pdgfb*^{ret/ret} BMDM-derived medium as assessed by ELISA ($n = 3$). (D) Representative photomicrographs of PDGF-B staining in *Pdgfb*^{WT/WT} and *Pdgfb*^{ret/ret} aortic root lesions. P; plaque, L; lumen. (E) Quantification of total PDGF-B plaque area relative to total MOMA-2 plaque area in adjacent sections of *Pdgfb*^{WT/WT} ($n = 13$) and *Pdgfb*^{ret/ret} ($n = 8$) aortic root lesions. Graphs represent mean \pm SEM. * $p < 0.05$, ** $p < 0.01$. Scale bars 200 μ m. Data were tested for normality (Shapiro-Wilk) and equal variances (F-test). Variables that did or did not pass, were analyzed using Student's t-test or Mann-Whitney U test, respectively. Data in C were transformed to ranks followed by a Student's t-test.

Thus, we investigated whether enhanced soluble PDGF-B secretion in *Pdgfb*^{ret/ret} mice results in changes in macrophage functions, such as apoptosis, lipid uptake, proliferation, migration and matrix metalloproteinase (MMP) activity explaining the fibrotic plaque phenotype and reduced macrophage content. Indeed, apoptosis upon incubation with cholesterol oxidation products 7-ketocholesterol (7-KC) or oxidized low-density lipoprotein (oxLDL) was significantly increased in *Pdgfb*^{ret/ret} compared to *Pdgfb*^{WT/WT} BMDMs *in vitro* (Figure 3A–D). Increased susceptibility to apoptosis was not caused by increased lipid uptake (Figure 3E). Likewise, pro-inflammatory cytokine secretion by *Pdgfb*^{ret/ret} BMDMs was unchanged (Figure S3A). To confirm whether, specifically, increased levels of extracellular soluble PDGF-B stimulate macrophage apoptosis, we incubated C57BL/6J BMDMs with 7-KC and a similar PDGF-B concentration as previously established in *Pdgfb*^{ret/ret} BMDM medium (Figure 2C, 140 pg/mL). Indeed, apoptosis was significantly increased upon combinatorial stimulation with both 7-KC and soluble PDGF-B versus stimulation with only 7-KC (Figure 3F and G). In line with these observations and with increased PDGF-B protein immunoreactivity per macrophage-positive plaque area, *in vivo* assessment confirmed enhanced plaque apoptosis (Figure 3H and I) and unaffected pro-inflammatory cytokine levels in plasma (Figure S3B). As basal BMDM migration

and proliferation *in vitro* were unchanged (**Figure 3J-K** and **S4**), enhanced apoptosis may be the underlying reason for reduced macrophage content.

Reduced macrophage content and thus lower net collagen degradation might partly explain the enhanced plaque collagen accumulation in *Pdgfb*^{ret/ret} versus *Pdgfb*^{WT/WT} mice. In addition, MMP activity was decreased in *Pdgfb*^{ret/ret} versus *Pdgfb*^{WT/WT} BMDMs (**Figure 3L**). Together, higher apoptotic rates in *Pdgfb*^{ret/ret} macrophages due to increased extracellular soluble PDGF-B might explain diminished plaque macrophage content. In parallel, lower levels of macrophages with reduced MMP activity may be partly responsible for larger and more fibrotic plaques.

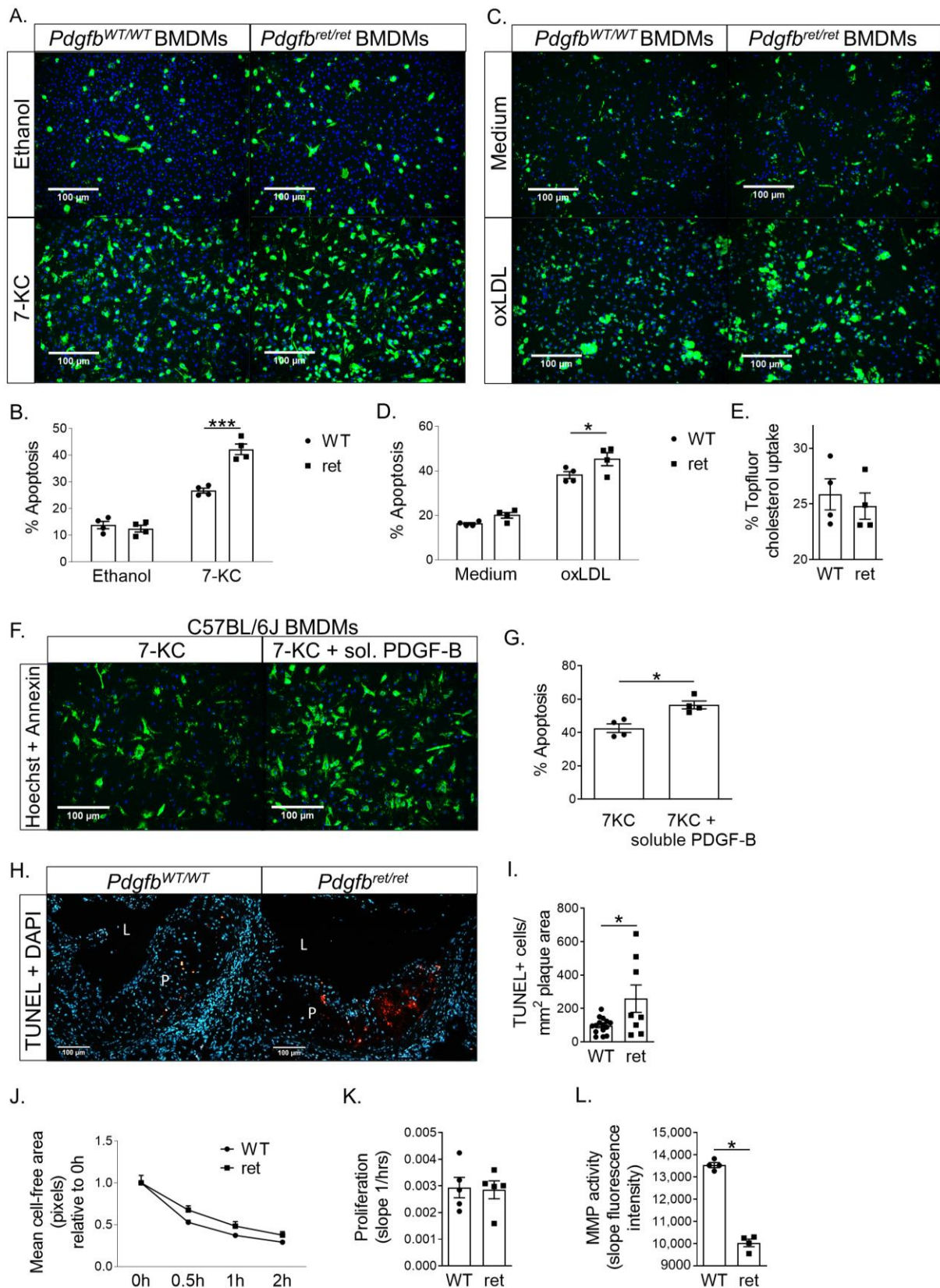


Figure 3: Increased apoptosis upon incubation with atherosclerosis-relevant stimuli and decreased MMP activity in *Pdgfb*^{ret/ret} BMDMs. All experiments in (A–E) and (J–L) were performed with *Pdgfb*^{WT/WT} and *Pdgfb*^{ret/ret} BMDMs. Representative photomicrographs of BMDM apoptosis stained with Annexin A5 (FP488, green) and

Hoechst 33342 (blue) after 24 h incubation with **(A)** ethanol or 7-ketocholesterol (7-KC) or **(C)** medium or oxidized LDL (oxLDL), with corresponding quantification ($n = 4$) in **(B)** and **(D)**. **(E)** Quantification of Topfluor-labeled cholesterol uptake by BMDMs after 3 h ($n = 4$). **(F)** Representative photomicrographs of C57BL/6J BMDM apoptosis stained with Annexin A5 (FP488, green) and Hoechst 33342 (blue) after 24 h incubation with 7-ketocholesterol and soluble (sol.) PDGF-B, with corresponding quantification ($n = 4$) in **(G)**. **(H)** Representative photomicrographs of TUNEL (red) and DAPI (blue) staining in *Pdgfb*^{WT/WT} ($n = 15$) and *Pdgfb*^{ret/ret} ($n = 8$) aortic root (AR) lesions and **(I)** quantification of TUNEL+ cells. P; plaque, L; lumen. **(J)** BMDM migration defined as mean cell-free area over time after scratch infliction ($n = 4$). **(K)** Mean BMDM proliferation measured as change in electrical impedance over time ($n = 5$). **(L)** Quantification of BMDM MMP activity with OmniMMP Fluorogenic Substrate ($n = 4$). Graphs represent mean \pm SEM. Scale bars 100 μ m. * $p < 0.05$, ** $p < 0.01$. Data were tested for normality (Shapiro-Wilk) and equal variances (F-test). Variables that did or did not pass were analyzed using Student's *t*-test or the Mann-Whitney U test, respectively. Data in **B** and **D**, and **J** were analyzed using two-way ANOVA and two-way repeated measures ANOVA, respectively, including Bonferroni's multiple comparisons test.

Differential systemic effects of *Pdgfb*^{ret/ret} on body weight and circulating immune cells

In addition to local vascular effects, we observed systemic effects of *Pdgfb*^{ret/ret} on body weight and circulating immune cells upon hypercholesterolemia. Body weight gain after 10 weeks of HCD was less in *Pdgfb*^{ret/ret} mice (**Figure S5A**), while 24 h food intake was unchanged between *Pdgfb*^{WT/WT} and *Pdgfb*^{ret/ret} mice (**Figure S5B**). Lower body weight gain could likely be explained by decreased weight of liver and epididymal white adipose tissue (eWAT) in *Pdgfb*^{ret/ret} mice, which is in line with histological observations of decreased fat accumulation in *Pdgfb*^{ret/ret} versus *Pdgfb*^{WT/WT} liver and eWAT (**Figure S5C** and **D**). Additionally, blood glucose levels were 45% lower in *Pdgfb*^{ret/ret} mice after the diet (**Figure S5E**). Thus, *Pdgfb*^{ret/ret} seems to protect against an unfavorable diet-induced (cardio) metabolic phenotype.

In contrast to beneficial vascular and metabolic effects, systemic inflammation was amplified in *Pdgfb*^{ret/ret} mice. Although immune cell counts were similar between *Pdgfb*^{ret/ret} and *Pdgfb*^{WT/WT} mice on a standard laboratory diet (**Figure S6A**), a striking general leukocytosis was observed in hypercholesterolemia (**Figure 4A–K**). The increased leukocytosis in *Pdgfb*^{ret/ret} mice during hypercholesterolemia is not associated with changes in systemic inflammation since circulating levels of inflammatory cytokines remain unchanged between *Pdgfb*^{ret/ret} and *Pdgfb*^{WT/WT} mice (**Figure S3B**).

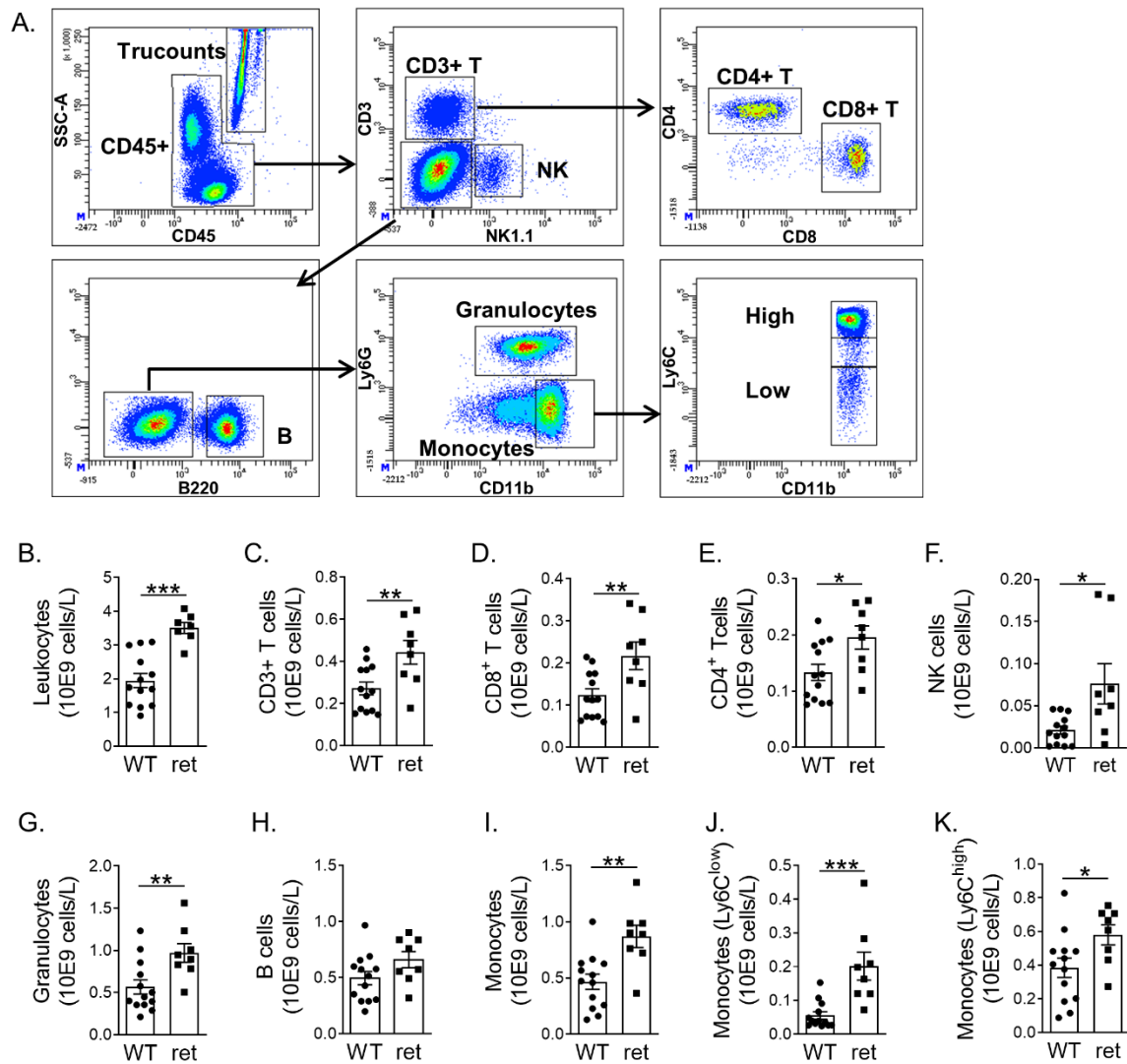


Figure 4: General leukocytosis in *Pdgfb^{ret/ret}* mice. (A) Flow cytometry gating strategy to assess absolute circulating leukocyte counts. **(B–K)** Absolute numbers of CD45+ leukocytes; CD3+, CD8+ and CD4+ T cells; NK (natural killer) cells; granulocytes; B cells and (lymphocyte antigen 6C (Ly6C)^{low} and Ly6C^{high}) monocytes in *Pdgfb^{WT/WT}* ($n = 13$) and *Pdgfb^{ret/ret}* ($n = 8$) blood. Graphs represent mean \pm SEM. * $p < 0.05$, ** $p < 0.01$, *** $p < 0.001$. Data were tested for normality (Shapiro-Wilk) and equal variances (F-test). Variables that did or did not pass were analyzed using Student's *t*-test or the Mann-Whitney U test, respectively.

Increased circulating immune cells may result from the increased proliferation of progenitor cells in bone marrow or spleen and/or leukocyte proliferation in circulation and spleen. Thus, we investigated if enhanced proliferation was underlying leukocytosis. Leukocytosis was again observed in this second experiment, reconfirming the phenotype (**Figure S6B**). EdU labeled similar fractions of bone marrow common myeloid progenitors (CMPs) and granulocyte monocyte progenitors (GMPs) in *Pdgfb^{ret/ret}* and *Pdgfb^{WT/WT}* mice, suggesting unchanged progenitor proliferation (**Figure 5A–C**). However, extramedullary hematopoiesis was heightened, as shown by increased relative EdU-positive counts within the splenic CMP and granulocyte populations. Moreover, increased EdU incorporation was observed in the CD8+ T cell population of the spleen (**Figure 5D–F** and **S6C–D**). In addition, the EdU-positive fraction of CD4+ and CD8+ T cells also increased in circulation (**Figure 5G** and **S6E**). In summary, increased proliferation largely drives extramedullary hematopoiesis and subsequent leukocytosis in *Pdgfb^{ret/ret}* during hypercholesterolemia. Overall, despite the amplification of the systemic inflammatory burden, *Pdgfb^{ret/ret}* prevents weight gain and lipid storage and supports the development of a fibrotic plaque phenotype in hypercholesterolemia.

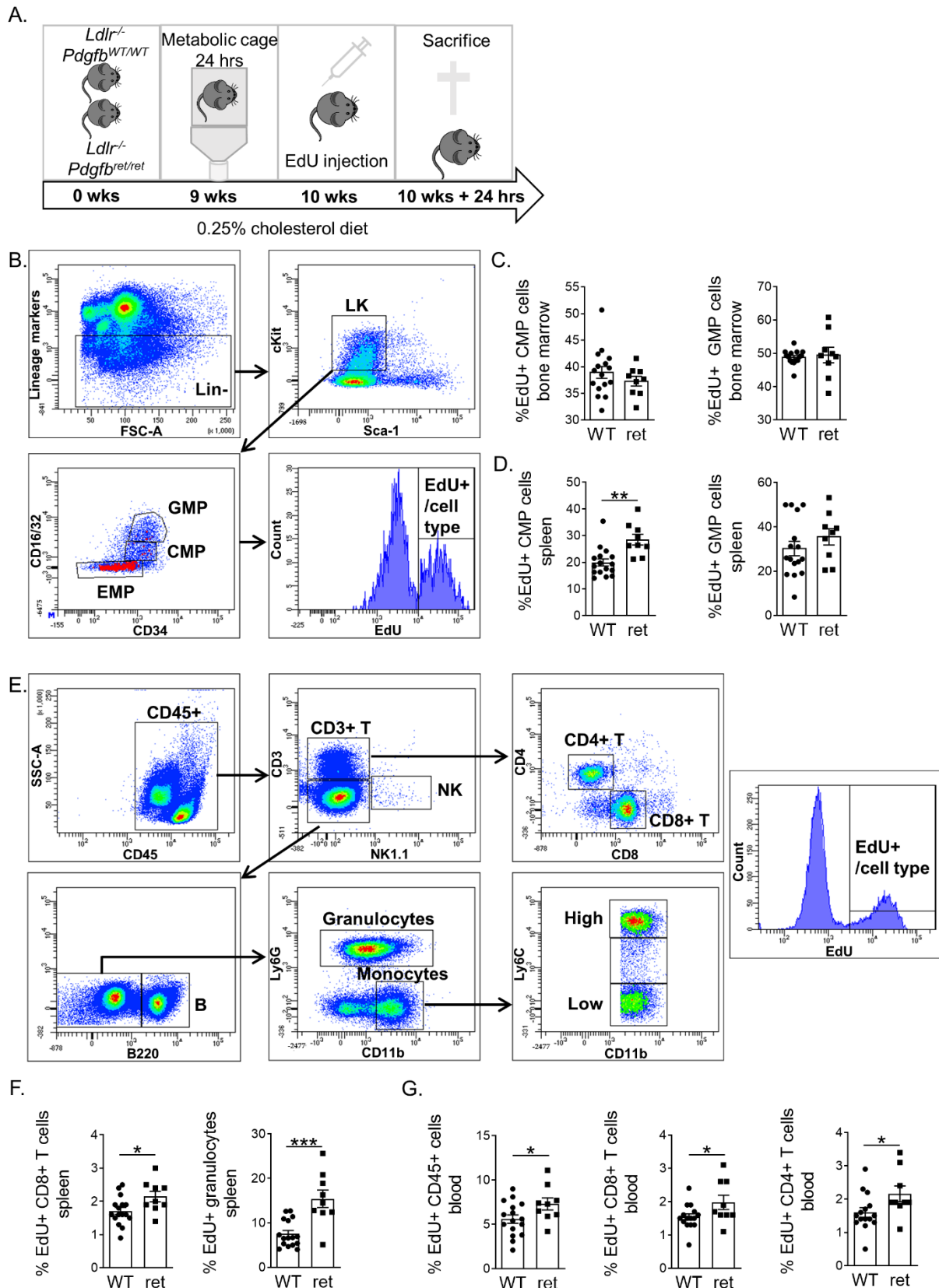


Figure 5: Increased extramedullary hematopoiesis and proliferation of leukocytes in *Pdgfb*^{ret/ret} mice. (A) Setup of second mouse experiment using *Ldlr*^{-/-}*Pdgfb*^{WT/WT} (*n* = 16) and *Ldlr*^{-/-}*Pdgfb*^{ret/ret} (*n* = 9) mice. **(B)** Flow cytometry gating strategy to assess hematopoietic progenitor cells and 5-ethynyl-2'-deoxyuridine (EdU) incorporation. **(C)** Percentage of EdU positive progenitor cells in *Pdgfb*^{WT/WT} (*n* = 16) and *Pdgfb*^{ret/ret} (*n* = 9) bone marrow and **(D)**

spleen. **(E)** Flow cytometry gating strategy to assess leukocytes and EdU incorporation. **(F)** Percentage of EdU positive leukocytes in *Pdgfb*^{WT/WT} ($n = 15-16$) and *Pdgfb*^{ret/ret} ($n = 9$) spleen and **(G)** blood. Graphs represent mean \pm SEM. * $p < 0.05$, ** $p < 0.01$, *** $p < 0.001$. Data were tested for normality (Shapiro-Wilk) and equal variances (F-test). Variables that did or did not pass were analyzed using Student's *t*-test or the Mann-Whitney U test, respectively.

Discussion

In our current study, we have disrupted PDGF-B's ability to anchor to the ECM or cell surface by deleting its retention motif (*Pdgfb^{ret/ret}*) and thus the cell-associated form. However, the soluble form of PDGF-B is, nonetheless, a biologically active protein^{16, 17}; it is produced and significantly more secreted by *Pdgfb^{ret/ret}* macrophages. The biological relevance of cell-associated and soluble PDGF-B is largely unknown. Here, we show the beneficial vascular and systemic effects of *Pdgfb^{ret/ret}* in hypercholesterolemia. Unexpectedly, plaque stability increased in *Pdgfb^{ret/ret}* mice, unrelated to intraplaque or adventitial microvessel quantity and leakage. Additionally, *Pdgfb^{ret/ret}* prevented body weight gain through decreased fat accumulation in liver and WAT. Contrary to beneficial local and systemic effects, we observed systemic leukocytosis in *Pdgfb^{ret/ret}* hypercholesterolemia, which is likely driven by increased extramedullary hematopoiesis.

Surprisingly, *Pdgfb^{ret/ret}* neither affected plaque or adventitial microvessel number nor leakage. It was reported previously that *Pdgfb^{ret/ret}* reduced retinal microvessel density⁹, suggesting reduced angiogenesis in normocholesterolemic *Pdgfb^{ret/ret}* mice. In the current study, no intra-plaque vessels were found in hypercholesterolemic mice, as expected. Our results coincide with numerous studies that did not observe plaque angiogenesis in the widely used *Ldlr^{-/-}* or *ApoE^{-/-}* mouse models of atherosclerosis³¹⁻³⁴. This may be related to scarcity of plaque neovascularization in mouse models or difficulties with the conventional detection of intraplaque microvessels through CD31 endothelial cell imaging³⁴. Indeed, additional interventions or genetic alterations are generally required to induce neovascularization and hemorrhage within the murine plaques. Adventitial microvessels are often studied, instead, as these have also been associated with atherosclerosis initiation and progression³⁴. However, in adventitia underlying the plaques, we also did not observe any changes in angiogenic density or leakage. Histological observations did show iron-laden macrophages and, thus, signs of blood vessel leakage in adult *Pdgfb^{ret/ret}* liver, possibly suggesting that PDGF-B remains an important factor for blood vessel stabilization even in hypercholesterolemia. However, this process seems to be organ-specific as it is dispensable for the permeability of arterial vasa vasorum. Therefore, we postulate that other factors such as vascular endothelial growth factors might be involved in the integrity of aortic intraplaque and adventitial microvessels in hypercholesterolemia³⁵.

Instead of affecting plaque or adventitial microvessel number and leakage, PDGF-B retention motif deletion showed protective local vascular and systemic effects. Although plaque size was increased, *Pdgfb^{ret/ret}* showed a more stable plaque phenotype as indicated by the increased collagen content and fibrous cap thickness and decreased macrophage content with similar MC content. While MC content was unaltered, PDGF-B is a well-established inducer of MC proliferation and has been associated with SMC migration from media to intima in

atherosclerosis³⁶. In line with our findings, normocholesterolemic *Pdgfb*^{ret/ret} mice without *Ldlr*^{-/-} background also increased collagen content without changing SMC numbers in the aortic media³⁷. In contrast, in *ApoE*^{-/-} mice with loss of both cell-associated and soluble PDGF-B in hematopoietic cells, fibrous cap formation and MC accumulation were reduced and the plaque size was unaffected³⁸. These results suggest that soluble PDGF-B is not responsible for MC content in early lesions, but does affect collagen accumulation in atherosclerotic plaque.

The increased plaque collagen content may partly be explained by increased plaque macrophage apoptosis. This could be due to reduced survival signaling or increased apoptosis signaling. In favor of the former, in a vascular graft model with a knockout of both soluble and cell-associated PDGF-B in myeloid cells, Onwuka et al. also observed increased macrophage apoptosis and suggested an autocrine role for PDGF-B in macrophage maintenance³⁹. Here, we show that enhanced secretion of soluble PDGF-B, in the absence of cell-associated PDGF-B, magnifies apoptosis induced by atherogenic stimuli such as 7-KC. Supplementation of soluble PDGF-B to BMDMs without genetic ablation of cell-associated PDGF-B also enhanced apoptosis. Thus, cell-associated PDGF-B might (partly) protect against apoptosis but, despite its presence, increased levels in soluble PDGF-B further stimulate apoptosis induced by cholesterol oxidation products. In this case, as previous studies mainly reported the protective effects of PDGF-B against apoptosis, the current study provides new insights regarding apoptosis-stimulating effects of soluble PDGF-B in atherosclerosis. In growth-arrested SMCs, soluble PDGF-B induced apoptosis through upregulation of B-cell leukemia/lymphoma (Bcl)-xs and downregulation of Bcl-2 and Bcl-xl gene expression⁴⁰. This remains to be confirmed for macrophages.

In addition to macrophage apoptosis, increased *Pdgfb*^{ret/ret} plaque collagen content could also be explained by reduced macrophage MMP activity. Several studies support enhanced MMP activity, specifically the activity of MMP-2 and -9, in response to PDGF-B. MMP-9 secretion was increased in human macrophages after PDGF-B stimulation, although the isoform was unspecified⁴¹. Additionally, total PDGF-B overexpression is associated with MMP-2 and MMP-9 expression in murine liver⁴². Moreover, a study in *ApoE*^{-/-} mice reported decreased plaque MMP-2 and MMP-9 expression after injection with AG1296, which is a PDGFR inhibitor⁴³. Together, these data suggest a stimulating effect of enhanced cell-associated PDGF-B on MMP activity and thus reduced local availability of cell-associated PDGF-B underlying reduced macrophage MMP activity.

In addition to beneficial vascular effects, we observed systemic protection of *Pdgfb*^{ret/ret} against adiposity. Similar results were reported in a model of tamoxifen-inducible systemic PDGFR β ablation in diet-induced obesity⁴⁴. Our observations seem linked to previous reports

of increased insulin signaling in *Pdgfb^{ret/ret}* liver that is caused by increased vascular permeability⁴⁵ and are thus in line with reduced local PDGF-B availability.

Contrary to decreased *Pdgfb^{ret/ret}* plaque inflammation, systemic leukocytosis was a prominent feature of *Pdgfb^{ret/ret}* mice, with expansion of almost all subsets in the circulation. This effect was only observed in hypercholesterolemia and not in *Pdgfb^{ret/ret}* mice on standard laboratory diet. This is in line with observations that hematopoietic PDGF-B was not essential for basal hematopoiesis in normolipidemia, although the spleen was not studied⁴⁶. Here, leukocytosis was likely caused by increased extramedullary hematopoiesis. Xue et al. overexpressed PDGF-B in subcutaneous tumors and reported heightened numbers of granulocyte-macrophage colony-forming units after isolation and stimulation of splenic progenitors in culture⁴⁷. Indeed, we observed a trend in the percentage of GMPs (**Figure S6C**) in *Pdgfb^{ret/ret}* spleen. Additionally, we report increased proliferation of CMPs in *Pdgfb^{ret/ret}* spleen *in vivo*. Thus, we show that extramedullary hematopoiesis is heightened due to increased progenitor proliferation and that PDGF-B already acts on CMPs to stimulate GMPs downstream, which has not been previously reported to the best of our knowledge. Moreover, Xue et al. reported PDGF-B-induced erythropoietin expression in PDGFR β -expressing stromal cells as a cause of increased extramedullary hematopoiesis⁴⁷. Thus, as the cell-associated PDGF-B is absent, the soluble PDGF-B isoform and possibly its increased secretion might be the main stimulator of splenic hematopoiesis in our model. We speculate that, in humans, the blockage of soluble PDGF-B by PDGFR inhibitors possibly underlies their immune suppressing effects¹⁴. Overall, PDGFR inhibition is associated with enhanced cardiovascular risk⁴⁸ and more insight into the PDGF-B isoforms may inform the design of future generation inhibitors. In the future, antibodies that specifically bind to the murine PDGF-B retention motif, which are currently unavailable, are warranted to further study the effects and affinity of PDGF-B isoforms and to clarify if underlying mechanisms are related to reduced bioavailability, altered (hetero)dimerization and/or signaling in PDGF-B-responsive and PDGF-B-producing cells.

In conclusion, *Pdgfb^{ret/ret}* has a dual effect in hypercholesterolemia as it results in more stable plaques and protects against an unfavorable diet-induced metabolic phenotype on one hand; on the other hand, it stimulates an immune response by increasing extramedullary hematopoiesis. Thus, the current study warrants further investigation of downstream pathways to isolate beneficial and detrimental effects of the PDGF-B isoforms and underlying mechanisms. Furthermore, integrity and density of intraplaque or adventitial microvessels seem to be independent of cell-associated PDGF-B.

Acknowledgements

The authors thank Clairly Dinjens for technical assistance.

Author contributions

Formal analysis, T.L.T. and R.J.H.A.T.; funding acquisition, J.C.S. and T.L.T.; investigation, T.L.T., K.v.K., J.d.B., L.T., M.G. and R.J.H.A.T.; methodology, C.B.; project administration, T.L.T. and R.J.H.A.T.; resources, C.B.; supervision, E.A.L.B. and J.C.S.; validation, R.J.H.A.T.; visualization, R.J.H.A.T.; writing—original draft, R.J.H.A.T. and J.C.S.; writing—review and editing; K.v.K., L.T., M.G., C.B., E.A.L.B., J.C.S. and R.J.H.A.T. All authors have read and agreed to the published version of the manuscript.

Funding sources

This work was supported by the following: VENI and VIDI fellowship of the Dutch Organization for scientific research (to JC Sluimer 016.116.017, 0.16.186.364), a Dr. Dekker senior postdoc fellowship of the Dutch Heart Foundation (to JC Sluimer, 2016T060) and a PhD student fellowship from the Cardiovascular Research Institute Maastricht (to T. Theelen).

Conflicts of interest

The authors declare no conflicts of interest.

References

1. Zaromitidou, M.; Siasos, G.; Papageorgiou, N.; Oikonomou, E.; Tousoulis, D. Chapter 2—Atherosclerosis and Coronary Artery Disease: From Basics to Genetics. In *Cardiovascular Diseases*; Papageorgiou, N., Ed.; Academic Press: Boston, MA, USA, 2016; pp. 3–24.
2. Gu, Q.; Paulose-Ram, R.; Burt, V.L.; Kit, B.K. Prescription cholesterol-lowering medication use in adults aged 40 and over: United States, 2003–2012. *NCHS Data Brief* 2014, *177*, 1–8.
3. Benjamin, E.J.; Blaha, M.J.; Chiuve, S.E.; Cushman, M.; Das, S.R.; Deo, R.; de Ferranti, S.D.; Floyd, J.; Fornage, M.; Gillespie, C.; et al. Heart Disease and Stroke Statistics-2017 Update: A Report from the American Heart Association. *Circulation* 2017, *135*, e146–e603.
4. Bentzon, J.F.; Otsuka, F.; Virmani, R.; Falk, E. Mechanisms of plaque formation and rupture. *Circ. Res.* 2014, *114*, 1852–1866.
5. Virmani, R.; Kolodgie, F.D.; Burke, A.P.; Finn, A.V.; Gold, H.K.; Tulenko, T.N.; Wrenn, S.P.; Narula, J. Atherosclerotic plaque progression and vulnerability to rupture: Angiogenesis as a source of intraplaque hemorrhage. *Arterioscler. Thromb. Vasc. Biol.* 2005, *25*, 2054–2061.
6. Parma, L.; Baganha, F.; Quax, P.H.; de Vries, M.R. Plaque angiogenesis and intraplaque hemorrhage in atherosclerosis. *Eur. J. Pharmacol.* 2017, *816*, 107–115.
7. Moreno, P.R.; Purushothaman, M.; Purushothaman, K.R. Plaque neovascularization: Defense mechanisms, betrayal, or a war in progress. *Ann. N. Y. Acad. Sci.* 2012, *1254*, 7–17.
8. Sluimer, J.C.; Kolodgie, F.D.; Bijmens, A.P.J.J.; Maxfield, K.; Pacheco, E.; Kutys, B.; Duimel, H.; Frederik, P.M.; van Hinsbergh, V.W.M.; Virmani, R.; et al. Thin-walled microvessels in human coronary atherosclerotic plaques show incomplete endothelial junctions: Relevance of compromised structural integrity for intraplaque microvascular leakage. *J. Am. Coll. Cardiol.* 2009, *53*, 1517–1527.
9. Lindblom, P.; Gerhardt, H.; Liebner, S.; Abramsson, A.; Enge, M.; Hellstrom, M.; Backstrom, G.; Fredriksson, S.; Landegren, U.; Nystrom, H.C.; et al. Endothelial PDGF-B retention is required for proper investment of pericytes in the microvessel wall. *Genes Dev.* 2003, *17*, 1835–1840.
10. Quaegebeur, A.; Lange, C.; Carmeliet, P. The Neurovascular Link in Health and Disease: Molecular Mechanisms and Therapeutic Implications. *Neuron* 2011, *71*, 406–424.
11. Armulik, A.; Genové, G.; Mäe, M.; Nisancioglu, M.H.; Wallgard, E.; Niaudet, C.; He, L.; Norlin, J.; Lindblom, P.; Strittmatter, K.; et al. Pericytes regulate the blood—Brain barrier. *Nature* 2010, *468*, 557–561.
12. Abramsson, A.; Lindblom, P.; Betsholtz, C. Endothelial and nonendothelial sources of PDGF-B regulate pericyte recruitment and influence vascular pattern formation in tumors. *J. Clin. Investig.* 2003, *112*, 1142–1151.
13. Levéen, P.; Pekny, M.; Gebre-Medhin, S.; Swolin, B.; Larsson, E.; Betsholtz, C. Mice deficient for PDGF B show renal, cardiovascular, and hematological abnormalities. *Genes Dev.* 1994, *8*, 1875–1887.
14. Rivera-Torres, J.; San José, E. Src Tyrosine Kinase Inhibitors: New Perspectives on Their Immune, Antiviral, and Senotherapeutic Potential. *Front. Pharmacol.* 2019, *10*, 1011–1011.
15. Heldin, C.H.; Westermark, B. Mechanism of action and in vivo role of platelet-derived growth factor. *Physiol. Rev.* 1999, *79*, 1283–1316.
16. Andrae, J.; Gallini, R.; Betsholtz, C. Role of platelet-derived growth factors in physiology and medicine. *Genes Dev.* 2008, *22*, 1276–1312.

17. Eming, S.A.; Yarmush, M.L.; Krueger, G.G.; Morgan, J.R. Regulation of the Spatial Organization of Mesenchymal Connective Tissue: Effects of Cell-Associated Versus Released Isoforms of Platelet-Derived Growth Factor. *Am. J. Pathol.* 1999, *154*, 281–289.
18. Deguchi, J.; Namba, T.; Hamada, H.; Nakaoka, T.; Abe, J.; Sato, O.; Miyata, T.; Makuuchi, M.; Kurokawa, K.; Takuwa, Y. Targeting endogenous platelet-derived growth factor B-chain by adenovirus-mediated gene transfer potently inhibits in vivo smooth muscle proliferation after arterial injury. *Gene Ther.* 1999, *6*, 956–965.
19. Fredriksson, L.; Li, H.; Eriksson, U. The PDGF family: Four gene products form five dimeric isoforms. *Cytokine Growth Factor Rev.* 2004, *15*, 197–204, doi:10.1016/j.cytogfr.2004.03.007.
20. Tang, J.; Kozaki, K.; Farr, A.G.; Martin, P.J.; Lindahl, P.; Betsholtz, C.; Raines, E.W. The absence of platelet-derived growth factor-B in circulating cells promotes immune and inflammatory responses in atherosclerosis-prone ApoE^{-/-} mice. *Am. J. Pathol.* 2005, *167*, 901–912.
21. Daugherty, A.; Tall, A.R.; Daemen, M.; Falk, E.; Fisher, E.A.; García-Cardena, G.; Lusis, A.J.; Owens, A.P.; Rosenfeld, M.E.; Virmani, R. Recommendation on Design, Execution, and Reporting of Animal Atherosclerosis Studies: A Scientific Statement From the American Heart Association. *Arter. Thromb. Vasc. Biol.* 2017, *37*, e131–e157.
22. Getz, G.S.; Reardon, C.A. Diet and Murine Atherosclerosis. *Arterioscler. Thromb. Vasc. Biol.* 2006, *26*, 242–249.
23. Seimon, T.A.; Wang, Y.; Han, S.; Senokuchi, T.; Schrijvers, D.M.; Kuriakose, G.; Tall, A.R.; Tabas, I.A. Macrophage deficiency of p38 α MAPK promotes apoptosis and plaque necrosis in advanced atherosclerotic lesions in mice. *J. Clin. Investig.* 2009, *119*, 886–898.
24. Vermes, I.; Haanen, C.; Steffens-Nakken, H.; Reutelingsperger, C. A novel assay for apoptosis flow cytometric detection of phosphatidylserine expression on early apoptotic cells using fluorescein labelled Annexin V. *J. Immunol. Methods* 1995, *184*, 39–51.
25. Wirka, R.C.; Wagh, D.; Paik, D.T.; Pjanic, M.; Nguyen, T.; Miller, C.L.; Kundu, R.; Nagao, M.; Collier, J.; Koyano, T.K.; et al. Atheroprotective roles of smooth muscle cell phenotypic modulation and the TCF21 disease gene as revealed by single-cell analysis. *Nat. Med.* 2019, *25*, 1280–1289.
26. Ma, W.F.; Hodonsky, C.J.; Turner, A.W.; Wong, D.; Song, Y.; Barrientos, N.B.; Mosquera, J.V.; Miller, C.L. Single-cell RNA-seq analysis of human coronary arteries using an enhanced workflow reveals SMC transitions and candidate drug targets. *BioRxiv* 2021, 2020.2010.2027.357715.
27. Gough, P.J.; Gomez, I.G.; Wille, P.T.; Raines, E.W. Macrophage expression of active MMP-9 induces acute plaque disruption in apoE-deficient mice. *J. Clin. Investig.* 2006, *116*, 59–69.
28. Rudijanto, A. The role of vascular smooth muscle cells on the pathogenesis of atherosclerosis. *Acta Med. Indones.* 2007, *39*, 86–93.
29. Barbieri, S.S.; Weksler, B.B. Tobacco smoke cooperates with interleukin-1 β to alter beta-catenin trafficking in vascular endothelium resulting in increased permeability and induction of cyclooxygenase-2 expression in vitro and in vivo. *FASEB J.* 2007, *21*, 1831–1843.
30. Gordts, P.L.S.M.; Esko, J.D. Heparan sulfate proteoglycans fine-tune macrophage inflammation via IFN- β . *Cytokine* 2015, *72*, 118–119.
31. Leppänen, P.; Koota, S.; Kholová, I.; Koponen, J.; Fieber, C.; Eriksson, U.; Alitalo, K.; Ylä-Herttuala, S. Gene Transfers of Vascular Endothelial Growth Factor-A, Vascular Endothelial Growth Factor-B, Vascular Endothelial Growth Factor-C, and Vascular Endothelial Growth Factor-D Have No

Effects on Atherosclerosis in Hypercholesterolemic Low-Density Lipoprotein-Receptor/Apolipoprotein B48-Deficient Mice. *Circulation* 2005, *112*, 1347–1352.

32. Perrotta, P.; Pintelon, I.; de Vries, M.R.; Quax, P.; Timmermans, J.P.; De Meyer, G.R.Y.; Martinet, W. Three-Dimensional Imaging of Intraplaque Neovascularization in a Mouse Model of Advanced Atherosclerosis. *J. Vasc. Res.* 2020, *57*, 348–354.

33. Petrovan, R.J.; Kaplan, C.D.; Reisfeld, R.A.; Curtiss, L.K. DNA vaccination against VEGF receptor 2 reduces atherosclerosis in LDL receptor-deficient mice. *Arter. Thromb. Vasc. Biol.* 2007, *27*, 1095–1100.

34. Sluimer, J.C.; Daemen, M.J. Novel concepts in atherogenesis: Angiogenesis and hypoxia in atherosclerosis. *J. Pathol.* 2009, *218*, 7–29.

35. Chistiakov, D.A.; Melnichenko, A.A.; Myasoedova, V.A.; Grechko, A.V.; Orekhov, A.N. Role of lipids and intraplaque hypoxia in the formation of neovascularization in atherosclerosis. *Ann. Med.* 2017, *49*, 661–677.

36. Ross, R.; Glomset, J.A. The Pathogenesis of Atherosclerosis. *N. Engl. J. Med.* 1976, *295*, 369–377.

37. Nyström, H.C.; Lindblom, P.; Wickman, A.; Andersson, I.; Norlin, J.; Fäldt, J.; Lindahl, P.; Skøtt, O.; Bjarnegård, M.; Fitzgerald, S.M.; et al. Platelet-derived growth factor B retention is essential for development of normal structure and function of conduit vessels and capillaries. *Cardiovasc. Res.* 2006, *71*, 557–565.

38. Kozaki, K.; Kaminski, W.E.; Tang, J.; Hollenbach, S.; Lindahl, P.; Sullivan, C.; Yu, J.-C.; Abe, K.; Martin, P.J.; Ross, R.; et al. Blockade of Platelet-Derived Growth Factor or Its Receptors Transiently Delays but Does Not Prevent Fibrous Cap Formation in ApoE Null Mice. *Am. J. Pathol.* 2002, *161*, 1395–1407.

39. Onwuka, E.; Best, C.; Sawyer, A.; Yi, T.; Heuer, E.; Sams, M.; Wiet, M.; Zheng, H.; Kyriakides, T.; Breuer, C. The role of myeloid cell-derived PDGF-B in neotissue formation in a tissue-engineered vascular graft. *Regen. Med.* 2017, *12*, 249–261.

40. Okura, T.; Igase, M.; Kitami, Y.; Fukuoka, T.; Maguchi, M.; Kohara, K.; Hiwada, K. Platelet-derived growth factor induces apoptosis in vascular smooth muscle cells: Roles of the Bcl-2 family. *Biochim. Biophys. Acta Mol. Cell Res.* 1998, *1403*, 245–253.

41. Lepidi, S.; Kenagy, R.D.; Raines, E.W.; Chiu, E.S.; Chait, A.; Ross, R.; Clowes, A.W. MMP9 production by human monocyte-derived macrophages is decreased on polymerized type I collagen. *J. Vasc. Surg.* 2001, *34*, 1111–1118.

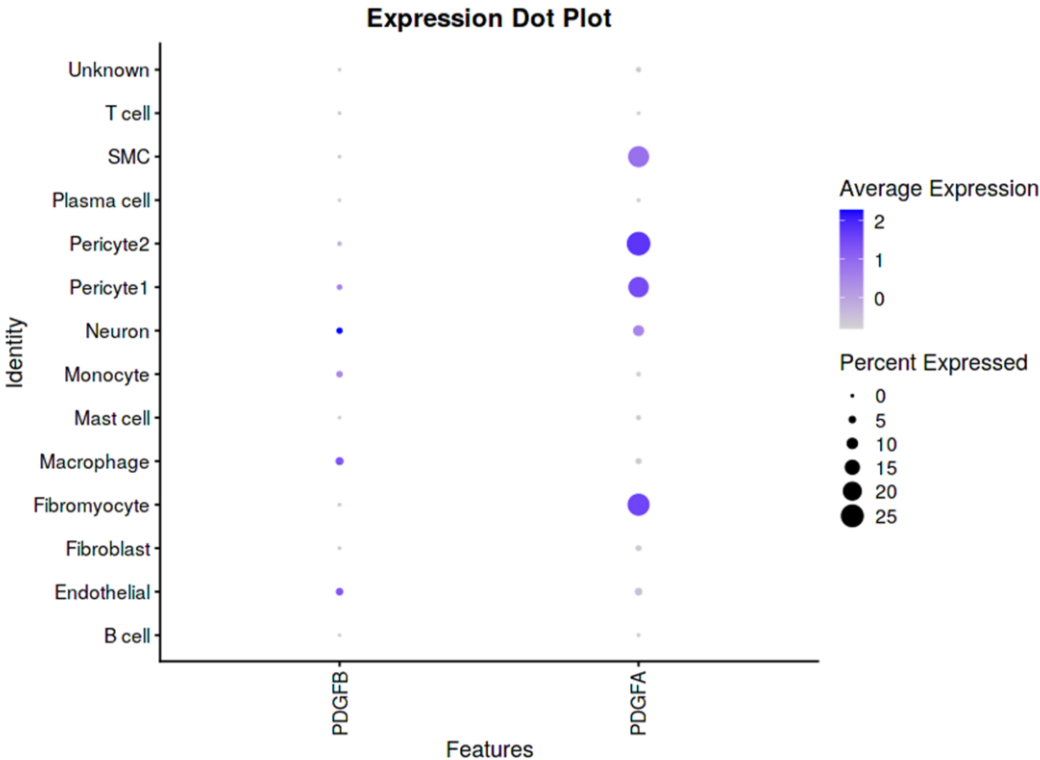
42. Czochra, P.; Klopčič, B.; Meyer, E.; Herkel, J.; Garcia-Lazaro, J.F.; Thieringer, F.; Schirmacher, P.; Biesterfeld, S.; Galle, P.R.; Lohse, A.W.; et al. Liver fibrosis induced by hepatic overexpression of PDGF-B in transgenic mice. *J. Hepatol.* 2006, *45*, 419–428.

43. Dong, M.; Zhou, C.; Ji, L.; Pan, B.; Zheng, L. AG1296 enhances plaque stability via inhibiting inflammatory responses and decreasing MMP-2 and MMP-9 expression in ApoE^{-/-} mice. *Biochem. Biophys. Res. Commun.* 2017, *489*, 426–431.

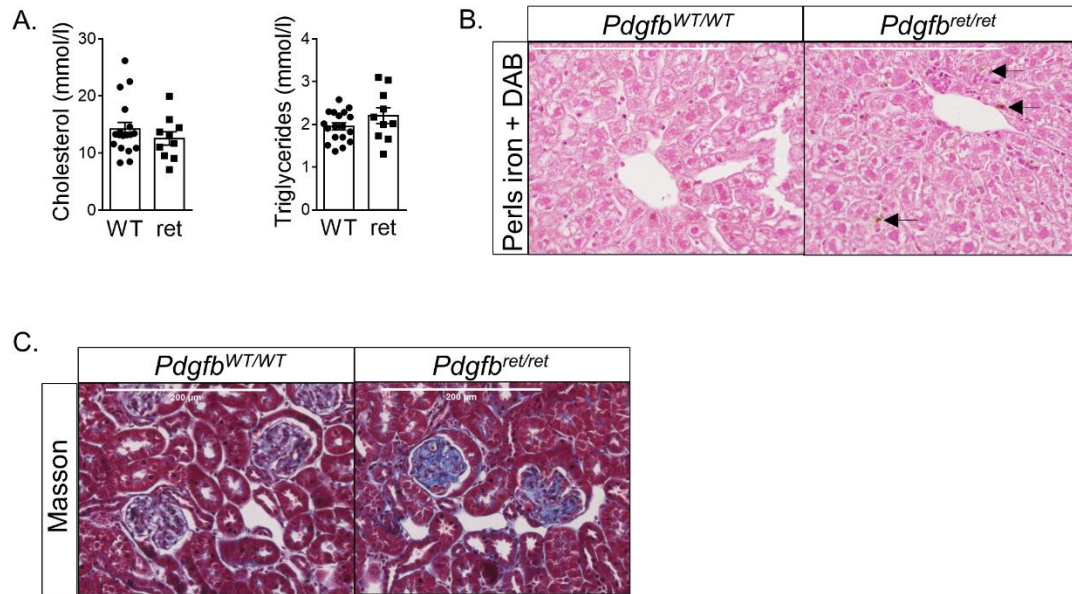
44. Onogi, Y.; Wada, T.; Kamiya, C.; Inata, K.; Matsuzawa, T.; Inaba, Y.; Kimura, K.; Inoue, H.; Yamamoto, S.; Ishii, Y.; et al. PDGFR β Regulates Adipose Tissue Expansion and Glucose Metabolism via Vascular Remodeling in Diet-Induced Obesity. *Diabetes* 2017, *66*, 1008–1021.

45. Raines, S.M.; Richards, O.C.; Schneider, L.R.; Schueler, K.L.; Rabaglia, M.E.; Oler, A.T.; Stapleton, D.S.; Genové, G.; Dawson, J.A.; Betsholtz, C.; et al. Loss of PDGF-B activity increases hepatic vascular permeability and enhances insulin sensitivity. *Am. J. Physiol. Endocrinol. Metab.* 2011, *301*, E517–E526.
46. Kaminski, W.E.; Lindahl, P.; Lin, N.L.; Broudy, V.C.; Crosby, J.R.; Hellström, M.; Swolin, B.; Bowen-Pope, D.F.; Martin, P.J.; Ross, R.; et al. Basis of hematopoietic defects in platelet-derived growth factor (PDGF)-B and PDGF beta-receptor null mice. *Blood* 2001, *97*, 1990–1998.
47. Xue, Y.; Lim, S.; Yang, Y.; Wang, Z.; Jensen, L.D.E.; Hedlund, E.-M.; Andersson, P.; Sasahara, M.; Larsson, O.; Galter, D.; et al. PDGF-BB modulates hematopoiesis and tumor angiogenesis by inducing erythropoietin production in stromal cells. *Nat. Med.* 2012, *18*, 100–110.
48. Damrongwatanasuk, R.; Fradley, M.G. Cardiovascular Complications of Targeted Therapies for Chronic Myeloid Leukemia. *Curr. Treat. Options Cardiovasc. Med.* 2017, *19*, 24.

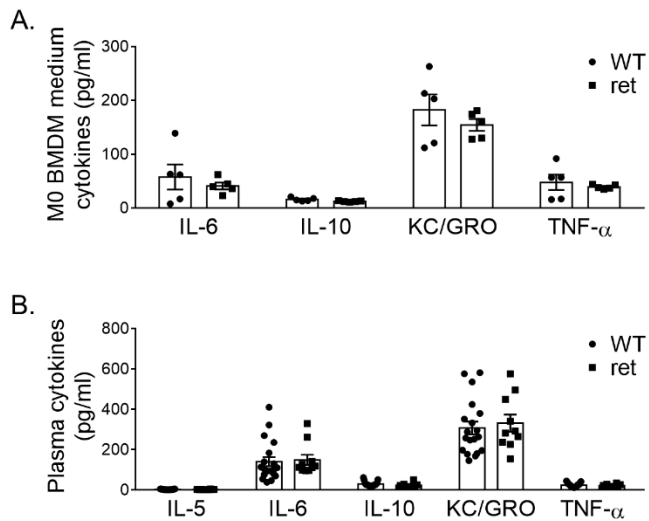
Supplementary data



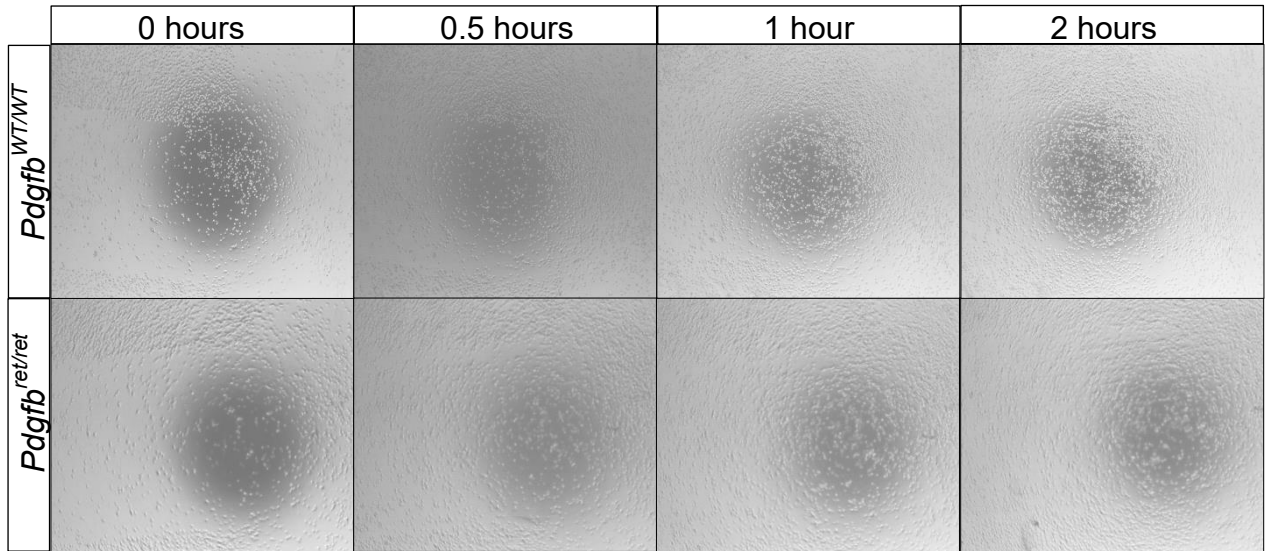
Supplementary Figure S1: PDGFB and PDGFA expression in human atherosclerosis. Dot plot of PDGFB and PDGFA expression in single-cell populations of human atherosclerotic coronary arteries (Wirka et al.²⁵). SMC; smooth muscle cell.



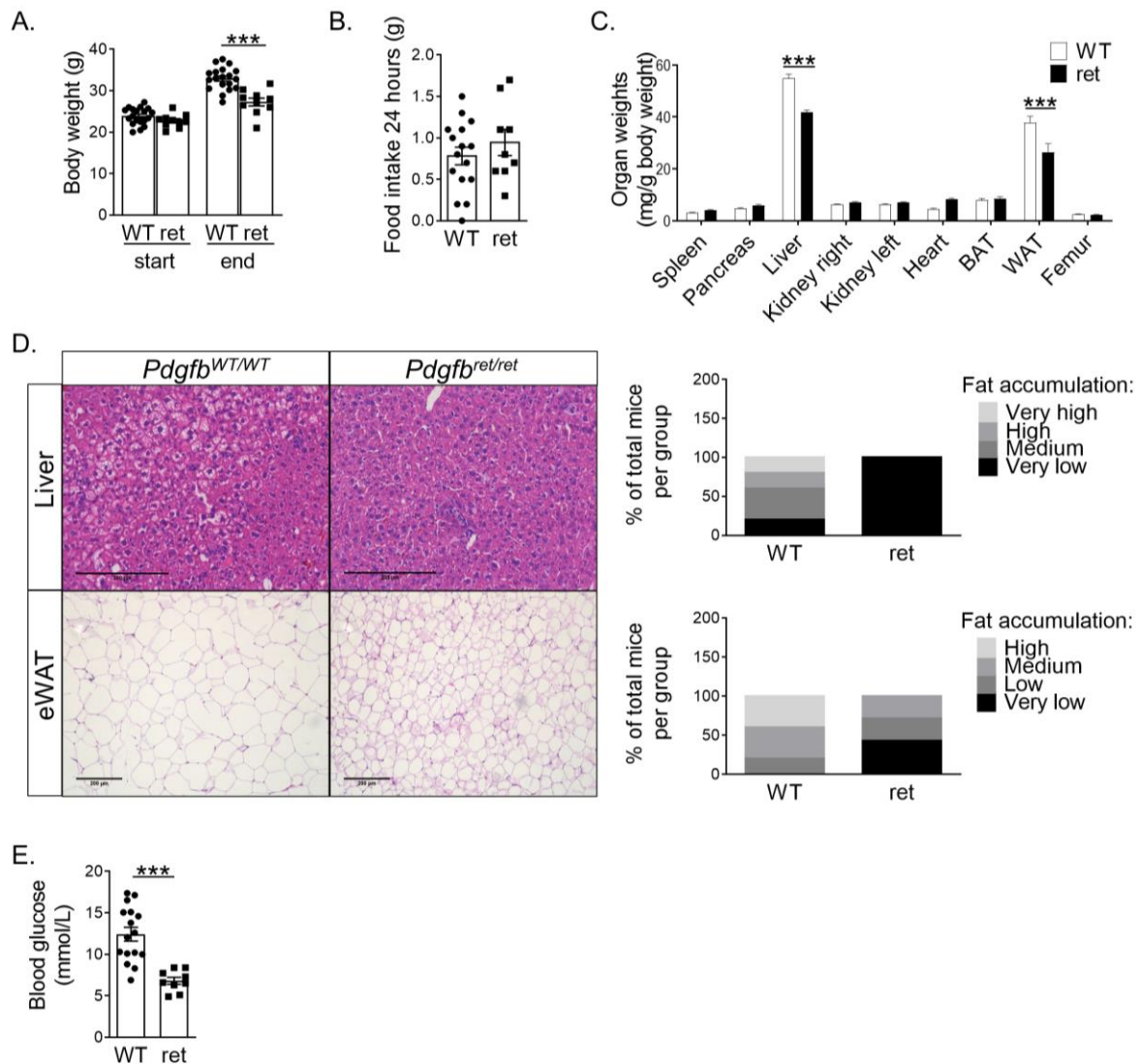
Supplementary Figure S2: Similar cholesterol and triglyceride levels in *Pdgfb*^{WT/WT} and *Pdgfb*^{ret/ret} plasma and affected *Pdgfb*^{ret/ret} liver and kidney. (A) Cholesterol and triglyceride levels in *Pdgfb*^{WT/WT} ($n = 18$) and *Pdgfb*^{ret/ret} ($n = 10$) plasma. (B) Representative photomicrographs of Perls iron staining combined with DAB in *Pdgfb*^{WT/WT} and *Pdgfb*^{ret/ret} liver. (C) Representative photomicrographs of Masson staining in *Pdgfb*^{WT/WT} and *Pdgfb*^{ret/ret} kidney, in which ECM is stained blue. Graphs represent mean \pm SEM. Scale bars 200 μ m. Data were tested for normality (Shapiro-Wilk) and equal variances (F-test). Variables that did not pass, were analyzed using Mann-Whitney U test. Variables that did pass, were analyzed using Student's t-test.



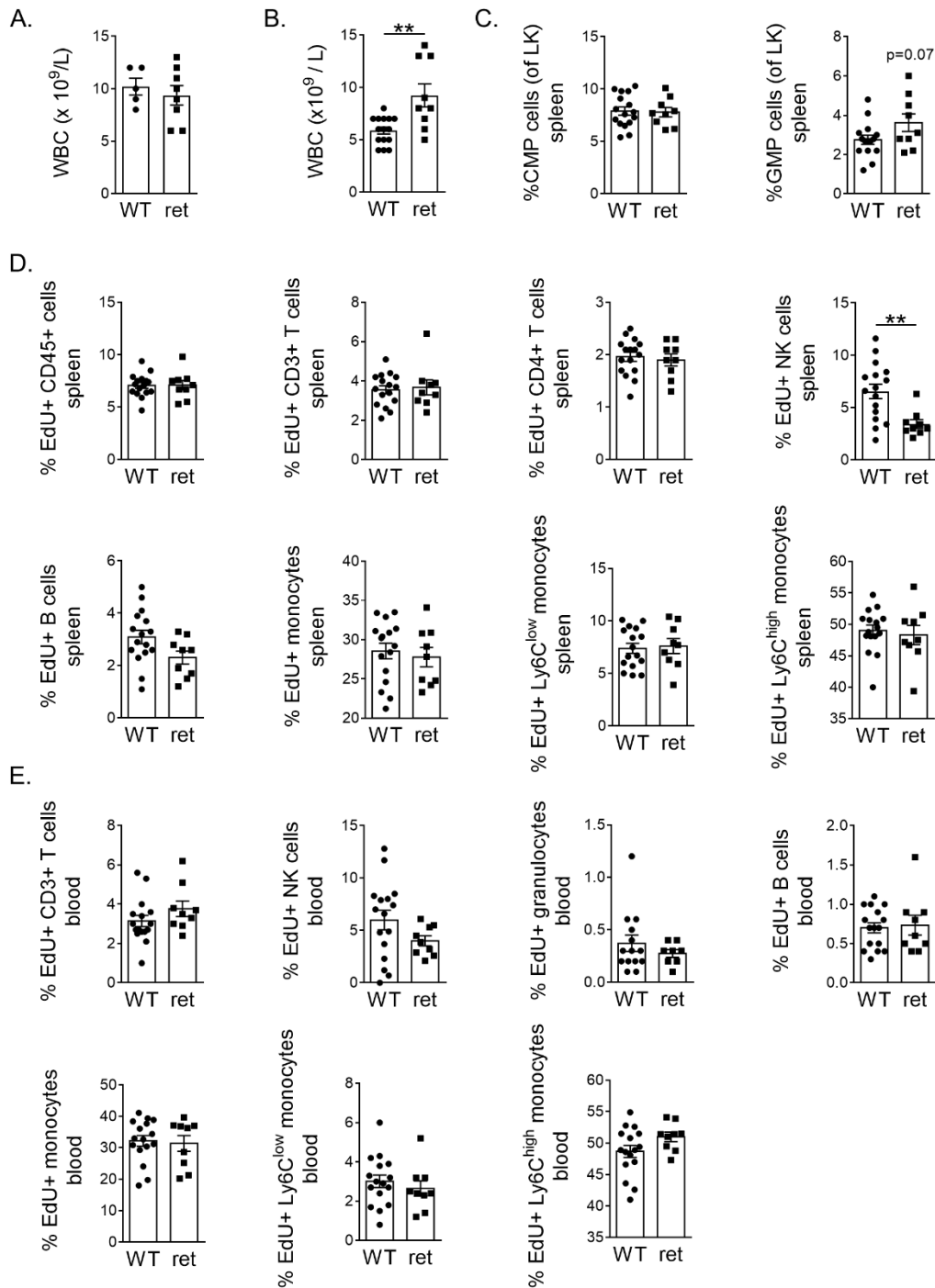
Supplementary Figure S3: Pro-inflammatory cytokine levels in plasma and BMDM conditioned medium unaffected. (A) Levels of interleukin 6 (IL-6), IL-10, keratinocyte-derived chemokine/growth-related oncogene (KC/GRO or CXCL1) and tumor necrosis factor- α (TNF α) in BMDM-derived medium ($n = 5$). IFN- γ , IL-1 β , IL-5, IL-12 p70, IL-2 and IL-4 levels were undetectable. (B) Levels of IL-5, IL-6, IL-10, KC/GRO and TNF- α in *Pdgfb*^{WT/WT} ($n = 19$) and *Pdgfb*^{ret/ret} ($n = 10$) plasma. Levels of interferon-gamma (IFN- γ), IL-1 β , IL-12 p70, IL-2 and IL-4 were undetectable. Graphs represent mean \pm SEM. Data were analyzed using two-way ANOVA.



Supplementary Figure S4: Pictures of BMDM scratch assay to assess migration *in vitro*. Representative pictures of *Pdgfb*^{WT/WT} and *Pdgfb*^{ret/ret} BMDM migration over time (t = 0, 0.5 hours, 1 hour and 2 hours) after scratch infliction.



Supplementary Figure S5: Decreased body weight gain and fat accumulation in *Pdgfb*^{ret/ret} liver and epididymal white adipose tissue (eWAT). (A) *Pdgfb*^{WT/WT} (n = 19) and *Pdgfb*^{ret/ret} (n = 10) body weight before and after 10 weeks of high cholesterol diet (HCD) (B) 24-hour food intake as assessed in metabolic cages, in the 9th week of HCD. (C) Organ weights after 10 weeks of HCD, relative to body weight. (D) Fat accumulation as assessed by visual analogue scores ranging from very low to very high fat accumulation in HE-stained *Pdgfb*^{WT/WT} (n = 5) and *Pdgfb*^{ret/ret} (n = 7) liver and eWAT, with corresponding photomicrographs. (E) Blood glucose levels after 10 weeks of HCD. Results shown in B, C and E were obtained using 16 *Pdgfb*^{WT/WT} and 9 *Pdgfb*^{ret/ret} mice. Scale bars 200 μ m. Graphs represent mean \pm SEM. *** p < 0.001. Data were tested for normality (Shapiro-Wilk) and equal variances (F-test). Variables that did not pass, were analyzed using Mann-Whitney U test. Variables that did pass, were analyzed using Student's t-test. Data in A and C were analyzed using two-way ANOVA, including Bonferroni's multiple comparisons test.



Supplementary Figure S6: *Pdgfb*^{ret/ret} leukocytosis confirmation in second mouse experiment after HCD and percentages of EdU positive leukocytes in blood and spleen. (A) White blood cell (WBC) counts in blood from *Pdgfb*^{WT/WT} ($n = 5$) and *Pdgfb*^{ret/ret} ($n = 8$) mice on standard laboratory diet. (B) WBC counts in *Pdgfb*^{WT/WT} ($n = 15$) and *Pdgfb*^{ret/ret} ($n = 9$) blood after 10 weeks HCD in the second mouse experiment. (C) Percentage progenitor cells of lineage^c-Kit⁺ cells in *Pdgfb*^{WT/WT} ($n = 15-16$) and *Pdgfb*^{ret/ret} ($n = 9$) spleen. CMP = common myeloid progenitor, GMP = granulocyte monocyte progenitor. (D) Percentage of EdU positive leukocytes in *Pdgfb*^{WT/WT} ($n = 14-16$) and *Pdgfb*^{ret/ret} ($n = 9$) spleen and (E) blood. Graphs represent mean \pm SEM. ** $p < 0.01$. Data were tested for normality (Shapiro-Wilk) and equal variances (F-test). Variables that did not pass, were analyzed using Mann-Whitney U test. Variables that did pass, were analyzed using Student's t-test.

Supplementary Table S1: Immunohistochemical staining protocols of murine aortic root cryosections

	αSMA Double staining with CD31	CD31 Double staining with αSMA	PDGF-B	MOMA-2
Fixation	Dry acetone		4% PFA in PBS	Dry acetone
Permeabilization	-		0.25% Triton-x100 in PBS	-
Blocking	0.3% H ₂ O ₂ in methanol Serum-free protein block (X0909, DAKO)		0.3% H ₂ O ₂ in methanol	0.3% H ₂ O ₂ in methanol PBS 4% FCS and avidin block 1:5 (SP-2001, Vector)
Primary antibody Cat. no and company	F3777, Sigma FITC-conjugated	550274, BD	Ab23914, Abcam	Molecular Genetics department Maastricht University
Primary antibody dilution and buffer	1:300 TBS	1:25 TBS	1:700 TBT (TBS + 1% BSA + 0.1% Tween)	1:50 PBS, 4% FCS, biotin block 1:5 (SP-2001, Vector)
Secondary antibody Cat. no and company	Sheep anti-FITC- HRP, 11.426.346.910 Roche	Biotinylated rabbit anti- rat, BA-4001, Vector	Brightvision poly- HRP-anti-rabbit, DPVR-55-HRP, Immunologic	Biotinylated rabbit anti-rat, Molecular Genetics department Maastricht University
Secondary antibody dilution and buffer	1:300 TBS	1:200 TBS	-	1:300 PBS, 2% normal mouse serum (X0910, DAKO), 4% FCS
Tertiary step/antibody Cat. no and company	-	ABC-AP kit (AK-5000, Vector)	-	ABC-HRP kit (PK-4000, Vector)
Stain development	3,3'- diaminobenzidine kit (K346811-2, Agilent)	Vector Blue substrate kit, alkaline phosphatase (SK-5300, Vector)	3,3'- diaminobenzidine kit (K346811-2, Agilent)	AEC kit (2% buffer, 3% AEC, 2% H ₂ O ₂ in milliQ, K3461, DAKO)

FCS; fetal calf serum, PBS; phosphate-buffered saline, PFA; paraformaldehyde, TBS; tris-buffered saline.

Supplementary Table S2: Primer sets used for genotype confirmation through PCR and electrophoresis

Gene	Forward primer (5' - 3')	Reverse primer (5' - 3')
<i>Pdgfb</i> ^{WT}	CATGCTGCCTTGTAATCCGTTC	CGGCGGATTCTCACCGT
<i>Pdgfb</i> ^{ret}	CTCGGGTGACCATTCCGTAA	TCTAAGTCACAGCCAGGGAGT AGC

Supplementary Table S3: Primer sets used for qPCR

Gene	Forward primer (5' - 3')	Reverse primer (5' - 3')
<i>18s rRNA</i>	GTAACCCGTTGAACCCATT	CCATCCAATCGGTAGTAGCG
<i>Pdgfb</i>	CGGTCCAGGTGAGAAAGATTG	CGTCTTGGCTCGCTGCTC
<i>Pdgfra</i>	AGAGAGAATCGGCCCCAGTG	CCATAGCTCCTGAGACCCGC
<i>Pdgfrb</i>	GGCCTTAGTGGTCCTTACCG	GCACAGGGTCCACGTAGATG

Supplementary Table S4: Antibodies used for flow cytometry

Antibody	Company	Catalog number	Dilution used
CD16/32	eBioscience	14-0161-82	1:100
CD45 PerCP	Biolegend	103130	1:100
CD3 eFluor 450	eBioscience	48-0032-82	1:100
NK-1.1 PE	BD Pharmingen	557391	1:100
Ly6G APC-Cy7	BD Pharmingen	560600	1:100
CD11b PE-Cy7	BD Pharmingen	552850	1:300
Ly-6C APC	Miltenyi Biotec	130-102-341	1:10
CD4 APC-H7	BD Pharmingen	560181	1:100
CD8 V500	BD Horizon	560776	1:200
CD8 FITC	eBioscience	11-0081-85	1:50
B220 V500	BD Horizon	561226	1:50
Sca-1 PerCP-Cyanine 5.5	eBioscience	45-5981-82	1:1000
c-Kit APC-eFluor780	eBioscience	47-1171-82	1:100
CD34 eFluor450	eBioscience	48-0341-82	1:50
CD16/32 PE-Cy7	eBioscience	25-0161-82	1:1000
B220 PE	BD Pharmingen	553089	1:100
CD3 PE	eBioscience	12-0031-82	1:800
CD11b PE	eBioscience	12-0112-82	1:800
Ly-6G PE	BD Pharmingen	551461	1:100
NK-1.1 PE	BD Pharmingen	557391	1:100
TER-119 PE	eBioscience	12-5921-82	1:200

Chapter 3

Partial inhibition of the 6-phosphofructo-2-kinase/fructose-2,6-bisphosphatase-3 (PFKFB3) enzyme in myeloid cells does not affect atherosclerosis

Renée J.H.A. Tillie, Jenny de Bruijn, Javier Perales-Patón, Lieve Temmerman, Yanal Ghosheh, Kim van Kuijk, Marion J. Gijbels, Peter Carmeliet, Klaus Ley, Julio Saez-Rodriguez, Judith C. Sluimer

Frontiers in Cell and Developmental Biology, 2021, Aug 12, 9:695684

Abstract

The protein 6-phosphofructo-2-kinase/fructose-2,6-bisphosphatase-3 (PFKFB3) is a key stimulator of glycolytic flux. Systemic, partial PFKFB3 inhibition previously decreased total plaque burden and increased plaque stability. However, it is unclear which cell type conferred these positive effects. Myeloid cells play an important role in atherogenesis, and mainly rely on glycolysis for energy supply. Thus, we studied whether myeloid inhibition of PFKFB3-mediated glycolysis in low-density lipoprotein receptor knockout (*Ldlr*^{-/-}) lysozyme M (*LysM*)*Cre*^{+/-}*Pfkfb3*^{fl/fl} (*Pfkfb3*^{fl/fl}) mice confers beneficial effects on plaque stability and alleviates cardiovascular disease burden compared to *Ldlr*^{-/-}*LysM**Cre*^{+/-}*Pfkfb3*^{wt/wt} control mice (*Pfkfb3*^{wt/wt}).

Analysis of atherosclerotic human and murine single-cell populations confirmed *PFKFB3/Pfkfb3* expression in myeloid cells, but also in lymphocytes, endothelial cells, fibroblasts and smooth muscle cells. *Pfkfb3*^{wt/wt} and *Pfkfb3*^{fl/fl} mice were fed a 0.25% cholesterol diet for 12 weeks. *Pfkfb3*^{fl/fl} bone marrow-derived macrophages (BMDMs) showed 50% knockdown of *Pfkfb3* mRNA. As expected based on partial glycolysis inhibition, extracellular acidification rate as a measure of glycolysis was partially reduced in *Pfkfb3*^{fl/fl} compared to *Pfkfb3*^{wt/wt} BMDMs. Unexpectedly, plaque and necrotic core size, as well as macrophage (MAC3), neutrophil (lymphocyte antigen 6G, Ly6G) and collagen (Sirius Red) content were unchanged in advanced *Pfkfb3*^{fl/fl} lesions. Similarly, early lesion plaque and necrotic core size and total plaque burden were unaffected.

In conclusion, partial myeloid knockdown of PFKFB3 did not affect atherosclerosis development in advanced or early lesions. Previously reported positive effects of systemic, partial PFKFB3 inhibition on lesion stabilization, do not seem conferred by monocytes, macrophages or neutrophils. Instead, other *Pfkfb3*-expressing cells in atherosclerosis might be responsible, such as DCs, smooth muscle cells or fibroblasts.

Introduction

Myeloid cells (i.e. monocytes, macrophages, neutrophils and dendritic cells (DCs)) play an active role in atherogenesis. Early pathogenesis of atherosclerotic plaques is characterized by activation of intimal endothelial cells (ECs) in arteries, followed by extravasation of low-density lipoprotein (LDL) cholesterol¹. In the subendothelial space, LDL is oxidized (oxLDL) by reactive oxygen species (ROS) and enzymes¹. This results in a pro-inflammatory response that triggers myeloid cell recruitment^{2, 3}. Recruited myeloid cells act in parallel to stimulate inflammation through cytokine secretion and other mechanisms. Recruited, activated neutrophils further stimulate monocyte recruitment and macrophage activation. Furthermore, neutrophils contribute to the pro-inflammatory environment by secretion of ROS and neutrophil extracellular traps (NETs), and to LDL oxidation by secreting myeloperoxidase³. DCs modulate T cell responses in atherosclerosis. Additionally, recruited monocytes can differentiate into macrophages or monocyte-derived DCs (moDCs), which ingest oxLDL and become lipid-laden foam cells^{2, 4, 5}. Excess uptake of oxLDL can result in leukocyte apoptosis. In advanced disease stages, accumulation of apoptotic leukocytes in combination with decreased phagocytic clearance contributes to formation of a detrimental necrotic core². Moreover, during atherogenesis, smooth muscle cells (SMCs) migrate into the plaque and synthesize collagen, forming a stabilizing fibrous cap. Secretion of matrix metalloproteinases, serine proteases and NETs by macrophages and neutrophils can cause fibrous cap thinning^{2, 3}. This increases the risk of plaque rupture, which can have detrimental consequences.

Activated neutrophils, DCs and pro-inflammatory macrophages highly depend on glycolysis for their energy production and function⁶⁻⁸. During glycolysis, glucose is metabolized to pyruvate, yielding ATP and NADH⁹. A rate-limiting step of glycolysis is the conversion of fructose-6-phosphate into fructose-1,6-bisphosphate, catalyzed by phosphofructokinase-1 (PFK-1). Another enzyme, 6-phosphofructo-2-kinase/fructose-2,6-bisphosphatase-3 (PFKFB3), catalyzes the conversion of fructose-6-phosphate into fructose-2,6-bisphosphate, which is an allosteric activator of PFK-1. Thus, PFKFB3 is a potent stimulator of glycolytic rate⁹, and possibly an attractive target to interfere with myeloid cell function in atherogenesis.

A few studies have indeed assessed the effect of systemic administration of 3-(3-pyridinyl)-1-(4-pyridinyl)-2-propen-1-one (3PO) or derivatives to partially inhibit PFKFB3 in atherosclerosis. These studies reported decreased total plaque burden¹⁰ and increased plaque stabilization, respectively^{11, 12}. However, as these studies entailed systemic pharmacological PFKFB3 inhibition, it is unclear which cell type confers these positive effects. Although *Pfkfb3* expression in atherosclerotic DCs and neutrophils remains to be assessed, Tawakol et al. reported increased *Pfkfb3* expression in macrophages incubated with atherosclerosis-relevant stimuli *in vitro*. This effect was exacerbated by hypoxia¹³. Still, the *in vivo* effect of partial

inhibition of PFKFB3-mediated glycolysis, specifically in myeloid cells, on atherogenesis has not been studied. Thus, we studied the hypothesis that myeloid inhibition of PFKFB3-mediated glycolysis in *Ldlr*^{-/-}*LysMCre*^{+/-}*Pfkfb3*^{fl/fl} (*Pfkfb3*^{fl/fl}) mice confers beneficial effects on plaque stability and alleviates cardiovascular disease burden compared to *Ldlr*^{-/-}*LysMCre*^{+/-}*Pfkfb3*^{wt/wt} control mice (*Pfkfb3*^{wt/wt}).

Materials and methods

Single-cell gene expression analysis

Single-cell RNA-sequencing (scRNA-seq) datasets from atherosclerotic plaques were collected from Gene Expression Omnibus (GEO) database or requested to corresponding authors: Wirka et al. 2019¹⁴ (4 human specimens, GSE131780), Zernecke et al. 2020¹⁵ (meta-analysis from 9 mice datasets), and Van Kuijk et al.¹⁶ (11 pooled *Ldlr*^{-/-}*LysMCre*^{+/-} mice, GSE150089). Seurat R package (v3.0.1) was used as toolbox for analysis¹⁷ in R (v3.6.1). Single-cell gene expression was normalized by library size, multiplied by a scaling factor of 10,000 and log-transformed. Original cell cluster annotations were used for analysis. *HIF1α/Hif1α* (hypoxia-inducible factor 1-alpha) transcription factor (TF) activity was estimated using DoRothEA (<https://saezlab.github.io/dorothea/>)¹⁸, using the TF regulons of A, B, and C confidence classes as previously described¹⁹. For 2-group comparison between cells undergoing and not undergoing hypoxia response, cells were stratified by the third quartile (Q3) of *HIF1A/Hif1a* TF activity within each cell cluster (high > Q3, low ≤ Q3). Differential *PFKFB3/Pfkfb3* expression was performed using Wilcoxon Rank Sum test. No test was performed when the sample size of any condition was lower than 5 observations. P-values were adjusted for multiple testing using the Benjamini & Hochberg method. R effect sizes from Wilcoxon Rank-Sum test were calculated as Z divided by the square root of total observations. The greater the absolute r value, the greater the effect size, with positive values for an effect in cells with High *HIF1A/Hif1a* activity. Dot plots show the percentage of cells within cell clusters that express the gene (size), and average expression of each cluster scaled across clusters. Violin plots show the normalized gene expression level of each cell cluster with individual observations (each cell) as data points, 50th percentile of the distribution as a horizontal line, and sample sizes (number of cells) at the bottom. For 2-group comparisons, violin plots are split by hypoxia response stratification, with Wilcoxon test statistics of FDR-adjusted p-values and r effect sizes at the top. Analysis code is available at https://github.com/saezlab/Myeloid_PFKFB3_atherosclerosis.

Experimental animals

Mouse experiments were approved by regulatory authorities of Maastricht University Medical Centre and performed in compliance with Dutch governmental guidelines and European Parliament Directive 2010/63/EU on protection of animals used for scientific purposes. Mice with a loxP-flanked *Pfkfb3* gene (*Pfkfb3*^{lox/lox})²⁰ were crossed to mice with both a low-density lipoprotein receptor knockout (*Ldlr*^{-/-}) to ensure atherosclerosis susceptibility, and hemizygous Cre-recombinase expression under control of the *Lyz2* gene promoter (*LysMCre*^{+/-}). *Lyz2* is highly expressed in macrophages, monocytes and neutrophils, and to a lower extent in DCs²¹ (**Supplementary (S) Figure S1A**). Thus, myeloid-specific Cre-mediated excision of the *Pfkfb3* gene could be ensured. Resulting mice (*Ldlr*^{-/-}*LysMCre*^{+/-}*Pfkfb3*^{fl/fl}) are referred to as *Pfkfb3*^{fl/fl}.

Ldlr^{-/-}LysMCre^{+/-}Pfkfb3^{wt/wt} mice were used as controls (*Pfkfb3^{wt/wt}*). Mice were housed in the Maastricht University laboratory animal facility under standard conditions, in individually ventilated cages (GM500, Techniplast) with up to 5 animals per cage, with bedding (corn cob, Technilab-BMI) and cage enrichment. Cages were changed weekly, reducing handling of mice during non-intervention periods.

Induction of atherosclerosis and tissue collection

To induce atherosclerosis, 11-week-old male *Pfkfb3^{wt/wt}* and *Pfkfb3^{fl/fl}* mice were fed a high cholesterol diet (HCD) for 12 weeks *ad libitum*, containing 0.25% cholesterol (824171, Special Diet Services). Mice were euthanized by intraperitoneal pentobarbital injection (100 mg/kg). Blood was withdrawn from the right ventricle and centrifuged (2100 rpm, 10 minutes, 4°C). Plasma aliquots were stored at -80°C. Brachiocephalic arteries (BCAs) and hearts were dissected, fixed in 1% PFA overnight and paraffin-embedded.

Plasma cholesterol and triglyceride levels

Plasma cholesterol (Cholesterol FS Ecoline, 113009990314; DiaSys Diagnostic Systems GmbH) and triglyceride (FS5' Ecoline, 157609990314; DiaSys Diagnostic Systems GmbH) levels were assessed by standard enzymatic techniques, automated on the Cobas Fara centrifugal analyzer (Roche).

Histology and immunohistochemistry

Paraffin-embedded BCA and aortic root (AR) were serially sectioned (4 µm) and stained with hematoxylin and eosin (H&E) to quantify plaque size and necrotic core content. For ARs, five consecutive H&E sections with 20 µm intervals were blinded and analyzed using computerized morphometry (Leica QWin V3, Cambridge, UK). The sum of plaque within three valves was averaged per mouse. Total plaque burden was quantified in BCA (\sum total plaque length/ \sum total vessel length). Furthermore, AR atherosclerotic plaques were analyzed for macrophage content (MAC3+ area/plaque area, 553322, BD), collagen content (Sirius Red+ area/plaque area, 09400, Polyscience) and neutrophil content (lymphocyte antigen 6G (Ly6G)+ cells/plaque area, 551459, BD). Antigen retrieval was performed with pepsin digestion (Ly6G) or at pH 6 (MAC3, Target Retrieval Solution, S2031, DAKO). Stainings were analyzed using Leica Qwin software (V3, Cambridge UK) or QuPath V0.2.3²².

Isolation and differentiation of bone marrow cells

Femur and tibia of *Pfkfb3^{wt/wt}* and *Pfkfb3^{fl/fl}* mice on standard laboratory diet were dissected. Bones were flushed with phosphate-buffered saline (PBS) and cells passed through a 70 µm cell strainer.

To obtain bone marrow-derived macrophages (BMDMs), bone marrow cells were cultured in RPMI 1640 medium (72400047, Gibco), with 15% L929-conditioned medium, 10% fetal bovine serum (FBS, FBS-12A, Capricorn Scientific) and 1% penicillin-streptomycin (15070-063, Gibco). After 7-day differentiation, BMDMs were detached with lidocaine and plated for downstream assays. For pro-inflammatory polarization of BMDMs, cells were incubated with lipopolysaccharide (LPS, 10 ng/mL, L2880, Sigma) and interferon-gamma (IFN- γ , 100 units/mL, HC1020, Hycult Biotech) for 24 hours after overnight attachment.

To obtain bone marrow-derived DCs, bone marrow cells were cultured in IMDM medium (21980032, Thermo Fisher Scientific), with 5% FBS, 0.029 mM 2-mercaptoethanol, 150 ng/mL Flt3 ligand (472-FL, R&D Systems) and 1% penicillin-streptomycin for 8 days. After differentiation, DCs were detached by rinsing.

Flow cytometry dendritic cells

Flow cytometry was performed to confirm cluster of differentiation (CD)11c protein expression in bone marrow-derived dendritic cells. Fc receptors were blocked (CD16/CD32 antibody, 1:100, 14-0161, Invitrogen) and LIVE/DEAD Fixable Aqua Stain was used to assess viability (1:1000, L34957, Invitrogen). Thereafter, cells were stained with a CD11c antibody (PE-Cy7 conjugated, 1:1000, 25-0114, Invitrogen). Flow cytometry samples were measured with a BD FACSCanto II and analyzed with BD FACSDiva Software Version 6.1.2 (BD Biosciences).

Quantitative PCR

RNA was isolated with TRIzol reagent (15596026, Thermo Fisher Scientific) according to manufacturer's protocol. RNA concentrations were determined by NanoDrop 2000 (Thermo Fisher Scientific) and reverse transcription performed following manufacturer's protocol (1708890, Bio-Rad and 04379012001, Roche). Real-time qPCR was performed using 10 ng cDNA, SYBR Green Supermix (1708885, Bio-Rad) and specific primer sets (**Table S1**). One housekeeping gene (18s rRNA) was used to correct for different mRNA quantities between samples.

Lactate and glucose levels

Lactate and glucose levels in *Pfkfb3*^{wt/wt} and *Pfkfb3*^{fl/fl} BMDM cell culture medium were assessed after 26 hours of conditioning, using a GEM Premier 4000 Analyzer and the manufacturer's protocol (Instrumentation Laboratory).

Seahorse

BMDMs were plated onto XF96 tissue culture microplates. Growth medium was replaced with glucose-free assay medium (RPMI-1640 (R1383, Sigma), 143 mM NaCl, 3 mg/L Phenol Red, 2 mM L-glutamine, in dH₂O, pH 7.35) and cells were incubated in a non-CO₂ incubator for 1 hour. Thereafter, the assay was performed according to manufacturer's protocol (103020-100, Agilent), using a 10 mM glucose stimulus, with a Seahorse XF96 Analyzer (Agilent).

Statistical analyses

Data are represented as mean \pm standard error of the mean (SEM). For results besides single-cell analysis, ROUT outlier analysis was performed and subsequently, normality (Shapiro-Wilk) and equal variances (F-test) analysis and corresponding parametric or non-parametric testing were performed for two-independent groups. * $p < 0.05$, ** $p < 0.01$ and *** $p < 0.001$.

Results

Expression of *PFKFB3/Pfkfb3* in human and murine plaques in both immune and stromal cells

We first sought to assess *PFKFB3/Pfkfb3* expression patterns in human and murine atherosclerotic plaques. The single-cell RNA-sequencing (scRNA-seq) dataset from human atherosclerotic coronary arteries by Wirka et al.¹⁴ showed *PFKFB3* expression mainly in macrophages, but also in ECs, fibroblasts and other leukocytes such as T cells (**Figure 1A**). This confirms *PFKFB3* expression in human atherosclerosis, and particularly in macrophages. Next, we analyzed murine *Pfkfb3* expression in myeloid cells specifically, from the scRNA-seq meta-analysis by Zernecke et al., including data from 9 atherosclerosis studies of murine aorta¹⁵. Traditionally, macrophages were classified into pro-inflammatory M1 and anti-inflammatory M2 macrophages²³. However, the rise of single-cell techniques has shown that macrophage phenotypes are diverse and has led to identification of 5 main macrophage subsets in atherosclerosis: resident-like macrophages, inflammatory macrophages, foamy “triggering receptor expressed on myeloid cells 2” (TREM2^{hi}) macrophages, interferon (IFN)-inducible macrophages, and so-called cavity macrophages, whose transcriptome resembles that of peritoneal macrophages^{15, 24}. Furthermore, DCs can be broadly classified into moDCs, plasmacytoid DCs (pDCs) and conventional DCs (cDCs)²⁵. Interestingly, of all myeloid cells, *Pfkfb3* expression was highest in mature DCs and pDCs. Furthermore, *Pfkfb3* was expressed across the 5 main macrophage subsets, albeit by a low percentage of cells (**Figure 1B**). Aside from the aforementioned DC and macrophage subsets, *Pfkfb3* expression was confirmed in monocytes, neutrophils, cluster of differentiation (CD)209a+ moDCs and cDCs.

The meta-analysis dataset contains only myeloid data from several murine atherosclerosis models. Considering the use of *Ldlr*^{-/-}*LysMCre*^{+/-} mice in the current study, we confirmed *Pfkfb3* expression in a scRNA-seq dataset from *Ldlr*^{-/-}*LysMCre*^{+/-} aortic arch lesions by Van Kuijk et al.¹⁶. Although the number of cells in this *Ldlr*^{-/-}*LysMCre*^{+/-} dataset is low, in accordance with the meta-analysis and human datasets, *Pfkfb3* was expressed in a wide range of plaque cells, including macrophage subsets, monocytes, neutrophils, DCs and lymphocytes, but also ECs, SMCs and fibroblasts (**Figure 1C**).

In line with *in vitro* analysis of hypoxia-inducible factor 1-alpha (HIF1 α)-dependent expression of *PFKFB3*¹³, *in vivo* *PFKFB3/Pfkfb3* expression was significantly increased in both human and murine atherosclerotic macrophages with high *HIF1 α /Hif1 α* signatures (**Figure 1D** and **E**). However, next to macrophages, a high *HIF1 α /Hif1 α* signature was associated with increased *PFKFB3/Pfkfb3* expression in human ECs, fibroblasts, B cells, neurons, natural killer (NK) cells, pericytes and plasma cells, and in murine CD209a+ moDCs and cDCs. Although cell number is

low in some populations, these data suggest that hypoxia regulates *PFKFB3/Pfkfb3* expression *in vivo*, both in humans and mice, in a wide range of cell types.

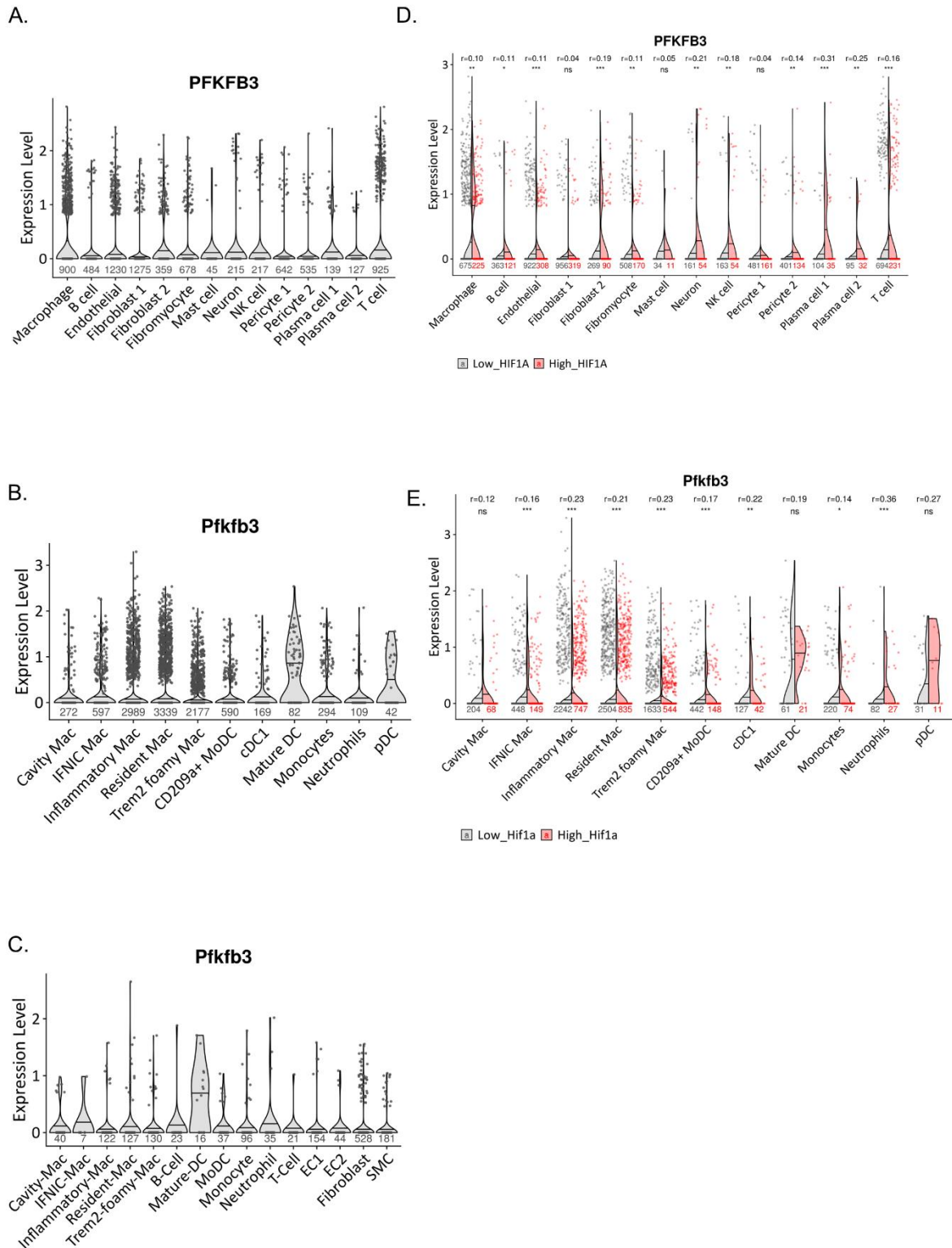


Figure 1: Expression pattern of *PFKFB3/Pfkfb3* in human and murine atherosclerosis. (A) Violin plot of *PFKFB3* expression in single-cell populations of human atherosclerotic coronary arteries¹⁴. **(B)** Violin plot of *Pfkfb3* expression in single-cell populations of murine atherosclerotic myeloid cells¹⁵. **(C)** Violin plot of *Pfkfb3* expression in single-cell populations of murine *Ldlr*^{-/-}*LysMCre*^{+/-} aortic arch lesions¹⁶. **(D)** Split violin plot of *PFKFB3* expression

in cells with high versus low *HIF1α* signature from human atherosclerotic coronary arteries¹⁴. **(E)** Split violin plot of *Pfkfb3* expression in murine atherosclerotic myeloid cells, with high versus low *Hif1α* signature¹⁵. In D and E, Wilcoxon test statistics of FDR-adjusted p-values and r effect sizes are indicated at the top. Sample sizes per cell type indicated under (split) violin plots. * p < 0.05, ** p < 0.01, *** p < 0.001. CD; cluster of differentiation, cDC; conventional dendritic cell, EC; endothelial cell, HIF1α; hypoxia-inducible factor 1-alpha, IFN γ ; interferon-inducible, Mac; macrophage, moDC; monocyte-derived dendritic cell, NK cell; natural killer cell, pDC; plasmacytoid DC, SMC; smooth muscle cell, TREM2; triggering receptor expressed on myeloid cells 2

Decreased glycolysis and pro-inflammatory profile in *Pfkfb3*^{fl/fl} macrophages

To study if myeloid cells were indeed responsible for the observed effects of systemic PFKFB3 inhibition, we generated *Ldlr*^{-/-}*LysMCre*^{+/-}*Pfkfb3*^{fl/fl} (*Pfkfb3*^{fl/fl}) mice, using *Ldlr*^{-/-}*LysMCre*^{+/-}*Pfkfb3*^{wt/wt} mice as controls (*Pfkfb3*^{wt/wt}). Partial myeloid *Pfkfb3* knockdown was confirmed in *Pfkfb3*^{fl/fl} versus *Pfkfb3*^{wt/wt} BMDMs (50%, **Figure 2A**). As available antibodies are non-specific, confirmation of PFKFB3 knockdown on a protein level was prevented. Therefore, we further sought to obtain functional confirmation of *Pfkfb3* knockdown. The (near-)complete inhibition of glycolysis ($\geq 80\%$) induces cell death²⁶. Thus, partial glycolysis inhibition is desirable to affect cell function, without compromising cell viability. Seahorse analysis after glucose dosing revealed decreased basal extracellular acidification rate (ECAR) in *Pfkfb3*^{fl/fl} BMDMs compared to controls (**Figure 2B**), indicating partially decreased glycolytic rates. During glycolysis, glucose is metabolized into pyruvate. Pyruvate can either be utilized in the tricarboxylic acid cycle to generate ATP, or metabolized into organic acids such as lactate⁹. As expected based on glycolysis disruption, residual glucose levels were increased, whereas lactate levels were decreased in *Pfkfb3*^{fl/fl} BMDM-conditioned medium (**Figure 2C and D**).

We previously mentioned that pro-inflammatory macrophages rely on glycolysis for their energy supply⁶. As PFKFB3 silencing using siRNA previously reduced glycolysis and pro-inflammatory activation of human macrophages¹³, we studied the effect of *Pfkfb3* knockdown on BMDM cytokine gene expression. Indeed, already in unstimulated *Pfkfb3*^{fl/fl} BMDMs, we observed increased expression of anti-inflammatory interleukin (*Il*)10 (**Figure 2E**). Thereafter, we stimulated *Pfkfb3*^{fl/fl} and *Pfkfb3*^{wt/wt} BMDMs with lipopolysaccharide (LPS) and interferon-gamma (IFN- γ) to mimic the plaque pro-inflammatory phenotype of these cells and showed that partial *Pfkfb3* knockdown was maintained (60%, **Figure 2F**). Moreover, pro-inflammatory *Il6* and *Il12b* expression were decreased in *Pfkfb3*^{fl/fl} versus *Pfkfb3*^{wt/wt} BMDMs after pro-inflammatory stimulation (**Figure 2G and H**). These results indicate a decreased pro-inflammatory profile in *Pfkfb3*^{fl/fl} macrophages, and thus confirm a role of *Pfkfb3* in pro-inflammatory macrophage polarization.

In our mouse model, Cre-recombinase expression is under control of the lysozyme 2 (*Lyz2*) promoter. Compared to macrophages, monocytes and neutrophils, *Lyz2* gene expression is low in DCs (**Supplementary (S) Figure S1A**). Nevertheless, we assessed if DCs were targeted

by our model, as *Pfkfb3* expression was abundant in this cell type (**Figure 1B** and **C**). We differentiated DCs from bone marrow cells and confirmed protein expression of the DC marker CD11c by flow cytometry (**Figure S1B**). As expected based on lower *Lyz2* gene expression, DCs were not targeted in our model, as *Pfkfb3* expression was unchanged between *Pfkfb3^{fl/fl}* and *Pfkfb3^{wt/wt}* DCs (**Figure 2I**).

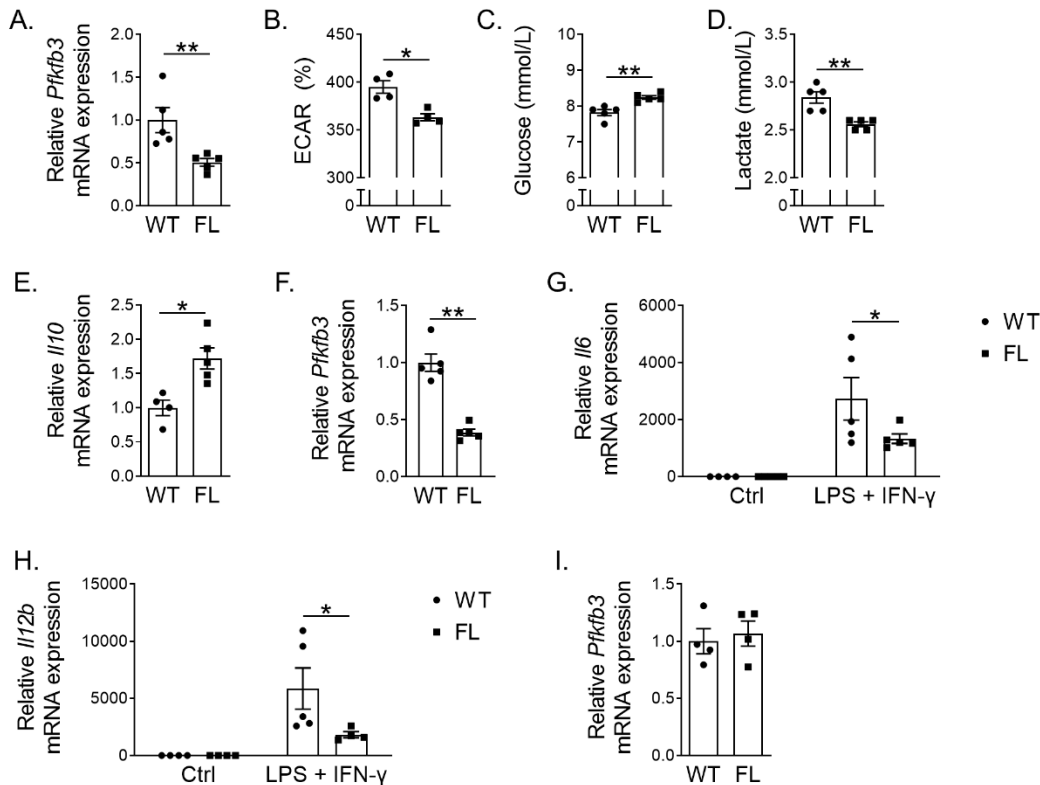


Figure 2: Decreased *Pfkfb3* expression and decreased glycolysis in *Pfkfb3^{fl/fl}* bone marrow-derived macrophages. (A) *Pfkfb3* mRNA expression in *Pfkfb3^{fl/fl}* (FL) relative to *Pfkfb3^{wt/wt}* (WT) bone marrow-derived macrophages (BMDM). (B) Extracellular acidification rate (ECAR, percentage of baseline) of *Pfkfb3^{fl/fl}* and *Pfkfb3^{wt/wt}* BMDMs after 10 mM glucose stimulus, as assessed with a Seahorse XF Analyzer. (C) Glucose and (D) lactate levels in *Pfkfb3^{fl/fl}* and *Pfkfb3^{wt/wt}* BMDM culture media after 26 hours of culture. (E) *Il10* mRNA expression in unstimulated *Pfkfb3^{fl/fl}* relative to *Pfkfb3^{wt/wt}* BMDMs. (F) *Pfkfb3* mRNA expression in *Pfkfb3^{fl/fl}* relative to *Pfkfb3^{wt/wt}* BMDMs after pro-inflammatory stimulation with LPS and IFN- γ . (G) *Il6* and (H) *Il12b* mRNA expression in *Pfkfb3^{fl/fl}* and *Pfkfb3^{wt/wt}* BMDMs cultured without additions (ctrl; control) or stimulated with LPS and IFN- γ . Expression is relative to unstimulated *Pfkfb3^{wt/wt}* BMDMs. (I) *Pfkfb3* mRNA expression in *Pfkfb3^{fl/fl}* relative to *Pfkfb3^{wt/wt}* bone marrow-derived dendritic cells. The graphs represent mean \pm standard error of the mean (SEM). * $p < 0.05$, ** $p < 0.01$. Data were analyzed using Mann-Whitney U test. ECAR; extracellular acidification rate

No effect of partial myeloid *Pfkfb3* disruption on atherosclerosis

After confirming partial *Pfkfb3* knockdown, functional disruption of glycolysis and a decreased pro-inflammatory profile in macrophages *in vitro*, we studied the effects of myeloid *Pfkfb3* disruption on atherosclerosis. Therefore, *Pfkfb3*^{fl/fl} and *Pfkfb3*^{wt/wt} mice were fed a high cholesterol diet (HCD) for 12 weeks (**Figure 3A**). We observed advanced atherosclerotic plaques in aortic roots (ARs) with a necrotic core and fibrous cap. Body weight and plasma cholesterol and triglyceride levels were similar between *Pfkfb3*^{fl/fl} and *Pfkfb3*^{wt/wt} mice after HCD (**Figure 3B-D**). Unexpectedly, plaque and necrotic core size, as well as plaque macrophage and collagen content were unaffected in *Pfkfb3*^{fl/fl} advanced AR lesions compared to controls (**Figure 3E-G**). Moreover, lymphocyte antigen 6G (Ly6G)⁺ neutrophil content was also unchanged between *Pfkfb3*^{wt/wt} and *Pfkfb3*^{fl/fl} AR lesions (**Figure 3H**). Similarly, no changes in plaque or necrotic core size were observed in early lesions without or with very little necrosis in brachiocephalic arteries (BCA) (**Figure S2A**). Besides plaque size, total plaque burden, as measured by plaque index¹⁰, was also unaffected in *Pfkfb3*^{fl/fl} BCA (**Figure S2B**).

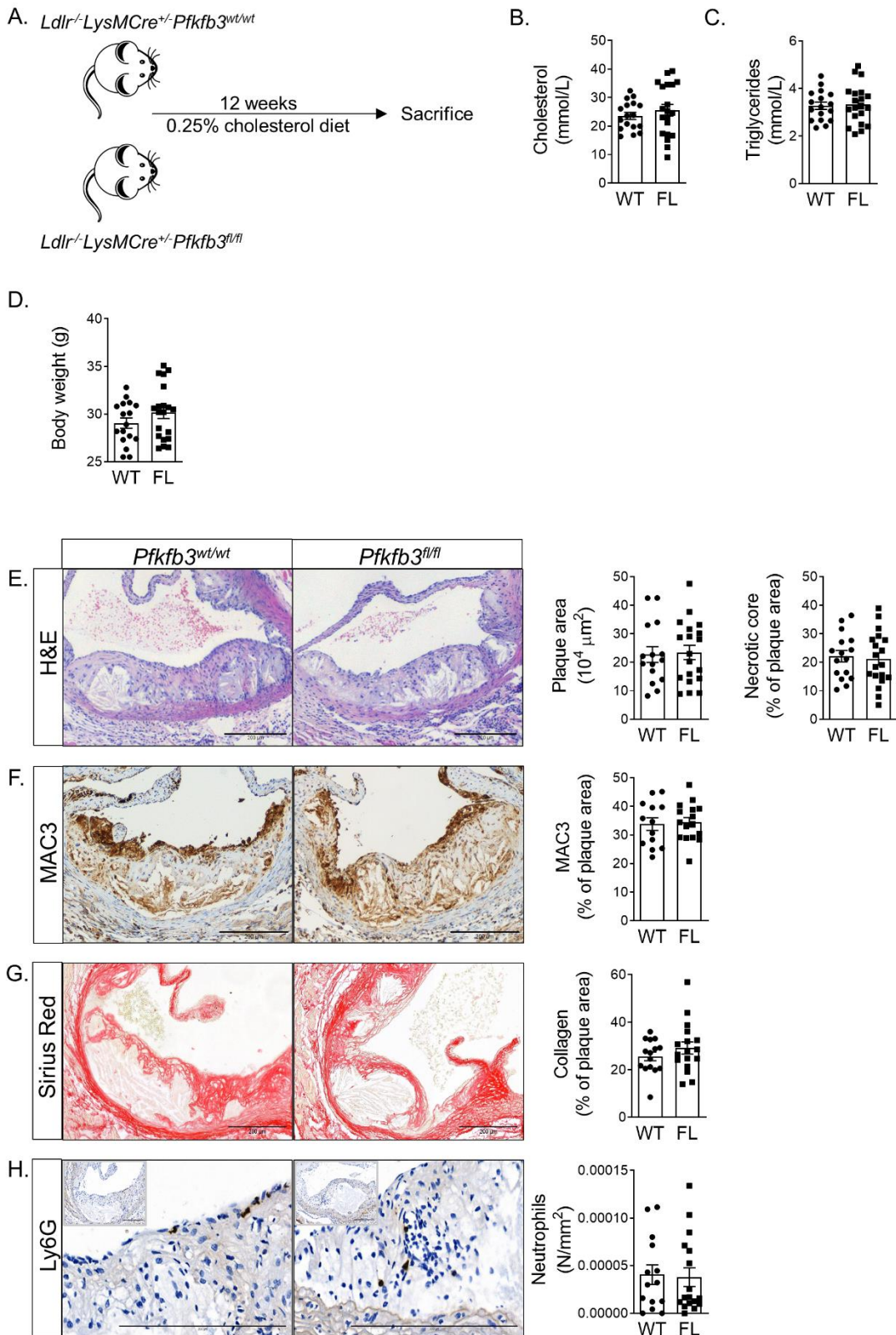


Figure 3: No effect of partial myeloid *Pfkfb3* disruption on advanced atherosclerotic lesions in aortic roots. (A) Setup of mouse experiment using *Ldlr*^{-/-}*LysMCre*^{+/-}*Pfkfb3*^{fl/fl} (*Pfkfb3*^{fl/fl}, n = 20) and *Ldlr*^{-/-}*LysMCre*^{+/-}*Pfkfb3*^{wt/wt} (*Pfkfb3*^{wt/wt}, n = 17) mice. **(B)** Cholesterol and **(C)** triglyceride levels in *Pfkfb3*^{wt/wt} (WT) and *Pfkfb3*^{fl/fl} (FL) plasma. **(D)** Body weight of *Pfkfb3*^{wt/wt} and *Pfkfb3*^{fl/fl} mice after 12 weeks of high cholesterol diet. **(E)** hematoxylin and

eosin (H&E), (F) MAC3, (G) Sirius Red and (H) Ly6G staining in *Pfkfb3*^{wt/wt} and *Pfkfb3*^{fl/fl} AR lesions and corresponding quantifications. The graphs represent mean \pm SEM. Scale bars 200 μ m. Data in B and H were analyzed using Mann-Whitney U test. Data in C-G were analyzed using Student's t-test

Pfkfb isoenzyme expression in plaque myeloid cells

To study potential genetic compensation by other *Pfkfb* isoenzymes keeping glycolytic rate above a certain threshold, we assessed expression of these isoenzymes in murine plaque myeloid cells. Expression of *Pfkfb1* and *Pfkfb2* was minimal in myeloid cells of the meta-analysis (Figure 4A and B) and *Ldlr*^{-/-}*LysMCre*^{+/-} datasets (Figure S3A and B). Similarly to *Pfkfb3*, *Pfkfb4* was expressed in macrophage and DC subsets, monocytes and neutrophils, albeit in a small proportion of cells (Figure 4C, S3C). To assess possible genetic compensation, we determined expression of *Pfkfb1*, *Pfkfb2* and *Pfkfb4* in *Pfkfb3*^{fl/fl} versus *Pfkfb3*^{wt/wt} BMDMs, which was unaffected (Figure 4D). Thus, genetic compensation by other *Pfkfb* isoenzymes seems absent in *Pfkfb3*^{fl/fl} BMDMs.

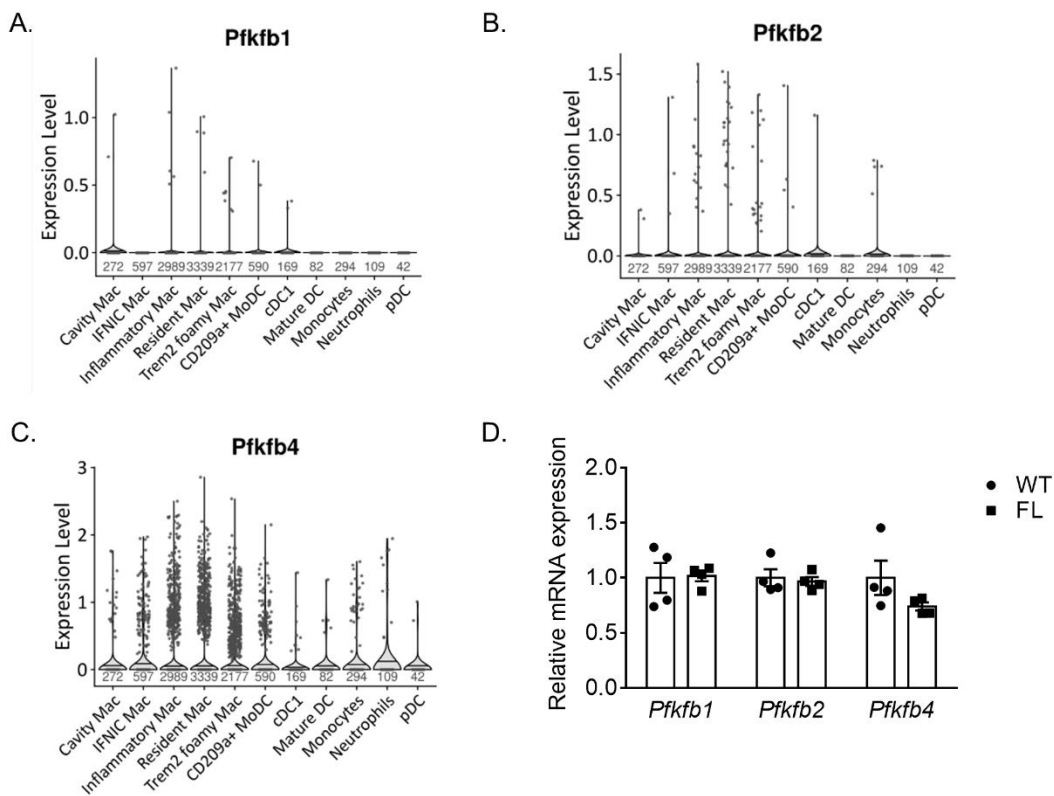


Figure 4: Expression of *Pfkfb* isoenzymes in plaque cells. Violin plot of (A) *Pfkfb1*, (B) *Pfkfb2* and (C) *Pfkfb4* expression in murine atherosclerotic myeloid cells (Zernecke et al.¹⁵). (D) *Pfkfb1*, *Pfkfb2* and *Pfkfb4* mRNA expression in *Pfkfb3*^{fl/fl} (FL) relative to *Pfkfb3*^{wt/wt} (WT) BMDMs. Data in D were analyzed using two-way ANOVA. Sample sizes per cell type indicated under violin plots. CD; cluster of differentiation, cDC; conventional dendritic cell, IFNIC; interferon-inducible, Mac; macrophage, moDC; monocyte-derived dendritic cell, pDC; plasmacytoid DC, TREM2; triggering receptor expressed on myeloid cells 2

Discussion

The current study assessed the effect of partial myeloid *Pfkfb3* disruption on atherosclerosis *in vivo*, after 12 weeks of HCD. Collectively, our findings suggest that although myeloid *Pfkfb3* disruption decreases the pro-inflammatory macrophage profile *in vitro*, it does not affect atherosclerosis development *in vivo*, neither in advanced, nor early lesions. No effects on circulating lipids, plaque size and composition, or total plaque burden were observed.

A few studies have looked into partial pharmacological inhibition of glycolysis in atherosclerosis by targeting PFKFB3, using 3PO(-derivatives). Similar to the current study, no effect on plaque size was reported¹⁰⁻¹². Although plaque size was unchanged, total plaque burden over the aorta length was reduced in 3PO-treated apolipoprotein E knockout (*ApoE*^{-/-}) and *ApoE*^{-/-} fibrillin 1 (*Fbn1*)^{C1039G+/-} mice¹⁰. This decreased plaque occurrence was independent of changes in plaque composition, such as macrophage content, necrosis, fibrosis or angiogenesis.

In contrast, other studies did report effects of 3PO treatment on plaque composition. Plaque stability was increased, as indicated by decreased necrotic core area and a thicker fibrous cap, in *Ldlr*^{-/-} mice treated with 3PO-derivative PFK158¹¹. While Perrotta et al. hypothesized that decreased plaque burden after 3PO treatment was linked to decreased expression of EC adhesion molecules during early lesion development¹⁰, no changes in EC adhesion molecules were observed in PFK158-treated *Ldlr*^{-/-} mice¹¹. It was suggested that glycolysis inhibition in macrophages and monocytes could be responsible for the observed plaque stabilization.

On the contrary, here, we show that partially decreased PFKFB3-mediated glycolysis in monocytes, macrophages and granulocytes does not affect atherogenesis. Possibly, opposing effects of *Pfkfb3* knockdown within myeloid cells and subsets, result in an absence of net effect. However, we did not observe changes in neutrophil and macrophage numbers. Thus, positive effects reported after systemic 3PO treatment are likely conferred by other myeloid or stromal cell types, that are affected by inhibition of PFKFB3-mediated glycolysis and are important in atherogenesis, such as DCs, SMCs and fibroblasts. Indeed, we show that our model does not induce *Pfkfb3* knockdown in DCs. However, *Pfkfb3* expression is high in atherosclerotic DCs, and DCs play a fundamental role in atherogenesis by contributing to activation of adaptive immunity, foam cell formation and pro-inflammatory cytokine secretion²⁷. Next to DCs and other myeloid cells, through analysis of scRNA-seq datasets, we showed that fibroblasts and SMCs, but also ECs and lymphocytes express *PFKFB3/Pfkfb3* in human and murine atherosclerosis. Importantly, increased alpha smooth muscle actin (α SMA)⁺ cells, i.e. SMCs and fibroblasts, were observed upon PFK158-treatment in *Ldlr*^{-/-} and upon 3PO-treatment in *ApoE*^{-/-} mice^{11, 12}. Additionally, EC activation and dysfunction are at the center of atherogenesis, while ECs also highly depend on glycolysis^{20, 28}. Both specific

PFKFB3/Pfkfb3 knockdown in ECs and 3PO treatment reduced EC sprouting *in vivo* and *in vitro*, by affecting EC migration and proliferation^{20, 26}. Moreover, 3PO decreased EC activation and increased endothelial barrier stability *in vitro*. However, while increasing plaque stability, 3PO treatment in *ApoE*^{-/-} mice did not affect plaque endothelial barrier function¹². Except for myeloid-specific *Pfkfb3* knockdown in the current study, effects of other cell-specific *Pfkfb3* knockdowns in atherosclerosis have not been studied yet. This could shine additional light on cell-specific effects of disrupted PFKFB3-mediated glycolysis on atherogenesis.

Another factor that might explain the lack of effect on atherosclerosis compared to studies utilizing 3PO treatment, is recent evidence that 3PO inhibits glycolysis through intracellular acidification, rather than specific PFKFB3 inhibition^{29, 30}. Thus, one should take possible unintended off-target effects of intracellular acidification into consideration when using 3PO(-derivatives). Small molecule AZ67 does bind to PFKFB3 specifically^{29, 31} and might be an interesting pharmacological inhibitor for future *in vivo* atherosclerosis studies, while keeping in mind that effects are likely not mediated by monocytes, macrophages or neutrophils.

In addition to greater relevance of PFKFB3-mediated glycolysis in other cell types in atherosclerosis, or off-target effects of reported inhibitors, other factors may explain the observed lack of effect of myeloid *Pfkfb3* inhibition on atherosclerosis.

Firstly, *Pfkfb3* knockdown in *Pfkfb3*^{fl/fl} BMDMs is only partial (~50-60%). The LysMCre-loxP system often results in ≥70% deletion efficiency in myeloid cells³². Efficiency of the Cre-lox system in our model could be complicated by *Pfkfb3* gene locus³³. Moreover, it should be noted that although we report expression of *Pfkfb3* in atherosclerotic myeloid cells, the percentage of monocytes, neutrophils and macrophages that express *Pfkfb3* is low (~10-20%, **Figure S4A**). Furthermore, as PFKFB3 is merely one of several stimulators of glycolytic flux³⁴, *Pfkfb3* inhibition reduces glycolysis only partially, in line with previous studies that targeted PFKFB3-mediated glycolysis^{20, 26, 35}. Nevertheless, glycolysis inhibition by 3PO treatment *in vivo* is also partial^{11, 26}, and a similar, partial approach was very successful to change EC function *in vivo*^{12, 20}.

Indeed, we focus only on PFKFB3-mediated glycolysis in the current study. Atherosclerotic plaques are associated with increased glycolytic activity³⁶. As glycolysis is controlled at different levels, other glycolytic regulators than PFKFB3 might be involved in this association, such as hexokinase 2, glucose transporter 1 or enolase 2, which should be studied in the future^{36, 37}.

Another factor that could explain the lack of effect, is the possible role of other PFKFB isoenzymes. Although we showed that *Pfkfb1*, *Pfkfb2* and *Pfkfb4* expression was unaffected

in *Pfkfb3^{fl/fl}* BMDMs, PFKFB isoenzyme activity could still be increased, independent of expression³⁸.

Finally, differences in experimental setup, gender, HCD length and composition, and vascular sites assessed may cause differences in observed effects between the current and previous studies (**Table S2**)³⁹⁻⁴¹. Moreover, glycolysis inhibition using chronic gene silencing by LysMCre from embryonic stage versus acute pharmacological protein inhibition or siRNA silencing in adult mice may result in different functional outcomes and may also explain a lack of effect in the current study⁴². As mentioned, the selectivity of pharmacological agents is often not entirely clear.

In conclusion, we showed that partial myeloid knockdown of PFKFB3 does not affect atherosclerosis development. Positive effects of systemic, partial glycolysis inhibition on lesion stabilization or total plaque burden that were previously reported, might be conferred by other *Pfkfb3*-expressing cells such as DCs, fibroblasts, SMCs and lymphocytes. Possibly, more severe reduction of myeloid glycolysis may be needed.

Acknowledgements

The authors gratefully acknowledge excellent technical assistance by Clairij Dinjens and Jacques Debets. We would like to thank Mieke Dewerchin and Guy Eelen for reading the manuscript and providing input.

Author contributions

JS, JdB, LT and RT devised and planned experiments. JdB, KvK and RT carried out experiments. JdB, KvK, MG and RT performed data analysis. JP-P, JS-R, YG and KL were responsible for single-cell sequencing data analysis. PC kindly provided *Pfkfb3*^{lox/lox} mice for the experiments. RT and JS wrote the manuscript. PC provided critical input to the manuscript. All authors reviewed and approved the manuscript.

Funding sources

J.S. reports grants from the Dutch Organization for Scientific Research (016.116.017 VENI fellowship, and VIDI fellowship 0.16.186.364), grants from dr. Dekker senior postdoc fellowship of the Dutch Heart Foundation 2016T060, and the Fondation Leducq (15CVD04) during the conduct of the study. J.S.R. reports grants from JRC for Computational Biomedicine partially funded by Bayer AG., during the conduct of the study; and grants from GSK, grants from Sanofi, personal fees from Traverre Therapeutics, outside the submitted work. P.C. reports grants from Methusalem funding (Flemish government) and an ERC Advanced Research Grant (EU- ERC743074).

Conflicts of interest

The authors declare that the research was conducted in the absence of any commercial or financial relationships that could be construed as a potential conflict of interest.

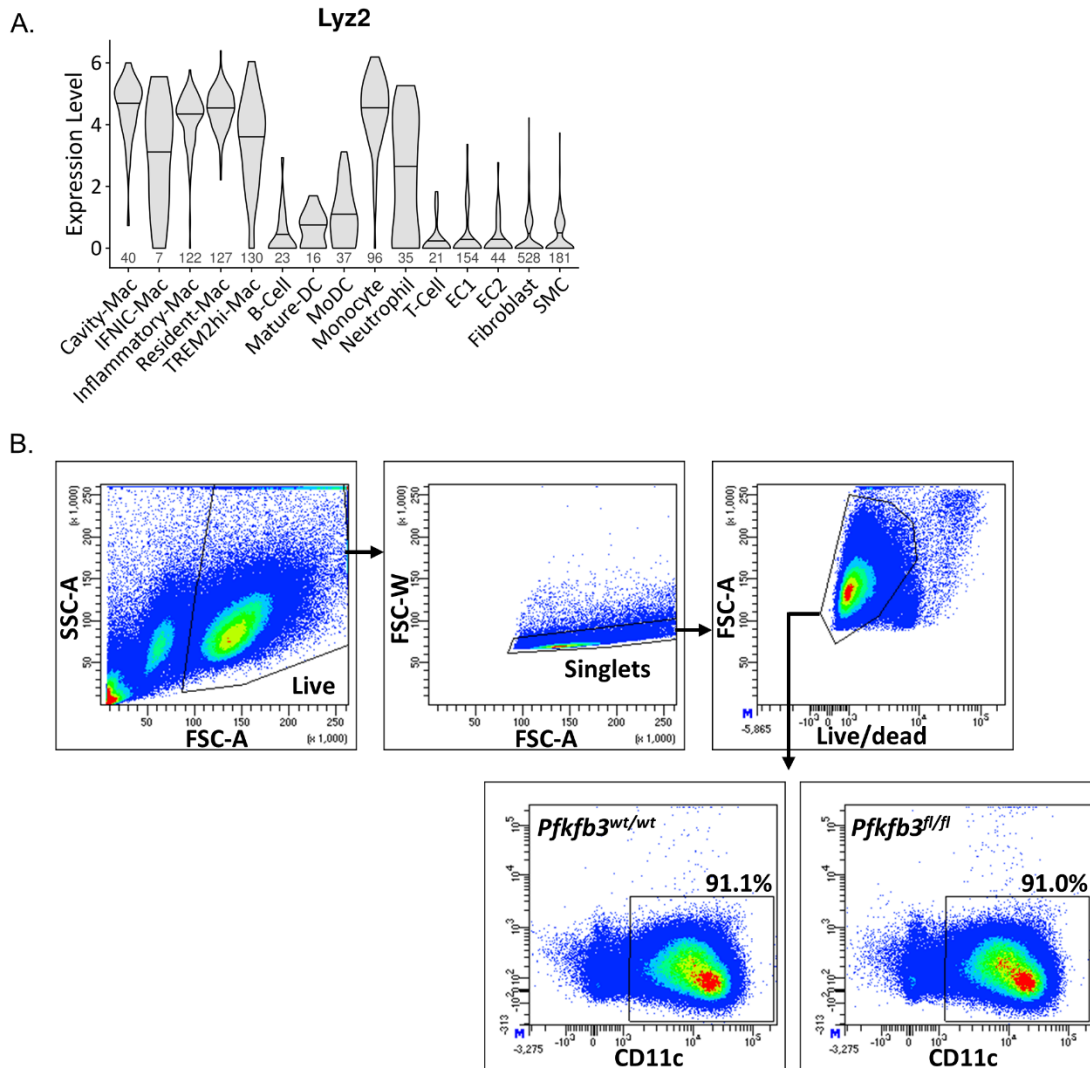
References

1. Tabas I, Williams KJ, Borén J. Subendothelial Lipoprotein Retention as the Initiating Process in Atherosclerosis. *Circulation*. 2007;116(16):1832-44.
2. Moore KJ, Tabas I. Macrophages in the pathogenesis of atherosclerosis. *Cell*. 2011;145(3):341-55.
3. Silvestre-Roig C, Braster Q, Ortega-Gomez A, Soehnlein O. Neutrophils as regulators of cardiovascular inflammation. *Nature Reviews Cardiology*. 2020;17(6):327-40.
4. Zerneck A. Dendritic Cells in Atherosclerosis. *Arteriosclerosis, Thrombosis, and Vascular Biology*. 2015;35(4):763-70.
5. Subramanian M, Tabas I. Dendritic cells in atherosclerosis. *Semin Immunopathol*. 2014;36(1):93-102.
6. Galván-Peña S, O'Neill LAJ. Metabolic reprogramming in macrophage polarization. *Front Immunol*. 2014;5:420-.
7. Wculek SK, Khouili SC, Priego E, Heras-Murillo I, Sancho D. Metabolic Control of Dendritic Cell Functions: Digesting Information. *Front Immunol*. 2019;10(775).
8. Kumar S, Dikshit M. Metabolic Insight of Neutrophils in Health and Disease. *Front Immunol*. 2019;10(2099).
9. Lunt SY, Heiden MG. Aerobic Glycolysis: Meeting the Metabolic Requirements of Cell Proliferation. *Annual Review of Cell and Developmental Biology*. 2011;27(1):441-64.
10. Perrotta P, Veken BVd, Veken PVD, Pintelon I, Roosens L, Adriaenssens E, et al. Partial Inhibition of Glycolysis Reduces Atherogenesis Independent of Intraplaque Neovascularization in Mice. *Arteriosclerosis, Thrombosis, and Vascular Biology*. 2020;40(5):1168-81.
11. Poels K, Schnitzler JG, Waissi F, Levels JHM, Stroes ESG, Daemen M, et al. Inhibition of PFKFB3 Hampers the Progression of Atherosclerosis and Promotes Plaque Stability. *Front Cell Dev Biol*. 2020;8:581641.
12. Beldman TJ, Malinova TS, Desclos E, Grootemaat AE, Misiak ALS, van der Velden S, et al. Nanoparticle-Aided Characterization of Arterial Endothelial Architecture during Atherosclerosis Progression and Metabolic Therapy. *ACS Nano*. 2019;13(12):13759-74.
13. Tawakol A, Singh P, Mojena M, Pimentel-Santillana M, Emami H, MacNabb M, et al. HIF-1 α and PFKFB3 Mediate a Tight Relationship Between Proinflammatory Activation and Anaerobic Metabolism in Atherosclerotic Macrophages. *Arterioscler Thromb Vasc Biol*. 2015;35(6):1463-71.
14. Wirka RC, Wagh D, Paik DT, Pjanic M, Nguyen T, Miller CL, et al. Atheroprotective roles of smooth muscle cell phenotypic modulation and the TCF21 disease gene as revealed by single-cell analysis. *Nature Medicine*. 2019;25(8):1280-9.
15. Zerneck A, Winkels H, Cochain C, Williams JW, Wolf D, Soehnlein O, et al. Meta-Analysis of Leukocyte Diversity in Atherosclerotic Mouse Aortas. *Circ Res*. 2020;127(3):402-26.
16. van Kuijk K, Demandt JAF, Perales-Patón J, Theelen TL, Kuppe C, Marsch E, et al. Deficiency of myeloid PHD proteins aggravates atherogenesis via macrophage apoptosis and paracrine fibrotic signalling. *Cardiovascular Research*. 2021.
17. Stuart T, Butler A, Hoffman P, Hafemeister C, Papalexi E, Mauck WM, 3rd, et al. Comprehensive Integration of Single-Cell Data. *Cell*. 2019;177(7):1888-902.e21.

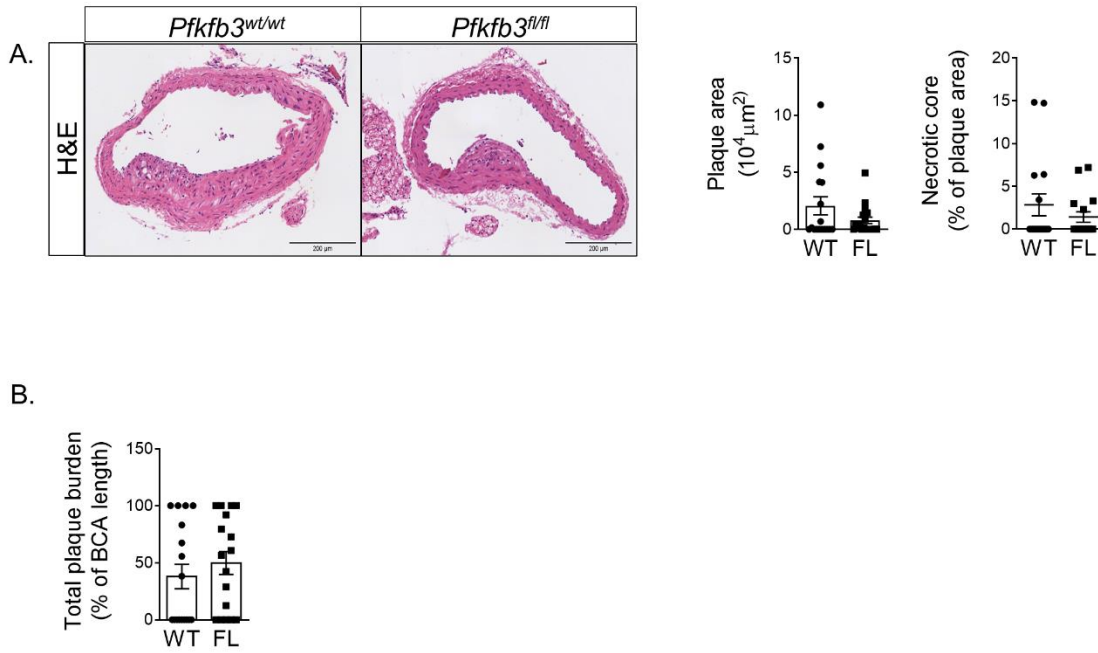
18. Garcia-Alonso L, Holland CH, Ibrahim MM, Turei D, Saez-Rodriguez J. Benchmark and integration of resources for the estimation of human transcription factor activities. *Genome Research*. 2019;29(8):1363-75.
19. Holland CH, Tanevski J, Perales-Patón J, Gleixner J, Kumar MP, Mereu E, et al. Robustness and applicability of transcription factor and pathway analysis tools on single-cell RNA-seq data. *Genome Biology*. 2020;21(1):36.
20. De Bock K, Georgiadou M, Schoors S, Kuchnio A, Wong Brian W, Cantelmo Anna R, et al. Role of PFKFB3-Driven Glycolysis in Vessel Sprouting. *Cell*. 2013;154(3):651-63.
21. Faust N, Varas F, Kelly LM, Heck S, Graf T. Insertion of enhanced green fluorescent protein into the lysozyme gene creates mice with green fluorescent granulocytes and macrophages. *Blood*. 2000;96(2):719-26.
22. Bankhead P, Loughrey MB, Fernández JA, Dombrowski Y, McArt DG, Dunne PD, et al. QuPath: Open source software for digital pathology image analysis. *Scientific Reports*. 2017;7(1):16878.
23. Mantovani A, Garlanda C, Locati M. Macrophage Diversity and Polarization in Atherosclerosis. *Arteriosclerosis, Thrombosis, and Vascular Biology*. 2009;29(10):1419-23.
24. Willemsen L, de Winther MP. Macrophage subsets in atherosclerosis as defined by single-cell technologies. *J Pathol*. 2020;250(5):705-14.
25. Eisenbarth SC. Dendritic cell subsets in T cell programming: location dictates function. *Nature Reviews Immunology*. 2019;19(2):89-103.
26. Schoors S, De Bock K, Cantelmo AR, Georgiadou M, Ghesquière B, Cauwenberghs S, et al. Partial and transient reduction of glycolysis by PFKFB3 blockade reduces pathological angiogenesis. *Cell Metab*. 2014;19(1):37-48.
27. Zhao Y, Zhang J, Zhang W, Xu Y. A myriad of roles of dendritic cells in atherosclerosis. *Clin Exp Immunol*. 2021.
28. Eelen G, de Zeeuw P, Simons M, Carmeliet P. Endothelial cell metabolism in normal and diseased vasculature. *Circulation research*. 2015;116(7):1231-44.
29. Emini Veseli B, Perrotta P, Van Wielendaele P, Lambeir AM, Abdali A, Bellosta S, et al. Small molecule 3PO inhibits glycolysis but does not bind to 6-phosphofructo-2-kinase/fructose-2,6-bisphosphatase-3 (PFKFB3). *FEBS Lett*. 2020;594(18):3067-75.
30. Burmistrova O, Olias-Arjona A, Lapresa R, Jimenez-Blasco D, Eremeeva T, Shishov D, et al. Targeting PFKFB3 alleviates cerebral ischemia-reperfusion injury in mice. *Scientific Reports*. 2019;9(1):11670.
31. Boyd S, Brookfield JL, Critchlow SE, Cumming IA, Curtis NJ, Debreczeni J, et al. Structure-Based Design of Potent and Selective Inhibitors of the Metabolic Kinase PFKFB3. *Journal of Medicinal Chemistry*. 2015;58(8):3611-25.
32. Clausen BE, Burkhardt C, Reith W, Renkawitz R, Förster I. Conditional gene targeting in macrophages and granulocytes using LysMcre mice. *Transgenic Res*. 1999;8(4):265-77.
33. Murray PJ, Wynn TA. Obstacles and opportunities for understanding macrophage polarization. *J Leukoc Biol*. 2011;89(4):557-63.
34. Mor I, Cheung EC, Vousden KH. Control of Glycolysis through Regulation of PFK1: Old Friends and Recent Additions. *Cold Spring Harbor Symposia on Quantitative Biology*. 2011;76:211-6.

35. Yetkin-Arik B, Vogels IMC, Nowak-Sliwinska P, Weiss A, Houtkooper RH, Van Noorden CJF, et al. The role of glycolysis and mitochondrial respiration in the formation and functioning of endothelial tip cells during angiogenesis. *Scientific Reports*. 2019;9(1):12608.
36. Ali L, Schnitzler JG, Kroon J. Metabolism: The road to inflammation and atherosclerosis. *Current Opinion in Lipidology*. 2018;29(6):474-80.
37. Berg JM TJ, Stryer L. Biochemistry. 5th edition. New York: W H Freeman; 2002.
38. Macut H, Hu X, Tarantino D, Gilardoni E, Clerici F, Regazzoni L, et al. Tuning PFKFB3 Bisphosphatase Activity Through Allosteric Interference. *Scientific Reports*. 2019;9(1):20333.
39. VanderLaan PA, Reardon CA, Getz GS. Site Specificity of Atherosclerosis. *Arteriosclerosis, Thrombosis, and Vascular Biology*. 2004;24(1):12-22.
40. Man JJ, Beckman JA, Jaffe IZ. Sex as a Biological Variable in Atherosclerosis. *Circulation Research*. 2020;126(9):1297-319.
41. Getz GS, Reardon CA. Diet and Murine Atherosclerosis. *Arteriosclerosis, Thrombosis, and Vascular Biology*. 2006;26(2):242-9.
42. Knight ZA, Shokat KM. Chemical Genetics: Where Genetics and Pharmacology Meet. *Cell*. 2007;128(3):425-30.

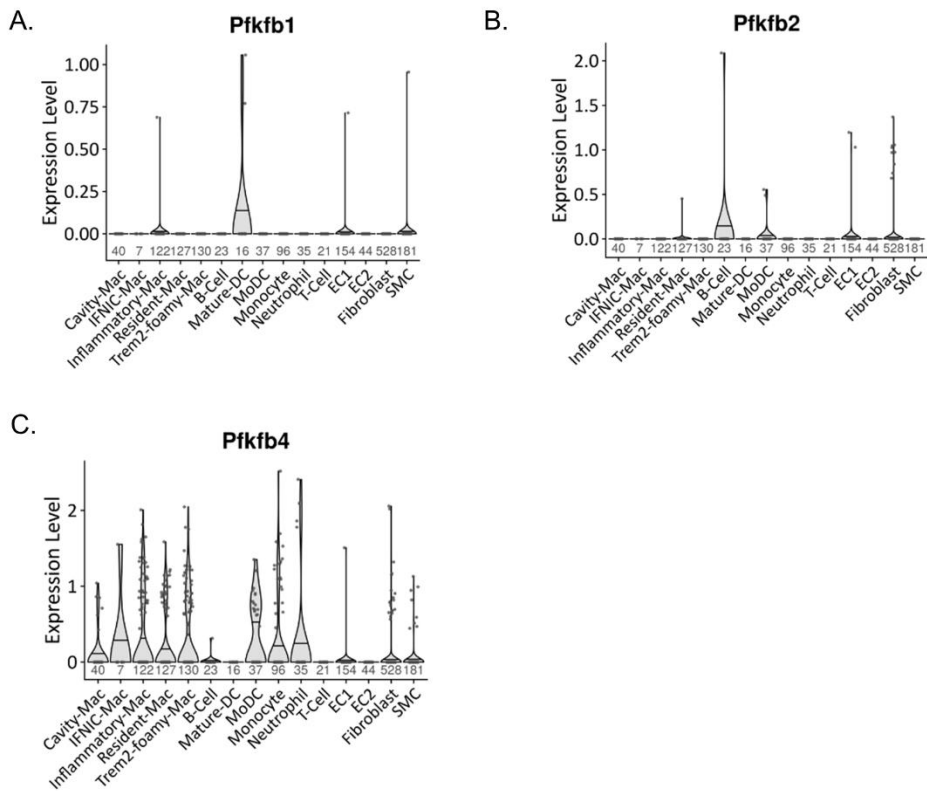
Supplementary data



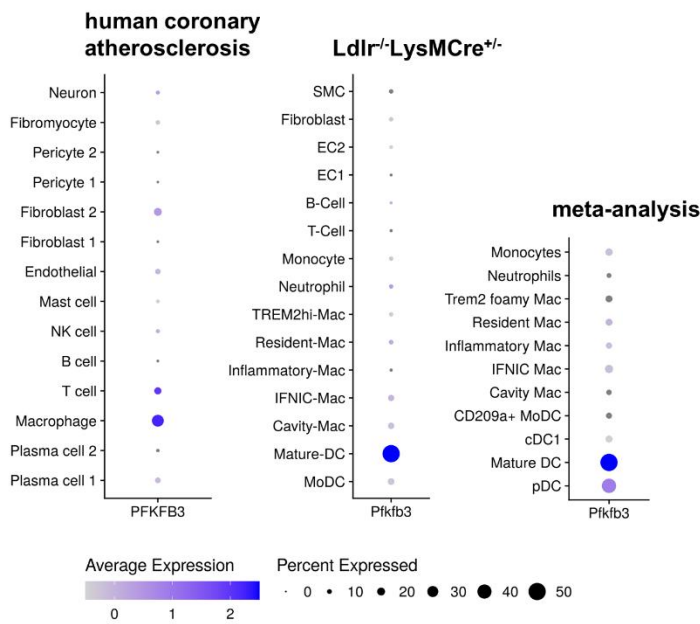
Supplementary Figure S1: Expression of *Lyz2* in *Ldlr*^{-/-}*LysMCre*^{+/-} plaque cells and confirmation of protein expression of CD11c in bone marrow-derived dendritic cells. (A) Violin plot of *Lyz2* expression in single-cell populations from murine *Ldlr*^{-/-}*LysMCre*^{+/-} aortic arch lesions¹⁶. Sample sizes per cell type indicated under violin plots. (B) Flow cytometry gating strategy and percentages of CD11c positive cells of living *Pfkfb3*^{wt/wt} and *Pfkfb3*^{fl/fl} bone marrow-derived dendritic cells. EC; endothelial cell, IFN-IC; interferon-inducible, Lyz2; lysozyme 2, Mac; macrophage, moDC; monocyte-derived dendritic cell, SMC; smooth muscle cell, TREM2; triggering receptor expressed on myeloid cells 2



Supplementary Figure S2: No effect of partial myeloid *Pfkfb3* disruption on early atherosclerotic lesions in brachiocephalic arteries. (A) Hematoxylin and eosin (H&E) staining in *Pfkfb3^{wt/wt}* (WT) and *Pfkfb3^{fl/fl}* (FL) brachiocephalic artery lesions and corresponding quantifications. (B) Total plaque burden in *Pfkfb3^{wt/wt}* and *Pfkfb3^{fl/fl}* brachiocephalic arteries. The graphs represent mean ± SEM. Scale bars 200 μm. Data were analyzed using Mann-Whitney U test. BCA; brachiocephalic artery



Supplementary Figure S3: Expression of *Pfkfb* isoforms in *Ldlr*^{-/-}*LysMCre*^{+/-} plaque cells. Violin plot of **(A)** *Pfkfb1*, **(B)** *Pfkfb2* and **(C)** *Pfkfb4* expression in single-cell populations from murine *Ldlr*^{-/-}*LysMCre*^{+/-} aortic arch lesions¹⁶. Sample sizes per cell type indicated under violin plots. EC; endothelial cell, IFN γ ; interferon-inducible, Mac; macrophage, moDC; monocyte-derived dendritic cell, SMC; smooth muscle cell, TREM2; triggering receptor expressed on myeloid cells 2



Supplementary Figure S4: Dot plots of *PFKFB3/Pfkfb3* expression in human and murine atherosclerosis. Dot plots of *PFKFB3/Pfkfb3* expression in single-cell populations of human atherosclerotic coronary arteries¹⁴, murine *Ldlr^{-/-}LysMCre^{+/-}* aortic arch lesions¹⁶ and murine atherosclerotic aorta (meta-analysis¹⁵). CD; cluster of differentiation, cDC; conventional dendritic cell, EC; endothelial cell, IFNIC; interferon-inducible, Lyz2; lysozyme 2, Mac; macrophage, moDC; monocyte-derived DC, NK cell; natural killer cell, pDC; plasmacytoid DC, SMC; smooth muscle cell, TREM2; triggering receptor expressed on myeloid cells 2

Supplementary Table S1: Primer sets used for qPCR

Gene	Forward primer (5'-3')	Reverse primer (5'-3')
<i>18s rRNA</i>	GTAACCCGTTGAACCCATT	CCATCCAATCGGTAGTAGCG
<i>Pfkfb1</i>	AGCCTTTGGATGAGGAATTG	GTGTGCCACATCGAAGAT
<i>Pfkfb2</i>	AATGAGATTGATGCTGGCGTG	ATTCCTCTGGGTACCGTTGC
<i>Pfkfb3</i>	CTATCCACGGGAGAGTCC	TGGCGCTCTAATTCCATGA
<i>Pfkfb4</i>	AACTGACCCAGAATCCCCTG	GTTAGTCATGCAGACACCACG

Supplementary Table S2: Characteristics and outcomes of glycolysis inhibition studies in murine atherosclerosis

Study	Intervention	Model	Gender	Composition /length diet	Sites assessed	Effect on plaque size/index	Effect on plaque composition
Current	<i>LysMCre^{+/-}</i> <i>Pfkfb3^{-/-}</i>	<i>Ldlr^{-/-}</i>	M	0.25% cholesterol, 12 weeks	AR, BCA	Size = Index =	Necrotic core = Macrophages = Collagen = MCs N/A
Poels et al., 2020	PFK158 2 µg/g 5 wks 3x/wk	<i>Ldlr^{-/-}</i>	M	0.15% cholesterol, 13 weeks	AR, AA	Size = Index N/A	Necrotic core ↓ Macrophages = Collagen N/A MCs ↑
Perrotta et al., 2020	3PO 50 µg/g <u>preventive:</u> 10 wks 2x/wk <u>curative:</u> 4 wks 4x/wk	<i>ApoE^{-/-}</i>	F	0.15% cholesterol, 14-20 weeks	CA, AA	Size = Index ↓	Necrotic core = Macrophages = Collagen = MCs =
Beldman et al., 2019	3PO 25 µg/g 6 wks 3x/wk	<i>ApoE^{-/-}</i>	F	0.2% cholesterol, 6 weeks	AR	Size = Index N/A	Necrotic core = Macrophages ↓ Collagen ↑ MCs ↑

M; male, F; female, AR; aortic root, BCA; brachiocephalic artery, AA; aortic arch, CA; carotid artery, N/A; not assessed, MCs; mesenchymal cells, =; unchanged, ↑; increased, ↓; decreased.

Chapter 4

Myeloid PFKFB3 knockdown exacerbates diet-induced MAFLD through stimulation of myeloid cell proliferation and hepatic steatosis

Renée J.H.A. Tille, Janny de Bruijn, Ross Dobie, Marion J. Gijbels, Gijs Goossens, Peter Carmeliet, Neil Henderson, Sander S. Rensen, Ludwig Dubois, Bart Ghesquiere, Kristiaan Wouters, Erik A.L. Biessen, Judith C. Sluimer

In preparation

Chapter 5

Fibroblasts in atherosclerosis: abundant, heterogeneous and plastic participants

Renée J.H.A. Tillie, Kim van Kuijk, Judith C. Sluimer

Current Opinion in Lipidology, 2020, Oct, 31(5):273-278

Abstract

Fibroblasts are very heterogeneous and plastic vascular cells. A growing interest in fibroblasts in healthy and atherosclerotic vasculature is observed, next to macrophages, endothelial cells and smooth muscle cells (SMCs). In this review, we discuss fibroblast presence, heterogeneity, origin and plasticity in health and atherosclerosis based on latest literature.

With help of single-cell sequencing (SCS) techniques, we have gained more insight into presence and functions of fibroblasts in atherosclerosis. Next to SMCs, fibroblasts are extracellular matrix (ECM)-producing cells abundant in the vasculature and involved in atherogenesis. Fibroblasts encompass a heterogeneous population and SCS data reveal several fibroblast clusters in healthy and atherosclerotic tissue with varying gene expression and function. Moreover, recent findings indicate interesting similarities between adventitial stem and/or progenitor cells and fibroblasts. Also, communication with inflammatory cells opens up a new therapeutic avenue.

In summary, because of their highly plastic and heterogeneous nature, modulating fibroblast cell function and communication in the atherosclerotic vessel might be useful in battling atherosclerosis from within the plaque.

Introduction

Atherosclerosis and its clinical manifestations, for example myocardial infarction and stroke, are currently still the leading causes of death worldwide¹. Atherosclerosis is characterized by lipid accumulation in the subendothelial space, intimal inflammation, smooth muscle cell (SMC) migration from the media to the outside of the newly formed plaque and ultimately plaque rupture². Different cell types, including endothelial cells (ECs), macrophages and SMCs, play prominent roles in this life-long process³⁻⁵. However, recent evidence suggests that an additional cell type, the fibroblast, is an important player in matrix production in atherosclerosis. Traditionally, fibroblasts are thought to arise from mesenchymal stem cells (MSCs) and are thus part of the mesenchymal cell category, also including pericytes and SMCs. In arterial injury, adventitial fibroblasts differentiate into activated fibroblasts (myofibroblasts) with *de novo* alpha smooth muscle actin (α SMA) expression in response to pro-inflammatory cytokines, matrix remodeling, and transforming growth factor beta (TGF- β) signaling. Myofibroblasts have been implicated in extracellular matrix (ECM) production, pro-inflammatory cytokine and matrix metalloproteinase (MMP) secretion and leukocyte recruitment⁶⁻⁸. However, these traditional views are being overturned by new insights and the advent of single-cell sequencing (SCS), which will be discussed in this review.

In fact, the ability to acquire stem cell properties by upregulating markers such as Stem cell antigen-1 (Sca-1) enables fibroblasts to be plastic and adaptable in numerous environmental situations^{9, 10}. Due to this heterogeneity and plasticity, currently used markers seem insufficient in unique identification of fibroblasts and/or covering the whole fibroblast population. Here, SCS will aid to find markers unique to fibroblasts. Indeed, SCS of healthy mouse brain confirmed the traditional marker platelet-derived growth factor alpha (*Pdgfra*) and yielded three new markers: decorin (*Dcn*), lumican (*Lum*) and *Mmp2*¹¹. However, both lumican and decorin have been associated with other cell types involved in the advent of atherosclerosis^{12, 13}. This may suggest disease- and/or organ-specificity of markers to identify fibroblasts. The lack of a one-size-fits-all marker makes investigating their role in atherosclerosis development challenging. In this review, we aim to elucidate the functional role of fibroblasts in healthy and atherosclerotic vasculature by discussing fibroblast presence, heterogeneity, origin and plasticity.

Fibroblasts in healthy vasculature

The arterial wall consists of three layers. The inner intima is composed of an EC monolayer. The middle medial layer consists of SMCs embedded in ECM. Lastly, the adventitia is the outer layer and is traditionally thought to harbor mesenchymal cells, that is fibroblasts, pericytes and SMCs, connective tissue, unmyelinated nerve fibers, resident leukocytes, small blood vessels with ECs surrounded by mesenchymal cells, and several progenitor cells⁸. Multiple

studies have shown the fibroblast's potential to extensively participate in organ homeostasis and repair mechanisms in response to stress¹⁴⁻¹⁶. The emergence of SCS has provided researchers the opportunity to study vascular cells in more depth. This technique has improved fibroblast annotation and revealed different subsets in multiple organs. Kalluri et al. used abovementioned technique to investigate all three layers of the healthy murine aorta¹⁷. The authors showed that SMCs comprise the largest cell population in the murine aorta (~40%), but surprisingly, also showed that fibroblasts make up for roughly 33% of aortic cells¹⁷. These fibroblasts consist of two subpopulations, with a phenotypic gradient rather than a rigid split between them. These fibroblasts are probably derived from the adventitia, although the authors removed perivascular fat – possibly including the adventitia. As their arterial wall location was not validated by immunohistochemistry or *in situ* hybridization, a possible medial location for one or both subpopulations is yet to be confirmed. Furthermore, their function, embryonic origin, cellular progeny and fate are yet unknown. Gu et al. studied the adventitia of healthy murine aorta and shed more light on their function. They uncovered four mesenchymal populations, whose differential gene expression suggests functions in ECM organization, immune regulation and bone formation¹⁸. These data suggest fibroblast heterogeneity, already present in a healthy steady-state.

Fibroblasts in atherosclerosis

The classical dogma in atherogenesis entails migration of medial SMCs to the newly formed plaque, producing ECM components for fibrous cap formation². This dogma has recently been challenged, as several groups have reported the presence of fibroblast-like cells in human atherosclerotic lesions^{12, 19}. Also, adventitial fibroblast-like cells have been functionally implicated in plaque ECM production^{19, 20}. Using apolipoprotein E knockout (*ApoE*^{-/-}) mice on a Western diet superimposed with chronic kidney disease, Kramann et al. showed that a subset of adventitial MSC-like cells, expressing GLI family zinc finger 1 (*Gli1*), *Sca-1* and *PDGFR β* , migrated into the media and neointima. *Gli1*+ cells contributed to calcification by differentiation into osteoblast-like cells²⁰. In contrast, Evrard et al. reported decreased collagen and increased MMP expression in another subset of endothelial-derived, fibroblast-like cells expressing fibroblast activation protein (FAP) or fibroblast-specific protein 1 (FSP1, *S100a4* gene) in atherosclerosis, indicating a role in matrix degradation¹⁹. In 2019, a key paper by Wirka et al. employed SCS to assess cellular composition in atherosclerotic plaques from human coronary artery and mouse aorta, and identified two fibroblast clusters¹². Interestingly, *Gli1*, *Fap* or *S100a4* were not among the top 100 differential genes in the two murine or human fibroblast subsets defined by Wirka, complicating the interpretation of the above reference studies and strongly suggesting heterogeneity. Together, these studies suggest that fibroblast clusters identified in healthy and diseased tissue differ in functionality, possibly due to different origin and/or differentiation fate.

Fibroblast plasticity, heterogeneity and origin in atherosclerosis

As described above, varying numbers of fibroblast clusters with corresponding differential gene sets have been identified in healthy and atherosclerotic tissue. Additionally, studies in other organs have shown that new fibroblast clusters can arise as a consequence of disease, further supporting plasticity and heterogeneity¹⁵. Heterogeneity makes it very difficult to identify the entire fibroblast population and a resulting lack of specific markers complicates fibroblast research. Common fibroblast markers, such as FAP, FSP1 and lumican are not specifically expressed by fibroblast-like cells only, and/or are not expressed by all fibroblasts²¹⁻²⁵. Fibroblast heterogeneity may be a result of their various origins and enormous plasticity, all enhanced as a result of adaptation to disease. Here, we describe evidence to support that fibroblasts in atherosclerosis originate from SMCs and/or ECs (**Figure 1**). Also, we discuss adventitial stem and/or progenitor cells as a source of fibroblasts or possibly a subset of fibroblasts.

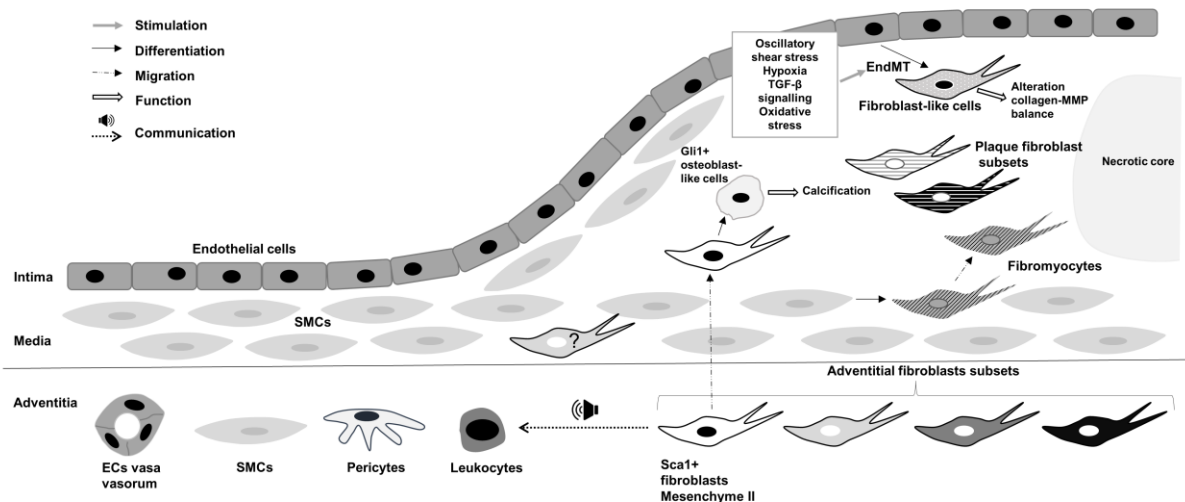


Figure 1: Presence and origin of fibroblasts in atherosclerosis and their suggested contributions. Four adventitial fibroblasts subsets have been discovered using single-cell sequencing (SCS). Sca-1+ fibroblasts may contribute to atherosclerosis by migrating into the neointima. Gli1+, Sca-1+ adventitial stem/progenitor cells have been shown to differentiate into osteoblast-like cells and hereby contribute to plaque calcification. Two fibroblast subsets have been identified with SCS, while prior studies showed that fibroblast(-like) cells in atherosclerosis can originate from medial smooth muscle cells (SMCs), called fibromyocytes, and from endothelial cells (ECs) through endothelial-to-mesenchymal transition (EndMT). It is unclear whether these are similar to or distinct from the two fibroblast subsets discovered by SCS. ? indicates possible medial localization of fibroblasts.

SMC origin

Wirka et al. studied SMC differentiation in and their contribution to atherosclerosis *in vivo* combining SCS and a fluorescent myosin heavy chain 11 (*Myh11*) reporter strain for SMCs on an *ApoE*^{-/-} background. In contrast to prevailing concepts of myofibroblast development from fibroblasts, they reported SMC differentiation into fibroblast-like, “fibromyocyte” cells upon

high-fat diet (HFD)¹². In addition to two fibroblast and two SMC clusters in *ApoE*^{-/-} mice on chow, a *Myh11* lineage-derived SMC cluster appeared and expanded with HFD feeding. This modulated SMC cluster showed decreased expression of SMC differentiation markers, and a clear transcriptional shift towards genes expressed by the fibroblast clusters, later confirmed in human coronary arteries¹². Nevertheless, the cells were transcriptionally distinct from fibroblasts and displayed positivity for the *Myh11*-reporter. These data highlighted the benefits of fluorescent fate tracking and lead one to wonder whether these fibroblast-like cells have reached the end stage of their dedifferentiation or will dedifferentiate further into actual fibroblasts. Another question is if the differentiation also occurs the other way around. Comparison between the modulated SMC cluster and a myofibroblast population could be interesting to avoid off-target effects in future cell-specific targeting.

Endothelial origin

Another possible fibroblast source are ECs, which can undergo endothelial to mesenchymal transitioning (EndMT). A review by Kovacic et al. emphasized the functional importance of EndMT in both healthy and diseased vasculature²⁶. EndMT results in downregulation of endothelial-associated genes, such as cluster of differentiation (CD)31 or VE-cadherin, and upregulation of mesenchymal genes, such as α SMA and FAP. These cells genetically present as mesenchymal cells and can execute mesenchymal functions like ECM production²⁶. Evrard et al. specifically showed that fibroblasts can arise through EndMT in atherosclerosis¹⁹. Using a tamoxifen-inducible endothelial lineage-tracking system in *ApoE*^{-/-} mice, they observed one-third of plaque cells positive for FAP were endothelial-derived after 8 weeks of HFD. The population expanded to nearly 50% in advanced atherosclerotic plaques¹⁹. They showed that EndMT is stimulated *in vitro* by severe hypoxia, TGF- β signaling, and oxidative stress, factors that are ubiquitous in atherosclerosis¹⁹. Oscillatory shear stress has also been identified as EndMT inducer in atherosclerosis²⁷. Importantly, Evrard et al. uncovered a relationship between the extent of EndMT and an unstable plaque phenotype in humans¹⁹. Notably, the data should be interpreted with slight caution, as the markers used to identify fibroblasts are not unique^{23, 24}. Current SCS publications have not explicitly reported on EndMT, either because it was unstudied or possibly due to lack of sufficient cells to model transitions. However, the reported two human fibroblast subsets could include EndMT-derived cells. The top 100 differential genes do not include endothelial markers, yet this does not exclude low marker expression¹². Hence, SCS using EC reporter strains are yet to fully confirm these findings. In addition, the functional differences between both EndMT- and SMC-derived fibroblast(-like) cells and their exact contribution to atherosclerosis remain to be elucidated.

Adventitial stem and/or progenitor cells

Fibroblasts have been suggested to originate from a pool of adventitial stem and/or progenitor cells. However, the identity of these cells is a point of discussion as fibroblasts also have the ability to re-acquire stem cell properties by upregulating markers such as Sca-1^{9, 10, 20, 28}. Additionally, MSCs and fibroblasts are morphologically similar and expression of MSC surface markers, such as CD105, CD73 and CD90, has been observed on fibroblasts. Vice versa, MSC expression of common fibroblast markers, i.e. vimentin and fibroblast surface protein (FSP), has been reported⁹. Similar to MSCs, fibroblasts seem capable of differentiation into adipogenic, osteoblastogenic and chondrogenic lineages⁹. These insights might suggest that adventitial MSCs and Sca-1+ progenitor cells, previously identified and studied by many groups, are in fact fibroblasts. Indeed, a recent paper by Ni et al. shows that 10% of c-Kit+ cells was positive for the fibroblast marker PDGFR α in healthy C57BL/6J aorta²⁹. Their findings were confirmed using an inducible Cre model, labeling c-Kit+ cells with tdTomato, showing ~20% overlap between PDGFR α and c-Kit²⁹. Moreover, Tang et al. also reported that 40% of adventitial Sca-1+ cells with progenitor properties co-expressed PDGFR α ^{21, 30}. These Sca-1+/PDGFR α +, progenitor-like cells generated new medial SMCs after severe artery injury³⁰. Similar to other recent studies that assessed vasculature cell populations by SCS, Gu et al. did not annotate mesenchymal clusters in adventitia of *ApoE*^{-/-} and WT aortas as stem or progenitor cells¹⁸. Yet, one of the four identified mesenchyme clusters showed high Sca-1+ expression, indicating stem cell properties of this cluster¹⁸. The distinction between true adventitial stem and/or progenitor cells and fibroblasts may thus be smaller than previously assumed, and expression of Sca-1+ indicative of fibroblast plasticity.

Together, these data suggest that fibroblasts show an even greater plasticity than previously thought. Cell transitioning of fibroblasts into other cell types and vice versa seems common and extensive in atherosclerosis. Whether all currently identified adventitial stem and/or progenitor cells are really adventitial fibroblasts and vice versa is an important remaining question to be resolved using reliable fibroblast reporter models. Based on this concept, another question is whether the fibroblast is an end stage cell or merely a collection of heterogeneous “in between” cells, actively transitioning between different cell types, or a combination of the two. It would be interesting to study if the acquisition of stem cell-like properties by fibroblasts occurs through dedifferentiation. Assessing the differentiation capacity of the distinct fibroblast clusters into other cell types could also shine some light on this discussion.

Fibroblast cell-cell communication and its therapeutic potential

In addition to heterogeneity and function of fibroblasts in the natural development of atherosclerosis, these cells could possibly be used as a new therapeutic approach based on their effect on surrounding inflammatory cells. A pro-inflammatory role of mesenchyme

clusters through increased intercellular communication with inflammatory macrophages has been computationally predicted in *ApoE*^{-/-} adventitia by Gu et al¹⁸. A recent paper by Mahdavi Gorabi et al. also reviewed the possibility of using MSCs as treatment for atherosclerosis by modulating inflammation³¹. Multiple studies discussed in this review showed a marked anti-inflammatory effect in murine atherosclerosis by decreased pro-inflammatory cytokines and NFκB signaling after bone marrow MSC administration. MSC therapy has been studied in clinical trials for diseases such as heart disease, cancer and peripheral artery disease, but not atherosclerosis. It is considered a promising future treatment option, but at the same time its safety and efficacy are questioned. Knowledge regarding precise *in vivo* mechanisms of action is still lacking and inconsistent results are observed due to cellular heterogeneity of MSCs and a lack of specific markers³². Donor characteristics, culture conditions, method and location of delivery, and host receptibility are all factors that can influence MSC therapy efficacy and efficiency³¹⁻³³. Moreover, risks of malignant transformation and pro-tumorigenic effects of MSCs have been reported. Thus, extensive additional research into improving efficiency and efficacy of MSC therapy is required before considering this a new therapy option.

Conclusions and future research

This review shows that in contrast to assumptions the classical dogmas contain, next to SMCs, fibroblasts are ECM-producing cells abundant in the vasculature and involved in atherosclerosis. Fibroblasts comprise a very heterogeneous population due to different cellular origins and an extensive repertoire of possible cell transitions. The origin and fate of fibroblasts in atherosclerotic plaques remains to be elucidated. Due to their heterogeneity, there is a lack of specific markers that encompass the entire population making it difficult to study fibroblast (sub)populations in atherosclerosis. Recent comparisons between fibroblasts and adventitial stem and/or progenitor cells indicate similarities between these cells. Moreover, recent SCS data did not identify any adventitial stem and/or progenitor cell clusters, supporting fibroblast identity of these cells. SCS data did identify multiple fibroblast clusters with differential gene expression and functionality per cluster in healthy and atherosclerotic tissue. Further research into subpopulations of fibroblasts and their different functions is needed to identify specific markers per subpopulation and to determine the contribution of each subpopulation to atherosclerosis. The emergence of SCS provides opportunities to find answers to the remaining questions in an unbiased way. In the future, modulating fibroblast cell communication in atherosclerotic vessels could be useful in battling atherosclerosis from within the plaque.

Key points

- Fibroblasts are ECM-producing cells abundant in the vasculature and involved in atherogenesis
- Fibroblasts encompass a very heterogeneous population as indicated by SCS data revealing several fibroblast clusters in healthy and atherosclerotic tissue with varying gene expression and function
- Fibroblast identity has been proposed for adventitial progenitor and/or stem cells and should be further investigated.

Acknowledgements

None.

Funding sources

Financial support is received from the Netherlands Scientific Organization (NWO VIDI 91718364 to J.C. Sluimer), and the Dutch Heart Foundation (Dr. Dekker fellowship 2016T060 to JC Sluimer).

Conflicts of interest

None.

References

1. Herrington W, Lacey B, Sherliker P, et al. Epidemiology of Atherosclerosis and the Potential to Reduce the Global Burden of Atherothrombotic Disease. *Circ Res*. 2016;118(4):535-46.
2. Libby P, Buring JE, Badimon L, et al. Atherosclerosis. *Nature Reviews Disease Primers*. 2019;5(1):56.
3. Basatemur GL, Jorgensen HF, Clarke MCH, et al. Vascular smooth muscle cells in atherosclerosis. *Nat Rev Cardiol*. 2019;16(12):727-44.
4. Li M, Qian M, Kyler K, Xu J. Endothelial-Vascular Smooth Muscle Cells Interactions in Atherosclerosis. *Front Cardiovasc Med*. 2018;5:151.
5. Moore KJ, Koplev S, Fisher EA, et al. Macrophage Trafficking, Inflammatory Resolution, and Genomics in Atherosclerosis: JACC Macrophage in CVD Series (Part 2). *J Am Coll Cardiol*. 2018;72(18):2181-97.
6. Shi Y, O'Brien JE, Jr., Fard A, Zalewski A. Transforming growth factor-beta 1 expression and myofibroblast formation during arterial repair. *Arterioscler Thromb Vasc Biol*. 1996;16(10):1298-305.
7. Sartore S, Chiavegato A, Faggini E, et al. Contribution of adventitial fibroblasts to neointima formation and vascular remodeling: from innocent bystander to active participant. *Circulation research*. 2001;89(12):1111-21.
8. Singh S, Torzewski M. Fibroblasts and Their Pathological Functions in the Fibrosis of Aortic Valve Sclerosis and Atherosclerosis. *Biomolecules*. 2019;9(9):472.
9. Soundararajan M, Kannan S. Fibroblasts and mesenchymal stem cells: Two sides of the same coin? *J Cell Physiol*. 2018;233(12):9099-109.
10. Ichim TE, O'Heeron P, Kesari S. Fibroblasts as a practical alternative to mesenchymal stem cells. *Journal of Translational Medicine*. 2018;16(1):212.
11. Vanlandewijck M, He L, Mae MA, et al. A molecular atlas of cell types and zonation in the brain vasculature. *Nature*. 2018;554(7693):475-80.
12. Wirka RC, Wagh D, Paik DT, et al. Atheroprotective roles of smooth muscle cell phenotypic modulation and the TCF21 disease gene as revealed by single-cell analysis. *Nat Med*. 2019;25(8):1280-9.
13. Do NN, Willenborg S, Eckes B, et al. Myeloid Cell–Restricted STAT3 Signaling Controls a Cell-Autonomous Antifibrotic Repair Program. *The Journal of Immunology*. 2018;201(2):663-74.
14. Guerrero-Juarez CF, Dedhia PH, Jin S, et al. Single-cell analysis reveals fibroblast heterogeneity and myeloid-derived adipocyte progenitors in murine skin wounds. *Nature Communications*. 2019;10(1):650.
15. Xie T, Wang Y, Deng N, et al. Single-Cell Deconvolution of Fibroblast Heterogeneity in Mouse Pulmonary Fibrosis. *Cell Rep*. 2018;22(13):3625-40.
16. Gladka MM, Molenaar B, de Ruiter H, et al. Single-Cell Sequencing of the Healthy and Diseased Heart Reveals Cytoskeleton-Associated Protein 4 as a New Modulator of Fibroblasts Activation. *Circulation*. 2018;138(2):166-80.
17. Kalluri AS, Vellarikkal SK, Edelman ER, et al. Single-Cell Analysis of the Normal Mouse Aorta Reveals Functionally Distinct Endothelial Cell Populations. *Circulation*. 2019;140(2):147-63.

18. Gu W, Ni Z, Tan YQ, et al. Adventitial Cell Atlas of wt (Wild Type) and ApoE (Apolipoprotein E)-Deficient Mice Defined by Single-Cell RNA Sequencing. *Arterioscler Thromb Vasc Biol.* 2019;39(6):1055-71.
19. Evrard SM, Lecce L, Michelis KC, et al. Endothelial to mesenchymal transition is common in atherosclerotic lesions and is associated with plaque instability. *Nat Commun.* 2016;7:11853.
20. Kramann R, Goettsch C, Wongboonsin J, et al. Adventitial MSC-like Cells Are Progenitors of Vascular Smooth Muscle Cells and Drive Vascular Calcification in Chronic Kidney Disease. *Cell Stem Cell.* 2016;19(5):628-42.
21. Kuwabara JT, Tallquist MD. Tracking Adventitial Fibroblast Contribution to Disease: A Review of Current Methods to Identify Resident Fibroblasts. *Arteriosclerosis, thrombosis, and vascular biology.* 2017;37(9):1598-607.
22. Dobnikar L, Taylor AL, Chappell J, et al. Disease-relevant transcriptional signatures identified in individual smooth muscle cells from healthy mouse vessels. *Nature Communications.* 2018;9(1):4567.
23. Osterreicher CH, Penz-Osterreicher M, Grivennikov SI, et al. Fibroblast-specific protein 1 identifies an inflammatory subpopulation of macrophages in the liver. *Proc Natl Acad Sci U S A.* 2011;108(1):308-13.
24. Kahounova Z, Kurfurstova D, Bouchal J, et al. The fibroblast surface markers FAP, anti-fibroblast, and FSP are expressed by cells of epithelial origin and may be altered during epithelial-to-mesenchymal transition. *Cytometry A.* 2018;93(9):941-51.
25. Lu YP, Ishiwata T, Kawahara K, et al. Expression of lumican in human colorectal cancer cells. *Pathol Int.* 2002;52(8):519-26.
26. Kovacic JC, Dimmeler S, Harvey RP, et al. Endothelial to Mesenchymal Transition in Cardiovascular Disease: JACC State-of-the-Art Review. *J Am Coll Cardiol.* 2019;73(2):190-209.
27. Lai B, Li Z, He M, et al. Atheroprone flow enhances the endothelial-to-mesenchymal transition. *Am J Physiol Heart Circ Physiol.* 2018;315(5):H1293-H303.
28. Yu B, Chen Q, Le Bras A, et al. Vascular Stem/Progenitor Cell Migration and Differentiation in Atherosclerosis. *Antioxid Redox Signal.* 2018;29(2):219-35.
29. Ni Z, Deng J, Potter CMF, et al. Recipient c-Kit Lineage Cells Repopulate Smooth Muscle Cells of Transplant Arteriosclerosis in Mouse Models. *Circ Res.* 2019;125(2):223-41.
30. Tang J, Wang H, Huang X, et al. Arterial Sca1+ Vascular Stem Cells Generate De Novo Smooth Muscle for Artery Repair and Regeneration. *Cell Stem Cell.* 2020;26(1):81-96.e4.
31. Mahdavi Gorabi A, Banach M, Reiner Z, et al. The Role of Mesenchymal Stem Cells in Atherosclerosis: Prospects for Therapy via the Modulation of Inflammatory Milieu. *J Clin Med.* 2019;8(9).
32. Lukomska B, Stanaszek L, Zuba-Surma E, et al. Challenges and Controversies in Human Mesenchymal Stem Cell Therapy. *Stem Cells Int.* 2019;2019:9628536.
33. Musiał-Wysocka A, Kot M, Majka M. The Pros and Cons of Mesenchymal Stem Cell-Based Therapies. *Cell Transplant.* 2019;28(7):801-12.

Chapter 6

Human and murine fibroblast single-cell transcriptomics reveals fibroblast clusters are differentially affected by ageing and serum cholesterol

Kim van Kuijk, Ian R. McCracken, **Renée J.H.A. Tillie**, Sebastiaan E.J. Asselberghs, Dizar A. Kheder, Stan Muijtens, Han Jin, Richard S. Taylor, Ruud Wichers Schreur, Christoph Kuppe, Ross Dobie, Prakesh Ramachandran, Marion J. Gijbels, Lieve Temmerman, Phoebe M. Kirkwood, Joris Luyten, Yanming Li, Heidi Noels, Pieter Goossens, John R. Wilson-Kanamori, Leon J. Schurgers, Ying H. Shen, Barend M.E. Mees, Erik A.L. Biessen, Neil C. Henderson, Rafael Kramann, Andrew H. Baker, Judith C. Sluimer

Cardiovascular Research, 2023, Jul 4, 119(7):1509-1523

Abstract

Specific fibroblast markers and in-depth heterogeneity analysis are currently lacking, hindering functional studies in cardiovascular diseases (CVDs). Here, we established cell-type markers and heterogeneity in murine and human arteries and studied the adventitial fibroblast response to CVD and its risk factors hypercholesterolemia and aging.

Murine aorta single-cell RNA-sequencing analysis of adventitial mesenchymal cells identified fibroblast-specific markers. Immunohistochemistry and flow cytometry validated platelet-derived growth factor receptor alpha (PDGFRA) and dipeptidase 1 (DPEP1) across human and murine aorta, carotid, and femoral arteries, whereas traditional markers such as cluster of differentiation (CD)90 and vimentin also marked transgelin+ vascular smooth muscle cells. Next, pseudotime analysis showed multiple fibroblast clusters differentiating along trajectories. Three trajectories, marked by CD55 (*Cd55+*), CXC motif chemokine ligand 14 (*Cxcl14+*) and lysyl oxidase (*Lox+*), were reproduced in an independent RNA-seq dataset. Gene ontology analysis showed divergent functional profiles of the three trajectories, related to vascular development, antigen presentation and/or collagen fibril organization, respectively. Trajectory-specific genes included significantly more genes with known genome-wide associations (GWAS) to CVD than expected by chance, implying a role in CVD. Indeed, differential regulation of fibroblast clusters by CVD risk factors was shown in adventitia of aged C57BL/6J mice, and mildly hypercholesterolemic *Ldlr* KO mice on chow by flow cytometry. The expansion of collagen-related CXCL14+ and LOX+ fibroblasts in aged and hypercholesterolemic aortic adventitia respectively, coincided with increased adventitial collagen. Immunohistochemistry, bulk and single-cell transcriptomics of human carotid and aorta specimens emphasized translational value as CD55+, CXCL14+ and LOX+ fibroblasts were observed in healthy and atherosclerotic specimens. Also, trajectory-specific gene sets differentially correlated with human atherosclerotic plaque traits.

In conclusion, we provide two adventitial fibroblast-specific markers, PDGFRA and DPEP1, and demonstrate fibroblast heterogeneity in health and CVD in humans and mice. Biological relevance is evident from regulation of fibroblast clusters by age and hypercholesterolemia *in vivo*, associations with human atherosclerotic plaque traits, and enrichment of genes with a GWAS for CVD.

Introduction

Cellular heterogeneity and plasticity are two fundamental concepts that are beginning to define both the healthy and diseased vasculature¹. This challenges the traditional approach to understanding previously distinct cellular compartments in the blood vessel wall, and the identities of cells that infiltrate the vessel wall in disease². One cell type in particular, known for its high plasticity and heterogeneity in numerous organs, is the fibroblast³⁻⁵. Fibroblasts mostly reside in the adventitial layer of the arterial wall, accompanied by other mesenchymal cells (e.g. pericytes and smooth muscle cells (SMCs)), immune cells and connective tissue⁶. Mainly fibroblasts express the stem cell marker Stem cell antigen 1 (Sca-1, encoded by the lymphocyte antigen 6 family member A gene, *Ly6a*), underpinning the potential of these cells to be reprogrammed into a diverse cell repertoire, supporting extensive plasticity^{7, 8}. Their functional role in fibrosis, inflammation, and angiogenesis in other organs^{9, 10} makes these cells an attractive candidate for therapeutic intervention in arterial pathologies, such as atherosclerosis and vascular ageing. However, presumably also due to this plasticity, markers specifically distinguishing fibroblasts at the mRNA and protein level from other vascular cells have been very difficult to define. For example, traditional markers such as collagen 1 alpha 1 (*Col1a1*), collagen 1 alpha 2 (*Col1a2*), fibroblast activation protein (*Fap*) and fibroblast-specific protein 1 (FSP1, encoded by the *S100a4* gene) lack the ability to distinguish between fibroblasts and other vascular cell types¹¹. In addition, other vascular mesenchymal cells exhibit phenotypes resembling that of fibroblasts upon vascular challenges^{12, 13}. Nevertheless, these markers have been used to detect fibroblast-like cells, originating from SMCs, or endothelial cells in atherosclerosis¹³⁻¹⁵. Thus, there is a need to resolve their fibroblast specificity to discern the impact or limitations of these studies. In addition, the role and regulation of potential fibroblast heterogeneity in vascular health and disease is not explored in sufficient detail but understanding disease-stimulating or -preventing phenotypes may impact therapeutic approaches.

Single-cell RNA-sequencing (scRNA-seq) and concomitant extensive validation could resolve the ambiguity of fibroblast identity markers and potential heterogeneity. Indeed, scRNA-seq has been key in identifying pan fibroblast-specific markers across the microvasculature in several major organs compared with mural cells (MCs) (consisting of pericytes and SMCs)¹⁶. Yet, it remains to be defined which markers are specific for arterial adventitial fibroblasts compared with other arterial cells. Previous scRNA-seq analyses of healthy murine vasculature have described transcriptomics of all arterial wall cell types, including fibroblasts, in a so-called atlas approach^{17, 18}. While both studies propose cell identity markers, and indicate the presence of multiple fibroblast clusters, the data stem from low number of fibroblasts, and results are not comprehensively validated on protein level. We hypothesize that a very detailed analysis of arterial fibroblasts would improve definition of fibroblast identity markers and detailed insight into fibroblast heterogeneity.

In the current study, we therefore investigated the fibroblast transcriptional landscape using scRNA-seq of fibroblast-enriched fractions from healthy murine adventitia. Fibroblast heterogeneity, and pseudotime differentiation trajectories were analyzed in-depth by bioinformatic analyses, such as Potential of Heat-diffusion for Affinity-based Transition Embedding (PHATE). The identified fibroblast identity and cluster markers were validated extensively on RNA and protein level using bulk, and single-cell sequencing, flow cytometry and immunohistochemistry of murine and human healthy and atherosclerotic arteries. We provide support for regulation of fibroblast heterogeneity in cardiovascular disease (CVD), as cardiovascular (CV) risk factors differentially affected fibroblast cluster expansion in aged and hypercholesteremic mice *in vivo*, cluster gene signatures harbored a significant number of genes with known genome-wide associations (GWAS) to CVD, and were associated with human atherosclerotic plaque traits. Together, this study provides a detailed fingerprint of arterial fibroblasts in health and CVD.

Materials and methods

Mouse models

All mouse experiments were approved by the regulatory authority of the Maastricht University Medical Centre and performed in compliance with the Dutch governmental guidelines and Directive 2010/63/EU of the European Parliament on the protection of animals used for scientific purposes. C57BL/6J mice (male, $n = 8$ per pool, 3-4 pools, 8-12 weeks old) were used as healthy controls. Aged C57BL/6J mice (male, $n = 5$ per pool, 3-4 pools, 72 weeks old) were obtained from Charles river and used to study the effect of aging. Male low-density lipoprotein receptor deficient mice (*Ldlr* KO) were fed chow (controls) or high-cholesterol diet (HCD, 0.25%, 824171, Tecnilab-BMI) for 16 weeks ($n = 15$ per pool for single-cell sequencing, $n = 5$ per pool, 3 pools for flow cytometry, 28-30 weeks old). *Ldlr* KO mice originated from Jaxx and were bred in Maastricht for <15 generations. *Pdgfra*-CreERT2-Rosa26-tdTomato and *Myh11*-CreERT2 eYFP were intraperitoneally injected with Tamoxifen (200 mg/kg) for three consecutive days, to induce tdTomato expression. Mice were euthanized with an overdose of pentobarbital (100 mg/kg), injected intraperitoneally.

Flow cytometry and cell sorting

Adventitia of the thoracic aorta (ranging from the aortic root until the diaphragm) was carefully microscopically dissociated from the underlying medial layer and collected in ice-cold phosphate buffered saline (PBS). Adventitial tissue of C57BL/6J or *Ldlr* KO mice was enzymatically digested for 15 minutes at 37°C using collagenase B (0.00284 g/mL, Sigma 110088807001), pronase (0.01 g/mL, Sigma 10165921001) and DNase (0.1 mg/mL, Roche 11284932001). This enzymatic cocktail ensures optimal isolation of mesenchymal cells¹⁹. Tissue was filtered through a 70 µm strainer and subjected to red blood cell lysis (8.4 g NH₄CL + 0.84 g NaHCO₃ in 1 liter H₂O, pH 7.2-7.4). Living, DAPI-negative, mesenchymal cells were sorted as CD45 negative (BioLegend, 103114), and ICAM2 negative cells (BioLegend, 400526) on FACS Aria III for scRNA-seq in case of 8 week old C57BL/6J mice or living, DAPI-negative, cells for *Ldlr* KO mice.

Cells isolated from adventitia originating from either young C57BL/6J mice (8 weeks, male), aged C57BL/6J mice (72 weeks, male), *Ldlr* KO mice on chow or high cholesterol diet for 16 weeks were used for protein validation using flow cytometry (FACS canto II). After FC receptor blocking (15246827, Thermofisher) cells were stained with the following antibodies: CD45 (Biolegend, 103154), Cdh5/VE-cadherin (Invitrogen, 53-1441-82 or eBioscience 46-1441-82), Transgelin (Novus biologicals, NBP2-47689PCP or NBP2-47689AF488), Platelet derived growth factor alpha (PDGFRA) (BD Pharmingen, 562774), Sca-1/Ly6a (eBioscience 61-5981-82), CD55 (Biolegend, 131804), CXCL14 (Abcam, ab264467) and Lysyl oxidase (LOX) (Novus biologicals, NB-100-2527AF647), live/dead fixable cell stain (Invitrogen, L34957). In case of CXCL14, the

antibody was labelled using a PE/Cy7 conjugation kit (Abcam, ab102903). For intracellular stainings (Transgelin, CXCL14 and LOX), fix & perm cell permeabilization kit was used (Invitrogen, GAS004). Data analysis was performed with BD FACS Diva software.

Immunohistochemical stainings

Murine tissue was fixed in 1% paraformaldehyde overnight, paraffin-embedded, and serially sectioned (4 µm). For stainings, only sections that had mature media (determined by elastin fiber presence) were used. Tissue was deparaffinized using xylene and rehydrated using an alcohol gradient (100-50% in dH₂O). Antigen retrieval was performed using low pH EnVision Dako target retrieval solution (Dako K800521-2), followed by blocking in 10% normal swine serum (Dako, X0901) in tris buffered saline (TBS). Immunohistochemical detection of the following proteins was performed: SMOC2 (Biorbyt, orb525072), COL14A1 (Novus biologicals, NBP2-15940), mouse PDGFRA (R&D, BAF1062), human PDGFRA (R&D, AF-307-NA), FBLN1 (Human Protein Atlas, HPA001613), LUMICAN (Abcam, ab168348), CCL11 (R&D, AF-420-NA), DPEP1 (Abcam, ab121308), MAC3 (Becton Dickinson), CD55 (ThermoFisher, PA5-78991), mouse CXCL14 (Abcam, ab13741), human CXCL14 (Proteintech, 10468-1-AP), LOX (Novus Biologicals, NB100-2527), Collagen type I (Abcam, ab21286), Vimentin (Abcam ab92547), CD90 (Biolegend 105307), and total collagen (Picosirius red, Polyscience 09400). Rabbit host primary antibodies were detected with a swine anti-rabbit secondary antibody (Dako, E0431), goat host primary antibodies were detected with a rabbit anti-goat secondary antibody (Dako, E046601-2), followed by signal amplification using Vectastain-ABC (Vector, AK-5000). Visualization was performed with 3,3'-diaminobenzidine (DAB, Agilent K346811-2) for single stains, while double stains were visualized with Vector Red/Blue (Vector, SK5100/5300). Pseudo-fluorescent images were created and adventitial co-localization quantified using the Nuance Multispectral Imaging System or Fiji. Quantification of adventitial area (defined as the area where medial elastin fibers end and the width is roughly similar to the width of the media), collagen 1 content (% adventitial area), and MAC3 (n/mm² adventitia) was done on images scanned with the Histotech P1000 scanner and analyzed with Qupath (v0.2.0-m8), while Sirius red was quantified on 20X images using Leica Qwin software. Representative images were selected based on the mean value of the corresponding analysis.

Human sample analysis

Human tissue collection was part of the Maastricht Pathology Tissue Collection (MPTC) and further storage and use of the tissue was in line with the Dutch Code for Proper Secondary use of Human Tissue and the local Medical Ethical Committee (protocol number 16-4-181). This code (https://elsi.health-ri.nl/sites/elsi/files/2022-01/Gedragscode_Gezondheidsonderzoek_2022.pdf) entails an opt-out arrangement and hence tissues were not used in the case of objection. The applicability of this code for this study was approved by the Maastricht University hospital (MUMC) local Medical Ethical

Committees. Human studies conducted by Li et al.²⁰ and Wirka et al.¹³ are approved by Institutional Review Board at Baylor College of Medicine and Stanford University Institutional Review Board, respectively, and follow the guidelines of the Declaration of Helsinki. Written informed consent was provided by all participants or the organ donors' legal representatives before enrollment. Formalin-fixed, paraffin-embedded (FFPE) carotid arteries were collected at autopsy ($n = 10$), carotid endarterectomy (CEA) procedure ($n = 63$ plaques, 43 patients), from the opposite site of the plaque ($n = 10$), or at carotid anastomosis during aortic bypass surgery ($n = 10$). Segments of 5 mm were alternated with frozen segments for histology and RNA isolation in case of CEA. A total of 43 plaque segments collected from 23 symptomatic patients undergoing CEA in the Maastricht Human Plaque Study (MaasHPS) were used for further microarray analysis. Library preparation, RNA extraction, data processing, normalization and additional information concerning plaque traits have been described in great detail elsewhere^{21,22}. Human carotid and aorta single-cell sequencing data was retrieved from data repositories and analyzed according to published methods^{13,20}.

Murine single-cell sequencing

After cell count number and viability check with Trypan Blue (>85%), a total of ~16,000 adventitial CD45-/ICAM2- cells from healthy 8 weeks old, male C57BL/6J mice were loaded on a Chromium single-cell controller using V2 reagent kit (10X Genomics). In case of *Ldlr* KO, a total of ~15,000 cells were loaded using V2 reagent kit (10X Genomics). Samples were loaded approximately 4 hours after tissue isolation. Libraries of cDNA were synthesized as suggested by 10X Genomics and used to create sequencing libraries. In short, in reaction vesicles (gel beads in emulsion, GEMs), cells were lysed and barcoded oligonucleotides reverse transcribed before clean-up and cDNA amplification. The Chromium Single-Cell 3' Library Kit was then used to generate indexed sequencing libraries. Sequencing was performed on Illumina HiSeq4000. In case of C57BL/6J, 5701 cells were yielded with ~87,000 reads per cell and for *Ldlr* KO, 4800 cells were yielded after chow diet and ~8000 cells after HCD, with 63,000 and 47,390 reads per cell respectively (**Supplementary (S) Table S1 and 2**).

Single-cell sequencing analysis C57BL/6J mice

The 10X Cell Ranger pipeline (v2.1.1) was used to perform alignment of raw sequencing reads to the mouse reference genome (mm10), filtering, barcode, and unique molecular identifiers (UMI) counting. Generated filtered expression matrices were subsequently used for additional quality control and subsequent analysis using the Seurat (v2.3) R package²³. Initial quality control was performed by removing low quality cells found to express less than 1500 genes, those with a UMI count greater 15,000, or those with more than 15% of reads aligning to mitochondrial genes (mito%, 654 cells removed in total). Global data normalization was then performed using the Normalize Data method²³, which normalizes gene expression in

individual cells based on the total gene expression, followed by multiplying by a factor of 10,000, and transforming the data by \log_e . Data was then scaled using the ScaleData method²³ and dimensionality reduction was performed using principal component analysis (PCA). PCA was carried out using the most variable genes in the dataset, identified by the FindVariableGenes method²³ selecting genes with a log variance to mean ratio (VMR) greater than 0.1. The appropriate number of principal components to be used for graph-based clustering and t-distributed stochastic neighbour embedding (tSNE) construction was determined by choosing the principal component (PC) after which the standard deviation of subsequent PCs remained approximately constant. Cluster identification was performed using the FindClusters method²³ using PCA as the chosen method of dimension reduction. Identified clusters were then visualized on a tSNE plot constructed using the appropriate number of PCs. Clusters found to have a low proportion of cells expressing *Pdgfrb* or containing cells positive for epithelial markers (*Krt19*, *Lgals7*, and *Cd82*) were removed from the dataset prior to re-clustering as described above (639 cells in total). Identified clusters were categorized based on their marker gene expression as either being smooth muscle (672 cells positive for *Myh11*, *Acta2*, *Tagln*, *Cnn1*) or fibroblast-like (3736 cells positive for *Col1a1*, *Col1a2*, *Ly6a*, *Mmp2*). Differential gene expression analysis compared smooth muscle cells to fibroblasts cells using the FindAllMarkers command²³. Only genes expressed in a minimum of 33% of cells in the given cell type, with a minimum \log_e fold change (logFC) in expression of 0.25, and with a difference in the fraction of positive cells between groups of at least 33%. Significantly differentially expressed markers were identified by the Wilcoxon rank sum test as having a Bonferroni adjusted P value <0.05. The top 20 markers based on logFC from each cell type were used for heatmap construction. Cell type markers were similar with mito% <10% and <15%.

Following sub-setting of data to contain only fibroblast-like cells, PHATE dimension reduction²⁴ was performed using the most variable genes in the fibroblast dataset. Highly variable genes were selected with an average expression (quantified as normalized $\ln(\text{UMI}+1)$) between 0.05 and 4 and with a log VMR between 0.075 and 10. Cluster identification within the fibroblast dataset was performed using the FindClusters method²³ with PHATE²⁴ used as the dimension reduction method. Identified clusters were then visualized on the PHATE plot using the DimPlot command²³. Markers from each fibroblast cluster were identified using the FindAllMarkers method²³ selecting genes only expressed in at least 25% of cells within the given cluster and with a logFC in expression threshold of at least 0.2. Comparative scRNA-seq datasets were imported directly as filtered count matrices and processed in accordance with the methods from the accompanying publications^{18,25,26}.

Single-cell sequencing analysis *Ldlr* KO mice

Filtered count matrices were generated using the 10X Cell Ranger V3.0.2 pipeline using the standard GRCh38-3.0.0 genome reference downloaded from 10X genomics (10X Genomics, Pleasanton, USA). The R package scater was used to perform cell filtering quality control on individual datasets²⁷. Cells with a UMI count exceeding 3 median absolute deviations (MADs) from the median UMI value were excluded from downstream analysis. Similarly, cells with a total gene count less than 200 genes or with a high proportion of reads originating from mitochondrial genes (>4MADs) were also excluded. Prior to combining the two datasets, data normalization was performed using the MultiBatchNormalisation method²⁸. Mitochondrial and ribosomal genes were excluded from the 2000 highly variable genes identified using the FindVariableFeatures function and the 'vst' selection method in Seurat V3.2.3²⁹. Following scaling of data, principal component analysis was performed using the previously identified list of highly variable genes. Clustering of cells was performed using the standard 'FindNeighbours' and 'FindClusters' methods including the first 12 principal components²⁹. Clustered data was then visualised in two dimensions using the Uniform Manifold Approximation and Projection (UMAP) method calculated using the 'RunUMAP' command²⁹. Differential gene expression analysis was performed using the 'FindAllMarkers' method selecting markers expressed in at least 30% of cells in the corresponding cluster and with a minimum log fold change in expression of 0.3 compared to the remainder of the dataset. Count data from cells belonging to the identified fibroblast cluster was extracted to further explore fibroblast heterogeneity using the same processing steps described above. Contaminating Schwann and mesothelial cells were excluded from further analysis of fibroblast heterogeneity. PHATE reduction analysis was performed as described below³⁰. Published datasets were reanalyzed per published methods^{13, 18, 20, 25, 31, 32}.

Cell signature scores

Cell signature scores were calculated as the scaled geometric mean of the expression of selected marker genes within each cell. All gene names within the dataset beginning with 'Mt' were included for generating the mitochondrial signature. All gene names beginning with 'Rpl' or 'Rps' within the dataset were included for calculating the ribosomal signature.

Pseudotime and RNA velocity analysis

Pseudotime cellular trajectories were calculated with the Monocle package (v2.10.1)³³. Subsets of fibroblast cells were first produced based on the localization of clusters within the branches of the previously generated PHATE plot. The FindMarkers method²³ was then used to identify markers of clusters localizing at the beginning and end of each PHATE branch. Marker genes with the highest logFC in expression were subsequently used for dimensionality reduction of data to two dimensions using the reduceDimension method³³. Pseudotime values

were then calculated using the `orderCells` command applying default Monocle parameters³³. Following scaling from 0 to 1, pseudotime values were subsequently mapped onto the corresponding cells on the previously generated PHATE plots. Directionality of cellular transitions were inferred by calculating the RNA velocity of individual cells using the `velocyto` R package³⁴. Reads were identified as mapping to either intronic or exonic sequences using the DropEst pipeline³⁵ utilising the previously generated binary alignment files from the Cell Ranger pipeline. Velocyto was then used to calculate RNA velocity using KNN pooling with $K_{cells} = 25$ and gamma fit performed using the full range of cellular expression magnitudes. RNA velocity vectors were then superimposed onto the previously generated PHATE plot.

Functional analysis using gene ontology (GO) terminology

Functional enrichment analysis was performed using G:profiler³⁶. A ranked list of the differentially expressed genes per end cluster was used as input. To increase the interpretative value, the size of the functional category range was set from 5 to 750. Electronic GO annotations were disabled and the size of query/term intersection was set to 3 to increase the reliability³⁷. The top-10 Go biological process terms per cluster were selected and plotted on an excel bubble chart where the diameter of the node represents the $-\log_{10}(p\text{-Value})$.

Enrichment analysis using hypergeometric testing

The DEGs from the full trajectories (F1, F2, F3, F4, $n = 216$; F5, F6, F7, $n = 235$; F8, F9, $n = 317$) were intersected with 1) GWAS CAD-associated genes, and 2) human aorta fibroblast DEGs from the study of Li et al²⁰. For this, a total of 329 CAD-associated genes were retrieved from the GWAS association file (v1.0, 2021-12-07; downloaded from the GWAS Catalog³⁸ website: <https://www.ebi.ac.uk/gwas/>) by searching the key word “coronary” in the term “disease/trait”. In addition, for each of the four human aorta fibroblast clusters reported by Li et al., we downloaded the top 20 DEGs from the original paper²⁰ and combined them as a comprehensive fibroblast gene set. Hypergeometric testing was used to evaluate the statistical significance of the overlap genes between trajectory genes and CAD or fibroblast genes. Mouse genes were converted to human genes by biomaRt R package (v2.50.1)³⁹.

Data availability

Data are deposited in a repository (GSE196395) and may be inspected on a web-based interface (Plaqview.com)⁴⁰. Count matrices and code are available upon reasonable request.

Statistical analysis

For human samples, correlations between genes and clinical traits were calculated using Pearson’s Correlation Coefficient. Only pairwise complete observations were included if missing values were contained in traits. Student P-value was calculated based on the correlations and sample size. Normality of the data was assessed through D’Agostino-Pearson

omnibus normality test and potential outliers were identified through the ROUT method. For mice flow cytometry analysis and Sirius red quantification, an ordinary two-way ANOVA was performed, followed by Tukey's multiple comparisons test. For immunohistochemistry analyses, depending on number of groups, unpaired T-test with Welch's correction or one-way ANOVA was used, followed by Bonferroni's multiple comparisons test. Statistical testing was done using GraphPad Prism 7.0.

Results

ScRNA-seq yields a seven-marker signature differentially regulated in fibroblasts compared to other cells in murine healthy vasculature

The adventitia of the thoracic aorta from 8 healthy male C57BL/6J mice was collected and pooled for isolation of DAPI⁻, cluster of differentiation (CD)45⁻, intercellular adhesion molecule 2 (ICAM2)⁻ cells to exclude immune and endothelial cells and enrich for the viable, mesenchymal population prior to scRNA analysis (**Supplementary (S) Figure S1A-C**). This approach allowed in-depth analysis of adventitial mesenchymal cells. In total, 5700 cells passed single-cell RNA quality control after removal of low-quality cells (< 1500 genes, >15% mitochondrial reads), and potential doublets (unique molecular identifier (UMI) count > 15,000) (**Table S1 and S2, Figure 1A-C**). Firstly, *in silico* selection of mesenchymal cells was done, based on expression of platelet-derived growth factor beta (*Pdgfrb*) (**Figure S1A**). Subsequently, annotation of the identified clusters was based on previously published markers for mural cells (myosin heavy chain 11 (*Myh11*), transgelin (*Tagln*), actin alpha 2 (*Acta2*), and calponin 1 (*Cnn1*)) and fibroblasts (*Col1a1*, *Col1a2*, matrix metalloproteinase 2 (*Mmp2*), and stem cell antigen-1 (*Sca-1/Ly6a*)¹⁶). These markers confirmed the presence of both fibroblasts and mural cells in healthy mouse adventitia (**Figure 1D and E**). The absence of macrophage (*Cd68*), endothelial cell (platelet endothelial cell adhesion molecule-1 (*Pecam1*)), neuron (RNA binding protein, fox-1 homolog 3 (*Rbfox3*)), and adipocyte (adiponectin (*Adipoq*)) markers confirmed the purity of our sorting strategy (**Table S3**). Differential gene expression analysis comparing fibroblast and mural cell populations revealed distinct expression profiles for both cell types (**Figure 1F**). Subsequent gene ontology (GO) enrichment analysis based on differentially expressed genes returned terms including 'extracellular matrix' and 'contractile fiber' corresponding to fibroblast and mural cell populations, respectively (**Figure S1D and E**).

Notably, many of the commonly proposed fibroblast markers from literature, including vimentin (*Vim*), *Mmp2*, CD90 (encoded by thymus cell antigen 1, *Thy1*), *Sca-1 (Ly6a)* and fibroblast activation protein (*Fap*), were not able to fully differentiate between fibroblasts and mural cells, as evidenced by RNA expression in pericytes and smooth muscle cells in three other single-cell RNA datasets (**Figure S2A and B**). Despite RNA levels being higher in fibroblasts than mural cells, protein co-expression with TAGLN⁺ smooth muscle cells was observed in healthy human and murine aorta (**Figure 1G-I, Figure S2C-D**). Thus, we next assessed genes differentially expressed between fibroblasts and mural cells to create a fibroblast-specific transcriptional signature. Differential gene expression (DEG) analysis provided twelve markers preferentially expressed in adventitial fibroblasts (**Figure 1J**). Enrichment of seven of these markers (platelet-derived growth factor alpha (*Pdgfra*), dipeptidase 1 (*Dpep1*), SPARC related modular calcium binding 2 (*Smoc2*), collagen 14 alpha 1

(*Col14a1*), fibulin 1 (*Fbln1*), lumican (*Lum*) and C-C motif chemokine ligand 11 (*Ccl11*) for mesenchymal fibroblasts remained after validation in two other available scRNA-seq datasets^{18, 25} (**Figure S1F-G**). Taken together, seven fibroblast markers (*Pdgfra*, *Lum*, *Smoc2*, *Col14a1*, *Fbln1*, *Dpep1*, and *Ccl11*) selected from our dataset were also expressed in fibroblasts and/or mesenchymal cells in two other datasets comprising healthy murine vasculature and a database including multiple murine organs.

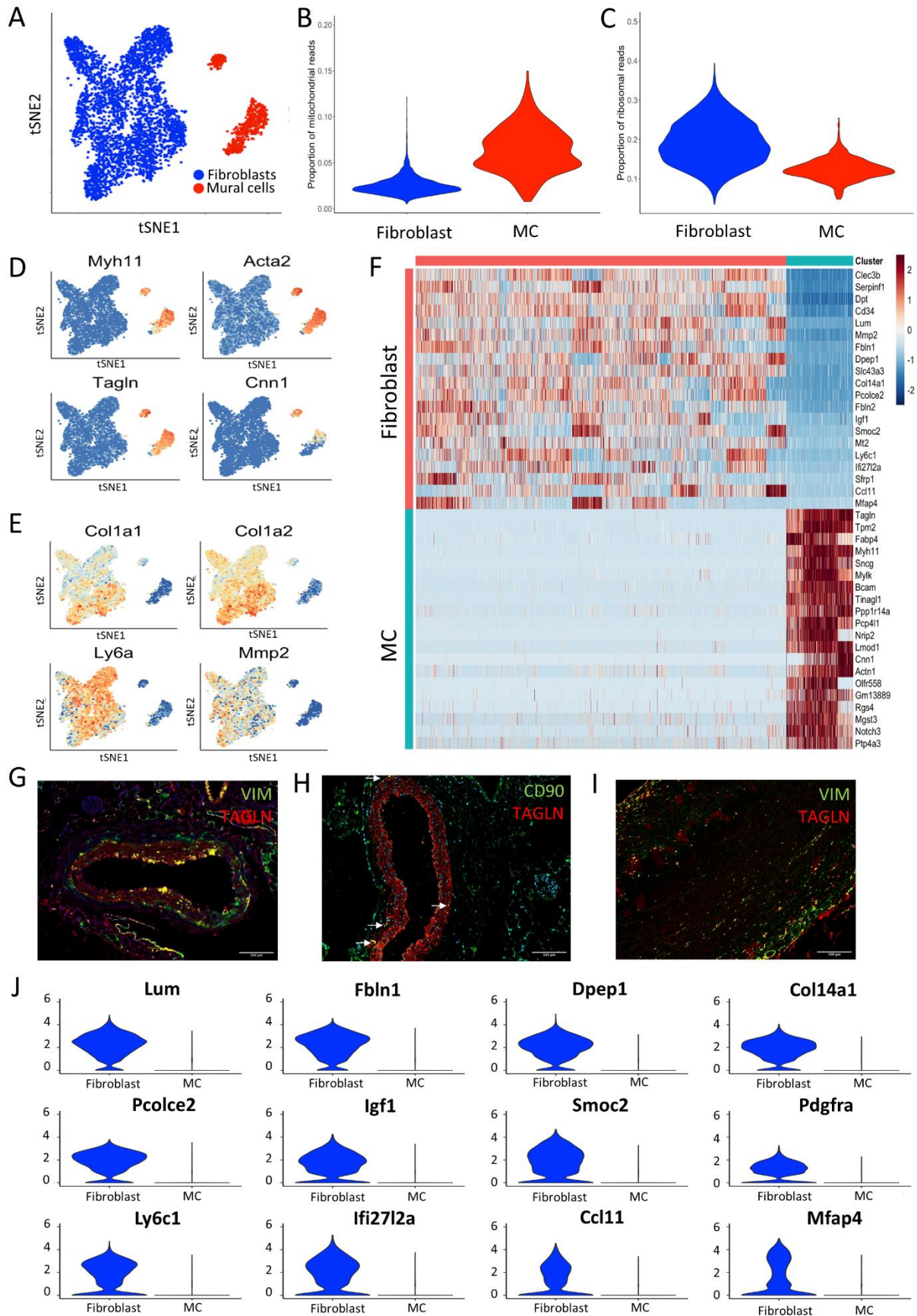


Figure 1: Single-cell RNA-sequencing reveals fibroblast transcriptional signature for healthy murine aortic adventitia. (A) T-distributed stochastic neighbour embedding (t-SNE) plot of single-cell sequencing data derived

from CD45-/ICAM2-/PDGFR β + adventitial cells from pool of 8 young C57BL/6J mice. **(B)** Mitochondrial signature of fibroblasts and mural cells (MC) post-filtering. **(C)** Ribosomal signature of fibroblasts and MCs post-filtering. **(D)** Expression of MC markers (*Myh11*, *Acta2*, *Tagln*, *Cnn1*), and **(E)** traditional fibroblast markers (*Col1a1*, *Col1a2*, *Ly6a*, *Mmp2*) projected on tSNE plot from Figure 1A shows cell type annotation. **(F)** Heatmap of differentially expressed genes (DEGs) in fibroblasts and MC. Immunohistochemical staining of SMC marker TAGLN (red) with traditional fibroblast markers (green) **(G)** vimentin (VIM) and **(H)** CD90 in mouse. **(I)** Immunohistochemical staining of SMC marker TAGLN (red) with traditional fibroblast marker vimentin (VIM, green) in human aorta. **(J)** Violin plots of twelve genes differentially expressed in fibroblasts compared to MC. Scale bars 100 μ m.

We next validated the fibroblast signature at the protein level using immunohistochemistry and confirmed adventitial localization in healthy mice and expression in spindle-like cells, resembling known fibroblast morphology for all markers, except CCL11. We used the following vascular beds: aortic root (AR), brachiocephalic artery (BCA), ascending aorta (Asc. A), thoracic aorta (Th. A), abdominal aorta (Abd. A) and carotid artery (CA) (**Figure 2**). PDGFRA and DPEP1 expression was specifically located in the adventitia across all arteries (**Figure 2A-B**), while LUM, SMOC2, COL14A1, and FBLN1 also showed expression in the media (**Figure 2C-F**). In case of the latter, it is in accordance with the recent detection of LUM+ fibroblast-like cells^{12, 13, 41}. Negative controls can be observed in **Figure S3A**. Importantly, flow cytometry confirmed that PDGFRA expression was largely similar across various vascular beds (**Figure 2G**). CCL11 was undetectable in aortic roots (**Figure S3B-C**), concordant with gene expression analyses in heart and aorta from the Tabula Muris consortium²⁶ (**Figure S1G**). Moreover, by making use of aorta tissue from smooth muscle cell *Myh11* reporter mice, and *Pdgfra* reporter mice, we were able to show very limited overlap between *Pdgfra* and *Myh11* (**Figure S3D-E**). This confirmed the highly selective nature of *Pdgfra*, prompting its use in further studies to delineate fibroblast distribution across arteries and heterogeneity.

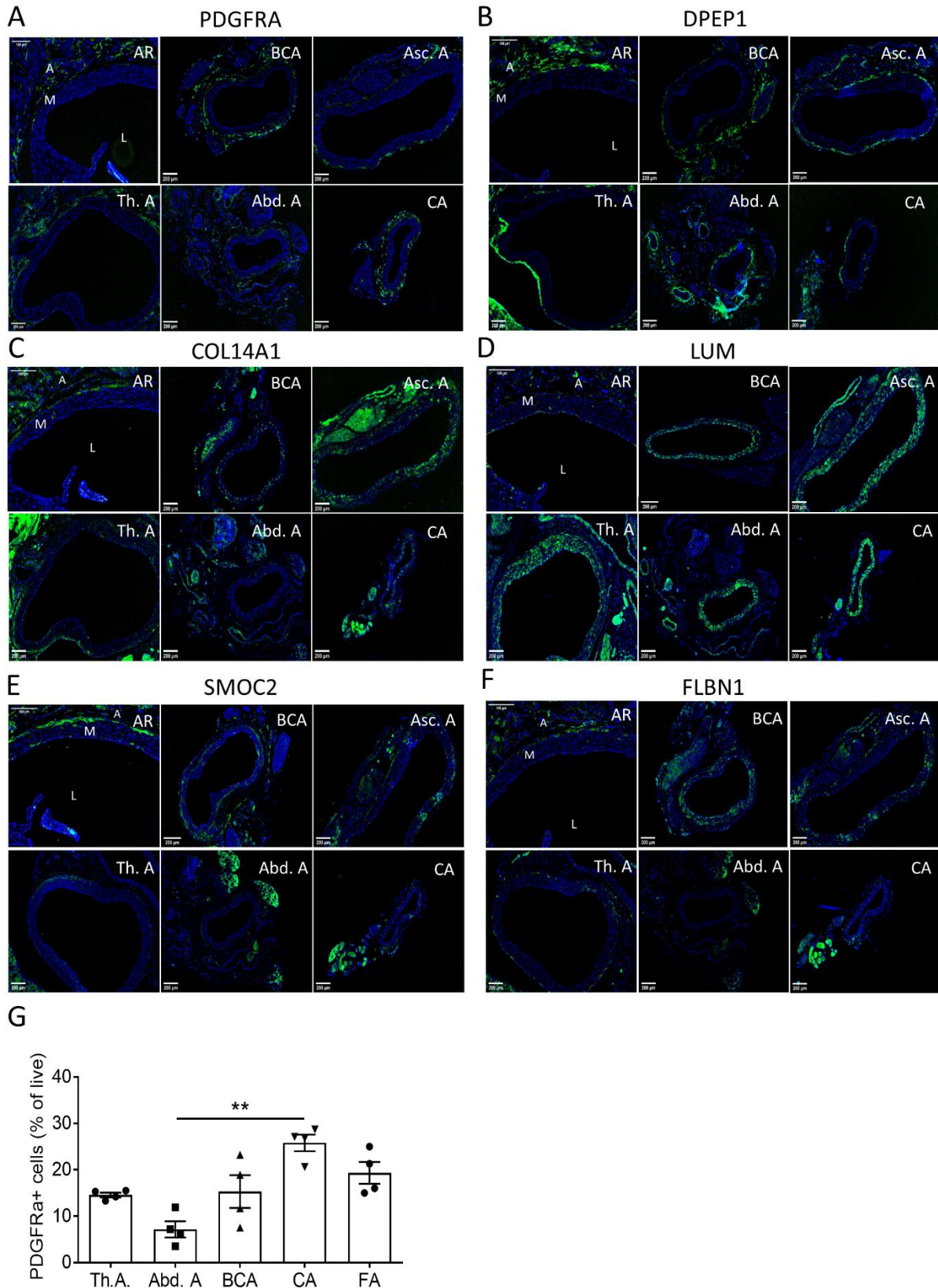


Figure 2: Validation of fibroblast signature across multiple vascular beds. Representative immunohistochemical staining of proposed fibroblast markers **(A)** platelet-derived growth factor alpha (PDGFRA), **(B)** dipeptidase 1 (DPEP1), **(C)** collagen 14 alpha 1 (COL14A1), **(D)** lumican (LUM), **(E)** SPARC related modular calcium binding 2 (SMOC2), and **(F)** fibulin 1 (FBLN1), in healthy murine C57BL/6J aortic roots (AR), brachiocephalic artery (BCA), ascending aorta (Asc. A), thoracic aorta (Th. A), abdominal aorta (Abd. A) and carotid artery (CA), $n = 10$. Nuclei

in blue, fibroblast markers in green. L indicates lumen, M indicates media, and A indicates adventitia. **(G)** PDGFRA+ frequencies within live CD45-/VE-cadherin- adventitial cells, across C57BL/6J arteries (thoracic aorta (Th. A), abdominal aorta (Abd. A), brachiocephalic artery (BCA), carotid artery (CA), and femoral artery (FA)), analyzed by flow cytometry ($n = 4$ pools of 5 mice each, 20 mice total). Results are shown as mean \pm standard error of the mean (SEM). * $p < 0.05$ vs Th. A. Scale bars 100 μm (AR) or 200 μm .

Trajectory inference analysis predicts the cellular dynamics of fibroblasts in healthy murine adventitia

The single-cell RNA-sequencing analysis not only supported the existence of two distinct cell types, but also suggested heterogeneity within the fibroblast population in a healthy, basal state (**Figure 3A**). To characterize the cellular dynamics underlying fibroblast heterogeneity, we applied Potential of Heat-diffusion for Affinity-based Trajectory Embedding (PHATE) dimensionality reduction analysis to the dataset to predict differentiation state. PHATE reduction is developed for optimal preservation of patterns in data structure such as continual progressions, branches and clusters, arising due to underlying biological processes, like differentiation³⁰. PHATE previously uncovered trajectories, that were undiscoverable by other methods³⁰. Subsequent clustering and visualization of data revealed multiple trajectories, suggestive of distinct fibroblast subtypes present in the arterial wall (**Figure 3B**). Expression of stem cell marker *Ly6a/Sca-1*⁴² in most (96.5%) fibroblasts, as shown in **Figure 1E**, supports the cellular differentiation potential of these cells. Interestingly, one of the three trajectories showed higher *Ly6a/Sca-1* expression throughout the whole trajectory (**Figure S4A**), whereas end-point clusters of the other two trajectories did not. PHATE analysis did not predict any *Ly6a/Sca-1* expressing fibroblasts to be differentiating into SMCs of the healthy murine adventitia (**Figure S4B**). To exclude that these trajectories were a result of differences in proliferation, protein synthesis or an artefact related to cell damage, the expression of proliferation markers, and ribosomal and mitochondrial genes, respectively, were investigated. Near absent expression of proliferation marker of proliferation Kiel 67 (*Mki67*), cyclin-dependent kinase (*Cdk1*, *Cdk2* and centromere protein F (*Cenpf*), and uniformly low expression of mitochondrial and ribosomal reads among all clusters was shown (**Figure S4C-F**).

We next mapped RNA velocities³⁴ onto the PHATE visualization. RNA velocity is estimated based on the proportions of spliced versus unspliced transcripts, allowing for prediction of future cell transcriptional state. In agreement with PHATE analysis, vectors pointing outwards toward branch extremities suggested the differentiation direction of three main trajectories (**Figure 3C**). Application of Monocle, a third trajectory inference tool³³ further supported the presence of identified trajectories (**Figure S4G**). The inference of the trajectory analysis was that all three trajectories originated from one or more clusters in the center (F1, F5 or F8), hence the possibility of a precursor population was further investigated. Gene signatures for each of these center clusters were constructed (**Table S4**) and the resulting signature scores

were presented in violin plots to suggest the origin of the three trajectories (**Figure S5**). This analysis implied that the differential expression of the F1 signature in clusters F2, F3, and F4 supported F1 as the origin of this trajectory (Trajectory 1). The F1 origin of F10 and F11 is likely, but differential expression of the F1 signature was less clear. Similarly, signature analysis suggested F5 as the likely origin of the F6-F7 (Trajectory 2) and F12 trajectories. F8 was inferred to be the likely origin of Trajectory 3 given the observed enrichment of its signature in F9.

Furthermore, the observed pattern was not a dataset specific phenomenon, as PHATE analysis of 840 “non-immune” adventitial cells in the dataset by Gu et al.¹⁸ also revealed three comparable differentiation trajectories (**Figure 3D**), supporting the results of our trajectory analysis. Expression of DEGs from the PHATE trajectories originating from the Gu dataset were also confined to three individual trajectories in our own PHATE analysis data (**Figure 3E**) demonstrating the reproducibility of our findings.

The DEGs in our dataset were further analyzed to investigate possible biological traits associated with the observed trajectories. GO term analysis of DEGs identified in the distal, most differentiated clusters (i.e. F4, F7, F9) of the three trajectories revealed differential annotation of gene ontology terms, and thus potentially different functions (**Figure 3F**). Trajectories 2 and 3 demonstrated expression of genes involved in extracellular matrix production. Trajectory 1 showed enrichment for terms involved in vasculature development and nucleotide sugar metabolism, trajectory 2 for cholesterol metabolism and antigen presentation and trajectory 3 for response and signaling upon growth factors, and collagen fibril organization. Together, the analysis supports a continuity of phenotype is apparent in adventitial fibroblasts, where most differentiated clusters have differential functional annotations.

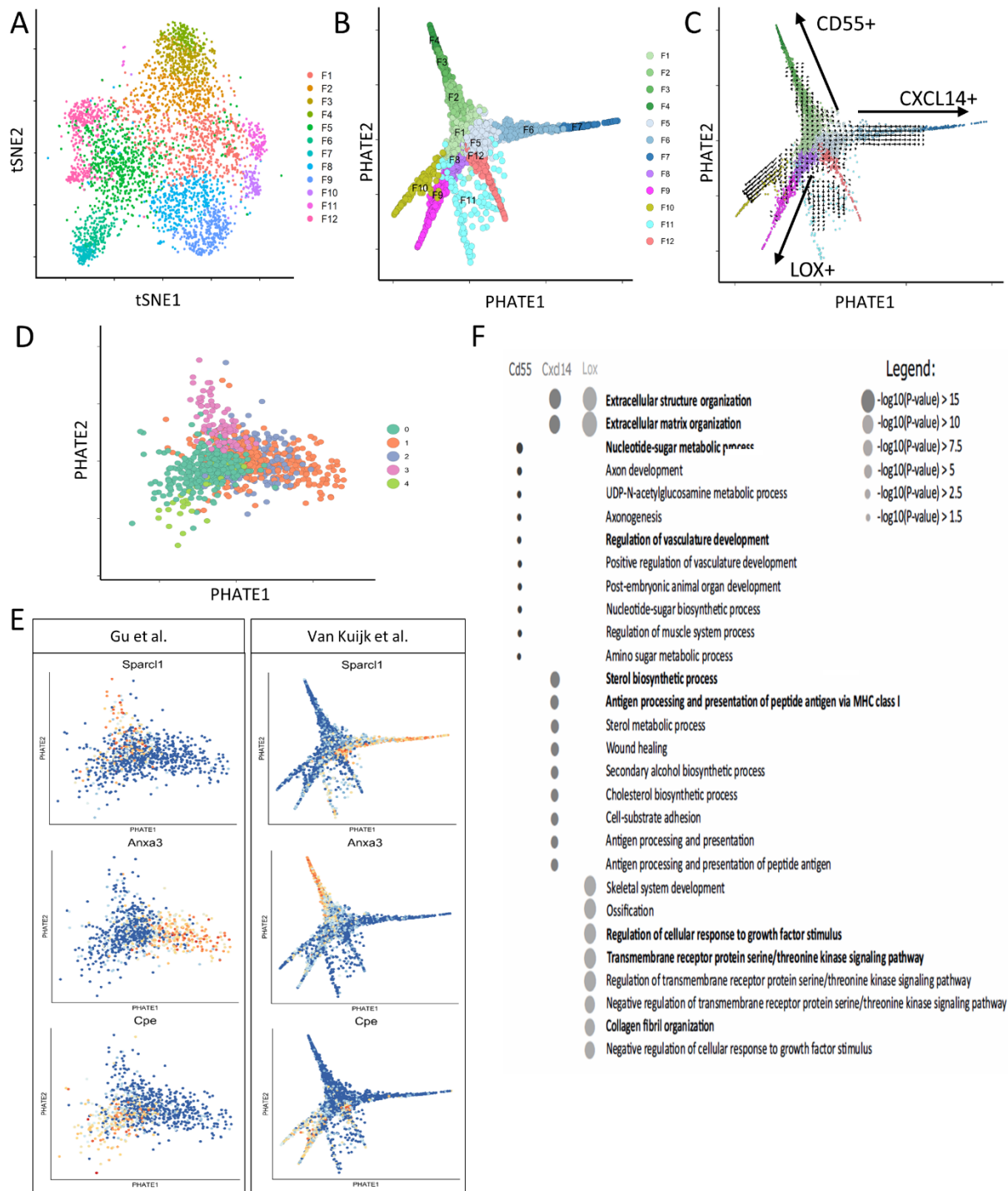


Figure 3: Trajectory analysis shows distinct phenotypes of fibroblasts in healthy murine adventitia. (A) tSNE plot of fibroblasts originating from Figure 1A. **(B)** PHATE pseudotime trajectory analysis of fibroblasts from Figure 1A depicting 12 clusters differentiating along several trajectory paths. **(C)** RNA velocity analysis on PHATE data from Figure 3B, arrows are indicating directionality. **(D)** Data was validated by PHATE analysis on an independent dataset from Gu et al.¹⁸ (840 cells from healthy murine adventitia) showing three trajectories. **(E)** Feature plots show expression of three differentially expressed genes in trajectories from Gu dataset on Gu PHATE map, and their expression in three trajectories of the PHATE map of our dataset (van Kuijk). **(F)** Dot plot of the gene ontology (GO) terms from the most differentiated clusters (F4, F7, F9) representing trajectories 1-3, respectively, with the most relevant GO terms in bold.

Fibroblast clusters validated in healthy murine vasculature

Genes selectively marking the most differentiated cluster of each fibroblast trajectory were identified for validation at the protein level, i.e. F4, F7 and F9 for trajectory 1 through 3 respectively (**Figure S6**). Candidates were selected based on reported expression in fibroblasts, cellular function related to the trajectory GO terms, gene function shown in animal studies, genome-wide associations to be related to known fibroblast functions, and/or processes involved in vascular disease, availability of antibodies for immunohistochemistry and flow cytometry, and/or preferential membrane expression. As an indicator of the most differentiated cluster in trajectory 1, cluster of differentiation 55 (*Cd55*, also known as decay-accelerating factor (*Daf*)) (**Figure 4A**) is involved in complement activation and a whole-body KO mouse presented with a protective phenotype against atherosclerosis^{43, 44}. The marker representing trajectory 2, CXC motif chemokine ligand 14 (*Cxcl14*) (**Figure 4A**) is involved in immune regulation and immune cell migration⁴⁵. Lastly, the marker representing trajectory 3, lysyl oxidase (*Lox*) is involved in the crosslinking and stabilization of extracellular matrix⁴⁶ (**Figure 4A**). All three markers (CD55, CXCL14 and LOX) located to the adventitia in healthy murine aortic roots, brachiocephalic arteries, carotid arteries and abdominal aorta, and co-localized with fibroblast marker PDGFRA (**Figure 4B-C, Figure S7A-B**). Flow cytometric analysis showed adventitial protein expression of all three markers in fibroblasts in a variety of vascular beds isolated from healthy C57BL/6J mice (**Figure 4D and E**). Important to note is that the observed percentages of each end-stage cluster in the thoracic aorta are similar to cluster percentages obtained from our scRNA-seq data (**Table S5**). CD55+ and CXCL14+ fibroblasts are similarly present between arteries, while the frequency of LOX+ fibroblasts varies. All clusters show different distributions within the same artery. These data validate the location, PDGFRA colocalization, frequency and protein expression of key markers for clusters representing each trajectory using two independent techniques.

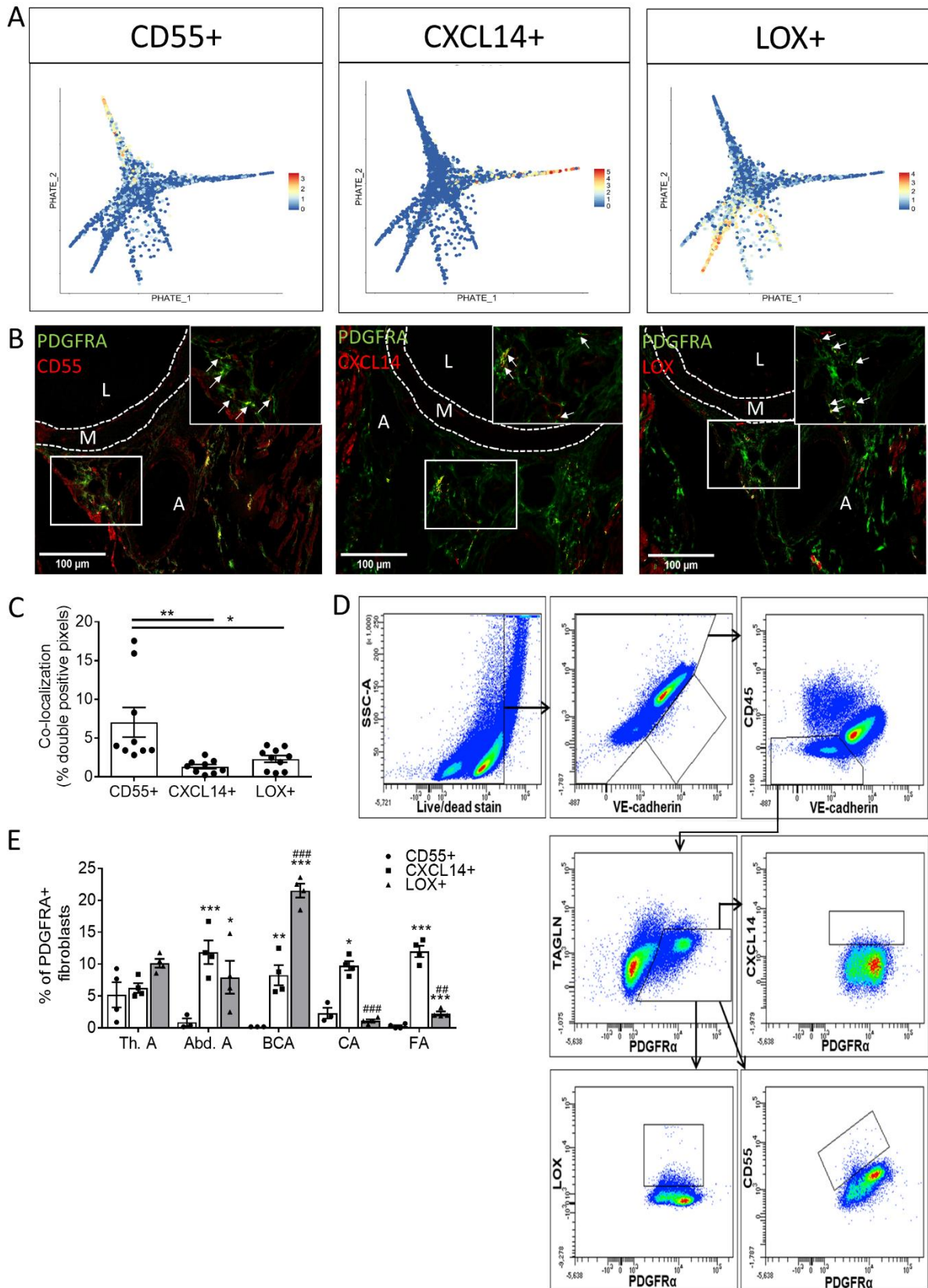


Figure 4: Fibroblast clusters representing three trajectories can be identified on transcriptional and protein level in healthy murine adventitia. (A) Projection of clusters markers representing the three trajectories *Cd55*, *Cxcl14* and *Lox* on PHATE plot from Figure 3B. **(B)** Immunohistochemical staining of CD55, CXCL14 and LOX in aortic roots of healthy C57BL/6J mice ($n = 10$). Pan-fibroblast marker PDGFRA in green and fibroblast trajectory

markers in red. Yellow areas indicate double-positive cells for PDGFRA and cluster marker (marked with arrows in 63X magnification). L indicates lumen, M indicates media, A indicates adventitia. **(C)** Quantification of double positive cells for each cluster in aortic roots of Figure 4B. **(D)** Flow cytometry gating strategy of each fibroblast cluster. **(E)** Fibroblast clusters in the adventitia of thoracic aorta (Th. A), abdominal aorta (Ab. A), brachiocephalic artery (BCA), carotid artery (CA), and femoral artery (FA) assessed by flow cytometry in 4 pools of 5 mice, 20 mice in total. Results are shown as mean \pm SEM. * $p < 0.05$, ** $p < 0.01$, or *** $p < 0.001$ vs. CD55+ fibroblasts in same artery; # $p < 0.05$ or ### $p < 0.001$ vs. same cluster in Th. A. Scale bars 100 μ m.

Cardiovascular risk factors differentially regulate fibroblast clusters

We next queried if the inferred trajectories would be involved in cardiovascular disease, and/or regulated by known CV risk factors. Indeed, we showed that DEGs from all three trajectories were significantly enriched in genes with a single nucleotide polymorphism related to coronary artery disease (**Table S6**). Interestingly, mainly DEGs in the *Cxcl14*+ trajectory showed a highly significant enrichment, and the involved DEGs could be linked to the GO terms of this trajectory, e.g. lipid metabolism and inflammation^{3, 47}. Thus, we studied if changes in the environment, such as in CVD, differentially affected the most differentiated fibroblast clusters in each trajectory. Cardiovascular risk factors ageing and mild dyslipidemia initiate early vascular changes and predispose to atherosclerosis, the main cause of cardiovascular disease⁴⁸. To assess the response to these early vascular changes, we used flow cytometry to dissect changes in CD55+, CXCL14+ and LOX+ fibroblasts between young and aged mice, and between normolipidemic wildtype mice and low-density lipoprotein receptor deficient (*Ldlr* KO) mice on a chow diet to induce mild hypercholesterolemia. Interestingly, fibroblast clusters were differentially altered upon ageing and lipidemia. Ageing preferentially increased CD55+ PDGFRA+ and CXCL14+ PDGFRA+ cell fractions, while mild dyslipidemia in *Ldlr* KO mice only increased the LOX+ PDGFRA+ cell fraction, representing the fibrosis-associated trajectory (**Figure 5A-B, Table S7**), suggesting the context-dependent importance of the inferred trajectories in progression of disease.

To interrogate whether these changes have functional relevance, we analyzed adventitial area, collagen and inflammatory cell accumulation. LOX is mainly involved in crosslinking immature collagen⁴⁹, and analysis of both mature collagen type I presence and Sirius Red analysis revealed an increase in mature collagen in adventitia from *Ldlr* KO mice (**Figure 5C and 5E, and Figure S8A, respectively**). Notably, the arteries in *Ldlr* KO or aged mice on chow did not show changes in adventitial area, or the major vascular cell populations (**Figure 5C-E, Table S8**), or any sign of atherosclerotic plaque development compared to C57BL/6J, as expected in only mild hypercholesterolemia and ageing (**Figure 5C-D**). Immune cell infiltration did not associate with CD55+ or CXCL14+ fibroblasts in ageing. Yet, CXCL14+ fibroblasts, also predicted to act in matrix metabolism, emerged simultaneously as adventitial collagen accumulation in ageing. Hence, the functional changes coinciding with an increase of LOX+ or CXCL14+ fibroblasts precede overt inflammatory, vascular disease.

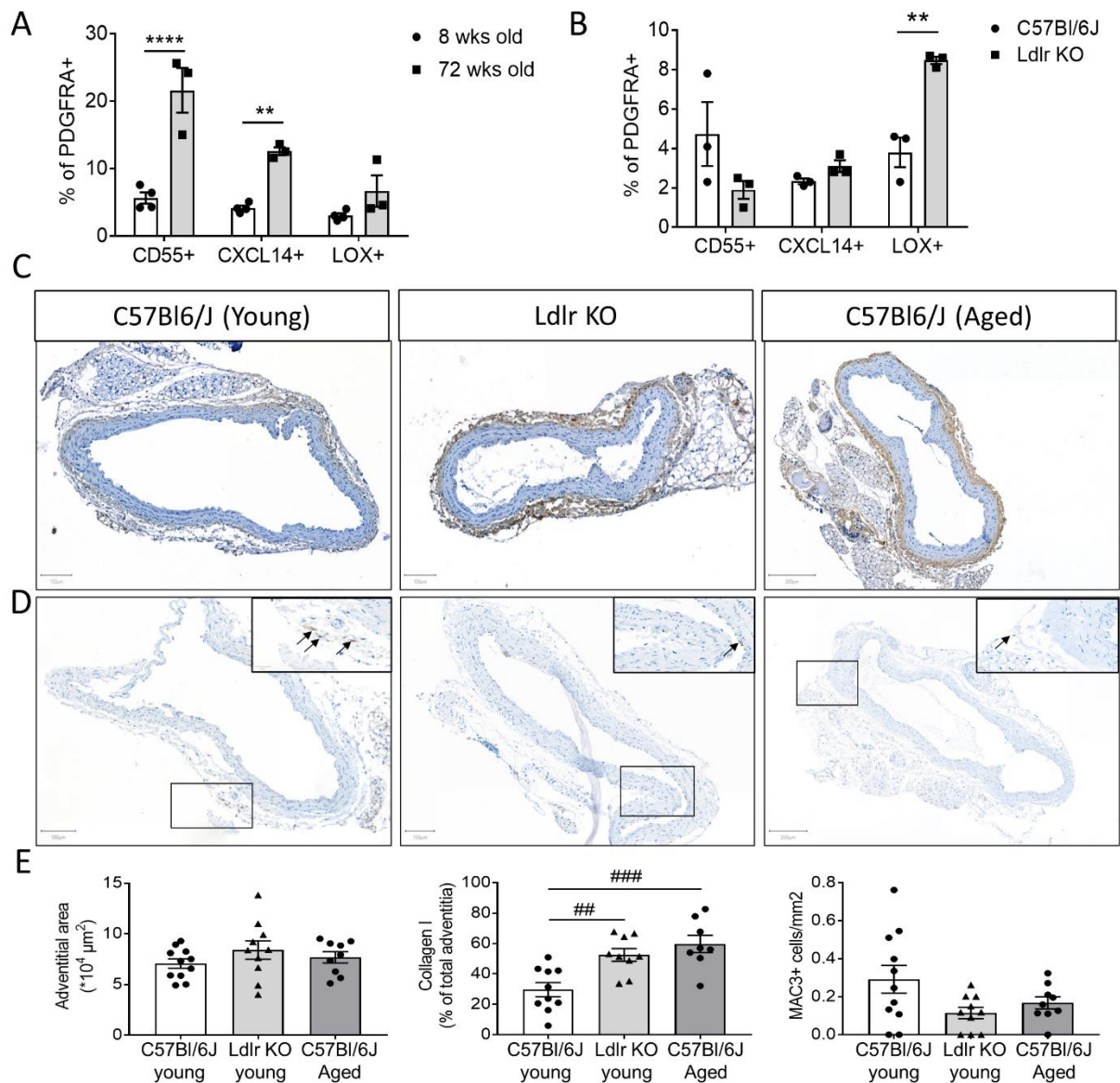


Figure 5: Fibroblast clusters representing three trajectories are differentially regulated upon cardiovascular risk factors. (A) Flow cytometry analysis of fibroblast clusters representing three trajectories in thoracic aorta adventitia from young or aged C57BL/6J mice, 12 or 72 weeks old respectively ($n = 4$ pools of young mice, 9 mice per pool (36 mice total) vs. $n = 3$ pools of aged mice, 4-5 mice per pools (14 mice total), respectively). Data are depicted as mean \pm SEM. (B) Flow cytometry analysis of fibroblast clusters representing trajectories in adventitia from *Ldlr* KO mice on chow diet vs. healthy C57BL/6J mice. ($n = 3$ pools, 4 mice per pool (12 mice total) vs. $n = 3$ pools, 6 mice per pool (18 mice total), respectively). Data are depicted as mean \pm SEM. (C) Representative images of collagen type I, (D) MAC3 immunohistochemical stainings, and (E) quantification of adventitial area, collagen type I and MAC3+ cells in adventitia of young, *Ldlr* KO and aged mice (11, 10, and 9 mice per group, respectively). Positive cells or area are observed in brown, nuclei in blue. ** $p < 0.0032$, **** $p < 0.0001$, ## $p < 0.0060$, ### $p < 0.0006$. Scale bars 100 or 200 μm .

Atherosclerosis-relevance of murine fibroblast clusters and trajectories

The differential regulation by early vascular changes, prompted us to study the response of adventitial fibroblast clusters to atherosclerosis using scRNA-seq transcriptomics of the adventitia in mild and severe hypercholesterolemic *Ldlr* KO mice. In chow fed mice, 4800 adventitial cells passed quality control and in HCD fed mice, almost 8000 adventitial cells passed the quality control (**Table S1** and **S2**). All expected major cell types in adventitia were identified, with sub-clustering of the identified fibroblast population revealing seven distinct clusters (**Figure 6A-B**, **Figure S8B-C**). Of note, fibroblast *Ly6a/Sca-1* expression was lower in disease, in line with variation in other datasets (**Table S9**). PHATE reduction analysis confirmed the presence of trajectories equivalent to the original three trajectories in healthy adventitia (**Figure 6C**). Expression patterns of *Cd55* and *Cxcl14* each remained confined to a single fibroblast trajectory (**Figure 6C**). This was to a lesser extent visible for *Lox*. *Lox* was less confined to one trajectory, although still mutually exclusive from cells expressing *Cd55* or *Cxcl14*. In line with mRNA expression patterns, protein expression of markers for all three trajectories were visualized in PDGFRA fibroblasts of the adventitia underlying advanced murine plaques (**Figure 6D**). LOX+ fibroblasts were the least prominent at the protein level in this disease condition. These data imply a role for LOX+ fibroblasts in very early stages of atherogenesis, rather than advanced atherosclerosis.

Interestingly, only CD55+ fibroblasts were observed in the atherosclerotic plaque, indicated by the white arrows, in addition to the adventitial layer (**Figure 6D**). Intriguingly, this trajectory (cluster 0 and 6) also highly expressed stem cell marker *Ly6a/Sca-1* (**Figure 6E**) and may represent the most plastic, progenitor-like trajectory. This is in line with our healthy scRNA-seq dataset, where the equivalent trajectory highly expressed *Ly6a/Sca-1*. Other groups have already shown that *Sca-1* positive cells have the capacity to contribute to neointima formation upon vascular injury^{50, 51}, yet it remains to be defined if these cells were of fibroblast, MC, or other origin. Our data shed new light on a possible role of specific fibroblast trajectories therein.

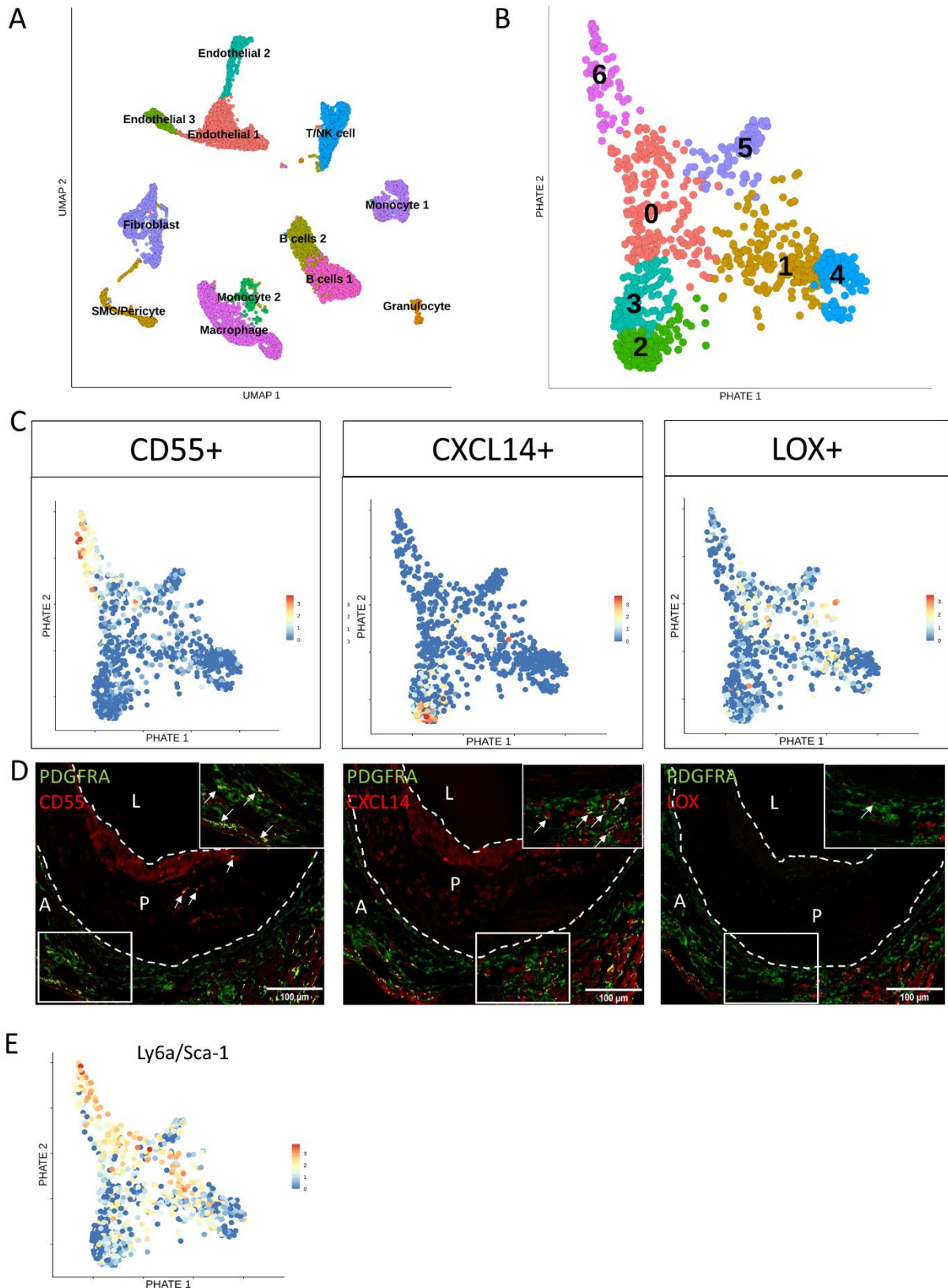


Figure 6: Fibroblast cluster markers representing three trajectories are still observed in atherosclerosis, while LOX+ fibroblasts reduced in presence. (A) Unsupervised clustering of single-cell sequencing data from *Ldlr* KO mice on chow or 16 weeks of high cholesterol diet (HCD). Results are visualized by Uniform Manifold Approximation and Projection (UMAP), colors represent individual clusters. **(B)** PHATE visualization of fibroblasts originating from the dataset in Figure 6A, colors represent individual clusters. **(C)** Cluster markers projected on

fibroblast PHATE plot of Figure 6B, representing trajectory 1 using *Cd55*, trajectory 2 using *Cxcl14*, and trajectory 3 using *Lox*. **(D)** Protein expression of each cluster marker visualized by immunohistochemistry in aortic roots from *Ldlr* KO mice after 16 weeks high cholesterol diet. Pan-fibroblast marker in green and fibroblast cluster markers in red. Yellow areas indicate double-positive cells for pan-fibroblast and cluster marker (marked with arrows). L indicates lumen, P indicates plaque, A indicates adventitia. **(E)** *Ly6a/Sca-1* mRNA expression visualized on PHATE map, originating from Figure 6B, depicting fibroblast clusters. Scale bars 100 μ m.

Fibroblast clusters are present in atherosclerotic human vasculature

To address the relevance of our murine fibroblast trajectories in human vasculature, we used specimens from carotid anastomosis during aortic bypass surgeries and carotid artery specimens acquired from the opposite side of the culprit plaques during carotid endarterectomy. Both specimens have the advantage that the adventitia is still attached to the vessel wall, allowing investigation of the trajectories in very early stage atherosclerotic human adventitia. Healthy specimens are almost impossible to retrieve in the western population, as even asymptomatic patients present with the earliest signs of intimal thickening (IT)⁵². This precludes the use of completely healthy arteries, as we obtained from mice. Nevertheless, all cluster markers representing the three trajectories could be observed in the adventitia of both surgical specimens (**Figure 7A**, **Figure S9A**), ensuring biological relevance of our identified clusters in human vasculature. In addition, in IT specimens obtained through autopsy from patients without CV symptoms, clusters could also be observed in the adventitia (**Figure S9B**). Moreover, spatial location might be of importance for function. In human intimal thickening sections, CD55+ fibroblasts were often observed on the border of the adventitia and media, while CXCL14+ and LOX+ trajectories were more observed surrounding the blood vessels in the adventitia.

To further confirm the presence of trajectories in human vasculature with early signs of disease, we obtained aorta scRNA-seq data from elderly individuals (median age 62) including all arterial wall layers²⁰. As these subjects presented with a history of smoking ($n = 2$), diabetes mellitus ($n = 1$), or hypertension ($n = 1$), aortae morphology is expected to show early sign of disease. After selection of the fibroblasts in the dataset, we performed PHATE analysis to assess the presence of trajectories. Also in human aorta with early atherosclerosis, trajectories could be observed that were transcriptionally divergent, although to a lesser extent than in young, healthy mouse adventitia (**Figure 7B**). Our murine cluster markers were expressed in human aorta fibroblasts, while only *CXCL14* was strictly confined to one human trajectory (**Figure 7C**). As this is a simplified view based on one marker gene, we tested if the complete gene set differentially expressed by each murine trajectory was significantly enriched in human fibroblasts. Important to note is that genes of the murine trajectories were indeed significantly enriched in the human fibroblasts (**Table S10**). Together, these data support human relevance of the observed fibroblast heterogeneity in mice.

We additionally confirm presence of the fibroblast clusters in advanced human atherosclerotic plaques of symptomatic patients undergoing carotid endarterectomy. Protein expression of each cluster marker was confirmed in adventitial PDGFRA+ fibroblasts, but also in the advanced plaque itself (**Figure 7D-E**) both on the adventitial as well as the luminal side. Additionally, we correlated differentially expressed genes by murine *CD55+*, *CXCL14+* and *LOX+* fibroblasts (46, 32, and 23 genes, respectively) to human plaque traits²². The traits were quantified in histology sections adjacent to the segment used for transcriptomics. The distribution of the individual correlations for all genes in a particular fibroblast cluster is shown in **Figure 7F**. Mostly genes of *LOX+* fibroblasts were shown to negatively correlate with detrimental plaque traits, such as plaque size, necrotic core and inflammatory macrophages (**Figure 7F**). These data suggest differential regulation and/or functions of fibroblast clusters representing the trajectories in human atherosclerosis, as we observed in mice.

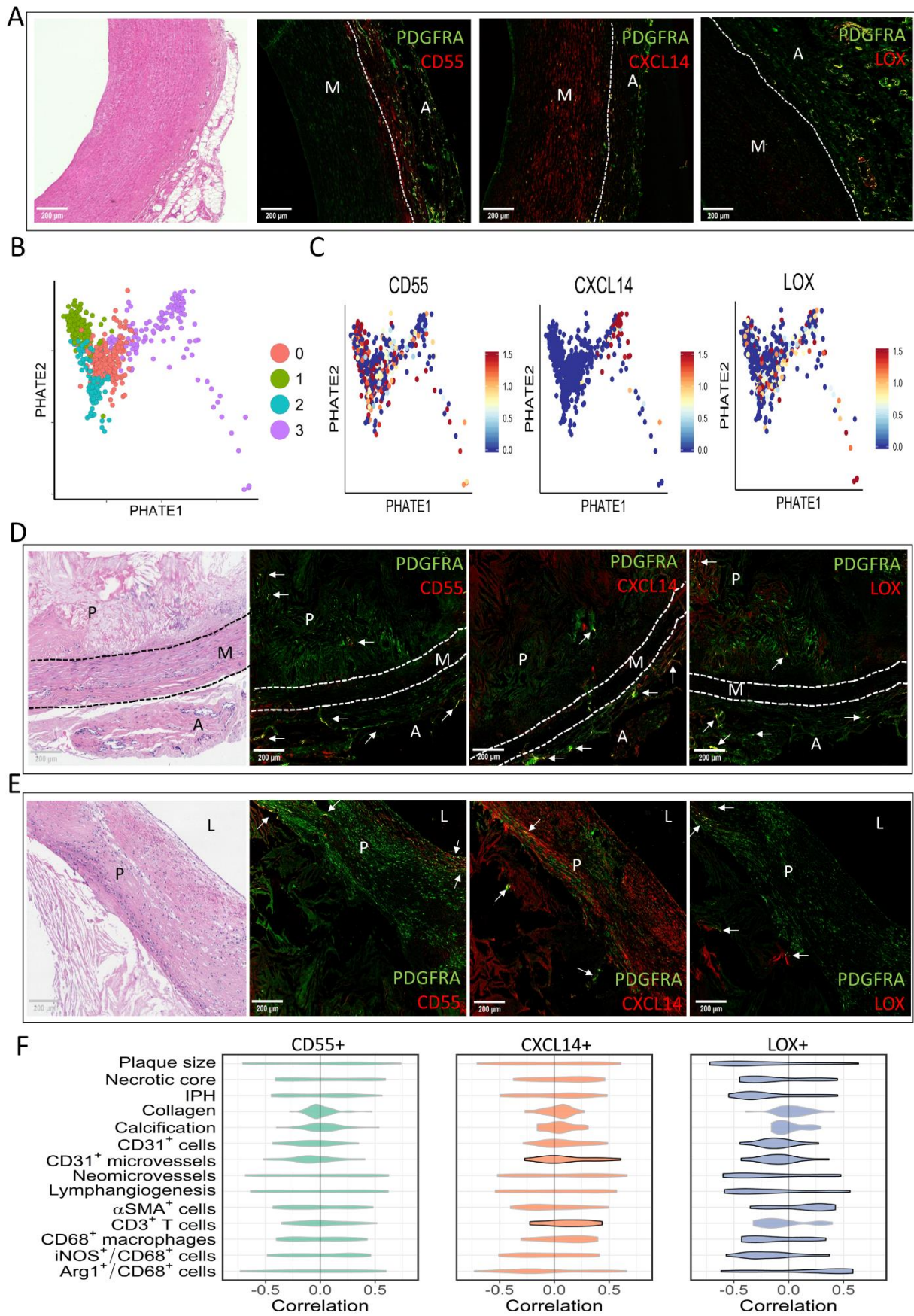


Figure 7: Fibroblast trajectories correlate differentially to human atherosclerotic plaque phenotype. (A) Immunohistochemical stainings of CD55⁺ fibroblasts, CXCL14⁺ fibroblasts, and LOX⁺ fibroblasts representing

trajectories 1-3, respectively, in human intimal thickening specimens collected through autopsy, accompanied with corresponding H&E, pan-fibroblast marker in green and fibroblast trajectory markers in red. Yellow areas indicate double-positive cells for pan-fibroblast and cluster marker. M indicates media, A indicates adventitia. **(B)** PHATE analysis of fibroblasts in scRNA-seq dataset by Li et al.²⁰ showing four clusters. **(C)** Fibroblast cluster markers representing the trajectories from mouse scRNA-seq data extrapolated to feature plots of human control data. Immunohistochemical stainings of CD55+ fibroblasts, CXCL14+ fibroblasts, and LOX+ fibroblasts representing trajectories 1-3, respectively, in advanced human atherosclerotic plaques, showing the adventitial side **(D)** and the luminal side **(E)**, accompanied by the corresponding H&E. Pan-fibroblast marker in green and fibroblast trajectory markers in red. Yellow areas indicate double-positive cells for pan-fibroblast and cluster marker. M, indicates media, P indicates plaque, A indicates adventitia. **(F)** Violin plots depicting correlations of all genes differentially expressed by each fibroblast trajectory with plaque traits in 43 human carotid plaque segments. Significant violin plots ($p < 0.05$) were denoted with a black border. Significance was assessed by positive and negative correlations and the unbalance thereof, which was defined as the sum of positive correlations minus the sum of absolute values of negative correlations. Furthermore, correlation skewness was compared between trajectory genes and a random gene set containing a similar number of genes. The permutation test was performed 100,000 times and the p-value is the frequency of the random gene sets that have higher correlation skewness than the trajectory gene set. Scale bars 200 μm .

Discussion

In this study, we identified arterial fibroblast cell type marker *Pdgfra* and *Dpep1* as most robust, and unveiled pseudotime trajectories of CD55+, CXCL14+ and LOX+ fibroblasts on RNA and protein level across five independent RNA datasets and using histology of five different murine and human arteries. We provide biological implications of these fibroblast clusters in disease in mice and humans: 1) CV risk factors and concomitant environmental triggers drive differential cluster distribution and associate with adventitial fibrosis; 2) ageing regulated adventitial CD55+ and CXCL14+ fibroblast expansion, and collagen accumulation; 3) mild hypercholesterolemia stimulated LOX+ fibroblast expansion and adventitial fibrosis preceding atherosclerosis; 4) fibroblast trajectories are present in human adventitia and plaques of symptomatic patients, 5) fibroblast trajectory genes differentially associated with human plaque traits and were enriched in GWAS genes, suggesting functional implication in human disease development. Together, these findings demonstrate a functional role for adventitial fibroblast trajectories, which could be of interest in disease progression and thus targeted treatments.

The identified arterial fibroblast cell type signature is of importance to the field to accurately distinguish arterial fibroblasts from other vascular cells, as expression of traditional fibroblast markers (e.g. COL1A1/2, VIM, CD90, FSP1, FAP, and DCN) is generally not restricted to fibroblasts as shown here and by others¹¹. Despite extensive *in silico* validation in three other single-cell transcriptomics datasets in healthy vasculature, protein validation only supported adventitial specificity of PDGFRA and DPEP1 across vascular beds, whereas LUM, COL14A1, SMOC2, and FBLN1 were additionally expressed in the media. Presumably, markers are shared with medial smooth muscle cells, in line with recent identification of LUM as marker for dedifferentiated SMCs in disease¹³. This is important information, as LUM has been coined as a fibroblast marker in several single-cell studies with mouse, primate, and human arteries, yet without proper validation^{17, 53, 54}. Alternatively, differences in embryonic origin between arteries could explain medial expression, in line with different embryonic origins of SMCs⁵⁵. The embryonic origin of adventitial fibroblasts in most arteries is not fully clear but is important to understand homeostasis and response to injury. Previous work showed that the neural crest was the origin of coronary artery adventitia⁵⁵, yet others excluded this origin in ascending aorta and support second heart field⁵⁶. Instead, dedifferentiation of medial Sca-1/*Ly6a*+ SMCs was shown²⁵, which offers a third explanation of ambiguity of our fibroblast signature. Trans differentiation between SMCs and fibroblasts in atherosclerosis is seemingly bi-directional^{13, 57}. Our data indeed suggest variation in embryonic origin and/or trans differentiation across arteries. Whether this also explains variation in trajectory dominance across arteries remains to be resolved using dual lineage reporter mice. Overall, the adventitial-specific location of PDGFRA and DPEP1 across arteries and absent medial co-localization of PDGFRA and SMC marker MYH11 in lineage reporter mice, support specificity

of this marker for arterial fibroblasts across healthy arteries, recommending this marker for future studies. A *Pdgfra* lineage tracing mouse would give insight in the location and distribution of fibroblasts in healthy but also diseased adventitia. In atherosclerosis, this would also reveal fate of adventitial fibroblasts, which is of interest considering evidence of endothelial or smooth muscle cell origin of fibroblast-like cells in plaques^{13, 14}. These studies are, however, beyond the scope of the current study.

The importance of adventitial cells in vascular pathology has been studied over the years, specifically focusing on the *Ly6a/Sca-1*+ progenitor population as a whole^{6, 57}, as recently reviewed by Jolly et al.¹ This population includes both mesenchymal and immune progenitors as shown by targeted phenotyping, and by our own data. Using our unbiased approach to phenotype adventitial mesenchymal cells, we show that the *Pdgfra/Dpep1* fibroblast population includes *Ly6a/Sca-1*+ cells, but also *Ly6a/Sca-1* low or negative cells. Moreover, *Ly6a/Sca-1*+ fibroblasts decrease in presence upon atherosclerosis, which might be a result of differentiation upon disease induction. On the other hand, we show that adventitial *Ly6a/Sca-1*+ cells include more than fibroblasts alone. Hence, *Ly6a/Sca-1*+ cells do not fully recapitulate PDGFRA+ cells, a concept which is important for interpretation of results. The CD55+ trajectory cells express high level and frequency of *Ly6a/Sca-1* and its function may thus most closely resemble published reports on adventitial *Ly6a/Sca-1*+ progenitor cells.

Biological implications of CD55+, CXCL14+ and LOX+ fibroblasts may be gained from their differential association and response to experimentally changed cardiovascular risk factors, i.e. age and serum lipids, and enrichment of genes with a GWAS to CAD. CD55+ fibroblasts were linked to vascular development and were increased upon aging. In endometrioid tumor, CD55 was found to be essential in self-renewal⁵⁸, which would be in line with our findings of coinciding expression of *Sca-1* in the CD55+ trajectory. Increasing the presence of the CD55+ trajectory might induce rejuvenation, through increased plasticity and potential to adapt to pathogenesis. In addition, CD55 has a role in complement regulation, and its stimulation may trigger detrimental vascular inflammation. This is in line with observations in atherosclerosis, where whole-body CD55 deficiency was shown to be atheroprotective in apolipoprotein E (*ApoE*) KO mice⁴³. As CD55 is one gene of 46, skewing the entire trajectory would probably not reflect the effect of the single CD55 knockout. CXCL14+ trajectory also expanded upon vascular aging. GO terms of the CXCL14+ trajectory included extracellular matrix organization, and antigen presentation, amongst others. In vascular ageing, we only observed an association of this trajectory with fibrosis, likely owing to the four collagen genes in this trajectory (*Col4a1*, *-5a3*, *-6a3*, *-15a1*). This is in line with a positive effect on fibrotic gene expression and proliferation of fibroblasts⁵⁹, and the absent effect of *Cxcl14* KO on immune cell recruitment in homeostasis⁶⁰. However, upon a stronger pro-inflammatory milieu, like in overt atherosclerosis, this aspect of CXCL14 function may be important. Indeed, this trajectory was

also detected in advanced plaques by histology and single-cell sequencing. In line, *Cxcl14* expression was enhanced in mouse primary macrophages by oxidized LDL, and peptide immune therapy diminished serum CXCL14 levels and murine atherosclerosis⁶¹. Although attributed to macrophages so far, conditional deletion of *Cxcl14* using existing *Pdgfra*- or future *Dpep1*-Cre models may unveil the effect of CXCL14+ fibroblasts in atherogenesis.

While CD55+ and CXCL14+ fibroblasts expanded upon vascular aging, expansion of LOX+ fibroblasts was triggered only by a mild increase in serum cholesterol. The early rise of LOX+ fibroblasts coinciding with adventitial collagen deposition prior to disease development, possibly implies a regenerative role for LOX+ fibroblasts to strengthen the vessel upon a lipid challenge. Higher total LOX protein abundance in plaques was associated with plaque stability, while, seemingly opposing, *Lox* mRNA levels predicted the risk of myocardial infarction⁶². Although these effects of LOX have thus far been attributed to SMCs⁶³, future studies are warranted to challenge this view. Together, we foresee skewing trajectories towards more favorable subsets through conditional knockout models, which might have great relevance for atherogenesis and vascular aging, like the improved balance between lung myogenic and lipofibroblasts spurring lung fibrosis⁶⁴. Likewise, dampening pro-inflammatory fibroblasts or promoting matrix-fibroblasts may be beneficial for plaque progression. An interesting addition to this is that lipid-lowering medications that are prescribed on a regular basis, e.g. statins, could already influence fibroblast abundance and matrix production⁶⁵. Studies investigating the beneficial lipid-lowering effect vs. the negative effect on fibroblast presence and functions are warranted.

The current study has some limitations. Current single-cell sequencing technology has limited sequencing depth and is therefore biased towards genes with high expression levels. Nevertheless, the resolution at single-cell level has already provided new insights in arterial biology in health and disease, as well as corroborated existing ones^{2, 18, 25, 66}. Enrichment of mesenchymal cells yielded sufficiently high fibroblast cell number to reveal transcriptional regulation of small subsets of cells, which remained obscured in two “atlas” datasets with smaller fibroblast numbers^{17, 18}. While their approach had the advantage to study all cells simultaneously, as well as cell-cell communication, our approach prevents analysis of cell-cell communication. Another limitation pertains to a causal implication of the observed association between the fibroblast trajectories and human plaque characteristics. Future studies with conditional depletion of trajectory genes or their master regulators in *Pdgfra*+/*Dpep1*+ fibroblasts would give us insight how targeted elimination of fibroblast trajectories would impact atherogenesis.

In conclusion, PDGFRA specifically marks arterial fibroblasts across arterial beds, with CD55+, CXCL14+ and LOX+ fibroblasts showing differential association to human cardiovascular

disease and response to cardiovascular risk factors. Together, these new insights will aid to determine the role of fibroblasts in disease progression and future targeted treatment plans.

Acknowledgements

The authors thank T. Abud, J. Debets, C. Dinjens, P. Leenders, and E. Wijnands for their technical assistance, and Gary K. Owens for providing *Myh11*-CreERT2 eYFP tissue sections. Flow-assisted cell sorting was done with support from the QMRI Flow Cytometry and cell sorting facility, University of Edinburgh, and at the Flow Cytometry Facility at RWTH Aachen.

Author contributions

J.C.S., A.H.B., K.V.K., I.R.M.: conceptualization; K.V.K., I.R.M., R.J.H.A.T., S.E.J.A., R.W.S., R.S.T., A.H.B., and J.C.S.: methodology; K.V.K., I.R.M., R.J.H.A.T., S.E.J.A., R.W.S., R.S.T., and J.C.S.: formal analysis; K.V.K., I.R.M., R.J.H.A.T., S.E.J.A., R.W.S., R.S.T., C.K., H.J., S.M., D.K., M.J.G., L.T., J.L., P.G.: investigation; R.D., P.R., Y.L., H.N., J.R.W.K., L.J.S., Y.H.S., B.M.E.M., E.A.L.B., N.C.H., and R.K.: resources; J.C.S. and K.V.K.: writing—original draft; K.V.K., I.R.M., A.H.B., J.C.S.: writing—review and editing; J.C.S.: funding acquisition; A.H.B., J.C.S.: supervision.

Funding sources

This work was funded by the Netherlands Organization for Scientific Research (NWO) VIDI grant (91718364) and ASPASIA grant (015.013.064) to J.C.S., a Senior Research Fellowship in Clinical Science from the Wellcome Trust (ref. 219542/Z/19/Z) to N.C.H., DFG/TRR219 M-05 to H.N., ERC advanced grant (VASC MIR) and Chair of Translational Cardiovascular Sciences from the British Heart Foundation to A.H.B.

References

1. Jolly AJ, Lu S, Strand KA, Dubner AM, Mutryn MF, Nemenoff RA, Majesky MW, Moulton KS, Weiser-Evans MCM. Heterogeneous subpopulations of adventitial progenitor cells regulate vascular homeostasis and pathological vascular remodeling. *Cardiovasc Res* 2021.
2. van Kuijk K, Kuppe C, Betsholtz C, Vanlandewijck M, Kramann R, Sluimer JC. Heterogeneity and plasticity in healthy and atherosclerotic vasculature explored by single-cell sequencing. *Cardiovasc Res* 2019;115:1705-1715.
3. Xie T, Wang Y, Deng N, Huang G, Taghavifar F, Geng Y, Liu N, Kulur V, Yao C, Chen P, Liu Z, Stripp B, Tang J, Liang J, Noble PW, Jiang D. Single-Cell Deconvolution of Fibroblast Heterogeneity in Mouse Pulmonary Fibrosis. *Cell Rep* 2018;22:3625-3640.
4. Guerrero-Juarez CF, Dedhia PH, Jin S, Ruiz-Vega R, Ma D, Liu Y, Yamaga K, Shestova O, Gay DL, Yang Z, Kessenbrock K, Nie Q, Pear WS, Cotsarelis G, Plikus MV. Single-cell analysis reveals fibroblast heterogeneity and myeloid-derived adipocyte progenitors in murine skin wounds. *Nat Commun* 2019;10:650.
5. Tillie R, van Kuijk K, Sluimer JC. Fibroblasts in atherosclerosis: heterogeneous and plastic participants. *Curr Opin Lipidol* 2020;31:273-278.
6. Majesky MW, Dong XR, Hognlund V, Daum G, Mahoney WM, Jr. The adventitia: a progenitor cell niche for the vessel wall. *Cells Tissues Organs* 2012;195:73-81.
7. Lee S, Park C, Han JW, Kim JY, Cho K, Kim EJ, Kim S, Lee SJ, Oh SY, Tanaka Y, Park IH, An HJ, Shin CM, Sharma S, Yoon YS. Direct Reprogramming of Human Dermal Fibroblasts Into Endothelial Cells Using ER71/ETV2. *Circ Res* 2017;120:848-861.
8. Xiao D, Liu X, Zhang M, Zou M, Deng Q, Sun D, Bian X, Cai Y, Guo Y, Liu S, Li S, Shiang E, Zhong H, Cheng L, Xu H, Jin K, Xiang M. Direct reprogramming of fibroblasts into neural stem cells by single non-neural progenitor transcription factor Ptf1a. *Nat Commun* 2018;9:2865.
9. Shi Y, O'Brien JE, Jr., Mannion JD, Morrison RC, Chung W, Fard A, Zalewski A. Remodeling of autologous saphenous vein grafts. The role of perivascular myofibroblasts. *Circulation* 1997;95:2684-2693.
10. Li M, Riddle S, Zhang H, D'Alessandro A, Flockton A, Serkova NJ, Hansen KC, Moldvan R, McKeon BA, Frid M, Kumar S, Li H, Liu H, Canovas A, Medrano JF, Thomas MG, Iloska D, Plecita-Hlavata L, Jezek P, Pullamsetti S, Fini MA, El Kasmi KC, Zhang Q, Stenmark KR. Metabolic Reprogramming Regulates the Proliferative and Inflammatory Phenotype of Adventitial Fibroblasts in Pulmonary Hypertension Through the Transcriptional Co-Repressor C-terminal Binding Protein-1. *Circulation* 2016.
11. Kuwabara JT, Tallquist MD. Tracking Adventitial Fibroblast Contribution to Disease: A Review of Current Methods to Identify Resident Fibroblasts. *Arterioscler Thromb Vasc Biol* 2017;37:1598-1607.
12. Alencar GF, Owsiany KM, Karnewar S, Sukhvasi K, Mocci G, Nguyen AT, Williams CM, Shamsuzzaman S, Mokry M, Henderson CA, Haskins R, Baylis RA, Finn AV, McNamara CA, Zunder ER, Venkata V, Pasterkamp G, Bjorkegren J, Bekiranov S, Owens GK. Stem Cell Pluripotency Genes Klf4 and Oct4 Regulate Complex SMC Phenotypic Changes Critical in Late-Stage Atherosclerotic Lesion Pathogenesis. *Circulation* 2020;142:2045-2059.
13. Wirka RC, Wagh D, Paik DT, Pjanic M, Nguyen T, Miller CL, Kundu R, Nagao M, Collier J, Koyano TK, Fong R, Woo YJ, Liu B, Montgomery SB, Wu JC, Zhu K, Chang R, Alamprese M, Tallquist MD, Kim JB,

Quertermous T. Atheroprotective roles of smooth muscle cell phenotypic modulation and the TCF21 disease gene as revealed by single-cell analysis. *Nat Med* 2019;25:1280-1289.

14. Evrard SM, Lecce L, Michelis KC, Nomura-Kitabayashi A, Pandey G, Purushothaman KR, d'Escamard V, Li JR, Hadri L, Fujitani K, Moreno PR, Benard L, Rimmele P, Cohain A, Mecham B, Randolph GJ, Nabel EG, Hajjar R, Fuster V, Boehm M, Kovacic JC. Endothelial to mesenchymal transition is common in atherosclerotic lesions and is associated with plaque instability. *Nat Commun* 2016;7:11853.

15. Kramann R, Schneider RK, DiRocco DP, Machado F, Fleig S, Bondzie PA, Henderson JM, Ebert BL, Humphreys BD. Perivascular Gli1+ progenitors are key contributors to injury-induced organ fibrosis. *Cell Stem Cell* 2015;16:51-66.

16. Muhl L, Genove G, Leptidis S, Liu J, He L, Mocci G, Sun Y, Gustafsson S, Buyandelger B, Chivukula IV, Segerstolpe A, Raschperger E, Hansson EM, Bjorkegren JLM, Peng XR, Vanlandewijck M, Lendahl U, Betsholtz C. Single-cell analysis uncovers fibroblast heterogeneity and criteria for fibroblast and mural cell identification and discrimination. *Nat Commun* 2020;11:3953.

17. Kalluri AS, Vellarikkal SK, Edelman ER, Nguyen L, Subramanian A, Ellinor PT, Regev A, Kathiresan S, Gupta RM. Single-Cell Analysis of the Normal Mouse Aorta Reveals Functionally Distinct Endothelial Cell Populations. *Circulation* 2019;140:147-163.

18. Gu W, Ni Z, Tan YQ, Deng J, Zhang SJ, Lv ZC, Wang XJ, Chen T, Zhang Z, Hu Y, Jing ZC, Xu Q. Adventitial Cell Atlas of wt (Wild Type) and ApoE (Apolipoprotein E)-Deficient Mice Defined by Single-Cell RNA Sequencing. *Arterioscler Thromb Vasc Biol* 2019;39:1055-1071.

19. Ramachandran P, Dobie R, Wilson-Kanamori JR, Dora EF, Henderson BEP, Luu NT, Portman JR, Matchett KP, Brice M, Marwick JA, Taylor RS, Efremova M, Vento-Tormo R, Carragher NO, Kendall TJ, Fallowfield JA, Harrison EM, Mole DJ, Wigmore SJ, Newsome PN, Weston CJ, Iredale JP, Tacke F, Pollard JW, Ponting CP, Marioni JC, Teichmann SA, Henderson NC. Resolving the fibrotic niche of human liver cirrhosis at single-cell level. *Nature* 2019;575:512-518.

20. Li Y, Ren P, Dawson A, Vasquez HG, Ageedi W, Zhang C, Luo W, Chen R, Li Y, Kim S, Lu HS, Cassis LA, Coselli JS, Daugherty A, Shen YH, LeMaire SA. Single-Cell Transcriptome Analysis Reveals Dynamic Cell Populations and Differential Gene Expression Patterns in Control and Aneurysmal Human Aortic Tissue. *Circulation* 2020;142:1374-1388.

21. Jin H, Mees BME, Biessen EAL, Sluimer JC. Transcriptional Sex Dimorphism in Human Atherosclerosis Relates to Plaque Type. *Circ Res* 2021;129:1175-1177.

22. Jin H, Goossens P, Juhasz P, Eijgelaar W, Manca M, Karel JMH, Smirnov E, Sikkink C, Mees BME, Waring O, van Kuijk K, Fazzi GE, Gijbels MJJ, Kutmon M, Evelo CTA, Hedin U, Daemen M, Sluimer JC, Matic L, Biessen EAL. Integrative multiomics analysis of human atherosclerosis reveals a serum response factor-driven network associated with intraplaque hemorrhage. *Clin Transl Med* 2021;11:e458.

23. Butler A, Hoffman P, Smibert P, Papalexi E, Satija R. Integrating single-cell transcriptomic data across different conditions, technologies, and species. *Nat Biotechnol*. United States, 2018:411-420.

24. Kevin R. Moon DvD, Zheng Wang, Scott Gigante, Daniel B. Burkhardt, William S. Chen, Kristina Yim, Antonia van den Elzen, Matthew J. Hirn, Ronald R. Coifman, Natalia B. Ivanova, Guy Wolf, Smita Krishnaswamy. PHATE: A Dimensionality Reduction Method for Visualizing Trajectory Structures in High-Dimensional Biological Data. *bioRxiv* 2017.

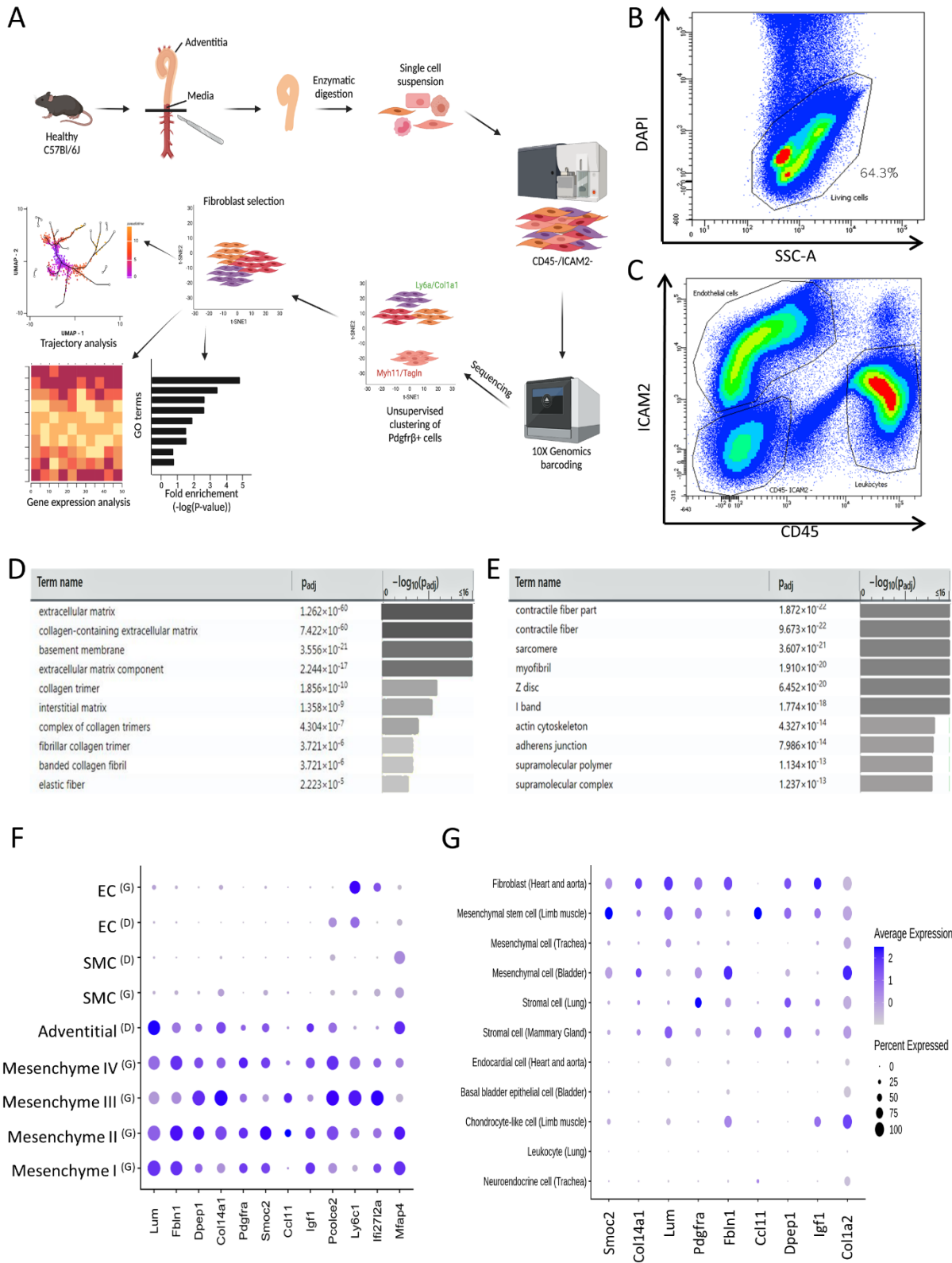
25. Dobnikar L, Taylor AL, Chappell J, Oldach P, Harman JL, Oerton E, Dzierzak E, Bennett MR, Spivakov M, Jorgensen HF. Disease-relevant transcriptional signatures identified in individual smooth muscle cells from healthy mouse vessels. *Nat Commun* 2018;9:4567.
26. Tabula Muris C. Single-cell transcriptomics of 20 mouse organs creates a Tabula Muris. *Nature* 2018;562:367-372.
27. McCarthy DJ, Campbell KR, Lun AT, Wills QF. Scater: pre-processing, quality control, normalization and visualization of single-cell RNA-seq data in R. *Bioinformatics* 2017;33:1179-1186.
28. Haghverdi L, Lun ATL, Morgan MD, Marioni JC. Batch effects in single-cell RNA-sequencing data are corrected by matching mutual nearest neighbors. *Nat Biotechnol* 2018;36:421-427.
29. Stuart T, Butler A, Hoffman P, Hafemeister C, Papalexi E, Mauck WM, 3rd, Hao Y, Stoeckius M, Smibert P, Satija R. Comprehensive Integration of Single-Cell Data. *Cell* 2019;177:1888-1902 e1821.
30. Moon KR, van Dijk D, Wang Z, Gigante S, Burkhardt DB, Chen WS, Yim K, Elzen AVD, Hirn MJ, Coifman RR, Ivanova NB, Wolf G, Krishnaswamy S. Visualizing structure and transitions in high-dimensional biological data. *Nat Biotechnol* 2019;37:1482-1492.
31. Cochain C, Vafadarnejad E, Arampatzi P, Pelisek J, Winkels H, Ley K, Wolf D, Saliba AE, Zernecke A. Single-Cell RNA-Seq Reveals the Transcriptional Landscape and Heterogeneity of Aortic Macrophages in Murine Atherosclerosis. *Circ Res* 2018;122:1661-1674.
32. Dawson A, Li Y, Li Y, Ren P, Vasquez HG, Zhang C, Rebello KR, Ageedi W, Azares AR, Mattar AB, Sheppard MB, Lu HS, Coselli JS, Cassis LA, Daugherty A, Shen YH, LeMaire SA. Single-Cell Analysis of Aneurysmal Aortic Tissue in Patients with Marfan Syndrome Reveals Dysfunctional TGF-beta Signaling. *Genes (Basel)* 2021;13.
33. Trapnell C, Cacchiarelli D, Grimsby J, Pokharel P, Li S, Morse M, Lennon NJ, Livak KJ, Mikkelsen TS, Rinn JL. The dynamics and regulators of cell fate decisions are revealed by pseudotemporal ordering of single cells. *Nat Biotechnol* 2014;32:381-386.
34. La Manno G, Soldatov R, Zeisel A, Braun E, Hochgerner H, Petukhov V, Lidschreiber K, Kastrioti ME, Lonnerberg P, Furlan A, Fan J, Borm LE, Liu Z, van Bruggen D, Guo J, He X, Barker R, Sundstrom E, Castelo-Branco G, Cramer P, Adameyko I, Linnarsson S, Kharchenko PV. RNA velocity of single cells. *Nature* 2018;560:494-498.
35. Petukhov V, Guo J, Baryawno N, Severe N, Scadden DT, Samsonova MG, Kharchenko PV. dropEst: pipeline for accurate estimation of molecular counts in droplet-based single-cell RNA-seq experiments. *Genome Biol* 2018;19:78
36. Raudvere U, Kolberg L, Kuzmin I, Arak T, Adler P, Peterson H, Vilo J. g:Profiler: a web server for functional enrichment analysis and conversions of gene lists (2019 update). *Nucleic Acids Res* 2019;47:W191-W198.
37. Reimand J, Isserlin R, Voisin V, Kucera M, Tannus-Lopes C, Rostamianfar A, Wadi L, Meyer M, Wong J, Xu C, Merico D, Bader GD. Pathway enrichment analysis and visualization of omics data using g:Profiler, GSEA, Cytoscape and EnrichmentMap. *Nat Protoc* 2019;14:482-517.
38. Buniello A, MacArthur JAL, Cerezo M, Harris LW, Hayhurst J, Malangone C, McMahon A, Morales J, Mountjoy E, Sollis E, Suveges D, Vrousitou O, Whetzel PL, Amode R, Guillen JA, Riat HS, Trevanion SJ, Hall P, Junkins H, Flicek P, Burdett T, Hindorf LA, Cunningham F, Parkinson H. The NHGRI-EBI GWAS Catalog of published genome-wide association studies, targeted arrays and summary statistics 2019. *Nucleic Acids Res* 2019;47:D1005-D1012.

39. Durinck S, Spellman PT, Birney E, Huber W. Mapping identifiers for the integration of genomic datasets with the R/Bioconductor package biomaRt. *Nat Protoc* 2009;4:1184-1191.
40. Ma WF, Hodonsky CJ, Turner AW, Wong D, Song Y, Mosquera JV, Ligay AV, Slenders L, Gancayco C, Pan H, Barrientos NB, Mai D, Alencar GF, Owsiany K, Owens GK, Reilly MP, Li M, Pasterkamp G, Mokry M, van der Laan SW, Khomtchouk BB, Miller CL. Enhanced single-cell RNA-seq workflow reveals coronary artery disease cellular cross-talk and candidate drug targets. *Atherosclerosis* 2022;340:12-22.
41. Pan H, Xue C, Auerbach BJ, Fan J, Bashore AC, Cui J, Yang DY, Trignano SB, Liu W, Shi J, Ihuegbu CO, Bush EC, Worley J, Vlahos L, Laise P, Solomon RA, Connolly ES, Califano A, Sims PA, Zhang H, Li M, Reilly MP. Single-Cell Genomics Reveals a Novel Cell State During Smooth Muscle Cell Phenotypic Switching and Potential Therapeutic Targets for Atherosclerosis in Mouse and Human. *Circulation* 2020;142:2060-2075.
42. Morikawa S, Mabuchi Y, Kubota Y, Nagai Y, Niibe K, Hiratsu E, Suzuki S, Miyauchi-Hara C, Nagoshi N, Sunabori T, Shimmura S, Miyawaki A, Nakagawa T, Suda T, Okano H, Matsuzaki Y. Prospective identification, isolation, and systemic transplantation of multipotent mesenchymal stem cells in murine bone marrow. *J Exp Med* 2009;206:2483-2496.
43. Lewis RD, Perry MJ, Guschina IA, Jackson CL, Morgan BP, Hughes TR. CD55 deficiency protects against atherosclerosis in ApoE-deficient mice via C3a modulation of lipid metabolism. *Am J Pathol* 2011;179:1601-1607.
44. Dho SH, Lim JC, Kim LK. Beyond the Role of CD55 as a Complement Component. *Immune Netw* 2018;18:e11.
45. Lu J, Chatterjee M, Schmid H, Beck S, Gawaz M. CXCL14 as an emerging immune and inflammatory modulator. *J Inflamm (Lond)* 2016;13:1.
46. Csiszar K. Lysyl oxidases: a novel multifunctional amine oxidase family. *Prog Nucleic Acid Res Mol Biol* 2001;70:1-32.
47. Arellano-Rodriguez M, Zapata-Benavides P, Arellano-Rodriguez NC, Izaguirre-Alvarez JM, Franco-Molina MA, F DEJTDM, Mendoza-Gamboa E, Soto-Dominguez A, Saavedra-Alonso S, Rodriguez-Padilla C. The Inflammatory Process Modulates the Expression and Localization of WT1 in Podocytes Leading to Kidney Damage. *In Vivo* 2021;35:3137-3146.
48. Frostegard J. Immunity, atherosclerosis and cardiovascular disease. *BMC Med* 2013;11:117.
49. Lucero HA, Kagan HM. Lysyl oxidase: an oxidative enzyme and effector of cell function. *Cell Mol Life Sci* 2006;63:2304-2316.
50. Kokkinopoulos I, Wong MM, Potter CMF, Xie Y, Yu B, Warren DT, Nowak WN, Le Bras A, Ni Z, Zhou C, Ruan X, Karamariti E, Hu Y, Zhang L, Xu Q. Adventitial SCA-1(+) Progenitor Cell Gene Sequencing Reveals the Mechanisms of Cell Migration in Response to Hyperlipidemia. *Stem Cell Reports* 2017;9:681-696.
51. Tang J, Wang H, Huang X, Li F, Zhu H, Li Y, He L, Zhang H, Pu W, Liu K, Zhao H, Bentzon JF, Yu Y, Ji Y, Nie Y, Tian X, Zhang L, Gao D, Zhou B. Arterial Sca1(+) Vascular Stem Cells Generate De Novo Smooth Muscle for Artery Repair and Regeneration. *Cell Stem Cell* 2020;26:81-96 e84.
52. Virmani R, Kolodgie FD, Burke AP, Farb A, Schwartz SM. Lessons from sudden coronary death: a comprehensive morphological classification scheme for atherosclerotic lesions. *Arterioscler Thromb Vasc Biol* 2000;20:1262-1275.

53. Zhang W, Zhang S, Yan P, Ren J, Song M, Li J, Lei J, Pan H, Wang S, Ma X, Ma S, Li H, Sun F, Wan H, Li W, Chan P, Zhou Q, Liu GH, Tang F, Qu J. A single-cell transcriptomic landscape of primate arterial aging. *Nat Commun* 2020;11:2202.
54. Hu Z, Liu W, Hua X, Chen X, Chang Y, Hu Y, Xu Z, Song J. Single-Cell Transcriptomic Atlas of Different Human Cardiac Arteries Identifies Cell Types Associated With Vascular Physiology. *Arterioscler Thromb Vasc Biol* 2021;41:1408-1427.
55. Sawada H, Rateri DL, Moorleggen JJ, Majesky MW, Daugherty A. Smooth Muscle Cells Derived From Second Heart Field and Cardiac Neural Crest Reside in Spatially Distinct Domains in the Media of the Ascending Aorta-Brief Report. *Arterioscler Thromb Vasc Biol* 2017;37:1722-1726.
56. Sawada H, Katsumata Y, Higashi H, Zhang C, Li Y, Morgan S, Lee LH, Singh SA, Chen JZ, Howatt DA, Moorleggen JJ, Franklin MK, Rateri DL, Shen YH, LeMaire SA, Aikawa M, Majesky MW, Lu HS, Daugherty A. Second Heart Field-derived Cells Contribute to Angiotensin II-mediated Ascending Aortopathies. *bioRxiv* 2022:2020.2002.2002.930917.
57. Hu Y, Zhang Z, Torsney E, Afzal AR, Davison F, Metzler B, Xu Q. Abundant progenitor cells in the adventitia contribute to atherosclerosis of vein grafts in ApoE-deficient mice. *J Clin Invest* 2004;113:1258-1265.
58. Saygin C, Wiechert A, Rao VS, Alluri R, Connor E, Thiagarajan PS, Hale JS, Li Y, Chumakova A, Jarrar A, Parker Y, Lindner DJ, Nagaraj AB, Kim JJ, DiFeo A, Abdul-Karim FW, Michener C, Rose PG, DeBernardo R, Mahdi H, McCrae KR, Lin F, Lathia JD, Reizes O. CD55 regulates self-renewal and cisplatin resistance in endometrioid tumors. *J Exp Med* 2017;214:2715-2732.
59. Li L, Li Q, Wei L, Wang Z, Ma W, Liu F, Shen Y, Zhang S, Zhang X, Li H, Qian Y. Chemokine (C-X-C motif) ligand 14 contributes to lipopolysaccharide-induced fibrogenesis in mouse L929 fibroblasts via modulating PPM1A. *J Cell Biochem* 2019;120:13372-13381.
60. Meuter S, Schaerli P, Roos RS, Brandau O, Bosl MR, von Andrian UH, Moser B. Murine CXCL14 is dispensable for dendritic cell function and localization within peripheral tissues. *Mol Cell Biol* 2007;27:983-992.
61. Tong W, Duan Y, Yang R, Wang Y, Peng C, Huo Z, Wang G. Foam Cell-Derived CXCL14 Multifunctionally Promotes Atherogenesis and Is a Potent Therapeutic Target in Atherosclerosis. *J Cardiovasc Transl Res* 2020;13:215-224.
62. Ovchinnikova OA, Folkersen L, Persson J, Lindeman JH, Ueland T, Aukrust P, Gavrishcheva N, Shlyakhto E, Paulsson-Berne G, Hedin U, Olofsson PS, Hansson GK. The collagen cross-linking enzyme lysyl oxidase is associated with the healing of human atherosclerotic lesions. *J Intern Med* 2014;276:525-536.
63. Martinez-Revelles S, Garcia-Redondo AB, Avendano MS, Varona S, Palao T, Orriols M, Roque FR, Fortuno A, Touyz RM, Martinez-Gonzalez J, Salaices M, Rodriguez C, Briones AM. Lysyl Oxidase Induces Vascular Oxidative Stress and Contributes to Arterial Stiffness and Abnormal Elastin Structure in Hypertension: Role of p38MAPK. *Antioxid Redox Signal* 2017;27:379-397.
64. El Agha E, Moiseenko A, Kheirollahi V, De Langhe S, Crnkovic S, Kwapiszewska G, Szibor M, Kosanovic D, Schwind F, Schermuly RT, Henneke I, MacKenzie B, Quantius J, Herold S, Ntokou A, Ahlbrecht K, Braun T, Morty RE, Gunther A, Seeger W, Bellusci S. Two-Way Conversion between Lipogenic and Myogenic Fibroblastic Phenotypes Marks the Progression and Resolution of Lung Fibrosis. *Cell Stem Cell* 2017;20:261-273 e263.

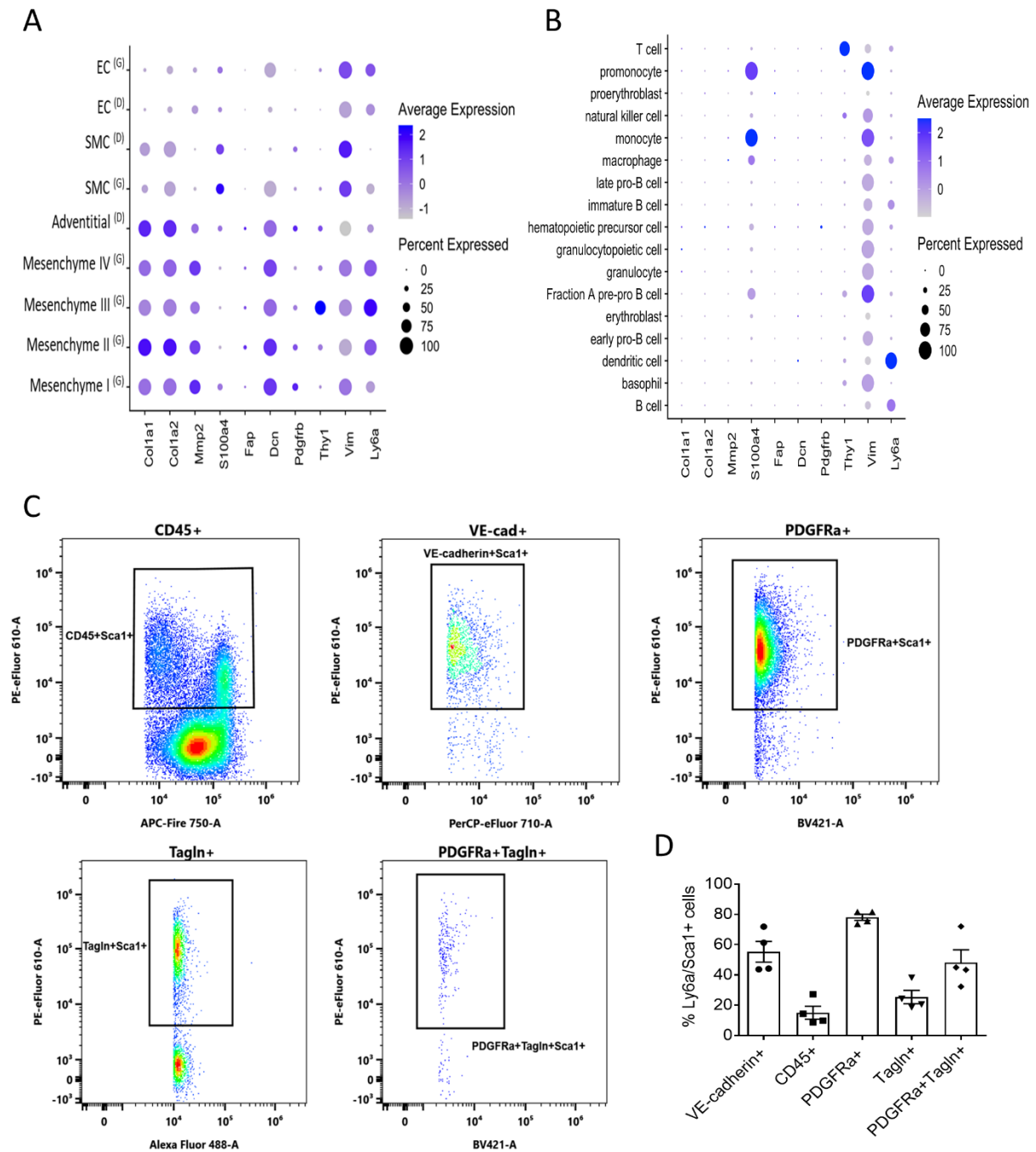
65. Porter KE, Turner NA, O'Regan DJ, Balmforth AJ, Ball SG. Simvastatin reduces human atrial myofibroblast proliferation independently of cholesterol lowering via inhibition of RhoA. *Cardiovasc Res* 2004;61:745-755.
66. Cochain C, Vafadarnejad E, Arampatzi P, Pelisek J, Winkels H, Ley K, Wolf D, Saliba AE, Zerneck A. Single-Cell RNA-Seq Reveals the Transcriptional Landscape and Heterogeneity of Aortic Macrophages in Murine Atherosclerosis. *Circ Res* 2018;122:1661-1674.

Supplementary data

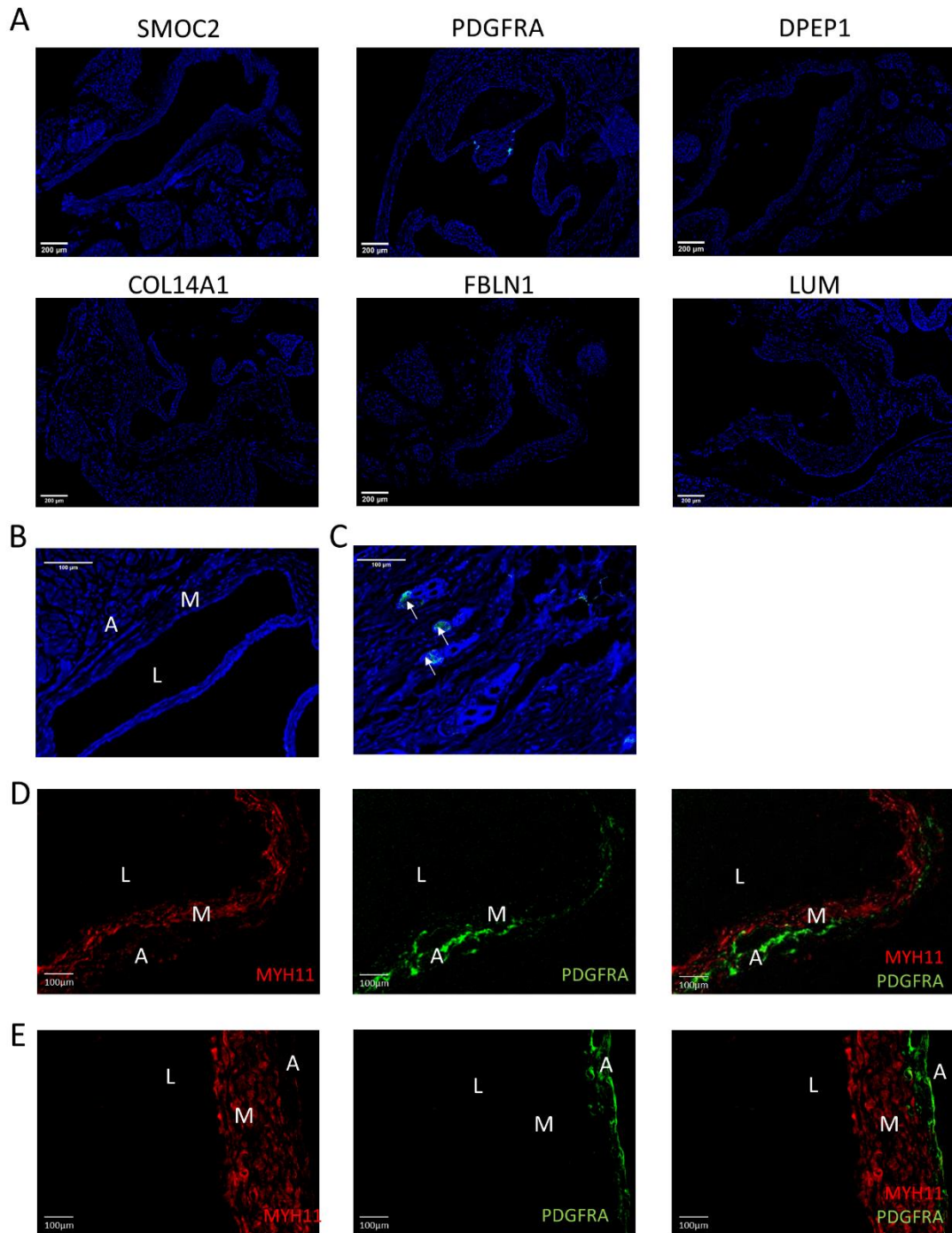


Supplementary Figure S1: Fibroblast characterization using single-cell sequencing. (A) Diagram depicting study approach from tissue isolation from healthy C57BL/6J mice and further processing. **(B)** Selection of living DAPI-cells (64.3%) from pooled adventitial samples of 8 male mice. **(C)** Flow cytometry gating strategy for selection of

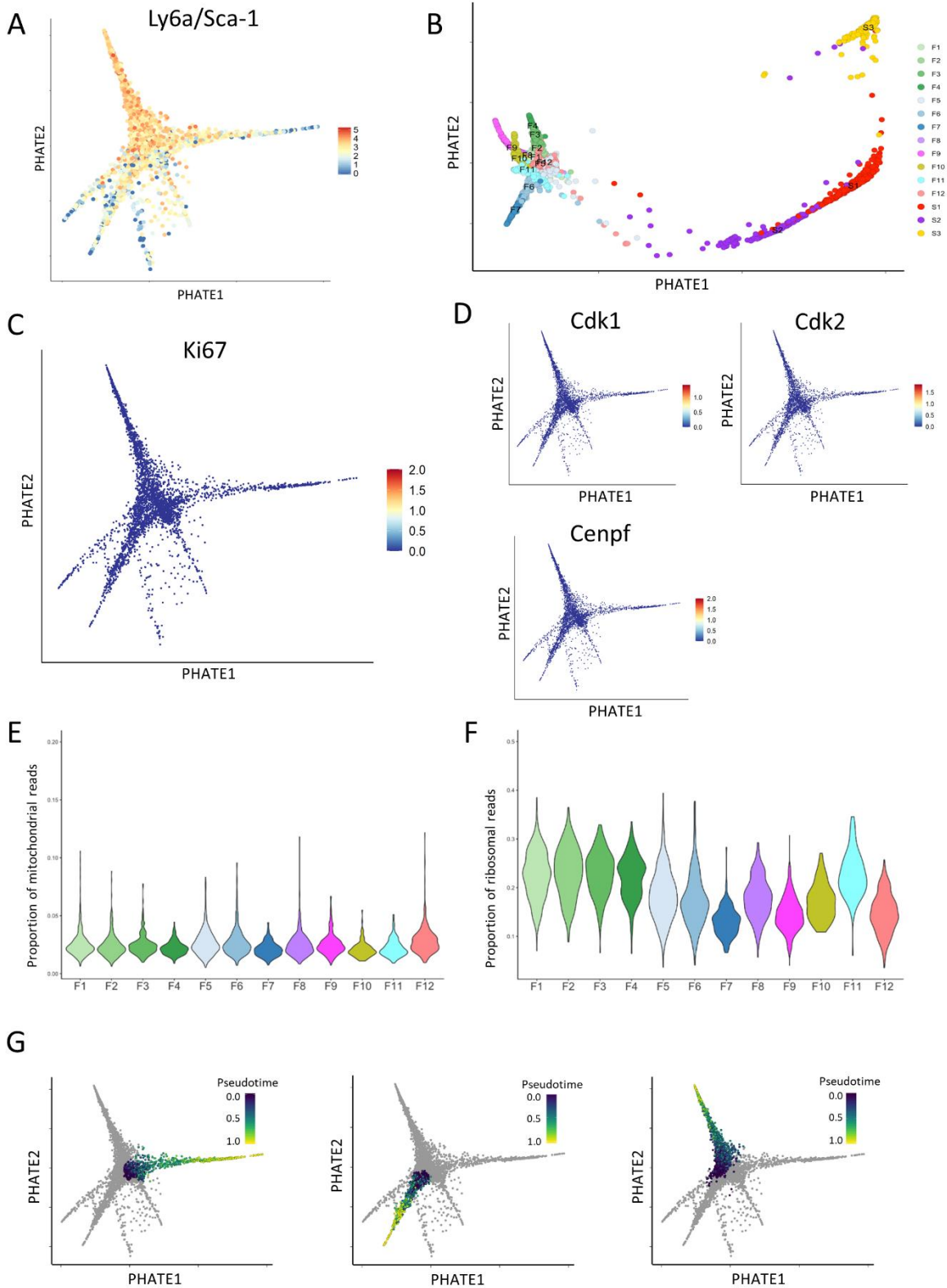
CD45-, ICAM2- cells from DAPI- cells (9.7% of living) from Figure S1B for scRNA-seq. **(D)** Top ten GO term analysis of cellular processes of fibroblasts, or **(E)** MCs. **(F)** Dot plot of marker specificity in healthy murine adventitia (G)¹⁸, and healthy media (D)²⁵. **(G)** Marker validation in mesenchymal and fibroblasts from single-cell expression data of Tabula Muris consortium²⁶. Annotation of cell types in F and G is according to the original paper.



Supplementary Figure S2: Expression traditional fibroblast markers not restricted to fibroblasts or mesenchymal cells. (A) Expression of traditional fibroblast markers in Gu dataset¹⁸ and Dobnikar dataset²⁵. **(B)** Expression of traditional fibroblast markers in spleen and bone marrow from Tabula Muris²⁶. Annotation of cell types is according to the original papers. **(C)** Flow cytometry gating strategy and **(D)** quantification of Sca-1 positivity in all vascular wall cell types, originating from thoracic aorta adventitia ($n = 4$ groups, 7 young C57BL/6J mice per group, total 28 mice).

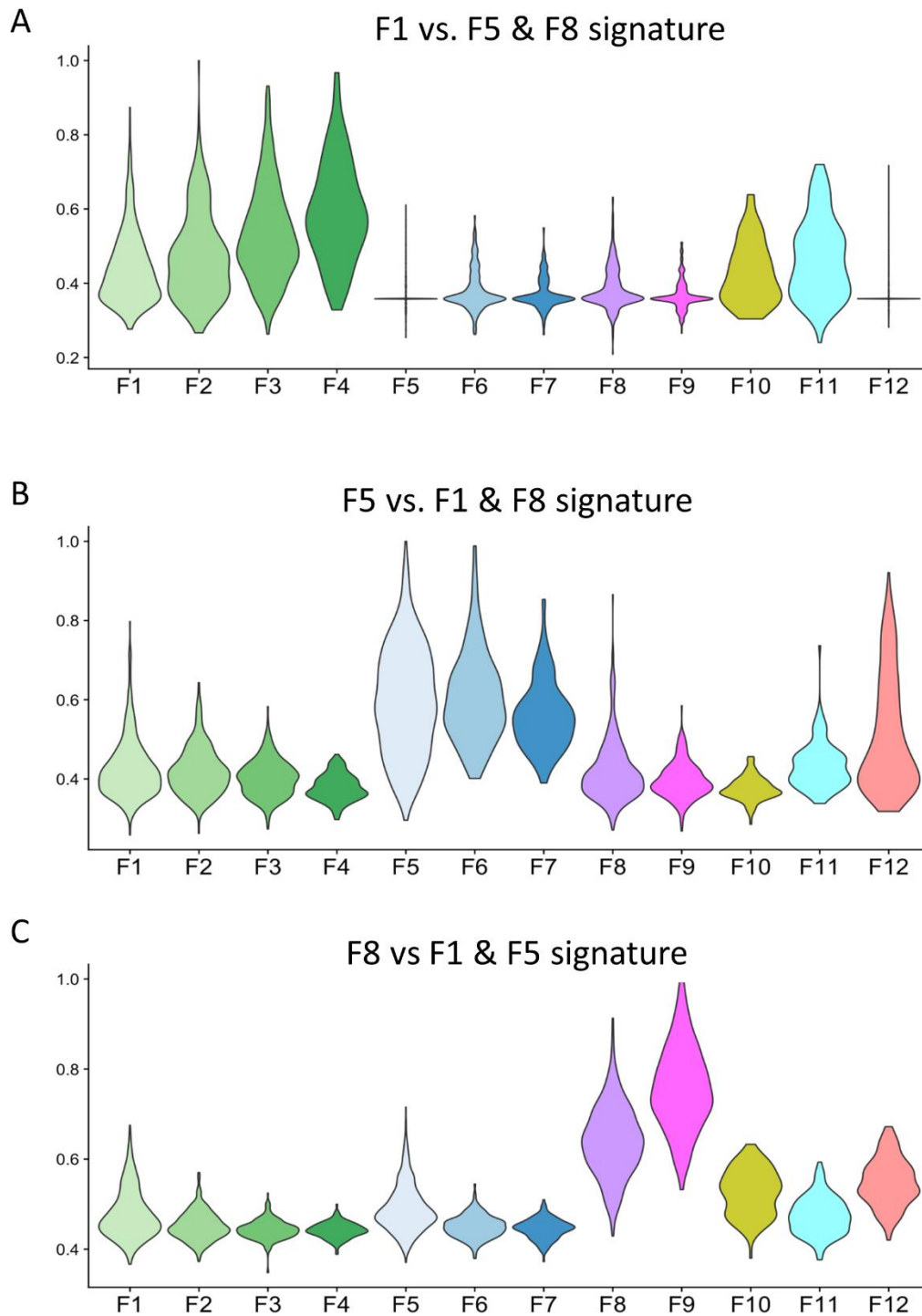


Supplementary Figure S3: Negative controls, immunohistochemical analysis of CCL11 in healthy C57BL/6J aortic roots, PDGFRA in *Myh11*-reporter mice and MYH11 in *Pdgfra*-reporter mice. (A) Negative controls for immunohistochemical stainings of fibroblast signature markers. **(B)** Murine aortic root immunohistochemically stained for CCL11. Adventitia indicated by A, media by M and lumen by L. **(C)** Positive control, murine dermis, with CCL11 expression in green. **(D)** PDGFRA expression in myosin heavy chain 11 (*Myh11*) reporter brachiocephalic artery. **(E)** MYH11 expression in aortic root of *Pdgfra*-tdTomato reporter. MYH11 in red, PDGFRA in green, co-localization (yellow) is absent. A indicates adventitia, M indicates media, and L indicates lumen. Scale bars 100 or 200 μm .

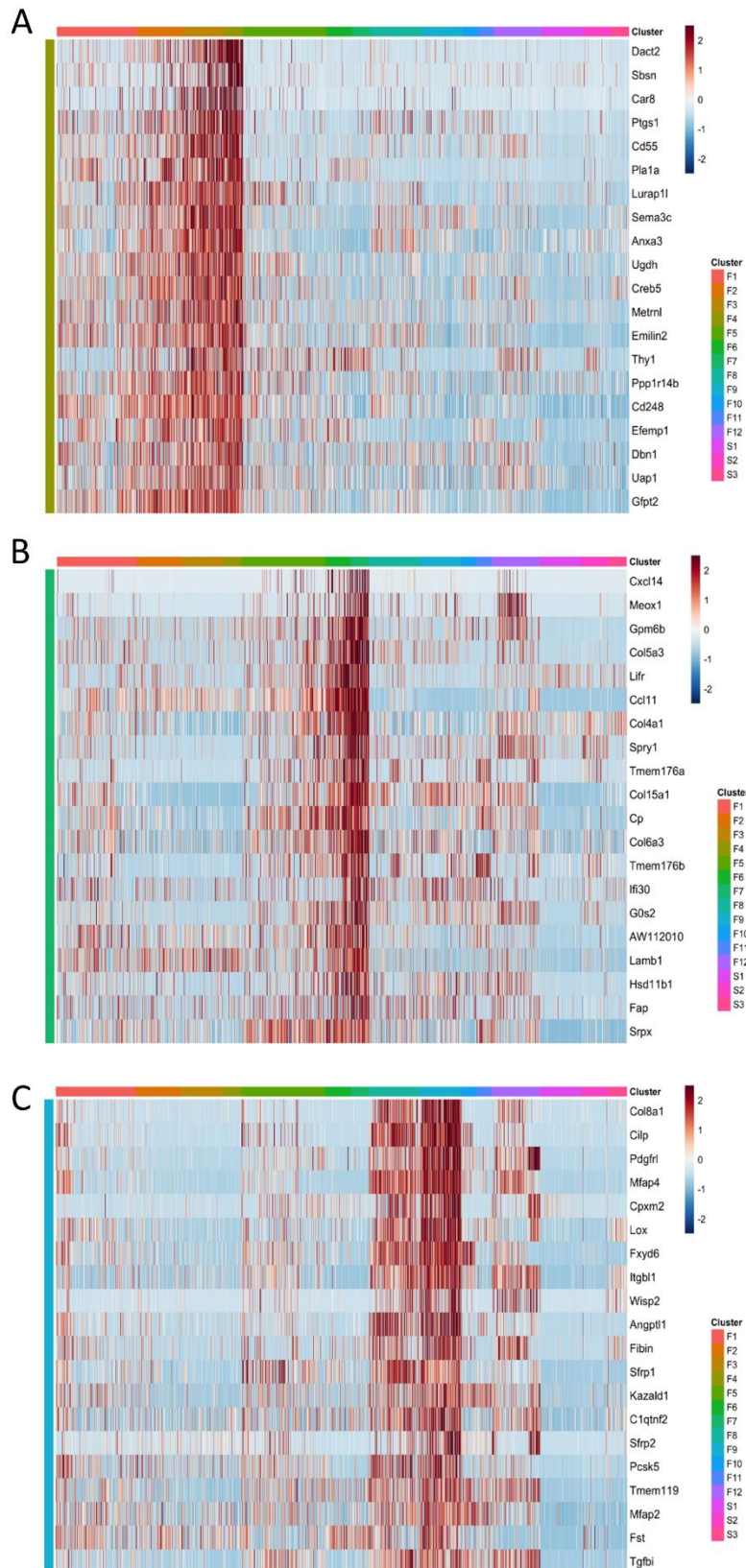


Supplementary Figure S4: Expression of proliferation markers, mitochondrial genes or ribosomal genes absent in fibroblasts. (A) *Ly6a/Sca-1* expression projected on PHATE plot of main Figure 3B. (B) PHATE dimensionality reduction on total dataset including fibroblasts and SMCs. (C) *Ki67* expression projected on PHATE plot of main Figure 3B. (D) Expression of proliferation markers cyclin-dependent kinase (*Cdk1*), *Cdk2* and centromere protein F (*Cenpf*) projected on PHATE plot of main Figure 3B. (E) Proportion of mitochondrial genes among the twelve

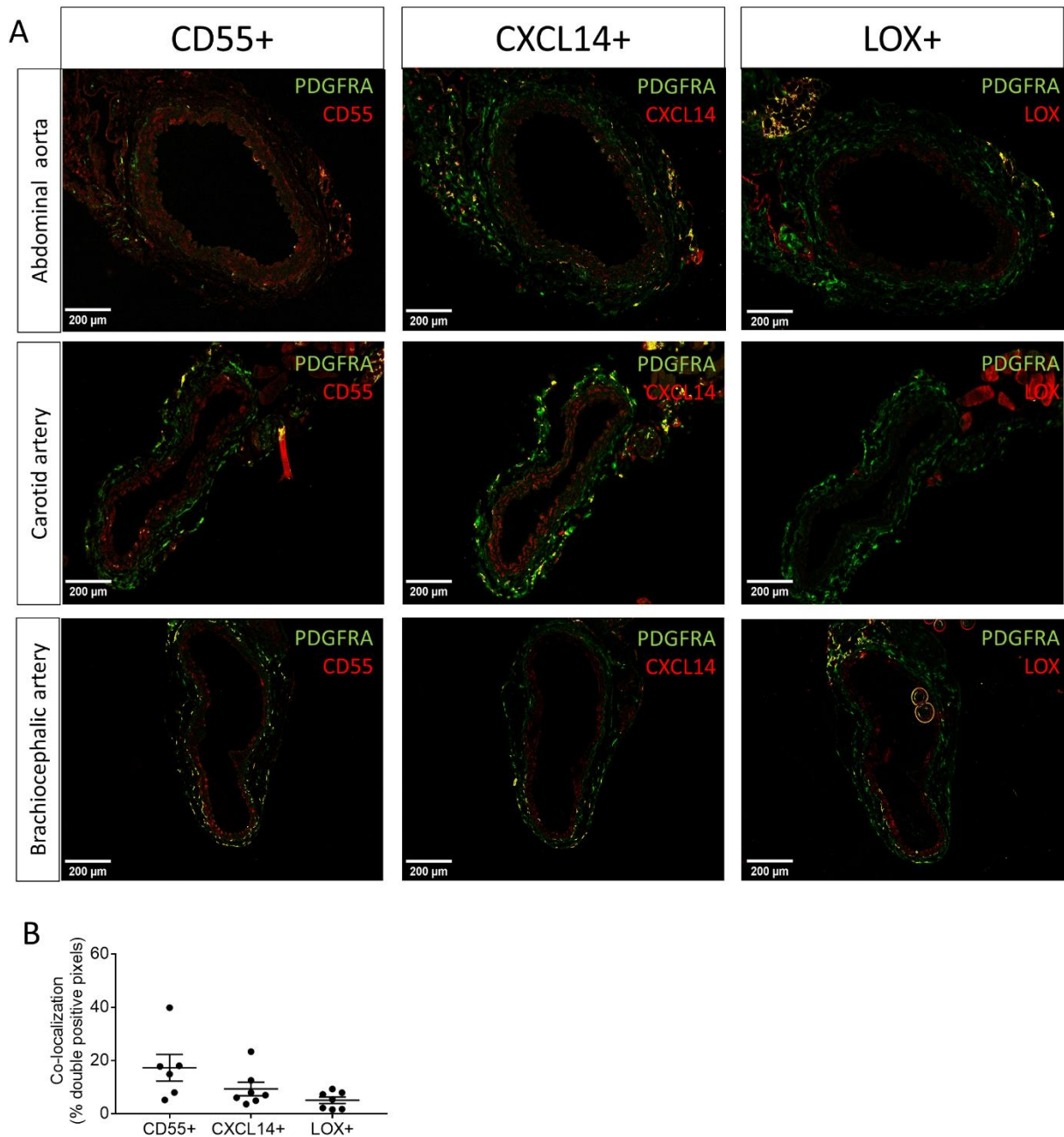
fibroblast clusters, **(F)** Proportion of ribosomal genes among the twelve fibroblast clusters. **(G)** Monocle pseudotime projection on each PHATE plot from main Figure 3B.



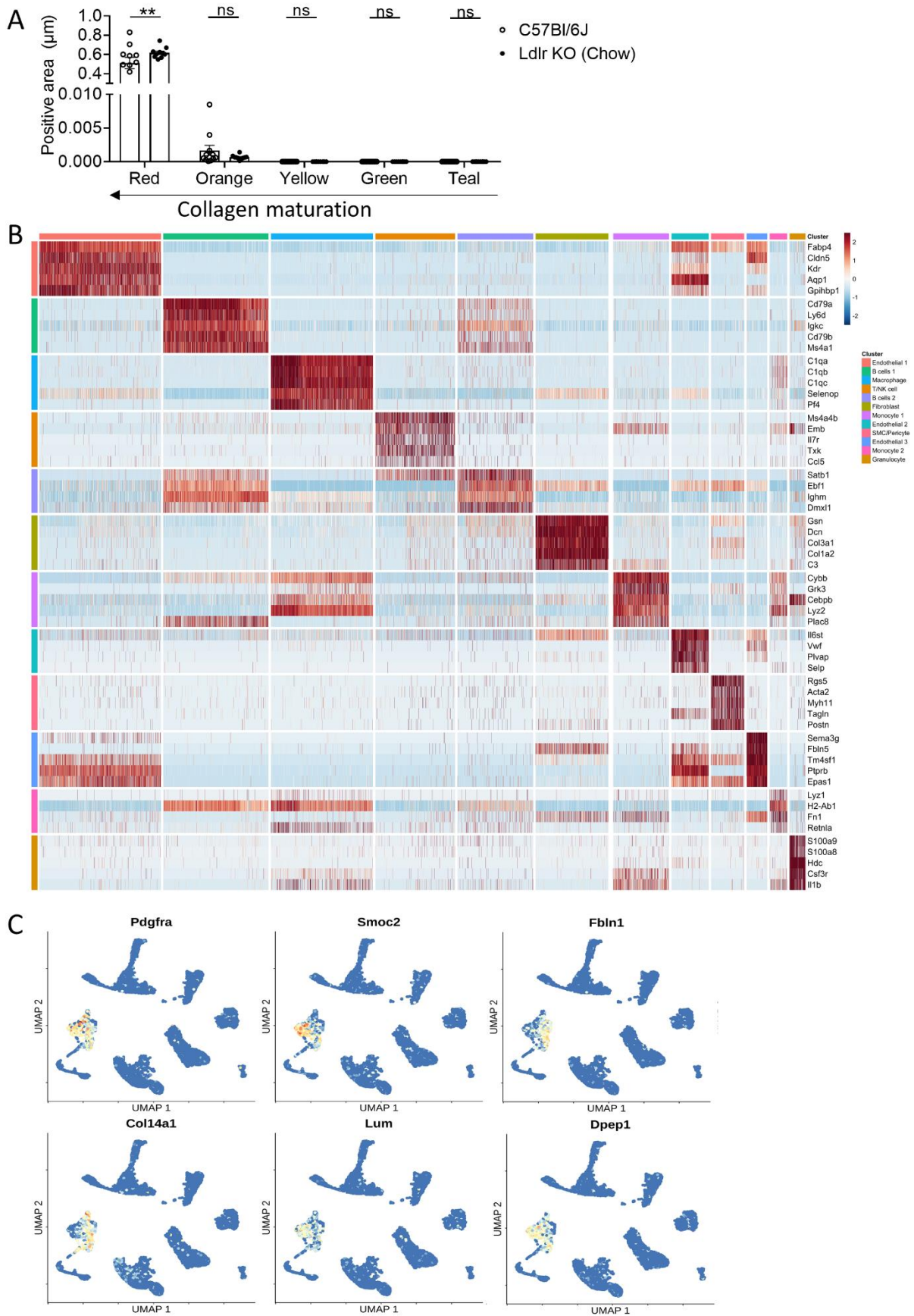
Supplementary Figure S5: Gene signatures for the different core clusters per differentiation trajectory. (A) Differential expression of signature for F1 vs F5+F8 in clusters F2, F3, F4, and to a lesser extent F10 and F11, suggesting these originate from F1. **(B)** Differential expression of F5 vs F1+F8 signature in clusters F6, F7 and F12. **(C)** Differential expression of F8 vs F5+F1 signature in population F9.



Supplementary Figure S6: Heatmaps depicting gene expression of trajectory specific markers. Heatmap for differentially expressed genes of trajectory 1 in **(A)** trajectory 2 in **(B)** and trajectory 3 in **(C)**. Criteria included expression of genes in >70% of cells in end-cluster of each trajectory and <35% of remaining cells.

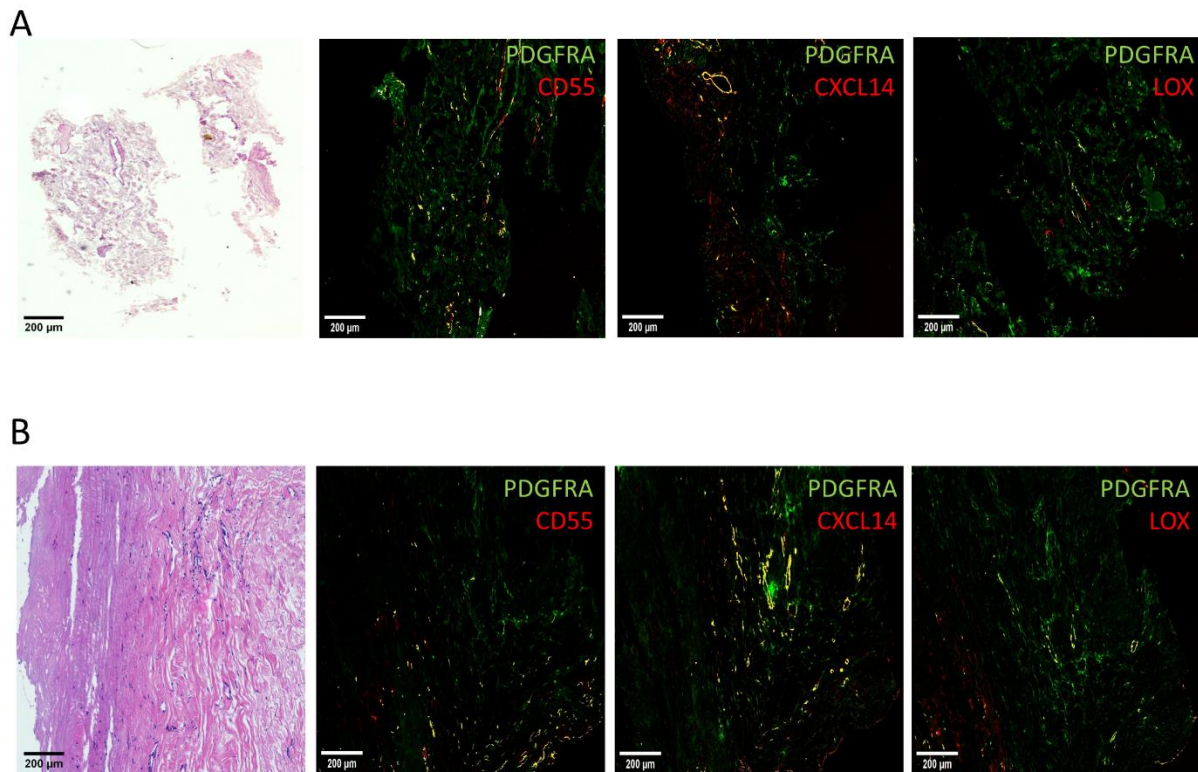


Supplementary Figure S7: Markers representing differentiated clusters presence in multiple vascular beds. (A) Immunohistochemical analysis of markers representing differentiated clusters for each trajectory in abdominal aorta, carotid artery and brachiocephalic artery. **(B)** Quantification of co-localization of trajectory markers CD55, CXCL14 and LOX with PDGFRA in adventitia of healthy C57BL/6J brachiocephalic arteries. Scale bars 200 μ m.



Supplementary Figure S8: Single-cell sequencing of adventitia from *Ldlr* KO mice. (A) Quantification of Sirius red staining in adventitia of healthy C57BL/6J and *Ldlr* KO BCA. Red represents mature collagen, while teal

presents the least mature collagen. **(B)** Heatmap for cell annotation of single-cell sequencing data, originating from *Ldlr* KO mice on chow and high cholesterol diet for 16 weeks. **(C)** Annotation of fibroblasts in *Ldlr* KO single-cell sequencing dataset making use of fibroblast-specific markers identified in main Figure 2. Visualization in UMAP. ** $p < 0.015$



Supplementary Figure S9: Fibroblast trajectories in human specimens. (A) Immunohistochemical stainings of CD55+ fibroblasts, CXCL14+ fibroblasts, and LOX+ fibroblasts representing trajectories 1-3, respectively, in specimens from carotid anastomosis during aortic bypass surgeries. **(B)** Trajectory presence in human carotid adventitia, obtained from the opposite side of the culprit plaques during carotid endarterectomy, with corresponding H&E. Overlap between PDGFRA and trajectory markers is shown in yellow. Scale bars 200 μm.

Supplementary Table S1: Cell counts after quality control as indicated in CellRanger software

Parameter	C57BL/6J (#)	<i>Ldlr</i> KO, chow (#)	<i>Ldlr</i> KO, 16 weeks HCD (#)
Estimated number of cells	5,701	4,822	7,989
Mean reads/cell	87,456	63,948	47,390
Median genes/cell	2,490	2,359	1,640
Median UMI counts/cell	7,169	6,794	3,545

Supplementary Table S2: Sequencing parameters for 10X Genomics samples

Sequencing	C57BL/6J (%)	<i>Ldlr</i> KO, chow (%)	<i>Ldlr</i> KO, 16 weeks HCD (%)
Valid barcodes	98.4	96.0	95.8
Reads mapped confidently to transcriptome	66.9	51.6	44.4
Reads mapped confidently to exonic regions	69.3	56.0	48.5
Reads mapped confidently to intronic regions	15.1	30.8	36.0
Reads mapped confidently to intergenic regions	2.8	4.3	5.0
Sequencing saturation	85.4	69.0	65.0

Supplementary Table S3: Expression of markers macrophages, endothelial cells, neurons and adipocytes in C57BL/6J scRNA-seq dataset

Markers	Cells with detected expression (%)
<i>Cd68</i> (macrophages)	0.25
<i>Pecam1</i> (endothelial cells)	6.13
<i>Rbfox3</i> (neurons)	1.45
<i>Adipoq</i> (adipocytes)	0.50

Supplementary Table S4: Differentially expressed genes (DEGs) in each individual core cluster compared to the other core clusters (F1 vs. F5 vs. F8)

F1 vs. F5 & F8 signature	F5 vs. F1 & F8 signature	F8 vs. F1 & F5 signature
Pla1a	Cxcl12	Mfap4
Gm12840	Gdf10	Col8a1
Ifi205	Steap4	Cilp
Sult1e1	Nrp1	Eln
Lrrn4cl	Ccl11	Angptl1
Ifi204	Clec11a	Fxyd6
Wt1		Itgbl1
Cotl1		Aspn
Efemp1		Sfrp1
		Lox
		Tgfb3
		Cpxm2
		Pdgfrl
		Wisp2
		C1qtnf2
		Fgl2
		Avpr1a
		Pcsk5
		Pmepa1
		Fibin
		Dkk2
		Hmcn2
		Crispld2
		Cpe
		Cdkn1c

Supplementary Table S5: Fibroblast cluster proportions represented as the percentages of the total population of fibroblast

Cluster	F1	F2	F3	F4	F5	F6	F7	F8	F9	F10	F11	F12
Proportion (%)	16.54	9.26	8.73	3.83	17.21	5.27	3.75	10.60	8.59	3.02	3.24	9.96

Supplementary Table S6: Enrichment of differentially expressed genes of each trajectory in GWAS for coronary artery disease (CAD) expressed as p-value

GWAS CAD	p-value	Intersected genes
CD55+ Trajectory (F1234)	$3.5 * 10^{-2}$	IL6R
CXCL14+ Trajectory (F567)	$<5 * 10^{-6}$	LPL, LOXL1, WT1, SERPINH1, COL6A3
LOX+ Trajectory (F89)	$2 * 10^{-3}$	TMEM204, GEM, ZEB2

Supplementary Table S7: Blood cholesterol levels of young C57BL/6J mice, aged C57BL/6J mice and *Ldlr* KO mice on chow diet or high cholesterol diet for 16 weeks

Mouse model	Diet	Cholesterol levels (mmol/L)
C57BL/6J (<i>n</i> = 36)	Chow (8 wks old)	1.30 ± 0.55
C57BL/6J (<i>n</i> = 14)	Chow (72 wks old)	1.28 ± 0.62
<i>Ldlr</i> KO (<i>n</i> = 11)	Chow	4.10 ± 2.25
<i>Ldlr</i> KO (<i>n</i> = 13)	16 weeks high cholesterol diet	14.23 ± 8.33

Supplementary Table S8: Adventitial cell populations of *Ldlr* KO mice on chow diet vs. normolipidemic C57BL/6J mice, proportional to relevant populations measured by flow cytometry. Values are represented as average from 3 pools, consisting of 3-6 mice

Mouse model	Endothelial cells (% of living)	Immune cells (% of living, VE-cadherin-)	Smooth muscle cells (% of living, VE-cadherin-, CD45-)	Fibroblasts (% of living, VE-cadherin-,CD45-)	Other (% of living)
C57BL/6J (<i>n</i> = 36)	0.2	1.2	3.0	31.0	64.6
<i>Ldlr</i> KO (<i>n</i> = 11)	0.8	0.8	3.8	26.5	68.1

Supplementary Table S9: Percentages of *Ly6a/Sca-1* expressing fibroblasts in single-cell sequencing datasets used in the current manuscript

Data	Publication	% of fibroblasts expressing <i>Ly6a/Sca-1</i>
Healthy C57BL/6J	This manuscript	94.8
Ldlr KO (Chow)	This manuscript	92.9
Ldlr KO (HCD)	This manuscript	59.3
C57BL/6J	Gu et al. 2019 ATVB	86.0
C57BL/6	Dobnikar et al. 2018 Nature Communications	43.6

Supplementary Table S10: Enrichment of murine trajectory-specific genes in human fibroblast population originating from dataset by Li et al.

Trajectory	-10log(p-value)
CD55+ trajectory (F1234)	2.17
CXCL14+ trajectory (F567)	15.32
LOX+ trajectory (F89)	21.24

Chapter 7

Identification of a pan-fibroblast marker and fibroblast subsets in atherosclerosis

Renée J.H.A. Tillie, Simrah Maryam, Kim van Kuijk, Monica T. Hannani, Hanjin Han, Stan Muijtens, Marion J. Gijbels, Sikander Hayat, Rafael Kramann, Judith C. Sluimer

In preparation

Chapter 8

General discussion

EMBARGOED

Chapter 9

Summary | Samenvatting

Summary

Cardiovascular disease (CVD) is a considerable global health concern, as it is a leading cause of mortality and morbidity worldwide, and thereby puts a substantial burden on healthcare systems and individuals. A key process that drives many cardiovascular diseases is atherosclerosis. This can eventually manifest itself in major clinical events such as angina pectoris, myocardial infarction and ischemic stroke. Atherosclerosis is a chronic, non-resolving inflammatory disease characterized by the progressive buildup of fatty deposits, also called plaque, in medium and large-sized arteries. It is caused by local endothelial cell dysfunction, followed by lipoprotein extravasation and retention, recruitment and accumulation of pro-inflammatory macrophages and other leukocytes, and foam cell formation in the subendothelial space. Moreover, mesenchymal cells produce extracellular matrix (ECM) components to create a stabilizing fibrous cap. At later stages, apoptosis of ECM-forming cap cells and thinning of the fibrous cap contributes to plaque destabilization and ultimately, plaque rupture. Additionally, advanced stages of atherosclerosis are characterized by neovascularization of the plaque. The resulting new microvessels are often unstable and leaky, which is also thought to contribute to plaque destabilization. The destabilized plaque may subsequently rupture (or erode), leading to thrombus formation and vessel occlusion, the immediate cause of clinical events such as myocardial infarction and ischemic stroke.

Thus, atherosclerosis involves a complex interplay of plaque stabilizing and destabilizing cell (sub)types, functions and processes. The complexity of the atherosclerotic disease process offers many leverage points to study atherosclerosis and potential interventions. Firstly, the role of intraplaque microvessel leakage in plaque destabilization remains to be confirmed. Secondly, interventions in cell types that are key for atherosclerosis initiation and progression, such as pro-inflammatory macrophages, may prevent or slow down disease progression. Pro-inflammatory macrophages are highly glycolytic, and inhibition of glycolysis has previously shown to decrease their pro-inflammatory activation *in vitro*. This offers interesting opportunities for manipulation of macrophage metabolism in inflammatory diseases. Lastly, the (functional) heterogeneity of fibroblasts, a mesenchymal cell type that was identified in atherosclerosis quite recently, remains to be explored. Thus, this thesis set out to study the role of these three potential regulators of plaque stability: microvessels, macrophage metabolism and fibroblasts in atherosclerosis. These studies may yield important opportunities for future therapeutic targets to prevent plaque progression and destabilization.

Platelet-derived growth factor B (PDGF-B) was previously shown to play an important role in recruitment of stabilizing mural cells towards sprouting microvessels, through its retention on the surface of the secreting cell and in the ECM. To investigate the potential causal role of microvascular permeability and hemorrhage in plaque destabilization, we studied the effects of removal of the PDGF-B retention motif, and thus a switch from cell-associated to soluble

PDGF-B, on atherosclerosis in **chapter 2**. We showed that integrity and density of atherosclerotic microvessels in the aortic root were independent of cell-associated PDGF-B. Instead, we showed that removal of the PDGF-B retention motif has dual effects, since it stimulated plaque stability and protected against an unfavorable diet-induced metabolic phenotype on one hand, but also stimulated leukocytosis through extramedullary hematopoiesis on the other hand. Further investigation of downstream pathways might allow us to isolate beneficial and detrimental effects of the PDGF-B isoforms for future prevention or treatment of atherosclerosis.

As mentioned above, pro-inflammatory macrophages have been shown to be highly dependent on glycolysis for their energy supply and functioning. Therefore, in **chapter 3**, we assessed the effects of myeloid-specific inhibition of PFKFB3 (3-phosphofructo-2-kinase/fructose-2,6-bisphosphatase 3), a key glycolytic enzyme, on atherosclerosis. Myeloid inhibition of PFKFB3 did not have any effects on circulating lipids, plaque size, burden or composition in *Ldlr*^{-/-} mice, neither in early nor advanced plaques of the brachiocephalic artery or aortic root, respectively.

Unexpectedly, we did observe that myeloid PFKFB3 inhibition stimulated diet-induced fatty liver disease, characterized by increased hepatic steatosis, inflammation and macrophage content, which we discussed in **chapter 4**. PFKFB3 knockout macrophages presented with an increased pro-inflammatory phenotype and proliferative capacities at basal state. The latter was likely facilitated by a shunt of glucose towards *de novo* synthesis of nucleobases. The protective effect of myeloid PFKFB3 on fatty liver disease could be a novel therapeutic target worth exploring.

Chapter 5 entails an introduction to a relatively new player in atherosclerosis, the fibroblast. We provided a detailed discussion on the current state of knowledge on fibroblast presence and heterogeneity in the healthy and atherosclerotic vasculature. We brought the validity of currently used fibroblast markers up for discussion, which complicates comprehensive fibroblast identification and research in the vasculature. Lastly, we speculated on possible cellular origins and cell transitions of fibroblasts in atherosclerosis.

In **chapter 6**, we explored fibroblast heterogeneity in healthy adventitia through single-cell RNA-sequencing (scRNA-seq). We showed that platelet-derived growth factor receptor alpha (PDGFR α) and dipeptidase 1 (DPEP1) are suitable markers to identify adventitial fibroblasts across healthy vascular beds on RNA and protein level. Importantly, these markers allowed proper distinction between fibroblasts and vascular smooth muscle cells (VSMCs). Moreover, we uncovered fibroblast heterogeneity and showed the existence of three fibroblast subsets. These three subsets could each be characterized by specific markers, namely cluster of

differentiation (CD)55, CXC motif chemokine ligand 14 (CXCL14) and lysyl oxidase (LOX). Moreover, they were predicted to exert divergent functions relevant to atherosclerosis, such as vascular development, antigen presentation and growth factor response, respectively. Additionally, proportions of the subsets changed in response to CVD risk factors such as ageing and mild hypercholesterolemia.

Next, we utilized scRNA-seq to explore the fibroblast transcriptomic landscape in atherosclerosis in **chapter 7**. We identified a potential new plaque (myo)fibroblast marker, which remains to be confirmed on mouse and human tissue sections. Moreover, we showed that expression of the plaque (myo)fibroblast marker was significantly correlated with vulnerable human plaques, and with detrimental human plaque traits. When looking into fibroblast subsets, we identified two myofibroblast clusters, and two fibroblast clusters. Next to overlapping and expected functions in ECM organization, fibroblast clusters were linked to different predicted functions, related to regulation of angiogenesis and the inflammatory response, respectively. We believe that the functions of these fibroblast clusters in atherosclerosis should be investigated further and could allow us to identify detrimental or protective fibroblast populations that could be of interest for therapeutic targeting.

Finally, we have put the findings of this thesis in a broader perspective in **chapter 8**. Amongst others, we have discussed the unexpected effects of PDGF-B retention motif deletion on atherosclerosis development. Moreover, we evaluated the suitability of mouse models to study intraplaque microvessels and hemorrhage. Next, we discussed the effects of myeloid PFKFB3 inhibition on atherosclerosis and fatty liver disease. We speculated on the protective effect of myeloid PFKFB3 on fatty liver disease and how it could be therapeutically targeted. We speculated about challenges associated with long-term genetic inhibition of PFKFB3. Lastly, we discussed fibroblast heterogeneity and markers in healthy and atherosclerotic vasculature and enumerated some of many outstanding questions regarding fibroblast research in atherosclerosis.

Samenvatting

Hart- en vaatziekten zijn wereldwijd een van de meest voorkomende oorzaken van sterfte en ziekte. Daardoor vormen hart- en vaatziekten een zware belasting voor zowel de volksgezondheid als de gezondheidszorg. Atherosclerose, ook wel aderverkalking genoemd, ligt vaak ten grondslag aan hart- en vaatziekten, en kan leiden tot een hart- of herseninfarct. Aderverkalking is een chronische ontstekingsziekte die gekenmerkt wordt door de voortschrijdende opstapeling van vetten, ontstekingscellen, kalk, en andere stoffen in middelgrote en grote slagaders. Deze opstapeling wordt ook wel plaque genoemd. Aderverkalking ontstaat vaak als gevolg van een verstoorde werking van de beschermende endotheellaag in de slagader, gevolgd door de ophoping van vetten, het aantrekken en ophopen van ontstekingsbevorderende macrofagen en andere immuuncellen, en de vorming van schuimcellen in de ruimte onder de endotheellaag. Mesenchymale cellen produceren bindweefsel, dat bijdraagt aan de vorming van een stabiliserend kapsel boven op de plaque. In latere stadia van de ziekte sterven deze bindweefsel-producerende cellen, waarbij het stabiliserend kapsel dunner wordt. Dit kan uiteindelijk leiden tot het instabiel worden en scheuren van de plaque. In vergevorderde stadia ontstaan er ook kleine bloedvaatjes in de plaque. Deze nieuw gevormde bloedvaatjes zijn vaak instabiel en lek. Er wordt gedacht dat dit verder bijdraagt aan de destabilisatie van de plaque. Klinische symptomen zoals hart- en herseninfarcten zijn het resultaat van het scheuren of afslijten van de plaque en de daaropvolgende vorming van stolsels.

Aderverkalking is dus het gevolg van een complex samenspel van cel (sub)typen, functies en processen die de plaque kunnen stabiliseren of juist destabiliseren. Het complexe karakter van aderverkalking biedt ook veel aanknopingspunten voor therapie. Ten eerste moet het oorzakelijk verband tussen lekkage van kleine bloedvaatjes in de plaque en destabilisatie nog worden bevestigd. Ten tweede bieden interventies in celtypen die essentieel zijn voor de initiatie en progressie van aderverkalking, zoals ontstekingsbevorderende macrofagen, kansen om ziekteprogressie te voorkomen of vertragen. Ontstekingsbevorderende macrofagen zijn zeer afhankelijk van de eerste stap van het suikermetabolisme, de glycolyse. Het is al eerder aangetoond dat remming van glycolyse de ontstekingsbevorderende activatie van macrofagen verlaagt *in vitro*. Dit biedt interessante mogelijkheden voor de manipulatie van macrofagen in ontstekingsziekten. Ten slotte is er nog veel onbekend over de diversiteit en functies van fibroblasten, een mesenchymaal celtype dat vrij recent werd geïdentificeerd in aderverkalking. Het doel van dit proefschrift was dan ook om de rol van kleine bloedvaatjes, het metabolisme van macrofagen, en fibroblasten in aderverkalking te bestuderen. Deze studies kunnen mogelijk belangrijke kansen bieden voor de identificatie van toekomstige therapeutische doelwitten, waarmee de verdere ontwikkeling of destabilisatie van de plaque kan worden voorkomen.

Platelet-derived growth factor B (PDGF-B) is een eiwit waarvan al eerder aangetoond is dat het een belangrijke rol speelt bij de aantrekking van stabiliserende cellen naar nieuwe bloedvaatjes. Deze aantrekking vindt plaats via binding van het eiwit aan het oppervlak van cellen die het eiwit afgeven, kortom de endotheelcellen die de nieuwe bloedvaatjes vormen, of door binding van het eiwit aan het nabijgelegen bindweefsel. Het retentiemotief is het gedeelte van het PDGF-B eiwit dat verantwoordelijk is voor deze binding aan het celoppervlak en nabijgelegen bindweefsel. In vorige studies resulteerde verwijdering van het retentiemotief in de afwezigheid van stabiliserende cellen in kleine bloedvaatjes. Dit zorgde voor instabiele en lekke bloedvaatjes. Om het mogelijk oorzakelijk verband te onderzoeken tussen lekkage van kleine bloedvaatjes in de plaque, en het instabiel worden van de plaque, bestudeerden we in **hoofdstuk 2** het effect van het verwijderen van het PDGF-B retentiemotief op aderverkalking. Dit zorgt dus voor een omschakeling van cel-geassocieerd naar vrij PDGF-B. We lieten zien dat dit onverwacht geen effect had op de integriteit en de dichtheid van de kleine bloedvaatjes in de verkalkte aorta. In plaats daarvan, toonden we aan dat het verwijderen van het PDGF-B retentiemotief enerzijds de stabiliteit van de plaque verhoogde en het metabool fenotype verbeterde, maar anderzijds ook een ontstekingsreactie stimuleerde in het bloed via verhoogde aanmaak van immuuncellen in de milt. Het verder bestuderen en identificeren van de mechanismen die gunstige en nadelige effecten van de PDGF-B isovormen teweegbrengen, zou voordelig kunnen zijn voor toekomstige preventie of behandeling van aderverkalking.

Het was al aangetoond dat ontstekingsbevorderende macrofagen voor hun energievoorziening en functioneren sterk afhankelijk zijn van de glycolyse. Daarom creëerden we in **hoofdstuk 3** muizen waarin PFKFB3 (3-phosphofructo-2-kinase/fructose-2,6-bisphosphatase 3), een belangrijk enzym in de glycolyse, specifiek geremd was in immuuncellen afkomstig uit het beenmerg, waaronder macrofagen. Vervolgens onderzochten we de effecten hiervan op aderverkalking. De remming bleek echter geen enkel effect te hebben op vetten in het bloed die aderverkalking bevorderen, zoals cholesterol, en de grootte of samenstelling van de plaque.

Onverwacht zagen we wel een effect van deze PFKFB3-remming op de muizenlever, besproken in **hoofdstuk 4**. Remming van PFKFB3 in immuuncellen uit het beenmerg stimuleerde vetstapeling, productie van ontstekingsfactoren en aanwezigheid van macrofagen in de lever. Dit zijn allemaal kenmerken van metabole leververvetting. PFKFB3-deficiënte macrofagen vertoonden daarnaast een ontstekingsbevorderend fenotype en verhoogde celgroei. Dit laatste werd waarschijnlijk mogelijk gemaakt door het verhoogde gebruik van glucose voor de aanmaak van bouwstenen van DNA. Aangezien PFKFB3 in immuuncellen uit het beenmerg dus een beschermend effect lijkt te hebben op

leververvetting, zou dit mogelijk een nieuw therapeutisch doelwit voor leververvetting kunnen vormen.

In **hoofdstuk 5** introduceerden we een relatief nieuwe speler in aderverkalking, een bindweefsel-producerende cel genaamd fibroblast. We gaven een gedetailleerd overzicht van de huidige stand van kennis over de aanwezigheid en diversiteit van fibroblasten in zowel de gezonde als verkalkte slagader. Bovendien bespraken we dat de genen die in de literatuur momenteel veel worden gebruikt voor de identificatie van fibroblasten, eigenlijk ongeschikt zijn. Dit gebrek aan goede markers bemoeilijkt het onderzoek naar fibroblasten in bloedvaten. Daarnaast speculeerden we over de mogelijke oorsprong van fibroblasten in de plaque, en de mogelijke transitie die fibroblasten kunnen ondergaan naar andere celtypen.

In **hoofdstuk 6** onderzochten we de diversiteit van fibroblasten in de buitenlaag van gezonde bloedvaten (de adventitia) middels een nieuwe analysetechniek, namelijk single-cell RNA-sequencing (scRNA-seq). We lieten zien dat twee eiwitten, platelet-derived growth factor alpha (PDGFR α) en dipeptidase 1 (DPEP1), enkel geproduceerd worden door fibroblasten in de buitenlaag van het gezonde vaatbed. Dat maakt ze zeer geschikt als marker voor dit celtype. Deze markers bleken ook goed in staat om een onderscheid te maken tussen gladde spiercellen en fibroblasten in aders. Bovendien toonden we de diversiteit van fibroblasten aan door de identificatie van drie subpopulaties. Deze subpopulaties werden gekenmerkt door de productie van verschillende markers, namelijk cluster of differentiation 55 (CD55), CXC motif chemokine ligand 14 (CXCL14) en lysyl oxidase (LOX), en leken ook verschillende functies te hebben, gerelateerd aan vaatontwikkeling, antistofherkenning en gevoeligheid voor groeifactoren, respectievelijk. Daarnaast reageerden de subpopulaties verschillend op bekende risicofactoren van hart- en vaatziekten, zoals veroudering en mild verhoogde cholesterolniveaus in het bloed.

Vervolgens pasten we scRNA-seq toe om het transcriptomisch landschap van fibroblasten in aderverkalking te verkennen in **hoofdstuk 7**. We identificeerden een potentiële nieuwe marker voor de herkenning van fibroblasten in de plaque. De geschiktheid van deze marker moet nog verder bevestigd worden op eiwitniveau met behulp van vaatweefsel uit mens en muis, maar we hebben al aangetoond dat de genexpressie van deze marker gecorreleerd is met (mogelijk) destabiliserende eigenschappen in de menselijke plaque. Naar aanleiding van verder onderzoek naar mogelijke fibroblast subgroepen, identificeerden we twee myofibroblast clusters en twee fibroblast clusters. Naast gedeelde functies omtrent bindweefselorganisatie, leken de twee fibroblast clusters ook divergerende functies te hebben, gerelateerd aan regulatie van bloedvataanleg en de ontstekingsreactie. De functies van deze fibroblast clusters moeten verder onderzocht worden *in vivo* en *in vitro*. Uiteindelijk

zou dit ons in staat kunnen stellen om schadelijke of juist beschermende fibroblastpopulaties te identificeren, die gebruikt kunnen worden als therapeutisch doelwit in aderverkalking.

Tot slot bundelden we de bevindingen van dit proefschrift en plaatsten we deze in een breder perspectief in **hoofdstuk 8**. Onder andere bespraken we hierin de onverwachte effecten van het ontbreken van het PDGF-B retentiemotief op de ontwikkeling van aderverkalking. Daarnaast bediscussieerden we de geschiktheid van muismodellen om kleine bloedvaatjes in de plaque te bestuderen. Vervolgens bespraken we de effecten van remming van PFKFB3 in immuuncellen uit het beenmerg op aderverkalking en leververvetting. We speculeerden over het beschermende effect van PFKFB3 in immuuncellen uit het beenmerg op leververvetting en hoe deze kennis gebruikt zou kunnen worden voor therapeutische behandeling. Daarnaast bespraken we uitdagingen die mogelijk verband houden met langdurige genetische remming van PFKFB3. Ten slotte bediscussieerden we de diversiteit van fibroblasten en markers in gezonde en verkalkte slagaders, en somden we enkele openstaande vragen en adviezen op met betrekking tot onderzoek naar fibroblasten in aderverkalking.

Chapter 10

Impact

In this thesis, we investigated the role of three potential determinants of plaque destabilization: intraplaque microvessel presence and dysfunction, macrophage metabolism and fibroblast presence in atherosclerosis. In this impact chapter, we will describe the implications of the findings of this thesis for science and society and how obtained results were or will be disseminated to society.

The socio-economic burden of cardiometabolic diseases

Cardiovascular disease (CVD) ranks among the leading causes of mortality worldwide, with an estimated 17.8 million deaths in 2017¹. It is the primary cause of death in Europe, in particular^{2, 3}. Coronary artery disease and ischemic stroke, often caused by atherosclerosis, globally account for 50% and 15% of deaths accountable to CVD, respectively^{1, 2}. Moreover, it has been predicted that if current risk factor trends persist, the number of CVD deaths will continue to rise⁴. The global burden of CVD is not limited to high mortality, as it is also associated with high morbidity and associated disability, hospitalization, and institutionalization^{2, 5, 6}. Thereby, next to high social costs, CVD also comes with high economic costs. Indeed, CVD costs were estimated at €210 billion (direct and indirect costs) in 2015 and \$320 billion (direct costs) in 2016 for the European Union and the United States, respectively^{3, 5}. Current treatment options, specifically for atherosclerosis, include lifestyle modifications, lipid lowering drugs, antihypertensives, anticoagulants and ultimately, invasive surgery. Evidently, these treatment options do not sufficiently decrease CVD-related mortality and morbidity.

Next to CVD, we unexpectedly touched upon another cardiometabolic disease during my studies, namely metabolic dysfunction-associated fatty liver disease (MAFLD). MAFLD development is associated with an obesogenic environment, and disturbed lipid handling and glucose homeostasis⁷. MAFLD is the major cause of liver cirrhosis, hepatocellular carcinoma, and eventually, the necessity for liver transplantation. Globally, MAFLD prevalence is estimated at 25%⁸, whereas annual direct medical costs approximate \$103 billion in the United States and €35 billion in the Europe-4 countries (France, Germany, United Kingdom, Italy)⁹. It is associated with several comorbidities such as obesity, type 2 diabetes mellitus, hypertension, hypercholesterolemia, and even cardiovascular risk. Indeed, MAFLD is an independent risk factor for CVD. Additionally, associations of MAFLD with dyslipidemia, dysregulation of glucose homeostasis, endothelial dysfunction and systemic inflammation all contribute to increased CVD risk. Thus, tackling MAFLD is likely to reduce the risk of CVD and CVD-related mortality as well¹⁰. Currently, as there is no approved drug available, treatment of MAFLD is aimed at lifestyle modifications and treatment of underlying risk factors associated with MAFLD development and fibrosis progression.

Taken together, the aforementioned numbers clearly show that new treatment options are imperative to decrease the social and economic burden of both CVD and MAFLD.

The ripple effect of scientific research: stimulating scientific and societal advances in cardiometabolic diseases

The scientific impact of my thesis can be deduced from the influence of my findings on scientific advancements, acquisition of new insights, methods and theories, and the stimulation of future research. Moreover, societal impact is based on the potential contribution of my main findings to current societal challenges, such as the socio-economic burden of cardiometabolic diseases, in the short and long term. On the short term, the results of this thesis mainly contribute to novel scientific insights. We envision that these novel insights will stimulate further research on the short and long term, as they yielded new theories and tools and allowed us to identify several new potential targets for therapeutic strategies. Thereby, although this thesis did not directly yield therapeutic treatments for atherosclerosis and MAFLD, we expect societal impact in the long term, too. Below, I will shortly summarize novel scientific insights obtained per thesis chapter. Moreover, I will address how we expect our findings to stimulate future research and to contribute to therapeutic interventions and thus societal impact in the long term.

In **chapter 2**, we showed that the switch of cell-associated to soluble PDGF-B stabilized the atherosclerotic plaque. PDGF-B retention motif deletion also ameliorated diet-induced body weight gain and fat accumulation in liver and white adipose tissue. However, simultaneously, an immune response was stimulated as circulating immune cell levels were increased. Currently, it is rather unclear whether individual effects were conferred by deletion of the cell-associated PDGF-B isoform, or due to increased availability and secretion of the soluble PDGF-B isoform. Therefore, future research could focus on unravelling isoform-specific effects per PDGF-B-reactive cell type *in vitro* and in mouse models, to isolate beneficial effects and possibly harness those for future therapeutic interventions.

Although myeloid PFKFB3 inhibition did not affect atherosclerosis in **chapter 3**, we uncovered protective effects of myeloid PFKFB3 on MAFLD development in **chapter 4**. These results seem promising, but there are some hurdles to take in order to exploit this finding for therapeutic purposes in the long term. Firstly, relevance of our observations and protective effects of myeloid PFKFB3 on MAFLD should be confirmed in the human disease setting. The association between hepatic macrophage PFKFB3 expression and MAFLD development could be assessed in healthy and MAFLD human liver sections. Moreover, multi-lineage human liver organoids or co-culture experiments could be utilized to assess macrophage PFKFB3 expression in a fatty liver-enhancing milieu, such as (physiologically relevant) free fatty acid exposure, and to perform macrophage-specific knockdown or overexpression experiments¹¹. For a therapeutic

treatment *in vivo*, it will be pivotal to target myeloid cells only, since in contrast to the protective effects of myeloid cell PFKFB3, hepatocyte PFKFB3 was associated with hepatic inflammation, macrophage recruitment and fibrogenesis in a liver injury model¹².

This could be accomplished using nanoparticles, carrying therapeutics that stimulate myeloid PFKFB3 levels, such as PFKFB3 mRNA or protein supplementation^{13, 14}. Nanoparticles allow easy administration through intravenous injection and preferably accumulate in macrophages of the mononuclear phagocyte system (liver, spleen and lymph nodes), which could be used to our advantage^{14, 15}. A recent review listed nanoparticle systems with preferential hepatic accumulation, and low to negligible accumulation in spleen and other organs¹⁵. Moreover, hepatic macrophage targeting could be further improved through addition of specific macrophage ligands to the nanoparticle, such as mannose¹⁶. Practically, it would be crucial to study the appropriate level of myeloid PFKFB3 overexpression or supplementation and confirm its protective effect on MAFLD development *in vitro* and in mouse models, and the absence of adverse side effects. In case of adverse side effects of PFKFB3 supplementation, it could be worthwhile to further explore the pathways that confer protective effects on MAFLD downstream of myeloid PFKFB3 inhibition, and target those. Lastly, our study only takes into account the effect of myeloid PFKFB3 inhibition from the start of fatty liver disease. MAFLD is usually only identified in patients in the clinic after progression to steatohepatitis or worse. Therefore, it will be essential to study whether myeloid PFKFB3 consistently confers protective effects throughout different stages of MAFLD and can induce regression of existing disease. This is required to establish suitable timepoints of treatment administration within the MAFLD disease process. Thereafter, the potential treatment would have to go through clinical trial phases. Taken together, we expect the entire track, from addressing remaining experimental questions until completion of clinical trials, to take another 10-15 years.

In **chapter 7**, we identified a pan plaque fibroblast marker which was associated with detrimental human plaque traits. This possibly indicates a harmful effect of fibroblasts in (certain stages of) atherosclerosis. Specifically, we also identified two fibroblast subclusters in the atherosclerotic plaque with divergent functions, related to regulation of angiogenesis and the inflammatory response. The identification of pan- and subset fibroblast markers is essential to increase understanding of fibroblast functions in disease, thereby driving scientific impact on the short term. Next to murine atherosclerosis, presence of the identified fibroblast subclusters and corresponding markers should be further validated in human atherosclerosis, using immunohistochemistry and scRNA-seq. Moreover, it will be crucial to further study the function of atherosclerotic fibroblasts in general, and of individual fibroblast subclusters, and their contribution to atherosclerosis. This could be achieved through fluorescence-activated cell sorting of fibroblasts from mouse and human plaques and subsequent *in vitro* investigation of functional characteristics and communication between fibroblasts and other cell types in atherosclerosis, such as macrophages. Alternatively, fibroblast (subcluster-

)specific ablation in mouse models could shine a light on the contribution of fibroblasts and individual subclusters to atherosclerosis development *in vivo*.

After further elucidation of fibroblast (subset) function in atherosclerosis, the identified pan- and subset markers will be pivotal for specific fibroblast targeting. Thereby, the findings of my thesis will drive scientific impact on the long term, and will potentially yield new leads for interventions. Indeed, specific targeting of detrimental or beneficial fibroblast subclusters could pose new avenues for therapeutic treatment. This could be accomplished using nanoparticles or extracellular vesicles, which is currently also under investigation for targeting tumor-associated fibroblasts^{17, 18}. These methods would yield interesting opportunities for subcluster-specific removal of fibroblasts, for the modulation of expression of fibroblast-specific genes that are detrimental or protective in atherosclerosis, or to steer fibroblast differentiation through identification and regulation of involved transcription factors.

Lastly, next to cardiometabolic diseases, PFKFB3-expressing macrophages, PDGF-B-expressing and -reactive cells and fibroblasts can be found throughout the body in health and disease. Thereby, knowledge generated and markers identified in this thesis might benefit other scientific disciplines and stimulate or shape development of therapeutic treatments for other diseases. One rather specific example entails small molecule inhibitor PFK158, an inhibitor of PFKFB3, which has recently entered clinical trials for the treatment of solid tumor patients¹⁹. Although PFKFB3 selectivity of the inhibitor is under debate, our study in **chapter 4**, showing detrimental effects of myeloid PFKFB3 inhibition on the development of fatty liver disease, raises a call for caution in its usage.

Spreading the knowledge: dissemination of scientific research results

Dissemination of the research results obtained in my thesis is a prerequisite to ensure impact and return of investment, since research efforts are established through public funding. If results obtained in this thesis can lead to the development of therapeutic treatments for atherosclerosis and MAFLD in the long term, this will benefit a large patient population and their clinicians. Moreover, it is pivotal to transfer the results of this thesis to important potential stakeholders, such as the scientific community and pharmaceutical companies, but also to the public, to increase knowledge, stimulate awareness and collaborations, raise support and to accelerate the realization of therapeutic treatments. To reach the stakeholders, several chapters (**chapter 2, 3, 5 and 6**) of this thesis have been published in scientific journals, predominantly open-access. Combined, these articles were read more than 10,000 times, underscoring the stakeholder's interests in my investigations. The other chapters (**chapter 4** and **chapter 7**) are also in preparation for publication. Moreover, findings of this thesis were shared multiple times at national and international conferences (such as the International Vascular Biology Meeting in Oakland, California, USA), symposia and social media platforms such as Twitter and LinkedIn. Additionally, I was selected to give a Ted talk in

layman's terms at the Papendal vascular biology training course for PhD candidates, organized by the Dutch Heart Foundation, which allowed me to further develop my skills to present scientific research results to a broader, non-scientific audience. Further dissemination of our results to a non-scientific audience (cardiometabolic disease patients, other interested parties) will occur through giving lectures (e.g. via Hart & Vaat Café, <https://www.hartenvaatonderzoekfondslimburg.nl/evenementen/hart-vaat-cafe>, Harteraad, www.harteraad.nl) and lay summaries of my research, such as the one found in this thesis. Importantly, scRNA-seq data from **chapter 6** were deposited in the Gene Expression Omnibus (GSE196395). Moreover, these scRNA-seq data have also been made available for interrogation through PlaqView, an open-source single-cell portal for cardiovascular research (plaqview.uvadcos.io). This enables other researchers to examine the data with their own research questions in mind.

In conclusion, the data presented in this thesis provide insight into the role of microvessels and fibroblasts in atherosclerosis, and the role of macrophage metabolism in atherosclerosis and MAFLD. Although more in-depth studies are still required, we identified several opportunities for future research and therapeutic targeting in atherosclerosis and MAFLD.

References

1. Roth GA, Abate D, Abate KH, Abay SM, Abbafati C, Abbasi N, et al. Global, regional, and national age-sex-specific mortality for 282 causes of death in 195 countries and territories, 1980–2017: a systematic analysis for the Global Burden of Disease Study 2017. *The Lancet*. 2018;392(10159):1736-88.
2. Townsend N, Kazakiewicz D, Lucy Wright F, Timmis A, Huculeci R, Torbica A, et al. Epidemiology of cardiovascular disease in Europe. *Nature Reviews Cardiology*. 2022;19(2):133-43.
3. Wilkins E WL, Wickramasinghe K, Bhatnagar P, Leal J, Luengo-Fernandez R, Burns R, Rayner M, Townsend N European Cardiovascular Disease Statistics 2017. European Heart Network, Brussels. 2017 [Available from: <https://ehnhheart.org/cvd-statistics/cvd-statistics-2017.html>].
4. Roth GA, Nguyen G, Forouzanfar MH, Mokdad AH, Naghavi M, Murray CJ. Estimates of global and regional premature cardiovascular mortality in 2025. *Circulation*. 2015;132(13):1270-82.
5. Yazdanyar A, Newman AB. The Burden of Cardiovascular Disease in the Elderly: Morbidity, Mortality, and Costs. *Clinics in Geriatric Medicine*. 2009;25(4):563-77.
6. Townsend N, Wilson L, Bhatnagar P, Wickramasinghe K, Rayner M, Nichols M. Cardiovascular disease in Europe: epidemiological update 2016. *European Heart Journal*. 2016;37(42):3232-45.
7. Eslam M, El-Serag HB, Francque S, Sarin SK, Wei L, Bugianesi E, et al. Metabolic (dysfunction)-associated fatty liver disease in individuals of normal weight. *Nature Reviews Gastroenterology & Hepatology*. 2022;19(10):638-51.
8. Younossi ZM, Koenig AB, Abdelatif D, Fazel Y, Henry L, Wymer M. Global epidemiology of nonalcoholic fatty liver disease-Meta-analytic assessment of prevalence, incidence, and outcomes. *Hepatology*. 2016;64(1):73-84.
9. Younossi ZM, Blissett D, Blissett R, Henry L, Stepanova M, Younossi Y, et al. The economic and clinical burden of nonalcoholic fatty liver disease in the United States and Europe. *Hepatology*. 2016;64(5):1577-86.
10. Duell PB, Welty FK, Miller M, Chait A, Hammond G, Ahmad Z, et al. Nonalcoholic Fatty Liver Disease and Cardiovascular Risk: A Scientific Statement From the American Heart Association. *Arteriosclerosis, Thrombosis, and Vascular Biology*. 2022;42(6):e168-e85.
11. Ouchi R, Togo S, Kimura M, Shinozawa T, Koido M, Koike H, et al. Modeling Steatohepatitis in Humans with Pluripotent Stem Cell-Derived Organoids. *Cell Metabolism*. 2019;30(2):374-84.e6.
12. Leslie J, Macia MG, Luli S, Worrell JC, Reilly WJ, Paish HL, et al. c-Rel orchestrates energy-dependent epithelial and macrophage reprogramming in fibrosis. *Nature Metabolism*. 2020;2(11):1350-67.
13. Hou X, Zaks T, Langer R, Dong Y. Lipid nanoparticles for mRNA delivery. *Nature Reviews Materials*. 2021;6(12):1078-94.
14. Colino CI, Lanao JM, Gutierrez-Millan C. Targeting of Hepatic Macrophages by Therapeutic Nanoparticles. *Frontiers in Immunology*. 2020;11.
15. Ngo W, Ahmed S, Blackadar C, Bussin B, Ji Q, Mladjenovic SM, et al. Why nanoparticles prefer liver macrophage cell uptake in vivo. *Advanced Drug Delivery Reviews*. 2022;185:114238.
16. Zhou J-E, Sun L, Liu L, Jia Y, Han Y, Shao J, et al. Hepatic macrophage targeted siRNA lipid nanoparticles treat non-alcoholic steatohepatitis. *Journal of Controlled Release*. 2022;343:175-86.

17. Li W, Little N, Park J, Foster CA, Chen J, Lu J. Tumor-Associated Fibroblast-Targeting Nanoparticles for Enhancing Solid Tumor Therapy: Progress and Challenges. *Mol Pharm.* 2021;18(8):2889-905.
18. Chen J, Tan Q, Yang Z, Jin Y. Engineered extracellular vesicles: potentials in cancer combination therapy. *J Nanobiotechnology.* 2022;20(1):132.
19. Telang S, O'Neal J, Tapolsky G, Clem B, Kerr A, Imbert-Ferndandez Y, et al. Discovery of a PFKFB3 inhibitor for phase I trial testing that synergizes with the B-Raf inhibitor vemurafenib. *Cancer & Metabolism.* 2014;2(1):P14.

Addendum

List of abbreviations

10-fTHF	10-formyltetrahydrofolate
3PO	3-[3-pyridinyl]-1-[4-pyridinyl]-2-propen-1-one
6-AN	6-aminonicotinamide
7-KC	7-ketocholesterol
ACAT2	acyl-coenzyme A:cholesterol acyltransferase 2
Acta2	actin alpha 2
Adgre1	adhesion G protein-coupled receptor E1
Adipoq	adiponectin
Ang-1	angiopoietin 1
Apo	apolipoprotein
ApoE ^{-/-}	apolipoprotein E knockout
AR	aortic root
BCA	brachiocephalic artery
Bcl	B-cell leukemia/lymphoma
BMDM	bone marrow-derived macrophage
CAD	coronary artery disease
Ccl11	C-C motif chemokine ligand 11
CD	cluster of differentiation
cDC	conventional dendritic cell
Cdh5	cadherin 5
Cdk	cyclin-dependent kinase
CEA	carotid endarterectomy
Cenpf	centromere protein F
c-Kit	stem cell factor receptor
CLEC4F	C-type lectin domain family 4 member F
CMP	common myeloid progenitor
CNN1	calponin 1
Col	collagen
Cox4i2	cytochrome C oxidase subunit 4i2
Ctps1	cytidine 5'-triphosphate synthase 1
Ctrl	control
CVD	cardiovascular disease
CXCL14	CXC motif chemokine ligand 14
CYGB	cytoglobin

DAB	3,3'-diaminobenzidine
DC	dendritic cell
Dcn	decorin
DEG	differentially expressed gene
DMEM	Dulbecco's Modified Eagle Medium
DPEP1	dipeptidase 1
Dpt	dermatopontin
EC	endothelial cell
ECAR	extracellular acidification rate
ECM	extracellular matrix
EDTA	ethylenediamine tetraacetic acid
EdU	5-ethynyl-2'-deoxyuridine
EndMT	endothelial-to-mesenchymal transition
Eng	endoglin
eNOS	endothelial nitric oxide synthase
Epha3	ephrin type-A receptor 3
eWAT	epididymal white adipose tissue
FACS	fluorescence-activated cell sorting
FAP	fibroblast activation protein
Fasn	fatty acid synthase
Fbln1	fibulin 1
Fbn1	fibrillin 1
FBS	fetal bovine serum
FC	fold change
FCCP	trifluoromethoxy carbonyl cyanide-4 phenylhydrazone
FFPE	formalin-fixed paraffin-embedded
FL	floxed
Foxp2	forkhead box P2
FSP	fibroblast surface protein
FSP1	fibroblast-specific protein 1
GEO	Gene Expression Omnibus
Gli1	GLI family zinc finger 1
GLUT1	glucose transporter 1
GMP	granulocyte monocyte progenitor

GO	gene ontology
Got	glutamic-oxaloacetic transaminase
GSEA	Gene Set Enrichment Analysis
GTT	glucose tolerance testing
GWAS	genome-wide association study
HCA	high content analyzer
HCD	high cholesterol diet
HE	hematoxylin and eosin
HFCd	high-fat-high-cholesterol diet
HFD	high-fat diet
HIF1 α	hypoxia-inducible factor 1-alpha
HLA-DR	human leukocyte antigen – DR isotype
ICAM	intercellular adhesion molecule
IFN γ	interferon-gamma
Ig	immunoglobulin
IL	interleukin
IPH	intraplaque hemorrhage
ISG15	interferon-stimulated gene 15
IT	intimal thickening
Itgax	integrin alpha X
ITT	insulin tolerance testing
KC	Kupffer cell
KC/GRO	keratinocyte-derived chemokine/growth-related oncogene
Klrc2	killer cell lectin-like receptor subfamily C member 2
KO	knockout
LCM	L929-conditioned medium
LDL	low-density lipoprotein
Ldlr	low-density lipoprotein receptor
Ldlr ^{-/-}	low-density lipoprotein receptor knockout
LOX	lysyl oxidase
LPS	lipopolysaccharide
Lsamp	limbic system associated membrane protein
Lum	lumican

Ly6	lymphocyte antigen 6
LysM	lysozyme M
LYVE1	lymphatic vessel endothelial hyaluronan receptor 1
Lyz2	lysozyme 2
MaasHPS	Maastricht Human Plaque Study
MAFLD	metabolic dysfunction-associated fatty liver disease
MC	mesenchymal cell mural cell
MCEC	mouse cardiac endothelial cell
MCP-1	monocyte chemoattractant protein 1
MMP	matrix metalloproteinase
moDC	monocyte-derived dendritic cell
MoM ϕ	monocyte-derived macrophage
MPTC	Maastricht Pathology Tissue Collection
MSC	mesenchymal stem/stromal cell
MTHFD2	methylenetetrahydrofolate dehydrogenase/cyclohydrolase
Mybl2	myeloblastosis oncogene-like 2
Myc	myelocytomatosis oncogene
Myh11	myosin heavy chain 11
NAFLD	non-alcoholic fatty liver disease
NES	Normalized Enrichment Scores
NET	neutrophil extracellular trap
Ng2	neural/glial antigen 2
NK cell	natural killer cell
NO	nitric oxide
Nt5e	5'-nucleotidase ecto
OCR	oxygen consumption rate
OCT	optimal cutting temperature
oxLDL	oxidized low-density lipoprotein
OXPPOS	oxidative phosphorylation
PA	palmitic acid
PBS	phosphate-buffered saline
PC	pericyte
PCA	principal component analysis

pDC	plasmacytoid dendritic cell
PDGF-B	platelet-derived growth factor B
PDGFR α	platelet-derived growth factor receptor alpha
PDGFR β	platelet-derived growth factor receptor beta
Pecam1	platelet endothelial cell adhesion molecule-1
PERK	protein kinase RNA-like endoplasmic reticulum kinase
PFA	paraformaldehyde
PFK-1	phosphofructokinase-1
PFKFB3	6-phosphofructo-2-kinase/fructose-2,6-bisphosphatase 3
PHATE	Potential of Heat-diffusion for Affinity-based Transition Embedding
Pi16	peptidase inhibitor 16
PPP	pentose phosphate pathway
P/S	penicillin/streptomycin
Psat1	phosphoserine aminotransferase 1
Ptprc	protein tyrosine phosphatase receptor type C
PTT	pyruvate tolerance testing
qPCR	quantitative polymerase chain reaction
Rbfox3	RNA binding protein, fox-1 homolog 3
Rgs5	regulator of G-protein signaling 5
ROS	reactive oxygen species
RPMI	Roswell Park Memorial Institute
rRNA	ribosomal RNA
RTCA	real-time cell analysis
S100A8	S100 calcium binding protein A8
S1P	sphingosine-1-phosphate
Sca-1	stem cell antigen 1
scRNA-seq	single-cell RNA-sequencing
SCS	single-cell sequencing
SEM	stem cell, endothelial cell, monocyte/macrophage standard error of the mean
Shmt2	serine hydroxymethyltransferase 2
Slc1a5	solute carrier family 1 member 5
SMC	smooth muscle cell
Smoc2	SPARC related modular calcium binding 2

Soat2	sterol O-acyltransferase 2
Srebf1	sterol regulatory element-binding transcription factor 1
Svep1	sushi, von Willebrand factor type A, EGF and pentraxin domain containing 1
Tagln	transgelin
TBE	tris-borate EDTA
TBS	tris buffered saline
TCA	tricarboxylic acid
TF	transcription factor
TGF- β	transforming growth factor beta
Thy1	thymus cell antigen 1, theta
Tie2	tyrosine kinase with immunoglobulin-like loops and epidermal growth factor homology domains-2
Tkt	transketolase
TNF	tumor necrosis factor
TREM2	triggering receptor expressed on myeloid cells 2
tSNE	t-distributed stochastic neighbour embedding
TUNEL	terminal deoxynucleotidyl transferase-mediated dUTP nick-end labeling
Ugdh	UDP-glucose 6-dehydrogenase
UMAP	Uniform Manifold Approximation and Projection
UMI	unique molecular identifier
VCAM-1	vascular cell adhesion molecule 1
VE-cadherin	vascular endothelial-cadherin
VEGF	vascular endothelial growth factor
VEGFR	vascular endothelial growth factor receptor
Vim	vimentin
VLDL	very low-density lipoprotein
VSMC	vascular smooth muscle cell
VWF	von Willebrand factor
WT	wildtype
α SMA	alpha smooth muscle actin

Addendum

Acknowledgements | Dankwoord

Dat was het dan, mijn promotietraject zit erop! Terwijl ik dit schrijf, kan ik het nog steeds niet geloven. Wat zijn de jaren snel omgevlogen en wat was het een indrukwekkend, mooi en leerzaam avontuur. Wanneer ik met een lach en een traan terugkijk, is het me duidelijk dat vele mensen hier op hun eigen unieke wijze aan hebben bijgedragen. Tot deze mensen wil ik mij graag richten in mijn dankwoord.

Prof. dr. Sluimer, beste **Judith**, natuurlijk ben jij de eerste die ik graag wil noemen in dit rijtje. Al in 2017 kwam ik als student jouw kantoor binnenlopen vanwege een sollicitatiegesprek voor de afstudeerstage van mijn master. Ik was meteen enthousiast om voor een inspirerende, ambitieuze, vrouwelijke wetenschapper als jij aan de slag te gaan. Na een succesvolle afstudeerstage, heb je mij ondersteund bij het aanvragen van een studentenbeurs bij de Hartstichting, die ik heb gebruikt om ook nog stage te lopen in Cambridge. Tegelijkertijd kwam toen het verlossende woord: jij had de VIDI binnengesleept en wilde mij na terugkomst graag aannemen als PhD student. Natuurlijk stemde ik volmondig in met dit aanbod! Ik wil je bedanken voor alles dat ik van je heb mogen leren. Ik kon altijd bij je terecht met een vraag, gesprek of discussie en je dacht altijd in mogelijkheden. Je hebt me daarnaast altijd gestimuleerd om het beste uit mezelf en mijn PhD te halen. Of het nou ging om het leren van een nieuwe experimentele techniek, het aanvragen van beurzen, het bezoeken van congressen, het geven van presentaties, het leren van R, het volgen van cursussen, het reviewen van artikelen en ga zo maar door: jij juichte het allemaal toe en was altijd actief op zoek naar nieuwe mogelijkheden en kansen ter bevordering van mijn ontwikkeling. Naast het professionele vlak, wil ik je ook bedanken voor je adviezen en alle gezellige feestjes (waaronder jullie prachtige bruiloft en jouw inauguratie!), etentjes en dansjes. Want ondanks het feit dat je een gedreven en ambitieuze wetenschapper bent, weet jij gelukkig ook heel goed hoe je een feestje moet bouwen! Wij waren the last ones standing, maar helaas is het voor mij nu ook tijd om team eggplant te verlaten. Bedankt voor alles!

Prof. dr. Biessen, beste **Erik**, natuurlijk wil ik jou ook graag bedanken voor al jouw input en al onze wetenschappelijke discussies de afgelopen jaren. Ik waardeer jouw positiviteit en was altijd onder de indruk van jouw eindeloze kennis over letterlijk alles. Ik moet eerlijk toegeven dat mijn hoofd vaak tolde wanneer ik uit een meeting met jou kwam.. Zo veel nieuwe ideeën, associaties en namen van genen of eiwitten waar ik nog nooit van had gehoord! Daarna volgde altijd een intensieve pubmed sessie, op zoek naar antwoorden. Helaas kon je niet aanwezig zijn bij mijn afscheidsdiner, en hoewel Judith het ook fantastisch deed, heb ik hopelijk toch nog een afscheidsspeech tegoed van jou...?

I would like to sincerely thank all the members of my assessment committee **prof. dr. Rory Koenen**, **prof. dr. Elizabeth Jones**, **dr. Jeffrey Kroon**, **dr. Annette Neele** and **prof. dr. Casper Schalkwijk** for your time and effort to read and assess my thesis.

Prof. dr. Axel zur Hausen, bedankt dat ik mocht promoveren bij de afdeling Pathologie.

I would also like to express my gratitude to **prof. dr. Baker**. Dear **Andy**, thank you for your input and for always bringing fresh perspectives to the table, which enriched our discussions and projects.

Dan natuurlijk mijn paranimfen, **Lieve** en **Mat**. **Lieve**, de vrolijkste wetenschapper van de afdeling. Hoewel je soms wat chaotisch kan zijn en we in dat opzicht tegenpolen zijn, komt toch altijd alles op zijn pootjes terecht bij jou. Wij hebben samen uren in het lab doorgebracht in Marseille en in Maastricht, voor de SCENITH experimenten.. De hele groep hebben we aan het werk gezet, en de gigantische tabellen, bergen aan plastic pipetpuntjes en buisjes, het samen tot in de ochtend achter de Cytex zitten terwijl we melig waren en Marion's reisblog bewonderden, zal ik nooit vergeten. Jij benadert alles in het leven met humor en optimisme, en dat kan ik enorm waarderen. Bedankt dat ik alles met je kon bespreken, voor je altijd opbouwende en goede wetenschappelijke input, nieuwsgierigheid en behulpzaamheid. Daarnaast heb ik genoten van je gezelligheid tijdens alle etentjes, feestjes en koffie/verse munt thee rondes en hebben we ontzettend met elkaar kunnen lachen. **Mat**, de constante factor en bron van kennis van de afdeling. Wanneer ik iets niet wist of iets niet kon vinden, was jij de eerste persoon waar ik naartoe ging. Geen vraag is jou te veel en je staat altijd klaar om te helpen. Ik ben je dankbaar voor het delen van al je kennis. Je bent een gewaardeerde collega die met rust en stabiliteit stiekem de hele afdeling draaiende houdt. Bedankt voor je vertrouwen en ook voor je geduld wanneer ik weer eens met een bestelling aankwam die toch wel snel de deur uit moest.. Daarnaast waardeer ik je oprechte interesse, adviezen, onze fijne gesprekken en je trots wanneer je foto's van je kinderen en kleinkinderen kwam laten zien. We delen ook onze passies voor reizen en eten. Je was net zo enthousiast over uitstapjes en gezelligheid met het lab, zoals de geliefde kerstborrel en het reisje naar Berlijn. Gelukkig heb jij dan ook het stokje van mij, Elias en Valeria overgenomen voor de organisatie van ons volgende lab reisje naar Parijs. Je hebt me ook geïntroduceerd aan de wonderlijke wereld van de Sligro en het Japans koken! Wat hebben wij met plezier een prachtig menu van 7 gangen op tafel getoverd voor mijn Bram en jouw lieve Astrid. **Lieve** en **Mat**, ik ben er trots op dat ik jullie tijdens mijn verdediging aan mijn zijde mag hebben als paranimfen.

Kim, ik had het geluk om jou als dagelijkse begeleider te hebben tijdens de afstudeerstage van mijn master. Ik keek enorm op naar jouw efficiëntie, professionaliteit, vaardigheden in het lab en de enorme hoeveelheden werk die je wist te verzetten. Ik heb veel van je mogen leren. Ik vond het hartstikke leuk dat ik vervolgens mocht blijven in het team en dat wij als collega's samen verder mochten werken. We waren altijd perfect op elkaar ingespeeld en je was echt een top collega. We hebben samen aan het fibroblasten project mogen werken, wat resulteerde in twee mooie publicaties. Carnaval, feestjes, koffie- en lunchpauzes en etentjes

waren ontzettend gezellig met jou. Ik vind het hartstikke stoer dat jij en Pim in Londen aan de slag zijn gegaan en wens jullie nog het allerbeste voor de toekomst.

Ik heb mijn stokje overgedragen aan de nieuwe senior PhD student van team Sluimer, **Sebastiaan**. Ik vind het indrukwekkend hoe jij jouw PhD in Maastricht combineert met het volgen van een master én het openen en runnen van een hamburgerrestaurant in Amsterdam. Samen hebben wij mogen werken aan drie verschillende studies. Ik hoop dat de twee resterende studies nog tot schitterende publicaties zullen leiden in jouw handen. Heel veel succes met het afronden van je PhD! **Baixue**, it was a pleasure to welcome you in our department. Thank you for your enthusiasm and kindness. You are a great addition to the team and I am absolutely sure that you will bring your PhD to a successful end. **Adele**, we go back a long way! We started out as interns, sitting next to each other in the immuno lab. And it was great to have you as a roomie again when we were PhD students later on. I am glad that you followed your heart and chose the scientific path, as you are very talented. I was always in awe of your creativity, whether you applied it in your work or personal life. I remember how, during our first secret santa event, you gave me a “how to survive your PhD” gift basket accompanied by a poem consisting of multiple pages in which you creatively included many details of my life that I shared with you. It was one of the nicest, most creative and thoughtful gifts that I ever received. Thank you for being such a wonderful person, for always being up for a (decaf) coffee/tea run, and for our many fun but also heartfelt conversations. I was honored to be at your side during your defense, you did an amazing job! **Valeria**, we started our PhD almost at the same time, and look at us now! I thoroughly enjoyed the fun times that we shared at countless parties, carnival, filming of PhD movies (I can still see you running around in a dinosaur suit) and other social events (Berlin trip!!). You were always up for a drink and a good talk. While we were the only ones left in the lab in the evening of a random weekday, we even ended up saving the department from flooding.. Especially during the last part of our PhD trajectory, I’m thankful that we could confide in each other about some of the struggles we experienced. I admire your strong voice and how you always know exactly what you want and how to get it. I want to wish you the best of luck in your new challenge! **Elias**, thank you for always being kind, sincere and helpful. You were one of the main instigators of social activities within the team, which I greatly appreciated. I had a lot of fun organizing our lab trip to Berlin with you, and am proud that we started this new tradition. Good luck with finishing your PhD! **Stan**, jij bent op onze afdeling begonnen als mijn stagiair. Jouw talent en je passie voor wetenschap werden al snel duidelijk. Het is daarom meer dan verdiend dat je bent aangenomen als promovendus in onze groep. Bedankt voor je inzet en bijdrage aan mijn projecten en heel veel succes met je PhD. Ik ben ervan overtuigd dat dit helemaal goed gaat komen! **Jenny**, ik wil nogmaals benadrukken hoe trots ik ben op het feit dat jij je hart hebt gevolgd. Ik wil je bedanken voor de tijd dat we als collega’s hebben samengewerkt. Je werkte keihard en was er altijd voor iedereen. Bedankt voor het leggen van de basis van het PFKFB3

project. Ik wens jou, Renzo en Marie nog heel veel geluk toe. **Thomas**, hoewel we nooit hebben samengewerkt als collega's, wil ik je graag bedanken voor het leggen van de fundering van het PDGF-B project. Mede dankzij jou heeft dit tot een mooie publicatie geleid. **Lele, Jan, Olivia and Laura**, thank you for your contribution to this thesis and the best of luck in finishing your PhD! **Jasper, Ruud, Margaux, Anke, Danielle, Chang, Suzan, Zhenyu, Dizar and Han**, thank you for the great scientific and non-scientific conversations over the years and for your contribution to my PhD trajectory.

Pieter, er is niemand die zo veel feitjes paraat heeft en zo veel leuke verhalen te vertellen heeft als jij. Bedankt voor je adviezen, het delen van je kennis en voor je hulp met de Nuance. Ik weet zeker dat er nog veel wetenschappelijke successen voor jou in het verschiet liggen. **Marion**, wat heb ik genoten van jouw directheid en humor. Bij jou is het echt "what you see is what you get". Je bent altijd eerlijk, tot op het hilarische af. Daarnaast is geen feestje compleet zonder jou. We deelden onze passie voor reizen met elkaar. Je hebt mij en Lieve door een lange avond en nacht heen gesleept met jouw reisblog. Toen de corona restricties eindelijk waren afgeschaft, hebben we een hele leuke tijd gehad in Marseille, samen met Thijs en Lieve. Muiswerk ging altijd hartstikke soepel en snel wanneer jij meehielp. Bedankt daarvoor, en voor het vele samen kijken naar coupes onder de microscoop. **Marjo**, bedankt voor je suggesties en kritische vragen tijdens labmeetings en andere presentaties. Je benaderde (onderdelen van) mijn projecten vaak vanuit een nieuwe hoek, waar ik veel van heb geleerd. Daarnaast wil ik je ook bedanken voor je oprechte interesse en je carrière adviezen.

Het rustpunt van team Sluimer, **Jacques**. Jij laat je niet gek maken en ik kon altijd op je rekenen. Ik ben enorm blij dat jij bij team Sluimer bent gekomen en dat ik met jou heb mogen samenwerken. Ik kon altijd bij je terecht voor een gezellig of serieus gesprek. Ik wil je bedanken voor je interesse, eerlijkheid en je hulp bij al het muiswerk en alle kleuringen. Deze krullenbol gaat jou missen! **Clairy**, dankjewel voor het uitvoeren van de vele genotyperingen en voor het eindeloos snijden van coupes voor mij. Je was een fijne collega en ik heb genoten van onze gesprekken. **Gregorio**, bedankt voor de gezelligheid tijdens feestjes en in Berlijn, en voor het delen van al je kennis over histologie. **Emiel, Dietbert en Jack**, bedankt voor jullie belangstelling tijdens lab meetings en voor jullie hulp wanneer ik vragen had. **Audrey**, bedankt dat je altijd voor mij en de rest van het team klaarstond wanneer er iets geregeld moest worden.

Peter, hartelijk dank voor je flexibiliteit, je opgewektheid en al je hulp bij grootschalige dierexperimenten. Ook veel dank aan **Erwin** voor je expertise en voor je hulp, uitleg en advies bij flow cytometrie en sort experimenten, wanneer ik weer met die vervelende vaten en

plaques aankwam.. Ook al werkte je niet meer bij de Pathologie bij aanvang van mijn PhD, waardeer ik je aanhoudende betrokkenheid.

Daarnaast wil ik ook alle mensen van het **CPV** bedanken, waaronder **Richard, Saskia, Nicole, Clarice, Rik, Anouk** en **Mandy**, voor de prettige samenwerking en het meedenken.

Leon, Niko en **Armand**: jaren geleden liep ik bij jullie rond op het lab voor de afstudeerstage van mijn bachelor. Ik ben nog steeds dankbaar voor de fijne begeleiding in die vroege jaren en voor de prettige samenwerking tussen onze afdelingen. Bedankt voor jullie hulp en voortdurende interesse! **Kristiaan**, enorm bedankt voor je waardevolle input op het PFKFB3 manuscript!

Thank you to all the former and current members of **I'mCARIM** and the **EPC** for your input over the years and for having me as a PhD representative.

Ik wil ook graag alle mensen bedanken waar we mee hebben samengewerkt buiten het MUMC en de UM. **Margreet** en **Thijs**, hartelijk dank voor de fijne samenwerking binnen de PHD2 studie. Hopelijk komt hier een mooie en verdiende publicatie uit. Thijs, veel succes nog met de afronding van je PhD. Verder wil ik **Bart** enorm bedanken voor het leveren van input op het PFKFB3 project en voor de onmisbare hulp bij de metabolomics experimenten. **Neil** and **Ross**, thank you for your help with the PFKFB3 project. Your input concerning the liver and fatty liver disease was of immeasurable value. **Julio, Javier, Rafael, Sikander, Sidrah** and **Monica**, thank you all for helping with the bioinformatics part of our projects. I am very proud of our published papers and manuscripts.

Lieve **familie en vrienden**, bedankt voor jullie interesse in mijn onderzoek en voor jullie onvoorwaardelijke steun en liefde. Ik waardeer de mooie, gezellige en leuke momenten die we hebben gedeeld, die mij opvrolijkten en mij ontspanning brachten, ongeacht de staat van mijn promotie.

Lieve **pap en mam**, bedankt dat jullie mij altijd hebben gestimuleerd om door te zetten en het beste uit mezelf te halen. Een slimme meid is inderdaad op haar toekomst voorbereid. Samen hebben we open dagen van universiteiten afgestruind door het hele land. En hier zijn we dan: nu heb ik naast mijn bachelor en master ook mijn PhD op zak. Hoewel het niet altijd goed te volgen was wat dat promotietraject nou allemaal inhield, hebben jullie mij gesteund en aangemoedigd in al mijn beslissingen. Ik wil jullie bedanken voor alle offers die jullie hebben gebracht en voor jullie liefde, adviezen en geloof in mijn capaciteiten. Het geeft mij een fijn gevoel wetende dat ik altijd op jullie terug kan vallen. Lieve **Ralf** en **Erik**, hoewel we elkaar soms wat weinig zien, weet ik wel dat ik altijd op jullie kan rekenen. Als grote broers zijn jullie altijd voorbeelden voor mij geweest. Tijdens mijn promotietraject zijn jullie allebei papa

geworden, en ik ben dan ook ongelofelijk trots op jullie, **Jasmien, Gabriëlle, Owen en Matthijs**. Jullie doen het geweldig en ik geniet van de tijd die we samen doorbrengen. Lieve **Anita en Jo, Ton en Elviera**, bedankt voor jullie support en interesse en voor het bieden van een tweede en derde thuis.

Lieve **oma**, jij feliciteerde me al voordat ik helemaal klaar was, zoveel vertrouwen had je erin! Jij ook bedankt voor je interesse en al je goede zorgen, hopelijk ben je trots. Wat had ik graag gewild dat **opa** dit moment ook nog had kunnen meemaken. Hij wordt ontzettend gemist ★ Lieve **Jeannie en Fred**, bedankt voor de belangstelling die jullie altijd toonden in mijn voortgang en de fijne gesprekken. Een speciaal dankwoord ook aan **Bennie**, voor je hulp met het ontwerp van de omslag van mijn thesis!

Lieve **Bram**, de laatste maar zeker niet de minste die ik wil bedanken. Ik ben enorm dankbaar dat ik jou in mijn leven heb. Jij hebt een grote bijdrage geleverd aan de totstandkoming van dit proefschrift. Ik durf te zeggen dat me dit zonder jou niet gelukt zou zijn! Jij hebt mijn PhD traject, met de vele bijbehorende ups en down, van dichtbij meegemaakt. Jij hebt me een stabiele en warme thuisbasis gegeven en mij door de moeilijke momenten heen gesleept. Soms was ik tot laat in de avond (of vroeg in de ochtend..) bezig met experimenten. Hoewel je daar vanuit je standpunt als psycholoog en liefhebbende vriend niet altijd blij mee was, kon ik er zeker van zijn dat je thuis op me stond te wachten met een kopje slaap lekker thee, Wally, Evy en een luisterend oor. Bedankt dat ik bij jou altijd mezelf kan zijn. Je bent niet alleen mijn partner, maar ook mijn beste vriend. Bedankt dat je alle successen trots met me hebt gevierd met heerlijke etentjes of lieve cadeautjes. Bedankt voor je troost wanneer er weer eens iets was misgegaan en ik teleurgesteld thuiskwam. Bedankt voor je flexibiliteit en begrip wanneer ik werk moest afmaken in de avonden en weekends. Bedankt voor alle leuke momenten en mooie reizen die we samen hebben gedeeld, die mij de positieve energie gaven om weer door te zetten. Kortom, bedankt voor je onvoorwaardelijke steun en liefde. Je standvastigheid, relativiseringsvermogen, adviezen en gevoel voor humor vormden voor mij een boei in de onstuimige PhD wateren. Op mijn beurt hoop ik nu hetzelfde voor jou te kunnen betekenen tijdens je opleidingstraject. Ik ben trots op jou, en op ons als koppel. Iech han diech jeer ♥

Addendum

Curriculum vitae

Personal information

Name: Renée Jozefien Hubertus Antoinette Tillie

Date of birth: 10th of March 1995

Place of birth: Heerlen, The Netherlands

Education

- Jan. 2019 – Jul. 2023 **PhD training in biomedical sciences**
 Department of Pathology, Maastricht University Medical Center
 The Netherlands
- Sept. 2016 – Jul. 2018 **Master Biomedical Sciences (MSc) – *cum laude***
 Maastricht University
 The Netherlands
- Sept. 2013 – Jul. 2016 **Bachelor Health Sciences (BSc), Biology & Health track – *cum laude***
 Maastricht University
 The Netherlands

Research & work experience

- Jan. 2019 – Jul. 2023 **PhD training in biomedical sciences**
 Department of Pathology, Maastricht University Medical Center
 The Netherlands
 Promotores: Prof. Dr. Judith C Sluimer and Prof. Dr. Erik AL Biessen
 Title: *Plaque stabilizing and destabilizing effects in atherosclerosis: the role of microvessels, macrophage metabolism and fibroblasts*
- Aug. 2018 – Dec. 2018 **Research intern - supported by dr. E Dekker student grant Dutch Heart Foundation**
 Department of Regenerative Medicine, Stem Cell Institute, University of Cambridge
 United Kingdom
 Supervisor: Prof. Dr. Sanjay Sinha
 Title: *Testing combinational treatment in an in vitro vascular model of Marfan syndrome derived from induced human pluripotent stem cells*
- Nov. 2017 – Jun. 2018 **MSc senior practical training**
 Department of Pathology, Maastricht University Medical Center
 The Netherlands
 Supervisor: Prof. Dr. Judith C Sluimer

- Title: *Deletion of the PDGF-B retention motif to mimic intraplaque microvessel hyperpermeability: its effects on plaque stability, macrophages and smooth muscle cells*
- Feb. 2017 – Jul. 2017 **MSc junior practical training**
Department of Gynecology and Obstetrics, Maastricht University
Medical Center
The Netherlands
Supervisor: Dr. Chahinda Ghossein-Doha
Title: *Novel circulating biomarkers for concentric remodeling in women with a history of preeclampsia*
- Apr. 2016 – Jun. 2016 **BSc practical training**
Department of Biochemistry, Maastricht University
The Netherlands
Supervisor: Prof. Dr. Leon Schurgers
Title: *The role of vitamin K1 in vascular calcification in porcine vascular smooth muscle cells*

Certificates & courses

- June 2022 **Time and project management**
European Doctoral Summer School, University of York
- June 2021 **Non-invasive Cardiovascular Imaging**
Cardiovascular Research Institute Maastricht (CARIM)
- October 2019 **Introduction to R**
Maastricht University
- October 2019 **Vascular Biology**
Dutch Heart Foundation Papendal course
- April 2019 **Art.9 permit to work with lab animals**
Maastricht University
- February 2017 **Biosafety certificate**
Maastricht University
- 2016 **Introductory course in principles of the PBL system**
Maastricht University
- 2012 **The Anglia Certificate of English**
Examinations in ESOL International
Level: AcCEPT Proficiency – equivalent to level C1

Other activities

- Oct. 2021, Mar. 2023 **Reviewer**
Communications Biology, Vascular Pharmacology
- Oct. 2019 – Dec. 2022 **PhD representative I'mCARIM**
Cardiovascular Research Institute Maastricht
- Aug. 2020 – Oct. 2020, **Tutor**
- Aug. 2021 – Oct. 2021 Threats & Defences, bachelor Biomedical Sciences, Maastricht University
- Sept. 2013 – Jul. 2016 **Study association MSV Santé – sports committee**
Chair and member

Conferences & seminars

**European Atherosclerosis Society
Conference 2023**
Mannheim (Germany)

Selected oral presentation (2x)

Human and murine single-cell RNA-sequencing reveal fibroblast heterogeneity in healthy and diseased vasculature and differential regulation by ageing and serum cholesterol

Partial myeloid inhibition of key glycolytic enzyme PFKFB3 increases hepatic steatosis and inflammation, but does not affect atherosclerosis

**International Vascular Biology Meeting
2022**
Oakland, CA (USA)

Selected oral presentation

Human and murine single-cell RNA-sequencing reveal fibroblast heterogeneity in healthy and diseased vasculature and differential regulation by ageing and serum cholesterol

Poster presentation

Partial myeloid inhibition of key glycolytic enzyme PFKFB3 increases hepatic steatosis and inflammation, but does not affect atherosclerosis

**Cardiovascular Research Institute
Maastricht Annual Symposium 2022**
Maastricht (The Netherlands)

Poster presentation

Partial myeloid inhibition of key glycolytic enzyme PFKFB3 increases hepatic steatosis and inflammation, but does not affect atherosclerosis

Department of Pathology

Science Day 2022

Valkenburg (The Netherlands)

Selected oral presentation

Single-cell sequencing reveals fibroblast heterogeneity in healthy and diseased vasculature

Poster presentation

Partial inhibition of the key glycolytic enzyme PFKFB3 in myeloid cells causes increased hepatic steatosis and inflammation

German Society for Microcirculation and Vascular Biology meeting 2021

Göttingen (Germany)

Poster presentation

Single-cell sequencing reveals fibroblast heterogeneity in healthy and diseased vasculature

British Atherosclerosis Society

Annual meeting 2021

Online

Poster presentation

Partial myeloid inhibition of glycolytic enzyme 6-phosphofructo-2-kinase/fructose-2,6-bisphosphatase-3 (PFKFB3) does not affect atherosclerosis

European Atherosclerosis Society Conference 2021

Online

Science at a Glance E-poster presentation

Single-cell sequencing reveals fibroblast heterogeneity in healthy and diseased vasculature

Keystone eSymposium Fatty Liver Disease and Multi-system Complications

Online

Poster presentation & sci-talk

Partial inhibition of the key glycolytic enzyme PFKFB3 in myeloid cells causes increased hepatic steatosis and inflammation

International Vascular Biology Meeting 2020

Online

Poster presentation

PDGF-B retention motif deletion has mural cell-independent effects including increased atherosclerotic plaque stability due to altered macrophage function and enhanced extramedullary hematopoiesis resulting in leukocytosis

Dutch Heart Foundation cardiovascular training course 2019

Papendal, Arnhem (The Netherlands)

Poster presentation and selected TEDMED Talk

Mural cell-independent effects of PDGF-retention motif deletion: leukocytosis and increased atherosclerotic plaque stability

European Atherosclerosis Society Conference 2019 Maastricht (The Netherlands)	Science at a Glance E-poster presentation <i>Mural cell-independent effects of PDGF-B retention motif deletion: leukocytosis and increased atherosclerotic plaque stability</i>
European Society for Microcirculation-European Vascular Biology Organisation Conference 2019 Maastricht (The Netherlands)	Poster presentation <i>Mural cell-independent effects of PDGF-B retention motif deletion: leukocytosis and increased atherosclerotic plaque stability</i>
Mosa Conference 2018 Maastricht (The Netherlands)	Selected oral presentation <i>Deletion of the PDGF-B retention motif to mimic intraplaque microvessel hyperpermeability: its effects on plaque stability and macrophages</i>

Awards & prizes

Young Investigator Fellowship	European Atherosclerosis Society conference 2023
Travel award	North American Vascular Biology Organization, for IVBM 2022
Travel award	Journal of Cardiovascular Development & Disease, for IVBM 2022
CARIM commitment award 2022	Cardiovascular Research Institute Maastricht
Poster prize	Cardiovascular Research Institute Maastricht Annual symposium 2022
HS-BAFTA fellowship for talented PhD candidates	Cardiovascular Research Institute Maastricht 2021
Young Investigator Fellowship	European Atherosclerosis Society conference 2021
Scholarship	Keystone eSymposium on Tissue Plasticity: Preservation and Alteration of Cellular Identity
Poster prize	European Society for Microcirculation-European Vascular Biology Organisation conference 2019
Dr. E. Dekker student grant	Dutch Heart Foundation 2018

Publications

Human and murine fibroblast single-cell transcriptomics reveals fibroblast clusters are differentially affected by ageing and serum cholesterol

Kim van Kuijk, Ian R. McCracken, **Renée J.H.A. Tillie**, Sebastiaan E.J. Asselberghs, Dizar A. Kheder, Stan Muijtens, Han Jin, Richard S. Taylor, Ruud Wichers Schreur, Christoph Kuppe, Ross Dobie, Prakesh Ramachandran, Marion J. Gijbels, Lieve Temmerman, Phoebe M. Kirkwood, Joris Luyten, Yanming Li, Heidi Noels, Pieter Goossens, John R. Wilson-Kanamori, Leon J. Schurgers, Ying H. Shen, Barend M.E. Mees, Erik A.L. Biessen, Neil C. Henderson, Rafael Kramann, Andrew H. Baker, Judith C. Sluimer

Cardiovascular Research, 2023, July 4

Partial inhibition of the 6-Phosphofructo-2-Kinase/Fructose-2,6-Bisphosphatase-3 (PFKFB3) Enzyme in Myeloid Cells Does Not Affect Atherosclerosis

Renée J.H.A. Tillie, Jenny de Bruijn, Javier Perales-Patón, Lieve Temmerman, Yanal Ghosheh, Kim van Kuijk, Marion J. Gijbels, Peter Carmeliet, Klaus Ley, Julio Saez-Rodriguez, Judith C. Sluimer

Frontiers in Cell and Developmental Biology, 2021, Aug 12

A switch from cell-associated to soluble PDGF-B protects against atherosclerosis, despite driving extramedullary hematopoiesis

Renée J.H.A. Tillie, Thomas L. Theelen, Kim van Kuijk, Lieve Temmerman, Jenny de Bruijn, Marion Gijbels, Christer Betsholtz, Erik A.L. Biessen, Judith C. Sluimer

Cells, 2021, July 10

Fibroblasts in atherosclerosis: heterogeneous and plastic participants

Renée J.H.A. Tillie, Kim van Kuijk, Judith C. Sluimer

Current Opinion in Lipidology, 2020, October 31

Myeloid PHD2 conditional knock-out improves intraplaque angiogenesis and vascular remodeling in a murine model of venous bypass grafting

Thijs J. Sluiter, **Renée J.H.A. Tillie**, Alwin de Jong, Jenny B.G. de Bruijn, Hendrika A.B. Peters, Remco van de Leijgraaf, Raghed Halawani, Michelle Westmaas, Lineke I.W. Starink, Paul H.A. Quax, Judith C. Sluimer, Margreet R. de Vries

Accepted for publication in *Journal of the American Heart Association (JAHA)*

Myeloid PFKFB3 knockdown exacerbates diet-induced MAFLD through stimulation of myeloid cell proliferation and hepatic steatosis

Renée J.H.A. Tillie, Jenny B.G. de Bruijn, Ross Dobie, Marion Gijbels, Gijs Goossens, Peter Carmeliet, Neil Henderson, Sander S. Rensen, Ludwig Dubois, Bart Ghesquière, Kristiaan Wouters, Erik A.L. Biessen, Judith C. Sluimer

In preparation

Identification of a pan fibroblast marker and fibroblast subsets in atherosclerosis

Renée J.H.A. Tillie, Sidrah Maryam, Kim van Kuijk, Monica T. Hannani, Han Jin, Stan Muijtens, Marion Gijbels, Sikander Hayat, Rafael Kramann, Judith C. Sluimer

In preparation

DPEP1 regulates age-related increases in diastolic blood pressure in humans and mice

Sebastiaan E.J. Asselberghs, Dlzar A. Kheder, Baixue Yu, **Renée J.H.A. Tillie**, Paul M.H. Schiffers, Ryszard Nosalski, Bart Spronck, Marion J. Gijbels, Donna Senger, Tomasz Guzik, Leon J. Schurgers, Andy H. Baker, Barend M.E. Mees, Judith C. Sluimer

In preparation

